

The influence of man-made structures on spatial variability of soft soils

A case study at the Leendert de Boerspolder
T. P. W. van Koelen

The influence of man-made structures on spatial variability of soft soils

A case study at the Leendert de Boerspolder

by

T. P. W. van Koelen

to obtain the degree of Master of Science in Civil Engineering
at the Delft University of Technology,
to be defended publicly on **31 January, 2019 at 15:30**.

Thesis committee:

Prof. Dr. M. A. Hicks (Chair)	TU Delft, Geo-Engineering
Dr. P. J. Vardon	TU Delft, Geo-Engineering
Ir. K. J. Reinders	TU Delft, Hydraulic Engineering
Ir. T. de Gast	TU Delft, Geo-Engineering

Cover image: Random Field by Tim van Koelen.

An electronic version of this thesis is available at <http://repository.tudelft.nl/>.

Summary

The subsurface is often modelled as multiple homogeneous soil layers. In reality, the soil properties of these layers are heterogeneous and spatially variable, making it difficult to properly deduct the engineering properties that are required in the design of geotechnical structures. This leads to uncertainty in the design. The probabilistic framework known as the random finite element method (RFEM) can take the spatial variability of soil properties into account in geotechnical designs in an effort to reduce the uncertainty. The spatial variability is represented by the mean, the standard deviation and the scale of fluctuation. The scale of fluctuation is defined as the distance in which a significant correlation is found within the soil properties and is related to the geological deposition of the soil layer. The calculated reliability of man-made structures, such as dykes, is the output of the RFEM and is influenced by the scales of fluctuation of the subsurface. Since many man-made structures in the Netherlands are constructed on soft soils, they cause deformations in the subsurface. These deformations change the geological layering of the soil. It is therefore expected that the deformations caused by man-made structures influence the scales of fluctuation and that the changed scales of fluctuation influence the calculated reliability of the man-made structures.

The objective of this thesis is to research how the spatial variability of soft soils is influenced by man-made structures. To research this, a case study is undertaken at the Leendert de Boerspolder in the Netherlands. One-hundred cone penetration tests (CPTs) have been taken in an area of 15 by 50 meters in the polder as well as in the dyke as part of the research programme Reliable Dykes. From the cone resistance data of the CPTs the spatial variability of the area can be estimated. The case study is accompanied by two theoretical studies. The first study aims to estimate the effect of deformations on the spatial variability of generated random field data for different types of deformations. The second study of this thesis will provide the deformations that have occurred in the area of the case study from a plane-strain finite element analysis of the dyke and polder.

The first part of the research focussed on four deformations that are often encountered in the proximity of a dyke: vertical compression, horizontal compression, simple shear and rotation. The effect of these deformations on the spatial variability has been studied by applying the deformations to three resolutions of random fields and then estimating the change in scales of fluctuation. Since no soil properties were assigned to the random fields, the results can only be used qualitatively.

The research is then continued with the estimation of the spatial variability of the Leendert de Boerspolder. It was necessary to identify the soil layers first. These are a top peat layer, a clay layer which shows a transition from organic at the top to silty at the bottom, and a bottom peat layer. For each of the CPT lines parallel to the dyke the outliers of the cone resistance data were removed for the different soil layers and the depth trends were removed. This resulted in normalised cone resistance data from which the spatial variability in different directions could be estimated.

Finally, a two-dimensional plane strain analysis of the soil layers at the Leendert de Boerspolder was made. In the first step of the analysis the depths of the soil layers are at the level before construction of the dyke. Then the dyke was constructed step-wise. This allowed the initial soil layers to deform as close as possible to the actual deformations under influence of the dyke. Finally, the following conclusions are made by combining the resulting deformations with the results of the other research. At the Leendert de Boerspolder, the spatial variability of the polder next to the dyke is not influenced by the dyke and can be used as the baseline spatial variability to which to compare the spatial variability in the proximity of the dyke. Underneath the crest a significant vertical compression causes both the vertical and horizontal scales of fluctuation to decrease, while a smaller amount causes a change in just the vertical scale of fluctuation. Underneath the slope and toe of the dyke, rotation increases the larger vertical scale of fluctuation and decreases the larger horizontal scale of fluctuation. Horizontal extension of the soft soil underneath the slope results in a larger horizontal scale of fluctuation. Horizontal compression underneath the toe results in a smaller horizontal scale of fluctuation.

This research has shown that man-made structures on soft soils influence the spatial variability of those soft soils. Future research is necessary to investigate whether the changed spatial variability influences the calculated reliability of the man-made structure.

Samenvatting

De ondergrond wordt vaak gemodelleerd als meerdere homogene grondlagen. In werkelijkheid zijn de grondparameters van deze lagen heterogeen en ruimtelijk variabel, waardoor het moeilijk is om de technische eigenschappen die moeten worden gebruikt bij het ontwerpen van geotechnische structuren correct af te leiden. Dit leidt tot onzekerheid in het ontwerp. Het probabilistische raamwerk genaamd de willekeurige eindige elementen methode (Engels: *random finite element method*) kan rekening houden met de ruimtelijke variabiliteit van de grondparameters in geotechnische ontwerpen in een poging de onzekerheid te verminderen. De ruimtelijke variabiliteit wordt beschreven door het gemiddelde, de standaarddeviatie en schaal van fluctuatie. De schaal van fluctuatie is gedefinieerd als de afstand waarin een significante correlatie wordt gevonden in de eigenschappen van de bodem en is gerelateerd aan de geologische depositie. De betrouwbaarheid van door de mens gemaakte structuren, zoals dijken, is de uitkomst van een willekeurige eindige elementen methode en wordt beïnvloed door de schalen van fluctuatie van de ondergrond. Omdat veel waterkeringsinfrastructuur in Nederland op slappe bodem is gebouwd, veroorzaken ze vervormingen in de ondergrond. Deze vervormingen veranderen de geologische gelaagdheid van de grond. Het is daarom te verwachten dat de vervormingen van door de mens gemaakte structuren de schalen van fluctuatie beïnvloeden van de slappe grond, die op hun beurt de betrouwbaarheid van de door de mens gemaakte structuren beïnvloeden.

Het doel van dit proefschrift is om te onderzoeken hoe de ruimtelijke variabiliteit van een slappe ondergrond wordt beïnvloed door door de mens gemaakte structuren. Om dit te onderzoeken, wordt gebruik gemaakt van een case study in de Leendert de Boerspolder in Nederland. Honderd sonderingen zijn in een gebied van 15 bij 50 meter in de polder en in de dijk genomen in het kader van het onderzoeksprogramma Reliable Dykes. Met behulp van de gemeten conusweerstand van de sonderingen kan de ruimtelijke variabiliteit van het gebied worden geschat. Naast de case study zijn twee theoretische studies ondernomen. De eerste studie heeft als doel het effect van vervormingen op de ruimtelijke variabiliteit van gegenereerde willekeurige gronddata voor verschillende soorten vervormingen te schatten. Het tweede onderzoek zal de vervormingen opleveren die in de buurt van het dijklichaam in het gebied van de case study zijn opgetreden, met behulp van een vlakke vervormingen eindige elementen analyse van de dijk en de polder.

Het eerste deel van dit onderzoek focuste op vier vervormingen die vaak voor komen in de nabijheid van een dijk: verticale samendrukking, horizontale samendrukking, simple shear en rotatie. Het effect van deze vervormingen op de ruimtelijke variabiliteit is bestudeerd door de vervormingen toe te passen op drie resoluties van willekeurige velden en vervolgens de verandering in schalen van fluctuatie te schatten. Omdat aan de willekeurige velden geen sterkte eigenschappen zijn toegewezen, kunnen de resultaten alleen kwalitatief worden gebruikt.

Het onderzoek is vervolgens verder toegespitst op de inschatting van de ruimtelijke variabiliteit van de Leendert de Boerspolder. Het was noodzakelijk eerst de grondlagen te identificeren. Dit resulteerde in een bovenste veenlaag, een kleilaag die organisch is aan de bovenkant en siltig aan de onderkant, en een onderste veenlaag. Voor elk van de lijnen met sonderingen parallel aan de dijk werden de uitschieters van de gemeten conusweerstand en de dieptetrends verwijderd voor elk van de grondlagen. Dit resulteerde in genormaliseerde conusweerstand data waaruit de ruimtelijke variabiliteit in verschillende richtingen kon worden geschat.

Tot slot werd een tweedimensionale vlakke vervormingen eindige elementen analyse van de dijk bij de Leendert de Boerspolder gemaakt. In de eerste stap van de analyse werd de diepte van de grondlagen gedefinieerd op de diepte waarop ze lagen voordat de dijk werd gebouwd. Vervolgens werd de dijk stapsgewijs gebouwd. Dit zorgde voor vervormingen van de initiële grondlagen die zo waarheidsgetrouw mogelijk waren als de echte vervormingen die plaats hebben gevonden onder de dijk. Uiteindelijk konden de volgende conclusies getrokken worden door de resulterende vervormingen te combineren met de resultaten van het andere onderzoek. In de Leendert de Boerspolder wordt de ruimtelijke variabiliteit van de polder naast de dijk niet beïnvloed door de dijk. Hierdoor kan deze worden gebruikt als de oorspronkelijke ruimtelijke variabiliteit waarmee de ruimtelijke variabiliteit in de nabijheid van de dijk kan worden vergeleken. Onder de kruin zorgt een significante hoeveelheid verticale samendrukking ervoor dat zowel de verticale als horizontale schalen van fluctuatie afnemen, terwijl een kleinere hoeveelheid alleen de verticale schaal van fluctuatie verkleint. Onder de helling en de teen van de dijk laat rotatie de grotere verticale schaal van fluctuatie afnemen en de grotere horizontale schaal van fluctuatie toenemen. Horizontale uitstreking van de slappe grond onder de helling resulteert in een grotere horizontale schaal van fluctuatie. Horizontale samendrukking onder de teen resulteert in een kleinere horizontale schaal van fluctuatie.

Dit onderzoek heeft aangetoond dat door de mens gemaakte structuren op slappe bodems de ruimtelijke variabiliteit van die slappe bodems beïnvloeden. Toekomstig onderzoek is nodig om te onderzoeken of de veranderingen van de ruimtelijke variabiliteit invloed hebben op de berekende betrouwbaarheid van de door de mens gemaakte structuur.

Preface

The heterogeneity of the subsurface is a challenging aspect of geotechnical engineering. It has an influence on every geotechnical design and ignoring it can lead to dangerous situations. Over the course of the master Geo-Engineering my interest for the heterogeneity of the subsurface has only grown stronger and working on this thesis allowed me to really dive into the topic.

When I started this project, I took on the challenge of investigating the influence of a man-made structure on the spatial variability of soft soils. Little did I know it would be such a battle. I calculated thousands of correlation lengths in which I had the pleasure of creating order in the chaos not just once, but multiple times as the methods by which I estimated the spatial variability improved. Furthermore, generating random fields by making use of a pre-compiled generator would seem straightforward, but after many hours trying to generate proper random fields on computers all over Delft and Rotterdam, I can tell you it is not. In the end, I have succeeded in bringing all the pieces of the puzzle together in this final work as a master student at the Delft University of Technology. The time has come to move on to a new challenge.

I would like to thank my supervisors, who have guided and supported me throughout the process. Special thanks to Tom for the weekly meetings even when your personal schedule was completely booked. Thanks to my parents for their support during this thesis and for accepting my little amount of visits over the past year. Friends and classmates, I want to thank you for the beers we drank together when times were tough and when times were good. Finally, I would like to thank you, the reader, for reading at least this one page and hopefully all pages that follow.

"If it would have been easy, it would have been called a Bachelor thesis." - M. Adriaanse

*T. P. W. van Koelen
Delft, 24 January 2019*

Contents

List of Figures	xi
List of Tables	xv
Nomenclature	xvii
1 Introduction	1
1.1 Background and Motivation	1
1.1.1 Soil Heterogeneity	1
1.1.2 The Influence of a Dyke on the Subsurface.	2
1.1.3 Reliability	3
1.1.4 The Case Study.	3
1.2 Problem Statement	4
1.3 Objective	4
1.4 Research Questions	4
1.5 Scope	4
1.6 Outline	5
2 Literature Review	7
2.1 Estimating Spatial Variability of Real Data	7
2.1.1 Cone Penetration Tests.	7
2.1.2 Trend Identification	9
2.1.3 Outlier Identification.	10
2.1.4 Identification of the Point Statistics	12
2.1.5 Determine the Scales of Fluctuation	12
2.2 Computing Spatial Variability.	14
2.2.1 Random Fields.	14
2.2.2 Monte Carlo Simulation	16
2.3 Safety Analysis including Spatial Variability.	16
3 Correlations of Deformed Random Fields	19
3.1 Random Field Generation.	19
3.2 Random Field Deformation.	21
3.2.1 Vertical Compression of the Random Fields	21
3.2.2 Horizontal Compression of the Random Fields	21
3.2.3 Simple Shear of the Random Fields	22
3.2.4 Rotation of the Random Fields	22
3.3 Observations on Spatial Variability when Deforming Random Fields	23
3.3.1 A Comparison between the Input or Domain Spatial Variability	23
3.3.2 Results of the Change in Spatial Variability for Different Resolutions of RFs	24
3.4 Discussion	25
4 Spatial Variability of the Leendert de Boerspolder	29
4.1 Soil Layers of the Leendert de Boerspolder	29
4.1.1 Disturbed and Unsaturated Top Layer	29
4.1.2 Analysis using the Sleeve Friction	29
4.1.3 Analysis using the Friction Ratio	30
4.1.4 Analysis using the Robertson's Soil Behaviour Types	30
4.1.5 Soil Layers of the Leendert de Boerspolder.	32
4.1.6 Layer Boundaries	33
4.1.7 Deviations and Abnormalities	33

4.2	Removing the Depth Trends.	35
4.2.1	Groups of CPTs.	35
4.2.2	Identifying the Depth Trend	35
4.2.3	Outliers in the Cone Resistance Data.	36
4.2.4	Trend Removal of the Lines of CPTs	37
4.2.5	Results of the Trend Removal	38
4.3	Calculating the Scales of Fluctuation	42
4.3.1	Matlab Code	42
4.4	Results	45
4.4.1	Spatial Variability of the First Peat Layer	46
4.4.2	Spatial Variability of the Clay Layer	48
4.4.3	Spatial Variability of the Second Peat Layer	50
4.5	Discussion	52
5	Linking Theory and Practice	55
5.1	Deformations from a Finite Element Analysis.	55
5.1.1	Input Parameters	55
5.1.2	The Finite Element Model	55
5.2	Results of the Peat Layer	56
5.2.1	Underneath the Crest	57
5.2.2	Underneath the Slope	58
5.2.3	Underneath the Toe	59
5.3	Results of the Organic Clay Layer	60
5.3.1	Underneath the Crest	60
5.3.2	Underneath the Slope	61
5.3.3	Underneath the Toe	62
5.4	Account for Changes in Spatial Variability within the RFEM.	62
5.5	Discussion	63
6	Conclusions and Recommendations	65
6.1	Conclusions per Research Question.	65
6.2	General Conclusion	66
6.3	Recommendations	67
	Bibliography	69
	Appendices	73
A	Leendert de Boerspolder	73
B	Change in Spatial Variability when Deforming Random Fields	75
C	Soil Layer Depth per CPT	95
D	Trend Identification and Removal	107
E	The Scales of Fluctuation	117
F	The Finite Element Model	139

List of Figures

1.1	The vertical soil variability within a uniform soil layer, after Phoon and Kulhawy (1999)	1
1.2	The soil property X , fluctuating with depth, follows a normal distribution with mean μ and standard deviation σ (Hicks, 2014)	2
1.3	An example of macro-instability of a dyke ('t Hart et al., 2016)	2
1.4	The Leendert de Boerspolder before the controlled dyke failure occurred, after de Gast (2019)	3
1.5	The layout of the cone penetration tests taken in the Leendert de Boerspolder (de Gast et al., 2017)	4
2.1	The CPTu cone	8
2.2	The net area ratio is equal to A_N/A_q	8
2.3	Normalised CPT soil behaviour type graph (Robertson, 1990) with the SBTn index contours (Robertson and Wride, 1998).	9
2.4	Comparison between the Ordinary Least Squares estimator and the Theil-Sen estimator for an arbitrary data set with outliers. The data set has been generated from the dashed green line by adding jitter and replacing some points by random outliers.	10
2.5	(a) Example of CPT cone resistance (q_c) data; (b) Detrended CPT cone resistance data; (c) The statistics of the detrended data	10
2.6	An example of a box-and-whisker plot for arbitrary data with a median of 66.5 and an outlier of 79	11
2.7	1D example of the determination of the experimental correlation function for a set of data with different lag distances. The data x_1, x_2, x_3 and x_5 have been removed of their trend already, so $x_j = \chi_j - \mu_j$. At x_4 there is no data available, but it is a visual aid to present different lag distances.	13
2.8	An example of the vertical and horizontal correlation functions, fitted with the Markov correlation model, from (Lloret-Cabot et al., 2014)	13
2.9	These four unique random fields are created based on the same input statistics (Hicks and Samy, 2002b)	14
2.10	Construction of a 1D local average process, making use of a top-down approach (Fenton and Vanmarcke, 1990)	15
2.11	The first three stages of the 2D local average process, where Stage 0 covers the entire domain with center \boxtimes , at Stage 1 it is split into four quadrants with centers $+$ and at Stage 2 it is split into 16 quadrants with centers \circ (Fenton and Vanmarcke, 1990)	15
2.12	Four random fields based on the same input statistics produce different slope failure mechanisms (Hicks and Samy, 2002b)	16
2.13	The results of a deterministic 2D slope reliability (left); and the results of a probabilistic 2D slope reliability (right); the analytical solution is shown by the red line (Hicks and Samy, 2002b)	16
2.14	The cumulative distribution function of 600 realisations of a probabilistic two-dimensional slope reliability problem (Hicks and Samy, 2002b)	17
3.1	The different deformations that occur along a circular slip failure; Rotation occurs within the slip circle (Bjerrum, 1973)	19
3.2	Example of a random field, with input $\theta_{hor} = 12.5m$ and $\theta_{ver} = 0.5m$, generated by covariance matrix decomposition	20
3.3	Example of a random field, with $\theta_{hor} = 12.5m$ and $\theta_{ver} = 0.5m$, generated by local average subdivision	20
3.4	Example of the high resolution random field of Figure 3.3 transformed to a low resolution random field	20
3.5	The high resolution random field after vertical compression by 1.60m with the frame of reference indicated by the black square	21

3.6	The high resolution random field after horizontal compression by 4.00m with the frame of reference indicated by the black square	22
3.7	The high resolution random field after simple shear by 35 degrees with the frame of reference indicated by the black square	22
3.8	The high resolution random field after rotation by 20 degrees with the frame of reference indicated by the black square	23
3.9	Change in θ_v due to vertical compression, normalised with the spatial variability of the input ($\theta_v(\cdot)/0.50m$)	23
3.10	Change in θ_v due to vertical compression, normalised with the spatial variability of the domain ($\theta_v(\cdot)/\theta_v(1)$)	24
3.11	The spatial variability with $\theta_h = 12.5m$ and $\theta_v = 0.5m$ visualised as an ellipse	25
3.12	Change in spatial variability due to rotation of high resolution random fields, normalised with the spatial variability of the domain ($\theta_{h,v}(\cdot)/\theta_{h,v}(1)$), fitted with the formula for rotation of an ellipsoid	25
4.1	The pore water pressure plotted over the depth for the first CPT	30
4.2	The sleeve friction and corrected cone resistance plotted over the depth for CPT 1	31
4.3	The friction ratio and corrected cone resistance plotted over the depth for CPT 1	31
4.4	Normalised Robertson soil behaviour type over the depth for CPT 1	31
4.5	Non-normalised Robertson soil behaviour type over the depth for CPT 1	31
4.6	Analysis of the first line of CPTs, located in the polder, furthest away from the dyke	32
4.7	Soil layers identified at the first line of CPTs by making use of the sleeve friction and margins	33
4.8	The additional layer at the top of the clay layer can be found in the shaded area at CPTs 8, 9, 10, 20, 21, 31, 32, 43, 53, 54, 62, 68, 77 and 78	34
4.9	The additional layer at the top of the clay layer is shown in red	34
4.10	The linear trend identified for the corrected cone resistance data for the first peat layer of the CPTs located in the crest of the dyke	36
4.11	The Quadratic trend identified for the corrected cone resistance data for the clay layer of the CPTs located in the crest of the dyke	36
4.12	The results for the outlier removal of the first and second peat layers underneath the crest of the dyke	37
4.13	The histogram of the q_t data of the first peat layer underneath the crest of the dyke before and after outlier removal	37
4.14	The detrended clay data, in this example of CPT line 3, follows a log-normal distribution	38
4.15	Trend removal for the first peat layer of CPT line 5: after trend removal the data is normally distributed	38
4.16	Summary of the trends that have been removed from the first peat layer. The detrended data follows a normal distribution.	39
4.17	Summary of the trends that have been removed from the clay layer. The detrended data follows a log-normal distribution.	40
4.18	Summary of the trends that have been removed from the clay layer when the additional layer is removed from the data. The detrended data follows a log-normal distribution.	41
4.19	Summary of the trends that have been removed from the second peat layer. The detrended data can be described by a normal distribution.	42
4.20	Besides the parallel lines, it is possible to analyse (part of) the perpendicular lines of CPTs and the lines under 45 degrees angles to the dyke	43
4.21	A flowchart summarising the code that has been used to estimate the scales of fluctuation. The explanation of the t-matrix, autocorrelation function (ACF) and autocorrelation model (ACM) can be found in Section 2.1.5.	44
4.22	Example of the CPT grid output of Matlab	45
4.23	Example of the CPT line output of Matlab	45
4.24	Example of the trend removal output of Matlab	45
4.25	Example of the histogram output of Matlab	45
4.26	Example of the horizontal spatial variability output of Matlab	45
4.27	Example of the vertical spatial variability output of Matlab	45
4.28	The vertical scales of fluctuation of the single CPTs for the first peat layer, per line	46

4.29	The vertical scales of fluctuation of the single CPTs for the clay layer, per line	48
4.30	The vertical scales of fluctuation of the single CPTs for the clay layer without the additional layer, per line	49
4.31	The vertical scales of fluctuation of the single CPTs for the second peat layer, per line	51
5.1	The results of the total displacements after the final analysis stage in Plaxis	56
5.2	The results of the total displacements after the final analysis stage in Plaxis, with the displacements visualised by arrows	57
5.3	The results of the displacements in the peat layer underneath the crest of the dyke	58
5.4	The results of the displacements in the peat layer underneath the slope of the dyke	58
5.5	The results of the displacements in the peat layer underneath the toe of the dyke	59
5.6	The results of the displacements in the clay layer underneath the crest of the dyke	60
5.7	The results of the displacements in the clay layer underneath the slope of the dyke	61
5.8	The results of the displacements in the clay layer underneath the toe of the dyke	62
5.9	An example of an RFEM realisation of the dyke at the Leendert de Boerspolder, with the undrained shear strength as spatially random parameter on a logarithmic scale in kPa, after de Gast et al. (2018a)	63

List of Tables

2.1	Common correlation models (Lloret-Cabot et al., 2014)	13
3.1	Summary of the change in spatial variability when deforming random fields, according to the Theil-Sen estimator	24
4.1	The statistical properties of the first peat layer for the CPT lines	39
4.2	The statistical properties of the clay layer for the CPT lines	40
4.3	The statistical properties of the clay layer without the additional layer for the CPT lines	41
4.4	The statistical properties of the second peat layer for the CPT lines	41
4.5	The scales of fluctuation for the parallel lines of the first peat layer	47
4.6	The vertical scales of fluctuation for the parallel lines of the first peat layer, calculated by de Gast et al. (2017). The average θ_v is calculated from the weighting factors and the double vertical scales of fluctuation.	47
4.7	The scales of fluctuation for the parallel lines of the clay layer	49
4.8	The scales of fluctuation for the parallel lines of the clay layer without the additional layer	50
4.9	The scales of fluctuation for the parallel lines of the second peat layer	51
5.1	The soil parameters for the Plaxis soil model, after de Gast (2019) and Eurocode 7 (2016)	56
5.2	The resulting layer depths of the FE analysis compared to the depths found at the Leendert de Boerspolder	56

Nomenclature

Abbreviations

2D	Two-dimensional
ACF	Autocorrelation function
ACM	Autocorrelation model
cdf	Cumulative distribution function
COV	Coefficient of variation
CPT	Cone penetration test
FE	Finite element
FEM	Finite element model
LAS	Local average subdivision
LS	Least squares
MAD	Median absolute deviation
NAP	Dutch: <i>Normaal Amsterdams peil</i>
OLS	Ordinary least squares
pdf	Probability density function
RFEM	Random finite element method
RMSE	Root mean squared error
SBTn	Normalised soil behaviour type
SPT	Standard penetration test
TS	Theil-Sen

Parameters

α	Angle	[rad]
ϕ'	Effective friction angle	[deg]
$\hat{\gamma}$	Estimate of the covariance	<i>Depends on property</i>
γ	Soil weight	[Pa]
ν	Poisson's ratio	[-]
θ	Scale of fluctuation	[m]
θ_h	Horizontal scale of fluctuation	[m]
θ_v	Vertical scale of fluctuation	[m]
μ	Mean	[Pa]
$\hat{\rho}$	Experimental correlation function	[-]
ρ	Correlation model	[-]
σ	Standard deviation	[Pa]
σ^2	Variance	[Pa ²]
σ_{v0}	Total vertical stress	[Pa]
σ'_{v0}	Effective vertical stress	[Pa]
τ	Lag distance	[m]
a	Net area ratio of the cone	[-]
A_N	Area of the sleeve	[m ²]
A_q	Area of the cone	[m ²]
c'	Effective cohesion	[Pa]
$c_{1,2}$	Weighting factors	[-]
C_C	One-dimensional compression index	[-]
C_s	One-dimensional swelling index	[-]
d	Depth	[m]
E	Stiffness	[Pa]

e_0	Initial void ratio	[-]
k	Total amount of observations	[-]
$k_{x,y}$	Hydraulic conductivity	[m/day]
COV	Coefficient of variation	[-]
E	Error	[-]
F	Safety factor	[-]
f_s	Sleeve friction	[Pa]
F_r	Normalised friction ratio	[-]
I_c	Normalised soil behaviour type index	[-]
I_{SBT}	Non-normalised soil behaviour type index	[-]
\mathbf{K}	Matrix of covariances	<i>Depends on property</i>
\mathbf{L}	Lower triangular matrix	<i>Depends on property</i>
n_d	Amount of observations	[-]
p_a	Atmospheric pressure	[Pa]
q_c	Cone resistance	[Pa]
q_t	Corrected cone resistance	[Pa]
Q_t	Normalised cone resistance	[-]
r_B	Bartlett's Limit	[-]
R_f	Friction ratio	[%]
t	Amount of data pairs	[-]
u_2	Pore pressure behind the cone	[Pa]
$ u $	Total displacement	[m]
u_x	Horizontal displacement	[m]
u_y	Vertical displacement	[m]
\mathbf{w}	Vector of random variables	<i>Depends on property</i>
X	Random soil property	<i>Depends on property</i>
\mathbf{X}	Random field soil properties	<i>Depends on property</i>
z	Depth	[m]
Z	Global or local averages	<i>Depends on property</i>

Introduction

In geotechnical analyses, the subsurface is often modelled as multiple homogeneous soil layers. However, within each of those soil layers the properties of the soil are found to be heterogeneous and spatially variable, over both long and small distances. An important aspect to consider regarding the soil heterogeneity is that it might be altered by external forces, such as a dyke. In this chapter an introduction is given to soil heterogeneity and the effect that a dyke has on the underlying soft layers. A research approach is proposed to find the effect of man-made structures on the soft soil layers that are often encountered in the Dutch subsoil. Finally the layout of the thesis is presented.

1.1. Background and Motivation

1.1.1. Soil Heterogeneity

A characteristic of geotechnical engineering that sets it apart from other engineering disciplines, is the heterogeneity of the subsoil and therewith the variability of the engineering properties of the soil. The heterogeneity of the subsoil makes it difficult to properly deduct the engineering properties that have to be used in the design of geotechnical structures, leading to uncertainty in the design.

The heterogeneity, or spatial variability, of the subsoil can be viewed from different perspectives: the first one being on a macroscopic scale, where the subsoil cannot be regarded as one layer, but is divided in different geological soil layers such as sand, clay and peat. The second scale of heterogeneity is much smaller and is described by the difference or similarity in soil properties within one soil layer (e.g. clay or peat).

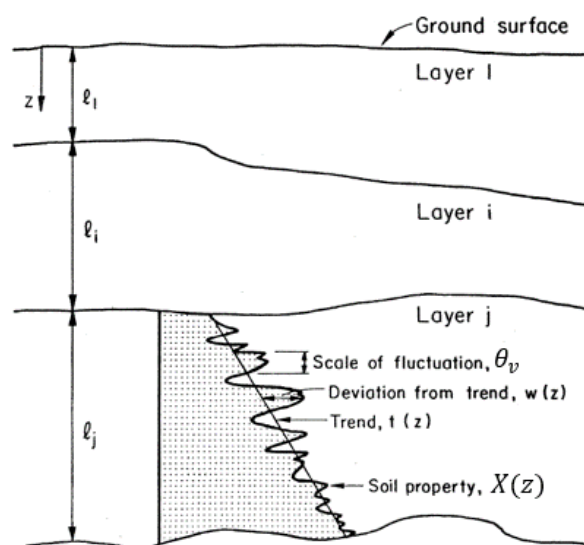


Figure 1.1: The vertical soil variability within a uniform soil layer, after Phoon and Kulhawy (1999)

A third scale is found on the microscopic scale of soil particles (Hicks, 2014). This thesis will focus on the second heterogeneity scale, described by the soil properties within a uniform soil layer, shown for the vertical direction in Figure 1.1.

If a property shows different values when measured at different spatial locations, this is referred to as spatial variability. In all soil bodies spatial variability is an inevitable characteristic that occurs naturally (Campbell, 1979), for example in the strength properties of soils, such as the friction angle and cohesion, but also for the permeability and other soil engineering properties.

Among other sources of uncertainty, such as model uncertainty, material properties uncertainty and uncertainty about the uncertainties (de Gast et al., 2018a), the spatial variability of soils leads to uncertainties in the design of geotechnical structures (Hicks, 2005). Current geotechnical practice does not properly account for the variability. The current practice makes use of a deterministic approach, where characteristic soil properties are used for the analysis of a soil layer, leading to a single factor of safety for the design.

The alternative to the deterministic approach is to make use of a probabilistic framework, known as the random finite element method (RFEM), in which the spatial variability of a soil property is represented by its statistics, which are the mean (μ), the standard deviation (σ) and the scale of fluctuation (θ) (Hicks, 2014). The first two define the probability density function of the soil property. An example of a soil property, fluctuating with depth, and its statistics is given in Figure 1.2. The scale of fluctuation is defined as the distance in which a significant correlation is found within the soil properties (Vanmarcke, 1983) and it is related to the geological deposition of the soil layer. Small values of the scale of fluctuation describe rapid changes of the soil property around the mean, whereas large values describe a soil property that varies more slowly around the mean.

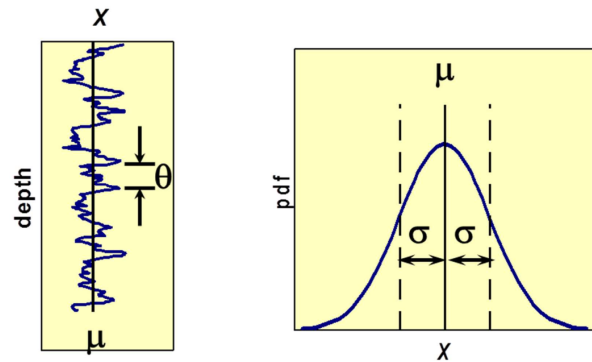


Figure 1.2: The soil property X , fluctuating with depth, follows a normal distribution with mean μ and standard deviation σ (Hicks, 2014)

1.1.2. The Influence of a Dyke on the Subsurface

In the Netherlands, many dykes have been constructed on soft soil layers such as peat and clay. The construction of a man-made structure will cause an increase in the vertical stress of the soil underneath the structure, causing settlement of the soft soil layers. The settlement can be divided in three components: immediate settlement, caused only by distortion of the soil layer, consolidation settlement, which is related to excess pore pressure dissipation, and creep or secondary consolidation settlement (Almeida and Marques, 2013). The compression is not limited to the vertical direction. Near the edges of the man-made structure the soft soil layers are compressed in the horizontal direction as well, since the soil is not confined.

Regarding the slope stability of dykes, it is known that macro-instability of the slope can occur, resulting

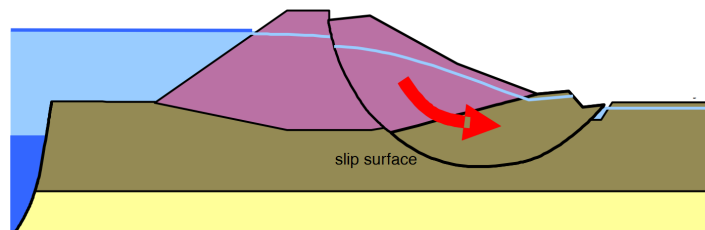


Figure 1.3: An example of macro-instability of a dyke ('t Hart et al., 2016)

in a rotation of the soil body along a circular slip circle. Due to an increase in pore water pressures, the effective stress of the soil decreases, which can result in the driving force, caused by the mass of the soil body, exceeding the resisting force, being the shear strength along the slip surface ('t Hart et al., 2016). An example of macro-instability is shown in Figure 1.3. It is possible that the soil is only slightly out of balance, resulting in a small rotation without failure of the slope.

1.1.3. Reliability

The inherent variability of soils leads to uncertainties in the design of dykes (Hicks, 2005). By making use of the random finite element method, the reliability, or the probability that failure of the dyke will not occur, can be determined. The RFEM makes use of so-called random fields, which are generated from the de-trended statistics of the tip resistance of the cone penetration tests of which the spatial variability is determined and can later be constrained (conditioned) at the CPT locations to further reduce the uncertainty in the design (van den Eijnden and Hicks, 2011). Each random field is then analysed in a finite element analysis, called a realisation, and multiple of these realisations are part of the random finite element method known as a Monte Carlo simulation.

Dykes or man-made structures influence the soil underneath, deforming the geological deposition of the layers. It is expected that this deformation also causes a change in the spatial variability of the subsurface. Since the spatial variability influences the reliability of dykes, research by de Gast et al. (2017) has made an effort to investigate the influence of the deformations underneath and around man-made structures on the scales of fluctuation. An influence of the man-made structure on the spatial variability was found, but more research would be needed to give a first insight into the influence of the change of the scales of fluctuation on the reliability of dykes.

1.1.4. The Case Study

This thesis will continue the research of de Gast et al. (2017) and use the results of 100 cone penetration tests (CPTs) made in the Leendert de Boerspolder as part of the Nederlandse Organisatie voor Wetenschappelijk Onderzoek (NWO) Toegepaste en Technische Wetenschappen (TTW) programme Reliable Dykes, which aims to provide the industry with focused scientific insight relating to rural dykes. The Leendert de Boerspolder is located to the West of the town Roelofarendsveen in the province of Zuid-Holland in the Netherlands. An overview of the area is shown in Appendix A and an aerial photograph of the polder is shown in Figure 1.4. The area will be referred to as a polder, because the measurements were taken before the controlled flooding in 2015 by the Water Board Rijnland, the foundation for applied water research STOWA and the Delft University of Technology. This had been done in order to obtain more knowledge about dykes on peat by performing a controlled failure at the dyke in the triangular section of Figure 1.4 that had not been flooded yet at the time of taking this aerial photo.



Figure 1.4: The Leendert de Boerspolder before the controlled dyke failure occurred, after de Gast (2019)

The measurement data used in this thesis is from a slightly different section of the polder and is indicated by the dashed blue square at the south west section of the dyke. The grid of the CPTs within the blue square is shown in Figure 1.5 and was designed such that the scales of fluctuation in different directions could be

obtained. The colour coding of the lines indicates the location of the measurements. The red lines (1 to 4) are the test locations in the polder, the blue lines (5 and 6) are test locations at the toe and the slope of the dyke respectively, and the green line indicates the test locations at the crest of the dyke.

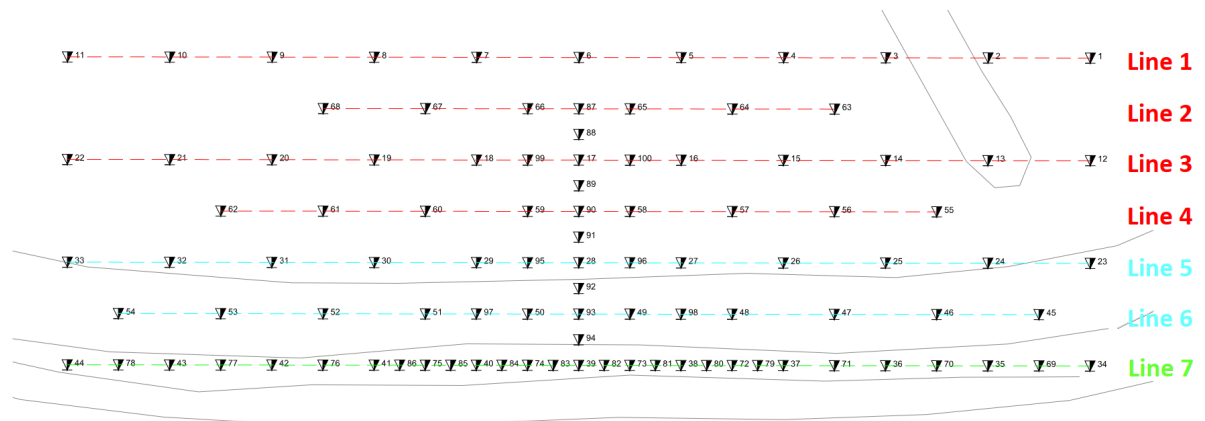


Figure 1.5: The layout of the cone penetration tests taken in the Leendert de Boerspolder (de Gast et al., 2017)

1.2. Problem Statement

In research by de Gast et al. (2017) it is hypothesised that due to deformations caused by dykes, the spatial variability of the soft soils in close proximity to the dyke is changed, influencing the reliability of the structure. When considering a limited amount of cone penetration tests, it is important to know how the dyke influences the correlations. Otherwise crucial information of the influence of the changed correlations on the reliability of the dyke could be missed by the limited dataset. More insight is needed into the influence of the dyke on the change in correlations, in order to make more appropriate analyses when the amount of cone penetration test data is limited.

1.3. Objective

The objective of this thesis is to calculate the spatial variability of the soft soil layers in the proximity of the dyke of the Leendert de Boerspolder and to find out how the spatial correlations under a man-made structure on soft soils are changed by that man-made structure by analysing the horizontal and vertical correlations. This analysis will be supported by simulations with random fields and a basic numerical analysis of the dyke at the Leendert de Boerspolder. Finally, the implications of the change in spatial variability for the calculated reliability of man-made structures will be discussed quantitatively.

1.4. Research Questions

Based on the objectives, three research questions have been formulated that will be investigated in this research.

1. How can spatial correlations be estimated from CPTs?
2. How do deformations caused by man-made structures on soft soils influence the spatial correlations of the soft soil layers?
3. How can the influence of spatial changes in spatial variability due to deformations caused by man-made structures on soft soils be taken into account in the RFEM?

1.5. Scope

The focus of this thesis lies on the change of the spatial variability of the soft soils at the Leendert de Boerspolder due to the influence of a man-made structure and the implications of the change in spatial variability on the calculated reliability of that man-made structure. In order to investigate the research questions, the scope of this thesis is as follows.

- The data that will be considered is derived from 100 cone penetration tests taken in close proximity of each other at the Leendert de Boerspolder, located in the Western part of the Netherlands, as part of the research of de Gast et al. (2017). Since this thesis will focus on soft soils, the CPT data of the dyke material and of the sand layer will not be taken into account.
- The spatial variability of the Leendert de Boerspolder will be calculated from the corrected cone resistance q_t of the CPTs. Many geotechnical engineering parameters can be derived from the cone resistance by using empirical relations. An example of one such parameter is the undrained shear strength. By using the q_t data the outcome of this research can be used for the other parameters.
- Different autocorrelation models can be considered to fit the autocorrelation function to obtain the scales of fluctuation. For the purpose of this thesis the only autocorrelation model that will be used is the double Markov exponential, also used in the research of de Gast et al. (2017). The single Markov exponential is commonly used in geotechnical engineering research and by using weighting factors and two scales of fluctuation it is possible to distinguish between smaller and larger scales of fluctuation in the soil layers.
- The effect of deformations on the spatial variability will be investigated by generating random fields and applying basic deformations to these random fields. The basic deformations found in the proximity of dykes are horizontal compression, vertical compression, simple shear and rotation. The generation method of the random fields will be limited to local average subdivision and covariance matrix decomposition.
- To find out what deformations occurred in the polder, a basic finite element analysis of the situation at the Leendert de Boerspolder will be made in Plaxis. The soft soil layers are modelled with the Soft Soil material model. The necessary parameters are determined from laboratory tests that have been carried out for the research of de Gast et al. (2017) and from Eurocode 7 (2016).

1.6. Outline

The first research question will be investigated by the literature study, presented in Chapter 2. It will elaborate on the spatial variability of soils and describe how the scales of fluctuation can be estimated from cone penetration test data. The scales of fluctuation are used in the random finite element method to generate random fields. The literature study will elaborate on these fields, which are one of the numerical studies used to investigate the second research question.

Chapter 3 presents a numerical study using random fields. As a basis of comparison for the results of the analyses performed in this thesis, several random fields with different resolutions have been deformed according to four deformations. The chapter is concluded with a discussion of the results.

In Chapter 4, the knowledge regarding the estimation of the scales of fluctuation that is obtained from the literature study will be applied to the cone penetration tests at the Leendert de Boerspolder to obtain the spatial variability of the area. The soil data has to be normalised first, by defining the soil layers, removing the outliers from the soil data and removing the depth trend of the soil data. When the boundary conditions that have been determined from the literature study are met, the spatial variability of the Leendert de Boerspolder is estimated and analysed in different orientations to the dyke. The main results are highlighted and discussed at the end of this chapter.

The results of Chapters 3 and 4 are linked together in Chapter 5. A numerical study, making use of the finite element program Plaxis, is undertaken to obtain the deformations that occurred near the dyke of the Leendert de Boerspolder. The results of the two numerical studies and the results of the spatial variability of the Leendert de Boerspolder are compared and the observations made in this research will be verified leading to a conclusion on the second research question. At the end of this chapter, the third research question will be answered qualitatively.

Finally, the conclusions and recommendations are given in Chapter 6.

2

Literature Review

The random finite element method can be used to account for soil heterogeneity in geotechnical design, reducing the uncertainty in comparison to a deterministic approach. This chapter gives an overview of the different stages of the random finite element method (Hicks, 2014):

1. Pre-analysis stage: Estimating spatial variability of real data
2. Analysis stage: Computing spatial variability
3. Post-analysis stage: Safety analysis including spatial variability

The focus of this thesis will mainly be on the pre-analysis stage of the RFEM and quantitatively treat the analysis and post-analysis stage.

2.1. Estimating Spatial Variability of Real Data

The first step of the pre-analysis stage is to determine the soil layering of the area under investigation and the second step is to characterise the spatial variability of the soil properties for each of the soil layers. This is done by making use of in situ continuous cone penetration test (CPT) profiles and the following steps (Hicks and Samy, 2002b):

- Identify the depth trend of the soil data.
- Identify its statistics $\mu(z)$ and $\sigma(z)$.
- Remove the depth trend of the soil data.
- Determine the scale of fluctuation in vertical and horizontal direction.

2.1.1. Cone Penetration Tests

For geotechnical engineering it is crucial to have a certain amount of knowledge of the subsoil, which is obtained by making use of in-situ tests and laboratory tests. Some of the most important soil parameters in terms of dyke design are the soil mass, shear behaviour, settlement and permeability. By making use of advanced laboratory tests, the parameters can be accurately estimated, but the downside of the laboratory tests is that the soil samples will have to be taken out of the underground, be brought to the laboratory and then prepared for the specific soil test before the test can be executed. Every step of this process disturbs the soil, which means that by the time the soil test is performed, the soil might not behave the same way as it would in the field. To prevent errors due to disturbance of the soil, in-situ soil tests are available which are performed, as the name implies, at the site.

In order to measure the undisturbed behaviour of the soil in the field (in-situ), soil tests such as the standard penetration test (SPT) and the cone penetration test (CPT) have been created. The SPT is executed by driving a tube into the soil and measuring the amount of blows necessary to hammer another sampler down a certain depth. The amount of blows, or the blow count, is used in empirical formulae to derive characteristics of the soil. The CPT is executed in a more continuous way than the SPT, by driving a tube down into the soil with at its front a cone and right behind it a sleeve. While pushing the cone down into the soil, the tip resistance is measured every centimetre and as soon as the sleeve enters the soil, the friction of the soil on the sleeve is measured every centimetre as well. It is possible to add a piezometer just behind the cone in order to measure the water pressure in the soil. This is called the CPTu. An overview of the CPTu is shown in Figure 2.1.

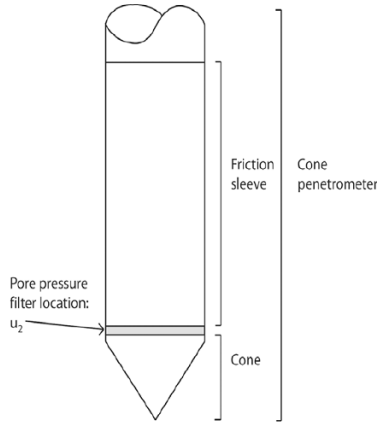
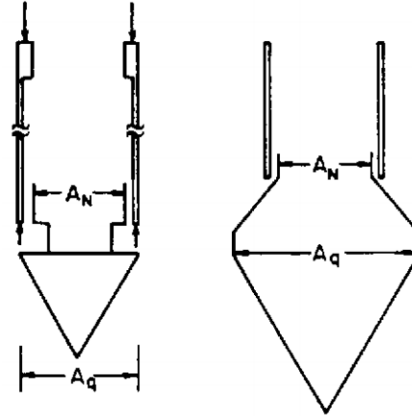


Figure 2.1: The CPTu cone

Figure 2.2: The net area ratio is equal to A_N/A_q

The SPT is not often used in the Netherlands, because the CPT has several advantages over the SPT:

- **Continuous soil profile:** In the SPT the sampler has to be hammered down 15 centimetres before a measurement of the blow count is taken, while with a CPT it is possible to measure multiple parameters every centimetre. These measurements are the cone resistance, the sleeve friction, the pore pressure and the inclination.
- **Accuracy:** Sensors near the cone and the sleeve of the CPT allow for accurate measurements of the parameters which are collected by a computer.
- **Not operator-dependent:** With modern CPT rigs, a computer controls the complete process. Therefore, the CPT measurements are repeatable and the data is more reliable.

CPT Measurements and Parameters

Several measurements are made during cone penetration tests. Before the cone is driven down into the soil, the location of the test is determined, as well as the elevation of the surface. Then the cone is pushed into the soil and measurements of the depth, cone resistance (q_c), sleeve friction (f_s), pore pressure (u_2) and gradient of the cone are recorded every centimetre.

Several other parameters can be determined from these measurements, the first of which is the friction ratio (R_f). The friction ratio is defined as the ratio of the sleeve friction over the cone resistance.

$$R_f = (f_s / q_c) \cdot 100\% \quad (2.1)$$

The friction ratio of sand is quite low, in the range of 1% to 2% due to the high permeability of sand in comparison to its interlocking. For peat layers the cone resistance is much lower than the sleeve friction, resulting in relatively high friction ratios of 8% to 10%. The friction ratio of clay typically lies in between the friction ratios for sand and peat and is commonly found to be approximately 5% (Verruijt, 2012).

In order to take the effects of the pore water pressure behind the cone and on the sleeve friction into account, the corrected cone resistance (q_t) is used (Campanella et al., 1983). The pore water pressures are taken into account, because in low permeability soils water pressures take more time to dissipate.

$$q_t = q_c + u_2 (1 - a) \quad (2.2)$$

where the net area ratio of the cone (a) is determined in a laboratory. The net area ratio of the cone is determined by the ratio of the sleeve area over the cone area, as shown in Figure 2.2. For the CPT used at the Leendert de Boerspolder, the net area ratio is equal to 0.85.

Research by Robertson (1990) resulted in a so-called normalised soil behaviour type graph, shown in Figure 2.3, to distinguish between soil layers. The different soil layers can be identified by the dimensionless parameters normalised cone resistance (Q_t) and normalised friction ratio (F_r).

$$Q_t = (q_t - \sigma_{v0}) / \sigma'_{v0} \quad (2.3)$$

$$F_r = (f_s / (q_t - \sigma_{v0})) \cdot 100\% \quad (2.4)$$

where σ_{v0} is the total vertical stress and σ'_{v0} is the effective vertical stress. The areas numbered one to nine indicate the different soil types, which are defined as:

1. Sensitive, fine grained
2. Organic soils - clay
3. Clays - silty clay to clay
4. Silt mixtures - clayey silt to silty clay
5. Sand mixtures - silty sand to sandy silt
6. Sands - clean sand to silty sand
7. Gravely sand to dense sand
8. Very stiff sand to clayey sand, heavily overconsolidated or cemented
9. Very stiff, fine grained, heavily overconsolidated or cemented

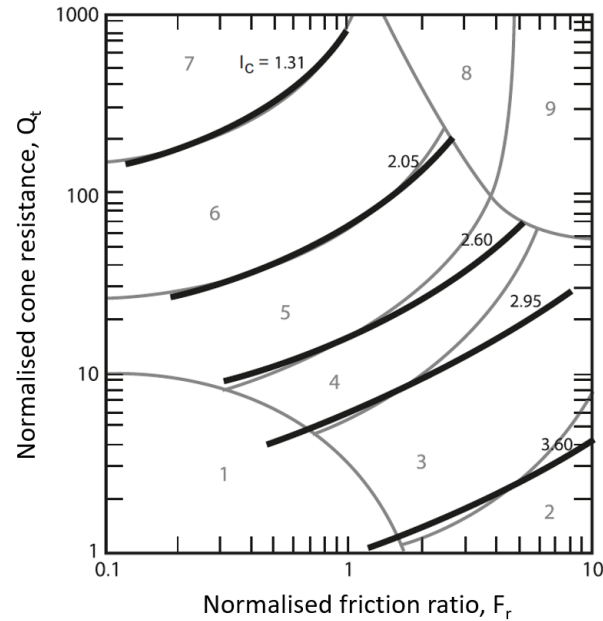


Figure 2.3: Normalised CPT soil behaviour type graph (Robertson, 1990) with the SBTn index contours (Robertson and Wride, 1998).

In order to estimate the soil type from CPT measurements, Robertson and Wride (1998) came up with a formula to estimate the contour lines shown as the bold lines in Figure 2.3. The normalised soil behaviour type index (I_c) makes use of the normalised cone resistance and the normalised friction ratio.

$$I_c = \left((3.47 - \log Q_t)^2 + (\log F_r + 1.22)^2 \right)^{\frac{1}{2}} \quad (2.5)$$

Later research by Robertson (2010) updated the normalised soil behaviour type index such that it could also be used with non-normalised soil parameters in case these could not be calculated, called the non-normalised soil behaviour type index (I_{SBT}).

$$I_{SBT} = \left((3.47 - \log(q_c/p_a))^2 + (\log R_f + 1.22)^2 \right)^{\frac{1}{2}} \quad (2.6)$$

where p_a is the atmospheric pressure. The non-normalised soil parameters will only result in the same estimation of the soil behaviour type as long as the effective in situ stresses are within the range of 50 to 150 kPa. If this is not the case, the normalised soil behaviour type index will allow for a more reliable analysis of the soil layers.

2.1.2. Trend Identification

In order to model the spatial variability, it is necessary to remove any depth trend from the CPT data. According to Jaksa et al. (1999) it is common practice to do this by removing a low-order polynomial trend from the data by using the ordinary least squares method, where the low-order polynomial is at most of a quadratic

form. Removing the depth trend from the data is the first criterion for stationary data, which simplifies the modelling of spatial variability. The other criteria are (Jaksa et al., 1999): the variance (σ^2) is constant with depth, there are no seasonal variations and there are no irregular fluctuations. For geotechnical engineering purposes, the data is sufficiently stationary when the mean and standard deviation do not change over the depth and that the correlation between two CPT locations only depends on the lag or separation distance (Lloret-Cabot et al., 2012). By identifying the soil layers and analysing each soil layer individually, these requirements are most likely to be met, since the fluctuations within a single soil layer are approximately uniform (Phoon and Kulhawy, 1999).

The most common method of identifying a linear trend is the ordinary least squares (OLS) method. However, the OLS method is sensitive to outliers in the data (Ohlson and Kim, 2014), as shown in Figure 2.4. A robust alternative is the Theil-Sen estimator, which makes use of the median of the slopes of all the possible data combinations, after which the overall estimator is determined by the median of all calculated medians (Sen, 1968). According to Huber and Ronchetti (2009) robustness is defined as insensitivity to small deviations from the assumptions.

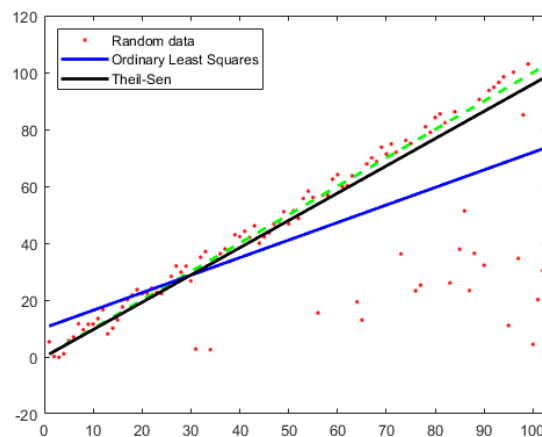


Figure 2.4: Comparison between the Ordinary Least Squares estimator and the Theil-Sen estimator for an arbitrary data set with outliers. The data set has been generated from the dashed green line by adding jitter and replacing some points by random outliers.

After identifying the trend, the following equation is used to end up with the detrended cone resistance data:

$$q_{c,\text{detrended}} = q_c - \text{trend} \quad (2.7)$$

An example of CPT cone resistance data, the trend identification and the detrended data after trend removal are shown in Figure 2.5.

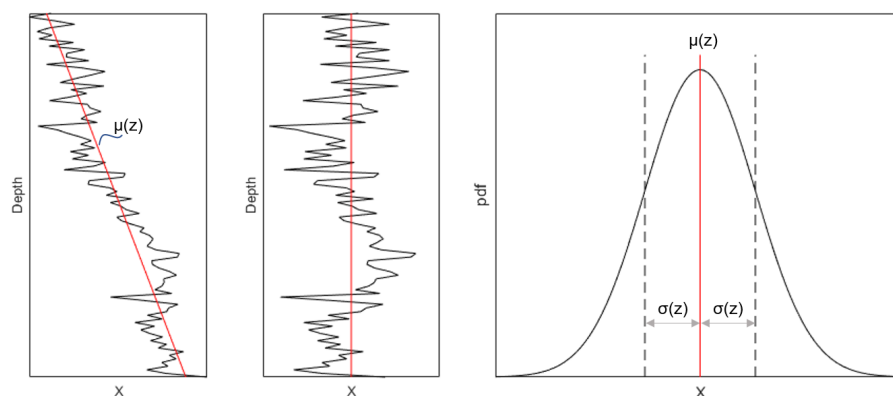


Figure 2.5: (a) Example of CPT cone resistance (q_c) data; (b) Detrended CPT cone resistance data; (c) The statistics of the detrended data

2.1.3. Outlier Identification

Outliers in the dataset can influence the result of the spatial variability found in the soil. This is due to the fact that the autocorrelation function that is used to estimate the scales of fluctuation, which will be treated

in Section 2.1.5, is not a robust model (Hampel, 1973). In order to calculate robust estimates of the scales of fluctuation it is necessary to remove the outliers from the data.

The outliers in the cone resistance measurements of CPTs often arise from pockets of soil that are different from the soil in which they are found, such as pockets of sand or gravel within a peat or clay layer. Other causes for outliers can be roots or debris, or measurement errors. The identification of outliers is often done by making use of one of three methods: the mean and the standard deviation, the interquartile range of boxplots or the median and the median absolute deviation.

Mean and Standard Deviation

Based on a normal distribution, 99.87% of the data is identified by the mean plus or minus three standard deviations, resulting in the identification of the data that falls out of this range as outliers. However, this introduces two problems (Leys et al., 2013). The first problem is the assumption that the data including the outliers follows a normal distribution. The second problem is that the mean and standard deviation are not robust estimators and are influenced by the outliers. Those outliers should be identified, but when they bias the detection, it is possible that some outliers are not identified as such.

A method to compare the mean method with the following methods is by looking at the breakdown point (Donoho and Huber, 1983). It is defined as the most contamination an estimator can take before it results in a false value. For the mean and standard deviation, an example is that when an array contains a single infinite value, the mean of the array becomes infinite, resulting in a breakdown point of 0 because a single value can cause a false value. A higher breakdown points allows more contamination, so other methods have to be analysed for their effectiveness in identifying outliers.

Interquartile Range

The second method to identify outliers is based on boxplots (Tukey, 1977), where quartiles are used to represent the data, as shown in Figure 2.6. The left side of the box represents the 25th percentile or first quartile and the right side of the box represents the 75th percentile or third quartile. The second quartile is the median, shown as the red line. The interquartile range is the range between the 25th and 75th percentiles. Outliers are identified as the datapoints that lie out of the range of the whiskers, of which the length is defined by the last value within 1.5 times the interquartile range from the first or third quartiles.

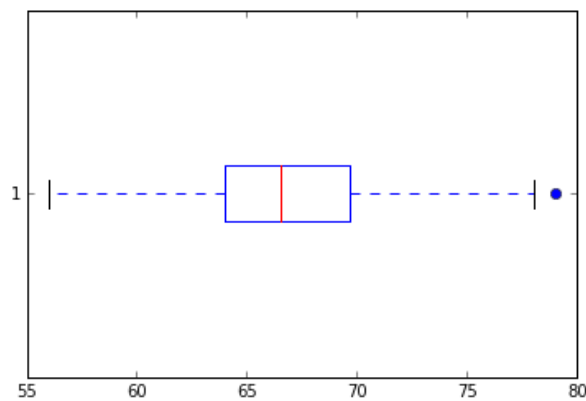


Figure 2.6: An example of a box-and-whisker plot for arbitrary data with a median of 66.5 and an outlier of 79

The breakdown point of the interquartile range is 0.25, as the name suggests, meaning that 25% of the data can be contaminated before the outlier detection is biased (Leys et al., 2013). This makes this method more robust to outliers and therefore more fit for the detection of outliers than the previous discussed method that makes use of the mean.

Median and Median Absolute Deviation

The last and most robust method to identify the outliers makes use of the median plus or minus three times the median absolute deviation. As discussed in Section 2.1.2, the Theil-Sen method that makes use of the median is a robust estimate for a linear trend. When identifying the outliers, the median will be combined with the median absolute deviation, calculated as (Huber and Ronchetti, 2009)

$$MAD = b \cdot \text{median}|x - \bar{x}| \quad (2.8)$$

where \bar{x} is the median of the data x , and b depends on the assumed distribution of the data, calculated as $b = 1/Q(0.75)$, where $Q(0.75)$ is the 75th percentile of the distribution. In case of a normal distribution $b = 1.4826$.

Investigating the breakdown point of the median method, it is found that half of the data has to be contaminated before the median is biased, resulting in a breakdown point of 0.5 (Leys et al., 2013). Therefore this is the most robust method for outlier detection of the three methods discussed.

2.1.4. Identification of the Point Statistics

From the trend and the soil data the point statistics can be determined, which are the mean of the trend $\mu(z)$ and the standard deviation of the trend $\sigma(z)$. These are used to determine the probability density function, which will be used in a later step of the probabilistic approach. According to Hicks and Samy (2002a), the variability of soil strength properties often follows a normal distribution.

In order to check the relative variability of the CPT data, the coefficient of variation can be calculated, which is a dimensionless parameter of inherent variability (Phoon and Kulhawy, 1999):

$$\text{COV} = \frac{\sigma}{\mu} \quad (2.9)$$

where μ is the mean of the data before trend removal and σ is the standard deviation of the data after trend removal. In order to determine the correct coefficient of variation, it is necessary to identify homogeneous geologic layers, exclude measurement errors, remove the trend of the data and make sure that the CPTs are performed within a time period in which no changes in the soil can occur. When all criteria are met, the COV, within the same soil layer, should show a consistency in the data.

2.1.5. Determine the Scales of Fluctuation

In order to determine the scale of fluctuation, θ , Vanmarcke et al. (1986) proposed the following equation:

$$\theta = 2 \int_0^{\infty} \hat{\rho}(\tau) d\tau \quad (2.10)$$

where $\hat{\rho}$ is the experimental correlation function and τ is the lag distance between measurements. The experimental correlation function is calculated as (Vanmarcke, 1983):

$$\hat{\rho}(\tau) = \frac{\hat{\gamma}(\tau)}{\hat{\gamma}(0)} \quad (2.11)$$

where the estimate of the covariance ($\hat{\gamma}$) is calculated as

$$\hat{\gamma}(\tau) = \frac{1}{t-1} \sum_{j=1}^t (X_j - \hat{\mu})(X_{j+\Delta_j} - \hat{\mu}) \quad (2.12)$$

and where X is the data, $\hat{\mu}$ is the trend of the data, τ is the lag distance or spacing between the measurement points, $j = 0, 1, 2, \dots, k$ where k is the total amount of observations, and t is the amount of data pairs at a certain lag distance τ . A visualisation of the experimental correlation function calculation for a one-dimensional data set with different lag distances is given in Figure 2.7.

In order to estimate the scale of fluctuation, a correlation model will have to be fit to the experimental correlation function in order to calculate the scale of fluctuation. Some correlation models that are commonly used in geotechnical engineering are shown in Table 2.1 (Lloret-Cabot et al., 2014). By making use of a correlation model, the error between the experimental correlation function, $\hat{\rho}(\tau)$, and the correlation model, $\rho(\tau)$, can be minimised in order to find the scale of fluctuation, according to:

$$E(\theta) = \sum (\rho(\tau) - \hat{\rho}(\tau))^2 \quad (2.13)$$

Research by (de Gast et al., 2017) proposed a correlation model made up of multiple weighed Markov correlation models:

$$\rho(\tau) = c_1 e^{-\frac{2|\tau|}{\theta_1}} + c_2 e^{-\frac{2|\tau|}{\theta_2}} + \dots + c_i e^{-\frac{2|\tau|}{\theta_i}} \quad (2.14)$$

where the different correlation models, and therewith the different scales of fluctuation, can be weighed by the weighing factors c_i , which should satisfy the following equation:

$$c_1 + c_2 + \dots + c_i = 1 \quad (2.15)$$

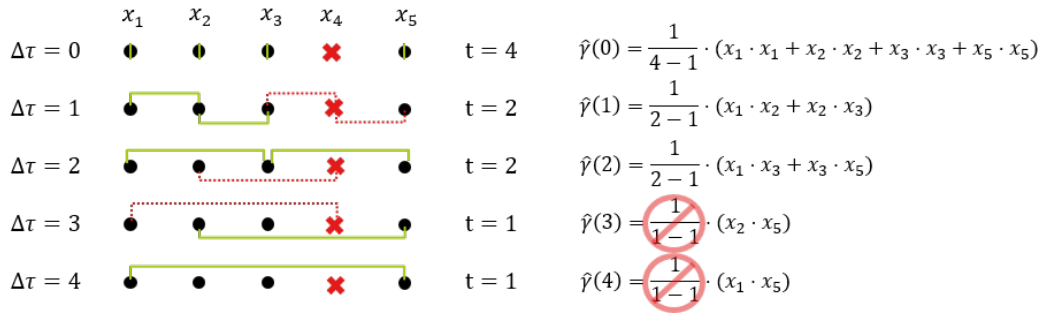


Figure 2.7: 1D example of the determination of the experimental correlation function for a set of data with different lag distances. The data x_1, x_2, x_3 and x_5 have been removed of their trend already, so $x_j = \chi_j - \mu_j$. At x_4 there is no data available, but it is a visual aid to present different lag distances.

Table 2.1: Common correlation models (Lloret-Cabot et al., 2014)

Correlation model	Formula
Markov	$\rho(\tau) = \exp\left\{\frac{-2 \tau }{\theta}\right\}$
Gaussian	$\rho(\tau) = \exp\left\{-\pi\left(\frac{ \tau }{\theta}\right)^2\right\}$
Triangular	$\rho(\tau) = \begin{cases} 1 - \frac{ \tau }{\theta} & \text{if } \tau \leq \theta \\ 0 & \text{if } \tau > \theta \end{cases}$
Spherical	$\rho(\tau) = \begin{cases} 1 - 1.5\left \frac{\tau}{\theta}\right + 0.5\left \frac{\tau}{\theta}\right ^3 & \text{if } \tau \leq \theta \\ 0 & \text{if } \tau > \theta \end{cases}$

In order to use Formula 2.14, it is necessary to calculate the average scale of fluctuation according to the unweighed Markov correlation model given in Table 2.1. Using this average scale of fluctuation, the weighed scales of fluctuation can be found by using the following formula:

$$c_1\theta_1 + c_2\theta_2 + \dots + c_i\theta_i = \theta_{\text{average}} \tag{2.16}$$

This allows multiple scales of fluctuation to be discovered in the soil, such as a small scale of fluctuation in the order of centimetres, and a large scale of fluctuation in the order of meters.

Examples of the vertical and horizontal correlation functions and the fitted Markov correlation models are shown in Figure 2.8. It can be seen that the smoothness is much higher for the vertical correlation function than for the horizontal correlation function. This is due to the fact that vertically the cone penetration test is able to measure the tip resistance or other soil parameters every centimetre, while in the horizontal direction the smoothness depends on the horizontal distance between CPTs, which is usually in the order of meters and therefore much less smooth. However, since the horizontal scale of fluctuation is often much larger than the vertical scale of fluctuation, due to the process at which soil is deposited, so it is expected that the results are accurate when the lag distance is small enough.

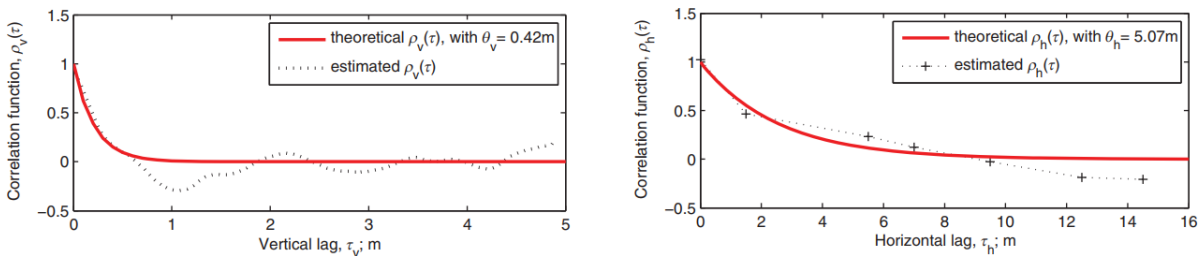


Figure 2.8: An example of the vertical and horizontal correlation functions, fitted with the Markov correlation model, from (Lloret-Cabot et al., 2014)

According to Phoon and Kulhawy (1999) a correlation of +1 or -1 between the soil properties that are compared indicates a perfect positive or negative linear relationship, respectively.

The Bartlett's Limit

It is accepted that the reliability of the correlation function drops with increasing lag distance. In order to fit the correlation model to just the part of the correlation function that is reliable, the Bartlett's limit can be used (Uzielli et al., 2005):

$$r_B = \frac{1.96}{\sqrt{n_d}} \quad (2.17)$$

where n_d is the amount of observations used to calculate the correlation function. Fitting the correlation model should only be done for the initial part of the correlation function which is larger than the Bartlett's limit.

2.2. Computing Spatial Variability

After the pre-analysis stage, the depth trend, soil property statistics and the scales of fluctuation are used to generate numerical predictions of the subsurface, so-called random fields. Each random field is used to analyse the geotechnical problem by mapping the field onto the finite element mesh. One such analysis is called a realisation and by using many random fields, many realisations can be made, known as a Monte Carlo simulation (Hicks, 2014).

2.2.1. Random Fields

The scales of fluctuation and soil property statistics are used to generate soil data in a random field. Because the same input statistics are used for every random field, each field seems similar to the other. However, the distribution of stronger and weaker zones within the random fields is different for each random field, as shown in Figure 2.9. As mentioned before, for geotechnical engineering applications, the vertical scale of fluctuation is often much smaller than the horizontal scale of fluctuation, due to the way soils are deposited.

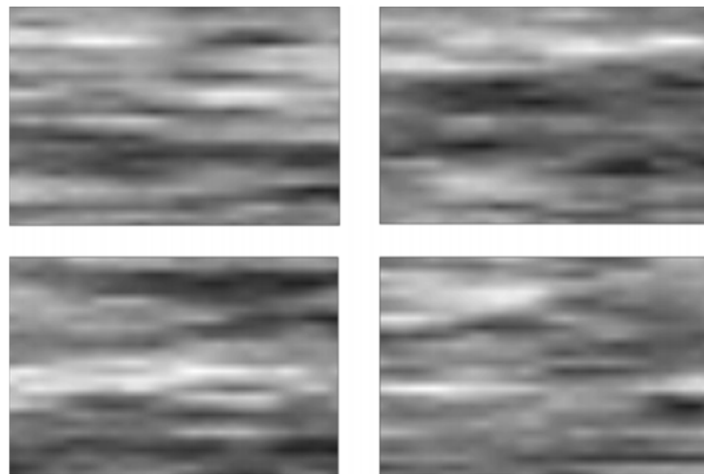


Figure 2.9: These four unique random fields are created based on the same input statistics (Hicks and Samy, 2002b)

Within a finite element program, a mesh is used to divide the soil continuum in elements for which the soil properties are set. By making use of the random field, the soil property that has been generated can be mapped onto the specific element. However, this method assumes that one value of the property is equal over the element, resulting in a discrete field instead of a continuous field (Hicks and Samy, 2002b). In order to take the size of a finite element into account, the statistics of the soil are adjusted by means of local average subdivision. Furthermore, the element size should be sufficiently small enough, relative to the scales of fluctuation, to prevent excessive local averaging of the soil property (Hicks and Onisiphorou, 2007).

Local Average Subdivision

Because most engineering properties are based on some average over a finite domain, for example the friction angle of a sand layer, Fenton and Vanmarcke (1990) introduced a method called Local Average Subdivision (LAS) which makes it possible to produce local averages over a distinct set of cells. Within a finite element model, the method also allows the resolution of the mesh to be changed easily in regions of interest.

By making use of a top-down approach, the construction of a one-dimensional local average process is shown in Figure 2.10. In stage 0 a normally distributed global average (Z_1^0) will be defined or the global mean of a process will be used if the global mean is known. For stage 1, the field is divided into two regions (Z_1^1 and Z_2^1) whose averages must preserve the parent value according to $Z_1^0 = \frac{1}{2}(Z_1^1 + Z_2^1)$ and the values must be appropriately correlated to each other. For the stages thereafter, another criterion that has to be met is that the two values, for example Z_1^2 and Z_2^2 , are correlated with the values derived from Z_1^1 , namely Z_3^2 and Z_4^2 .

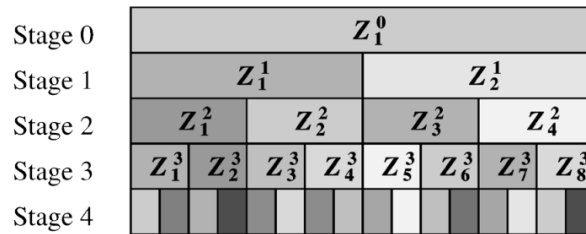


Figure 2.10: Construction of a 1D local average process, making use of a top-down approach (Fenton and Vanmarcke, 1990)

For the two-dimensional case, a rectangular domain is subdivided into four rectangles with an equal area for each stage. To three of the rectangles a random noise is added, while the value of fourth rectangle is determined by preserving upwards averaging of the four quadrants. Figure 2.11 shows the first three stages of the two-dimensional local average process, where the center of the local averages have been marked.

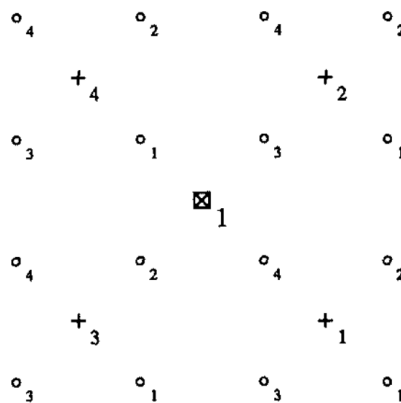


Figure 2.11: The first three stages of the 2D local average process, where Stage 0 covers the entire domain with center \boxtimes , at Stage 1 it is split into four quadrants with centers $+$ and at Stage 2 it is split into 16 quadrants with centers \circ (Fenton and Vanmarcke, 1990)

The advantages of the LAS algorithm are:

1. By using local averages the realisation can simply be conditioned.
2. The realisations are scale dependent and at any resolution they show to proper covariance between local averages.
3. The realisation can efficiently be used in finite element models, since each element property can be ascribed a local average.
4. Other methods show problems such as aliasing, which are avoided with the LAS method.

Covariance Matrix Decomposition

Another method to construct random fields is by covariance matrix decomposition, where the square root of the matrix of covariances is computed using Cholesky decomposition. It is a highly accurate method, because the generation takes all possible nodal correlation values into account (Fang and Tacher, 2003). However, due to the Cholesky decomposition and the storage size of the realisation, there is a limitation on the number of nodes.

The covariance matrix decomposition works as follows (Davis, 1987). The values of points in the random field, $\mathbf{X} = \{X_1, X_2, \dots, X_n\}^T$, can be simulated by

$$\mathbf{X} = \mathbf{L}\mathbf{w} \tag{2.18}$$

where w is a vector of n independent $N(0, 1)$ random variables, and L is the lower triangular matrix fulfilling $K = LL^T$ in which K is the matrix of covariances $\text{Cov}[X_i, X_j]$. The lower triangular matrix L can be referred to as the square root of the matrix of covariances, computed using Cholesky decomposition, mentioned before.

2.2.2. Monte Carlo Simulation

For every realisation of the Monte Carlo simulation, one of the generated random fields will be mapped onto the finite element mesh of the geotechnical problem for analysis in a finite element analysis, ensuring each element is assigned a different value of the property. When mapping the random field onto the FE mesh, the averaging of the value to the element should be accounted for in the method of generating the random field, such that the values are equal to the underlying continuous field (Hicks, 2014).

Figure 2.12 shows the results of four realisations of a slope failure in which random fields of the shear strength have been used with the same input statistics. The coloured lines indicate the shear strain invariants of the soil at failure.

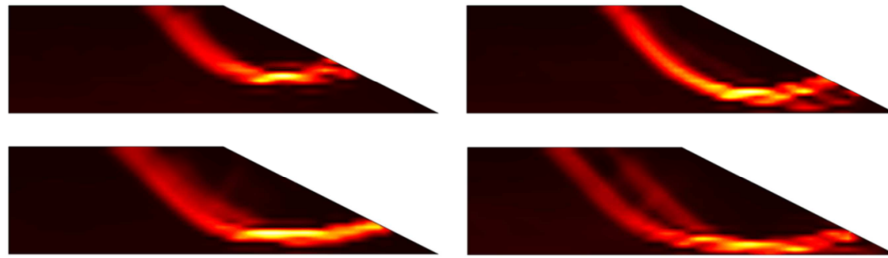


Figure 2.12: Four random fields based on the same input statistics produce different slope failure mechanisms (Hicks and Samy, 2002b)

When the Monte Carlo simulation reaches convergence of the results, the simulation is stopped. Due to the spatial averaging in the random fields, the number of realisations necessary to reach convergence with the RFEM is significantly less than for a probabilistic analysis that makes use of the probability density function of the soil parameter (Hicks, 2014).

2.3. Safety Analysis including Spatial Variability

In the post-analysis stage, the results of the Monte Carlo simulation are analysed by means of a probability density function of which the probability of failure is calculated from the area under the pdf. Another method to obtain the probability of failure is from a cumulative distribution function from which it can be seen directly (Hicks, 2014).

The results of a deterministic solution and a probabilistic solution of a 2D slope reliability problem are shown in Figure 2.13. The factor of safety is calculated by a strength reduction method, reducing the undrained shear strength in steps by dividing through the factor of safety F . Comparing the result of the deterministic solution, where the spatial variability is equal to zero, with the probabilistic results, it is seen that the spatial variability in the random fields leads to a range of solutions.

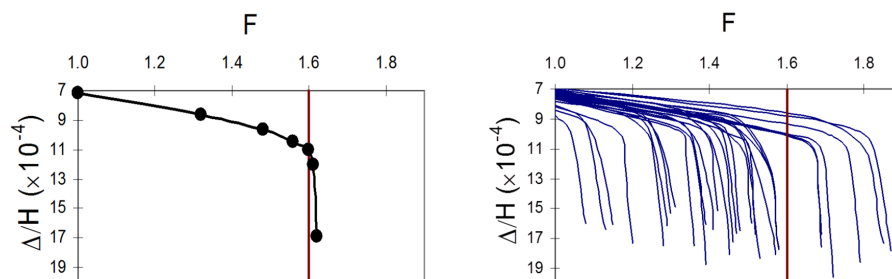


Figure 2.13: The results of a deterministic 2D slope reliability (left); and the results of a probabilistic 2D slope reliability (right); the analytical solution is shown by the red line (Hicks and Samy, 2002b)

The result of a Monte Carlo simulation is shown in Figure 2.14. For a reliability, which is defined as the probability that failure will not occur (Hicks, 2014), of 95% the safety factor F can be found where the cdf is equal to 0.05.

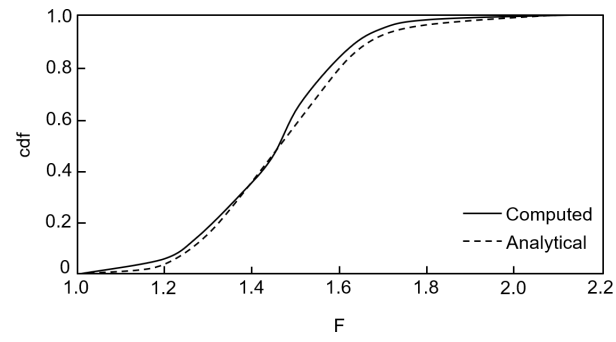


Figure 2.14: The cumulative distribution function of 600 realisations of a probabilistic two-dimensional slope reliability problem (Hicks and Samy, 2002b)

3

Correlations of Deformed Random Fields

A dyke imposes deformations to the soil in the proximity of the dyke. Figure 3.1 gives an overview of three deformations that occur along the circular slip failure of the dyke. At the centre of the slip circle a fourth deformation occurs, namely rotation. In order to investigate the effect of these deformations on the spatial correlations, random fields will be deformed according to these four deformations and the correlations will be analysed for every step of deformation. This will create a first insight into the change in spatial variability due to the deformations in the proximity of a dyke and will facilitate a comparison in the next chapters.

This chapter begins with the method by which the random fields are generated and deformed. It will then continue with the results of the change in spatial variability for the different deformations and conclude with a discussion of the results.

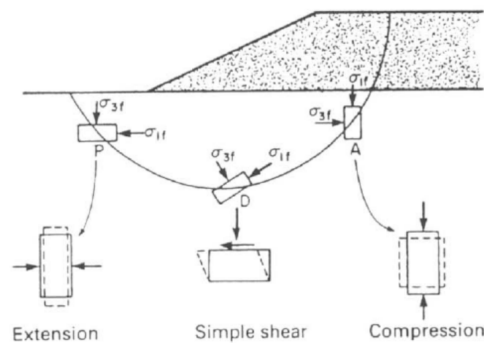


Figure 3.1: The different deformations that occur along a circular slip failure; Rotation occurs within the slip circle (Bjerrum, 1973)

3.1. Random Field Generation

Section 2.2.1 discussed two methods to generate random fields: the local average subdivision (LAS) and the covariance matrix decomposition. Since the latter results in more accurate results, the random fields are generated by making use of the covariance matrix decomposition and the random field generator of the Geotechnical Engineering department of the Delft University of Technology. The input statistics for the random fields are loosely based on the first results of the spatial variability in the field:

- Horizontal scale of fluctuation of 12.5 meters;
- Vertical scale of fluctuation of 0.5 meters;
- Normal distribution with a mean of zero and standard deviation of 1;
- Because this thesis is focussed on the Markov exponential, this is used for the kernel option;
- Horizontal and vertical mesh size of 0.1 meter, limited due to the covariance matrix decomposition method;
- Domain depth of 5 meters and domain width of 20 meters.

An example of such a random field is shown in Figure 3.2, where the random data should be interpreted as detrended q_t data.

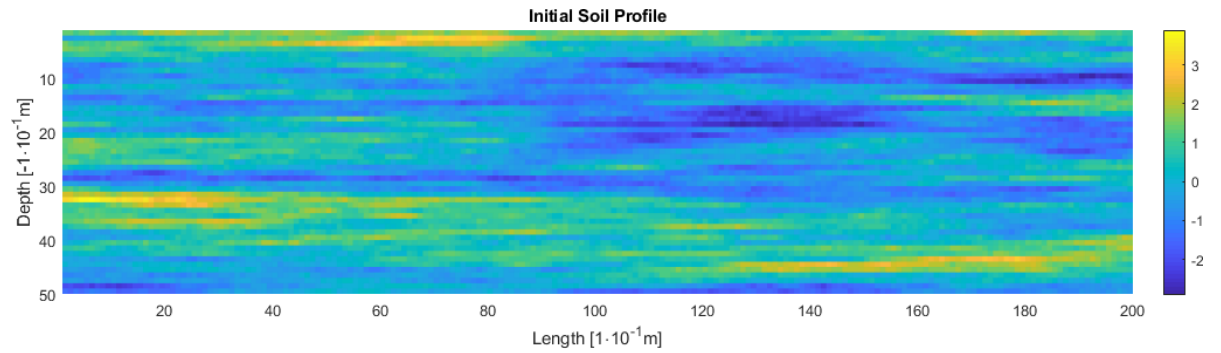


Figure 3.2: Example of a random field, with input $\theta_{hor} = 12.5m$ and $\theta_{ver} = 0.5m$, generated by covariance matrix decomposition

It is observed that the random field shown in Figure 3.2 is of low quality, because of the limitations of the Cholesky decomposition and of the storage limit. This can result in unwanted effects due to the interpolation methods of the deformations and lead to an increase of the interpolation error. Random fields with a higher resolution of 0.01m by 0.01m elements have therefore been generated by making use of the less memory intensive LAS method. An example of a high resolution random field is shown in Figure 3.3.

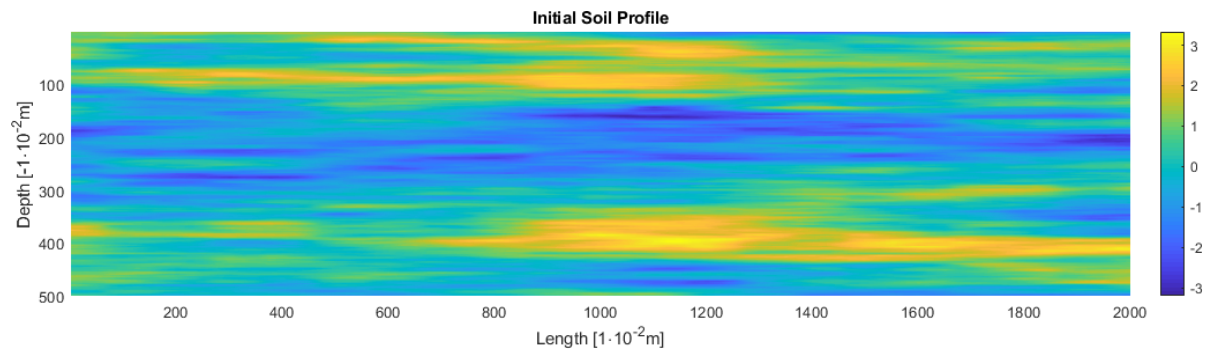


Figure 3.3: Example of a random field, with $\theta_{hor} = 12.5m$ and $\theta_{ver} = 0.5m$, generated by local average subdivision

In order to find the optimum element size through which the influence of the deformations on the spatial variability can be calculated most accurately, a comparison will be made between three different resolutions of random fields:

1. Using the low resolution random fields and sampling the data at every datapoint, so every 10cm.
2. Using the high resolution random fields and sampling the data every 10cm, to mimic the sampling of the low resolution random fields.
3. Using a low resolution interpolated version of the high resolution random fields, such that the mesh size becomes 0.1m by 0.1m, similar to the low resolution random fields, and sampling the data at every datapoint, so every 10cm.

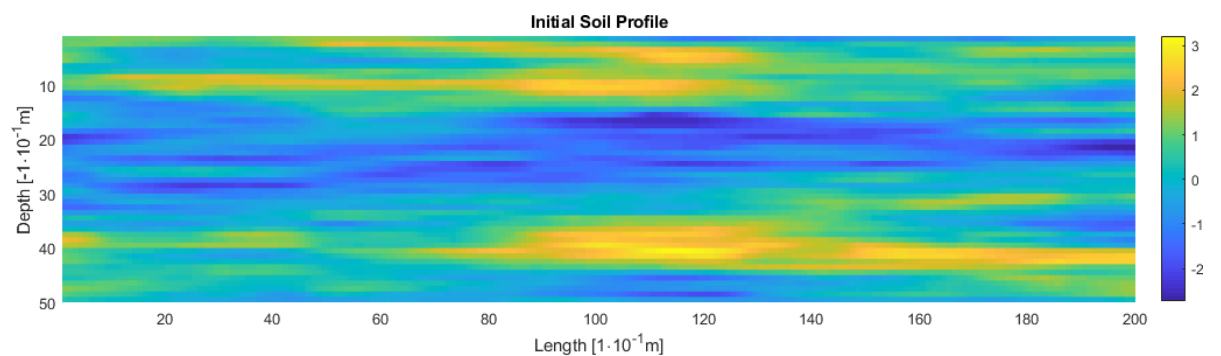


Figure 3.4: Example of the high resolution random field of Figure 3.3 transformed to a low resolution random field

The high resolution random fields will be transformed to low resolution random fields by means of bicubic interpolation. This interpolation method makes use of the nearest 4 by 4 neighbourhood of values to combine them into a single value by making use of weighting factors for each of the values according to their distance from the final cell. The results of transforming the high resolution random field of Figure 3.3 to a low resolution random field are shown in Figure 3.4. When applying a deformation to the transformed field, the random field will first be deformed and then be transformed to the low resolution version of the high resolution deformation to minimise the interpolation error of the deformation.

3.2. Random Field Deformation

The deformations are applied stepwise to the random fields by increasing the amount of compression or by increasing the angle. In total 145 low resolution and 145 high resolution random fields are generated and analysed. By using more than 100 random fields, the results will represent the input statistics accurately (de Gast et al., 2018b).

To compare the spatial variability before, during and at the end of the deformation, a so-called frame of reference is applied to every random field for each of the deformations, which is the section of the field in which the correlations are calculated. The frame of reference does not change during the deformation, but the random field within the frame changes according to the deformation. The deformations are pushed to the extreme, e.g. rotation until an angle of 45 degrees, in order to gain an understanding of the effect of different deformations.

The initial random field is used as input for every single step of the deformations. This prevents the accumulation of interpolation errors that could occur when continuing on the previous deformation step with the next.

3.2.1. Vertical Compression of the Random Fields

Due to the overburden pressure of the dyke, the soil consolidates vertically. To investigate the changes in the correlations due to this consolidation, the random fields are compressed vertically to half the vertical domain, which is 2.5 meters, over the complete width. The frame of reference is set to the bottom half of the complete random field domain.

The vertical compression is achieved by the Matlab function `imresize` with bicubic interpolation. The vertical compression is one-dimensional, so only the top is pressed downwards. Figure 3.5 shows one step of the vertical compression of a random field.

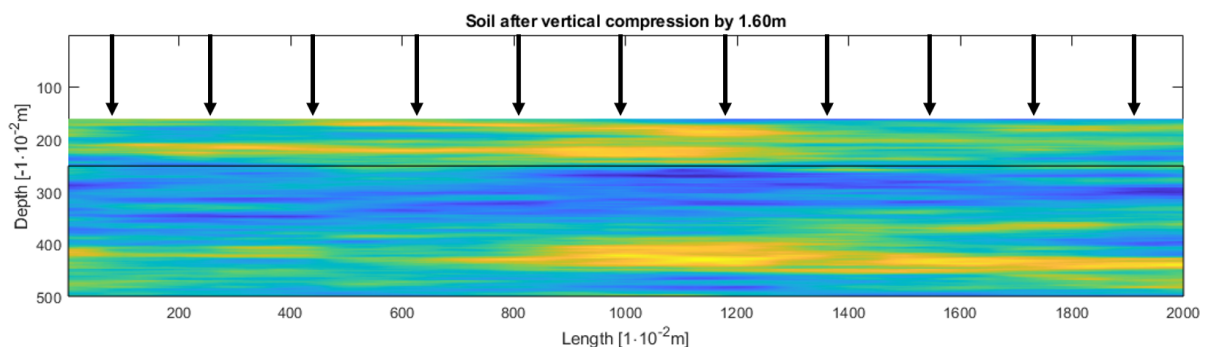


Figure 3.5: The high resolution random field after vertical compression by 1.60m with the frame of reference indicated by the black square

3.2.2. Horizontal Compression of the Random Fields

Horizontal compression of the soil can occur due to macro-instability of the dyke, which causes the soil body to rotate over a slip surface. In between the first part of the rotation where soil moves downwards, mostly underneath the dyke due to the overburden pressures, and the second part where the soil moves upwards due to lack of overburden pressure, the horizontal compression of a soil can take place. To investigate the change in spatial variability due to horizontal compression, the random fields are compressed until 5.00 meters, that is 25% of the domain width, over the complete height of the domain.

Similar to vertical compression, the Matlab function `imresize` is used with bicubic interpolation to com-

press the random field. The compression occurs one-dimensional, pressing the left side of the random fields to the right. Figure 3.6 shows one step of the horizontal compression of a random field.

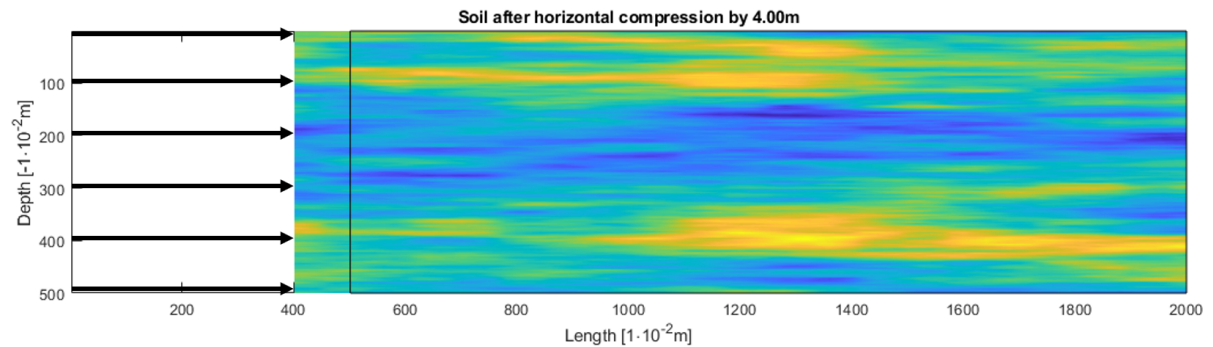


Figure 3.6: The high resolution random field after horizontal compression by 4.00m with the frame of reference indicated by the black square

3.2.3. Simple Shear of the Random Fields

Simple shear is a deformation found at the horizontal shear zone underneath a dyke and soil is commonly tested for its shear strength by means of a direct simple shear test. Since simple shear deformation could have occurred at the Leendert de Boerspolder, its influence on the spatial variability is tested as well.

The Matlab function `imwarp` is used to apply the simple shear deformation to the random fields. This function makes use of another function called `affine2d`, which describes a geometric transformation, with no transformation corresponding to the matrix $\begin{bmatrix} 1 & 0 & 0 \\ a & 1 & 0 \\ 0 & 0 & 1 \end{bmatrix}$ if $a = 0$. In order to apply simple shear to the matrix, the value of a will be increased in 46 steps from 0 to -1, where the latter corresponds to an angle of 45 degrees, such that each step is equal to an angle of one degree. Since the simple shear deformation pushes the horizontal layers of the random field to the right, the interpolation method is chosen to be linear interpolation. Figure 3.7 shows one step of the simple shear of a random field.

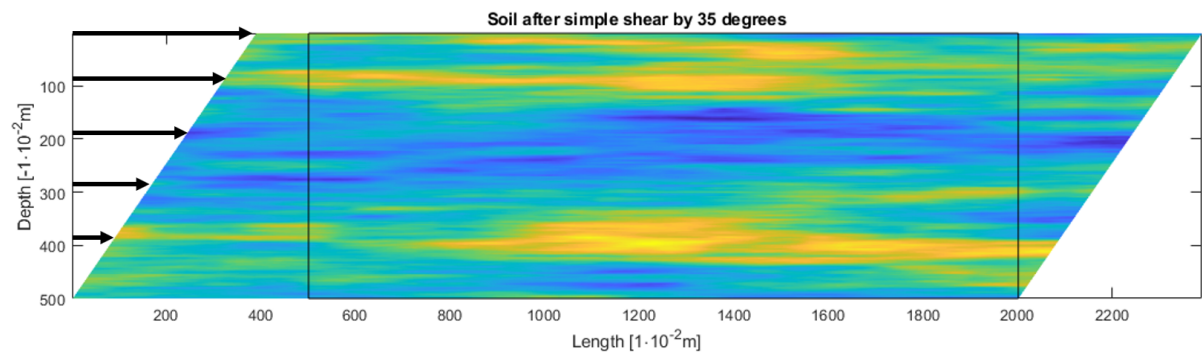


Figure 3.7: The high resolution random field after simple shear by 35 degrees with the frame of reference indicated by the black square

3.2.4. Rotation of the Random Fields

Macro-instability is characterised by a failure circle rotating away from the dyke. In order to investigate the effect of rotation on the spatial variability, the entire random field is rotated counter-clockwise and the spatial variability is analysed in the frame of reference shown in Figure 3.8. This frame is relatively small in comparison to the complete domain, but at a rotation of 45 degrees this is the largest frame that is possible to include soil data at all elements.

The rotation is done by using the `imrotate` Matlab function, rotating the random field around its centre. The interpolation method used is the nearest-neighbour interpolation which, as the name suggests, uses only the value of the nearest cell to determine the value of a cell. This method does not change the value of the initial cells and only changes their location. One step of the rotation of an entire random field is shown in Figure 3.8.

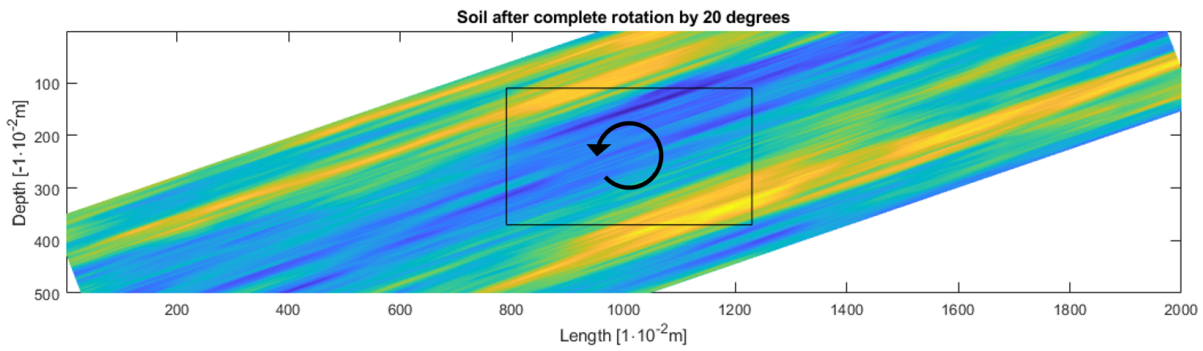


Figure 3.8: The high resolution random field after rotation by 20 degrees with the frame of reference indicated by the black square

3.3. Observations on Spatial Variability when Deforming Random Fields

This section will show the results of the change in spatial variability when deforming random fields. First, an insight will be given into two comparisons that can be made: one to the input spatial variability and one to the domain spatial variability. After this, the results of the different deformations for the different resolutions of random fields will be shown.

3.3.1. A Comparison between the Input or Domain Spatial Variability

The results of the spatial variability for the deformations of the different resolutions of random fields can be normalised to simplify the comparison. The normalisation is done by either comparing the results to the input statistics, which were $\theta_h = 12.50m$ and $\theta_v = 0.50m$, or to the calculated spatial variability of each of the random fields when no deformations have been applied yet.

As an example the results of the vertical compression of the high resolution random fields are used. The spatial variability is calculated after every deformation step for each of the random fields and the resulting spatial variability is plotted against the deformation steps. Boxplots are used in order to improve the readability of the large amount of results and then the least squares and Theil-Sen estimators are fitted to the data to discover a trend and the change in spatial variability after all deformations are made. Figure 3.9 shows an example of the results of the change in vertical scale of fluctuation due to vertical compression when normalising the results to the input statistics.

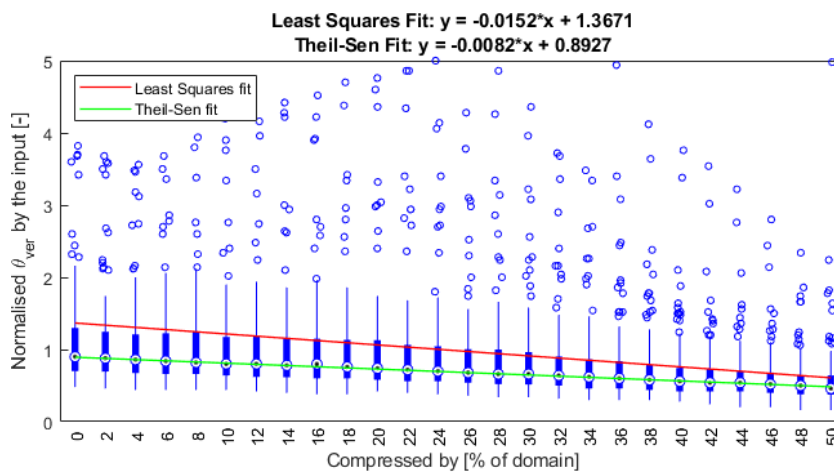


Figure 3.9: Change in θ_v due to vertical compression, normalised with the spatial variability of the input ($\theta_v(\cdot)/0.50m$)

For each of the random fields, the calculated vertical scales of fluctuation can also be normalised with the θ_v initially calculated before any deformation was applied to the random field. At no deformation, the results will always be equal to one, as shown in the example of Figure 3.10.

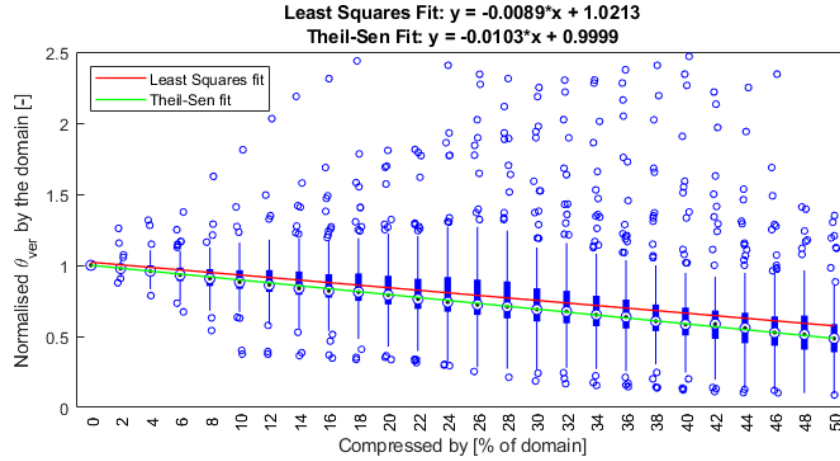


Figure 3.10: Change in θ_v due to vertical compression, normalised with the spatial variability of the domain ($\theta_v(\cdot)/\theta_v(1)$)

3.3.2. Results of the Change in Spatial Variability for Different Resolutions of RFs

The deformations shown in Section 3.2 have been applied to the different resolutions of random fields shown in Section 3.1. All results for both normalisation methods discussed before will be given in this section. From the results it became clear that the vertical compression, horizontal compression and simple shear caused linear changes in the spatial variability, but rotating the random fields did not cause a linear change. Therefore, the results of the linear changes will be shown first, and the rotation will be treated separately.

Linear Changes in Spatial Variability

Section 2.1.2 of the literature study showed that the Theil-Sen estimator is a robust estimator that is not influenced by outliers as much as the least squares estimator. It was found that for the linear change in spatial variability this holds true, as can be seen from Figures 3.9 and 3.10. Therefore, to reduce bias by the outliers, the change in spatial variability will be calculated from the results of the Theil-Sen estimator. The results are summarised in Table 3.1 for each of the different resolutions of random fields. The complete results can be found in Appendix B.

Table 3.1: Summary of the change in spatial variability when deforming random fields, according to the Theil-Sen estimator

Low Resolution	$\Delta\theta_{h,domain}$	$\Delta\theta_{v,domain}$	$\Delta\theta_{h,input}$	$\Delta\theta_{v,input}$
Vertical compression	+13.1%	-38.0%	+22.0%	-33.6%
Horizontal compression	-24.7%	0%	-24.5%	0%
Simple shear	-4.1%	0%	-3.8%	0%
High Resolution	$\Delta\theta_{h,domain}$	$\Delta\theta_{v,domain}$	$\Delta\theta_{h,input}$	$\Delta\theta_{v,input}$
Vertical compression	-5.3%	-51.4%	-2.6%	-45.8%
Horizontal compression	-24.2%	0%	-23.0%	0%
Simple shear	-1.8%	0%	-2.6%	0%
High to Low Resolution	$\Delta\theta_{h,domain}$	$\Delta\theta_{v,domain}$	$\Delta\theta_{h,input}$	$\Delta\theta_{v,input}$
Vertical compression	+2.3%	-40.4%	+6.9%	-34.2%
Horizontal compression	-24.9%	0%	-23.8%	0%
Simple shear	-2.7%	0%	-3.0%	0%

Changes in Spatial Variability due to Rotation

The results of the change in spatial variability due to rotation of the random fields, shown in Figure 3.12, could not be fitted by a linear trend or other common estimators. It was found that the horizontal and vertical scales of fluctuation of the high resolution random field, normalised to the domain, change according to the rotation of an ellipse with a width of $2 \cdot \theta_h$ and a height of $2 \cdot \theta_v$. A visualisation of the ellipsoid is given in Figure 3.11.

The formula for the rotation of an ellipsoid, with the width and height as scales of fluctuation, is

$$\frac{(x \cdot \cos \alpha - y \cdot \sin \alpha)^2}{\theta_h^2} + \frac{(x \cdot \sin \alpha + y \cdot \cos \alpha)^2}{\theta_v^2} = 1 \quad (3.1)$$

where α is the angle of rotation in radians. The results of Formula 3.1 fit the data accurately when ignoring the outliers, and result in a change in scales of fluctuation of $\Delta\theta_{h,domain} = -94.34\%$ and $\Delta\theta_{v,domain} = +41.40\%$. When the random fields are rotated by 45 degrees, the horizontal scale of fluctuation has become equal to the vertical scale of fluctuation.



Figure 3.11: The spatial variability with $\theta_h = 12.5m$ and $\theta_v = 0.5m$ visualised as an ellipse

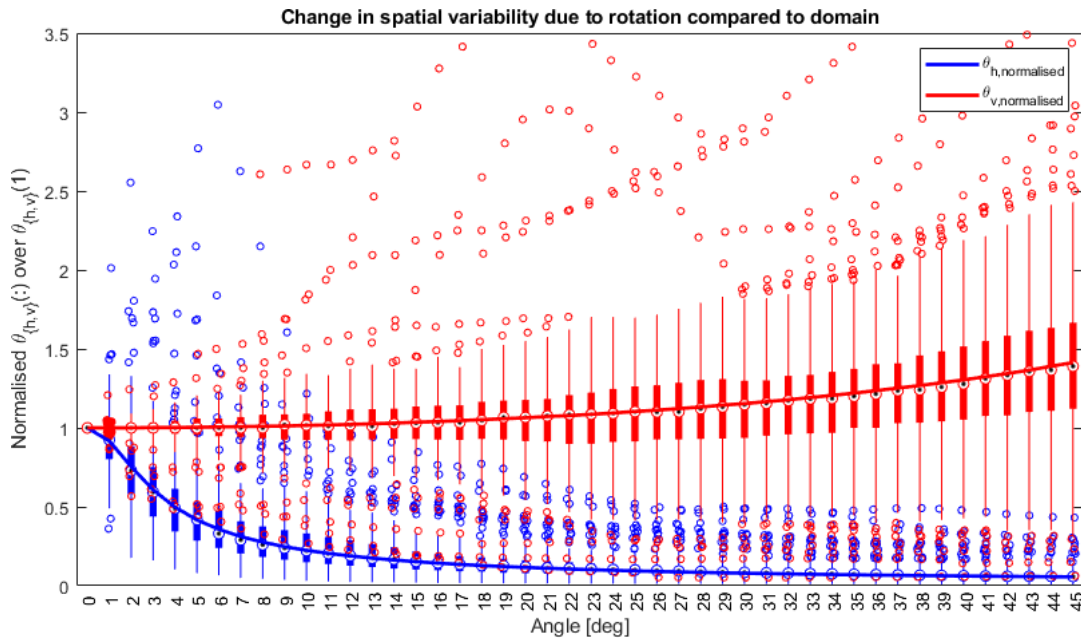


Figure 3.12: Change in spatial variability due to rotation of high resolution random fields, normalised with the spatial variability of the domain ($\theta_{h,v}(\cdot)/\theta_{h,v}(1)$), fitted with the formula for rotation of an ellipsoid

3.4. Discussion

The results of the change in correlation when deforming random fields will be discussed in this section. The limitations of the method applied in this research are discussed first. Then, a comparison between the results normalised to the domain or to the input is made. This discussion will conclude with a comparison of the results of the different resolutions of random fields.

Limitations of this research

The random fields generated in this research were not assigned soil properties before the fields were deformed. Therefore, this research is essentially deforming pictures and calculating the changing horizontal and vertical scales of fluctuation of the deformed pictures. It can be expected that the results of a compression of 50% in either the horizontal or vertical direction will result in a decrease of the correlation length in that direction of 50%. In case actual soil properties would have been assigned to the random fields, different deformations would occur at different locations. For example, at an equal stress, the areas with a larger stiffness would show less strain than the areas with a lower stiffness.

Therefore, the results of this research should not be used quantitatively, but the results can be used for future research. By using the mesh size that resulted in the best approximation of the scales of fluctuation,

mistakes in future random field generation can be prevented. The results can also be used qualitatively as a first estimate of the kind of change in spatial variability that occurs for different deformations.

Change normalised to the domain or input spatial variability

Even though the random fields are generated with the input statistics equal to $\theta_h = 12.50m$ and $\theta_v = 0.50m$, the initial spatial variability of each random field could be different. This research used 145 random fields to make sure that the average random field has a spatial variability equal to the input statistics. However, calculating the results normalised to the domain or normalised to the input spatial variability gave different results, as was shown in Table 3.1.

This research investigated the change in spatial variability due to deformations of random fields. It was not the goal to investigate the amount of random fields that were necessary to calculate an initial spatial variability equal to the input statistics for the average random field. Therefore, the best option is to normalise the change in spatial variability to the initial domain spatial variability, as this will result in the relative change for every random field and only depend on the deformation that was applied to the random fields.

The difference in results between the change normalised to the domain or to the input spatial variability could be explained by the amount of outliers found when normalising to the input. It was found that the amount and magnitude of the outliers was much larger when normalising to the input spatial variability. As discussed in Section 2.1.3, the breakdown point of the median is equal to 0.5, meaning that if more than 50% of the data is contaminated, the resulting median is biased. Possibly the results of the spatial variability normalised to the input statistics contained slightly more than 50% contaminated results, explaining the difference between the Theil-Sen estimators for both normalisation methods.

The different resolution random fields

Three different resolution random fields have been analysed. The first set was made up of low resolution random field with elements of 0.1m by 0.1m, the second was made up of high resolution random fields with an element size of 0.01m by 0.01m and the third set was made up of random fields with an element size of 0.1m by 0.1m, interpolated from the high resolution random fields. A comparison of the different resolutions will be made, after which this discussion will conclude with the most accurate random field resolution.

The first method by which the resolutions can be compared is by investigating the generation of the random fields and the interpolation errors. The low resolution random fields were generated by using covariance matrix decomposition, and the high resolution random fields were generated by local average subdivision. Both methods were discussed in Section 2.2.1 and it was discussed that the covariance matrix decomposition is a highly accurate method, but it is limited in the number of nodes it can generate, hence the low resolution of the random fields when generating a relatively large random field domain. When deforming these low resolution random fields, interpolation between the elements will occur, causing an interpolation error. This interpolation is less of an issue for the high resolution random fields, since, compared to the low resolution random fields, 9 additional data points are known in between the 10 centimetre data points. The transformed random fields are transformed from high to low resolution after the deformation had been applied to the random field, so the interpolation error due to deformations is equal to that of the high resolution random fields. However, the resulting correlations will be less accurate, because the data points used to calculate the autocorrelation function are based on interpolated sampling points. It is concluded that the high resolution random fields result in the lowest interpolation error and are therefore best suited to calculate the change in spatial variability.

Since a certain amount of compression of the random fields should approximately result in an equal change in spatial variability, it can be investigated whether the high resolution random fields actually outperform the other resolution random fields. Since it was discussed that this research is essentially deforming pictures, it is expected that a horizontal compression of 25% results in a change in horizontal scale of fluctuation of -25%. For the vertical compression of 50% a change in vertical scale of fluctuation of -50% is expected and for the simple shear, which is essentially a horizontal displacement, little to no change in the spatial variability is expected. The high resolution random fields approximately confirm these expectations, but for the horizontal compression the transformed random fields outperform the high resolution random fields.

The qualitative changes in spatial variability due to deformations

Since the change in spatial variability normalised to the domain is best predicted by the high resolution random fields, these results will be used for the changes in spatial variability due to deformations.

Due to vertical compression of random fields, a decrease in both the horizontal and vertical scales of fluctuation is found. The decrease of the horizontal correlation length is approximately 10% of the decrease

of the vertical correlation length. The low resolution and transformed random fields resulted in an increase of the horizontal correlation length, so the results of the horizontal change should be used with caution. The decrease in vertical correlation length is confirmed by the low resolution and transformed random fields.

The horizontal compression showed a decrease of the horizontal scale of fluctuation and no change of the vertical scale of fluctuation. The other resolutions confirm these findings.

Deforming random fields by simple shear shows a slight decrease in the horizontal correlation length and no change of the vertical correlation length. All resolution random fields confirm these findings, but the amount by which the horizontal correlations change is small enough that it could be possible that no change in the spatial variability occurs due to simple shear.

Rotation of random fields resulted in a change in spatial variability that could be estimated by the rotation of an ellipse. The general findings were that the horizontal scale of fluctuation decreases and the vertical scale of fluctuation increases, to eventually become equal to each other at 45 degrees rotation.

4

Spatial Variability of the Leendert de Boerspolder

Research by de Gast et al. (2017) hypothesised that under influence of a man-made structure, such as a dyke, the spatial variability of soft soils in the proximity of the man-made structure is changed. This chapter will test this hypothesis by investigating the one-hundred cone penetration tests of the Leendert de Boerspolder. Before the scales of fluctuation can be estimated, the soil layers that are present in the polder have to be determined. Subsequently, the outliers will be removed as well as the depth trend. Afterwards the spatial variability can be estimated. The chapter concludes with the results and discussion of those results.

4.1. Soil Layers of the Leendert de Boerspolder

In order to meet the requirements for stationary data, explained in Section 2.1.2, the soil layers of the Leendert de Boerspolder will have to be identified. For each of the soil layers it is then possible to calculate the scales of fluctuation. By making use of the following methods, the soil layering will be identified:

1. Sleeve friction (f_s) versus corrected cone resistance (q_t)
2. Friction ratio (R_f) versus corrected cone resistance (q_t)
3. Normalised soil behaviour type index (I_c)
4. Non-normalised soil behaviour type index (I_{SBT})

4.1.1. Disturbed and Unsaturated Top Layer

Before starting the soil layer analysis, the observation is made that the top layer of the soil has been disturbed and is in an unsaturated state. In the plot of the pore water pressure over the depth, shown in Figure 4.1, the unsaturated state of the top layer can be clearly seen in the soil layer until -2.75 m+NAP by the negative pore water pressures. The disturbance is likely caused by the agricultural activity that took place over the years in which this area was a polder and the unsaturated state is caused by the poldering of the Leendert de Boerspolder. Due to the disturbed and unsaturated state, the top layer of the soil will be identified for every soil investigation and then be excluded from the analysis, even if this is not mentioned specifically.

4.1.2. Analysis using the Sleeve Friction

A first indication of the different soil layers can be obtained by plotting the sleeve friction and the corrected cone resistance in one figure, as shown in Figure 4.2. The sleeve friction of organic soils is higher than the sleeve friction of clay, even though the corrected cone resistance can seem quite similar. Applying this to the measurements of CPT 1, shown in Figure 4.2, the following layers can be distinguished:

1. Below the top layer a sleeve friction of approximately 0.01 MPa is measured, from approximately -2.75 m+NAP to -4.50 m+NAP, indicating a peat layer;
2. From approximately -4.50 m+NAP to -11.00 m+NAP the sleeve friction is lower than the peat layer and increases with depth, indicating a clay layer;
3. Between -5.50 m+NAP and -7.00 m+NAP an increase in sleeve friction could indicate an organic clay;
4. From approximately -11.00 m+NAP to -11.90 m+NAP a high sleeve friction is measured, indicating a second peat layer;

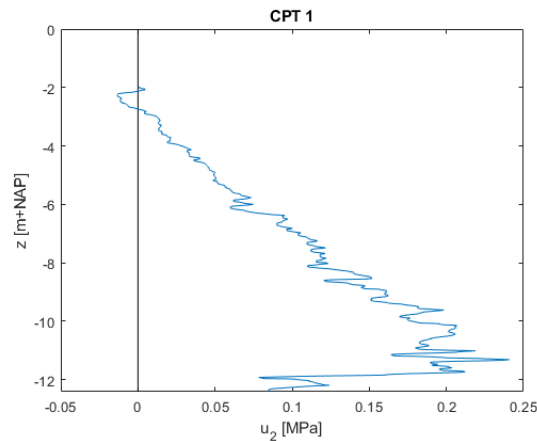


Figure 4.1: The pore water pressure plotted over the depth for the first CPT

5. Deeper than -11.90 m+NAP the corrected cone resistance increases, indicating a sand layer. Since the cone penetration tests are made in close proximity, it is expected that the layers described here will be found at the other locations as well.

4.1.3. Analysis using the Friction Ratio

Another method to identify the soil layers is by combining the sleeve friction and the cone resistance measurements in the friction ratio. The friction ratio is defined as the ratio of the sleeve friction and the cone resistance and gives a clear indication of the soil layers. Typical measurement values of the friction ratio for sands are 1% to 2%, for clays the ratio is approximately 5% and for peat higher values of approximately 8% to 10% are measured (Verruijt, 2012). Applying this to the measurements of CPT 1, shown in Figure 4.3, the same layers as found with the sleeve friction can be identified:

1. Underneath the top layer a friction ratio above 6% is measured, indicating a peat layer until approximately -4.50 m+NAP;
2. From approximately -4.50 m+NAP to -11.00 m+NAP the friction ratio remains more or less constant at 3%, which applies to a clay layer.
3. Between -5.8 m+NAP and -6.2 m+NAP the increase in the friction ratio could indicate an organic clay;
4. From approximately -11.00 m+NAP to -11.90 m+NAP the friction ratio increases to 6% indicating a second peat layer;
5. Continuing below -11.90 m+NAP a sand layer is encountered, indicated by a friction ratio of 1%.

4.1.4. Analysis using the Robertson's Soil Behaviour Types

The final two methods to verify the soil layers found from the previous methods are the normalised and non-normalised soil behaviour type indices, I_c and I_{SBT} respectively. By plotting these indices against the depth and using the values for the contour lines shown in Figure 2.3 the different soil layers can be identified. These indices have been calculated for the one hundred cone penetration tests available according to Formulae 2.5 and 2.6. An example of both I_c and I_{SBT} of the first CPT is shown in Figures 4.4 and 4.5 respectively.

The non-normalised and the normalised indices do not indicate the same soil type. As mentioned in Section 2.1.1, the normalised parameters allow for a more reliable analysis of the soil layers. Therefore the normalised soil behaviour type index will be used for the analysis. It should be mentioned that if the effective in-situ stresses are within the range of 50 to 150 kPa, the non-normalised parameters should result in a similarly accurate analysis. This can be seen in Figures 4.4 and 4.5 in which the results for CPT 1 are given as example. Below a depth of -11.65 m+NAP the effective in-situ stresses are higher than 50 kPa. As seen from the two graphs, the results below that depth are very similar, but the results above that depth are different. Therefore, the non-normalised index cannot be used for an accurate analysis of the soil layers. The results of the normalised soil behaviour type index (I_c) will be discussed in more detail.

By making use of the soil behaviour type graph in Figure 2.3, the following layers can be distinguished.

1. A layer of peat and organic clay is found between -2.7 and -4.5 m+NAP as seen by a value of I_c in the second zone;

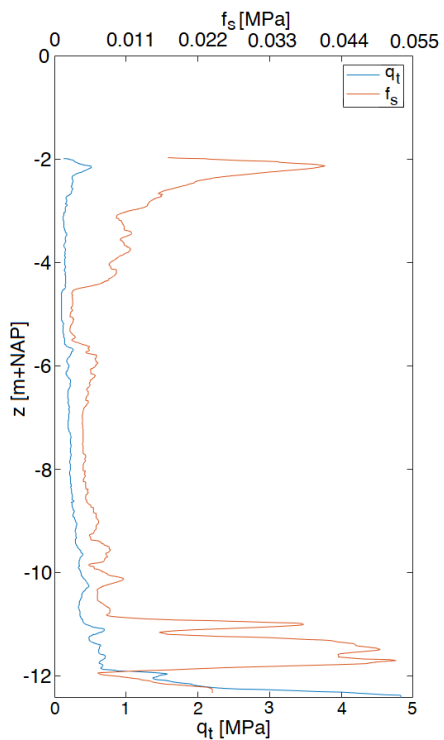


Figure 4.2: The sleeve friction and corrected cone resistance plotted over the depth for CPT 1

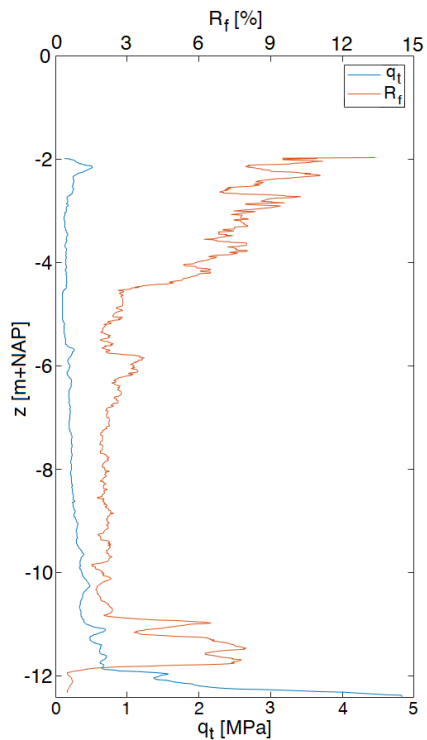


Figure 4.3: The friction ratio and corrected cone resistance plotted over the depth for CPT 1

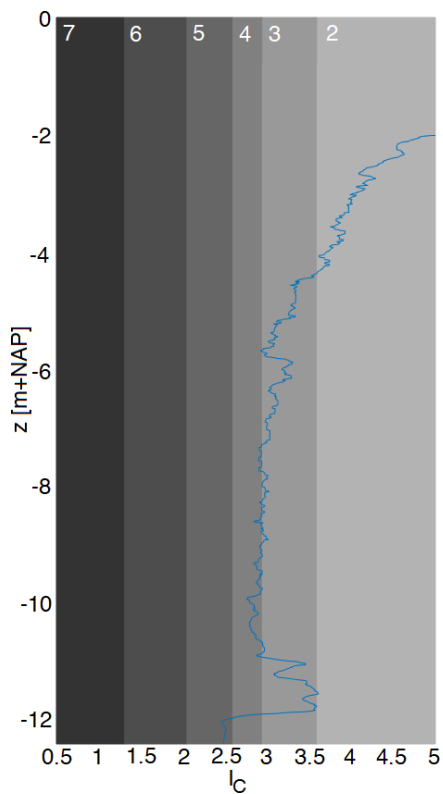


Figure 4.4: Normalised Robertson soil behaviour type over the depth for CPT 1

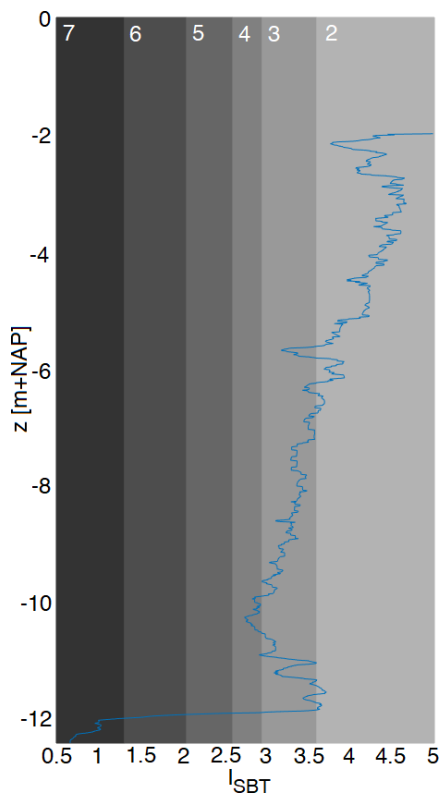


Figure 4.5: Non-normalised Robertson soil behaviour type over the depth for CPT 1

2. Around -4.5 m+NAP there is a drop in the value to the third zone, indicating that clay can be expected from there on down;
3. Around -6.0 m+NAP an increase in the normalised soil behaviour type index is seen, similar to the increase in cone resistance, sleeve friction and friction ratio around that depth. But even though the value increases, the soil type is still clay;
4. Deeper into the ground, it is seen that the I_c value begins to fluctuate around the border of zones 3 and 4, indicating a more silty clay;
5. At -10.0 and -10.5 m+NAP there are two small layers where it is possible that a clayey silt is located;
6. Finally the index value increases almost to an organic soil in between -11.0 and -11.9 m+NAP before continuing to the sandy zone.

4.1.5. Soil Layers of the Leendert de Boerspolder

From the three methods from which the soil layering could be determined, it is discovered that each method makes a similar prediction of the underground. Since the cone penetration tests have been made in close proximity to one another, it is expected that the layers discovered in the first CPT will be found in the other tests as well. The main goal is to find the depth at which the first and second peat layers and the clay layer in between are located, because these layers are large enough to determine their spatial variability. Since the sleeve friction measurements show a clear transition between these different layers and repeating patterns between CPTs, the sleeve friction will be used to identify the layering for every CPT.

Using the sleeve friction for the determination of the soil layers, every CPT has been analysed in order to define the different soil layers that are present at the Leendert de Boerspolder. This has been done by plotting the sleeve friction of multiple CPTs in one plot and comparing the plots, as shown in Figure 4.6.

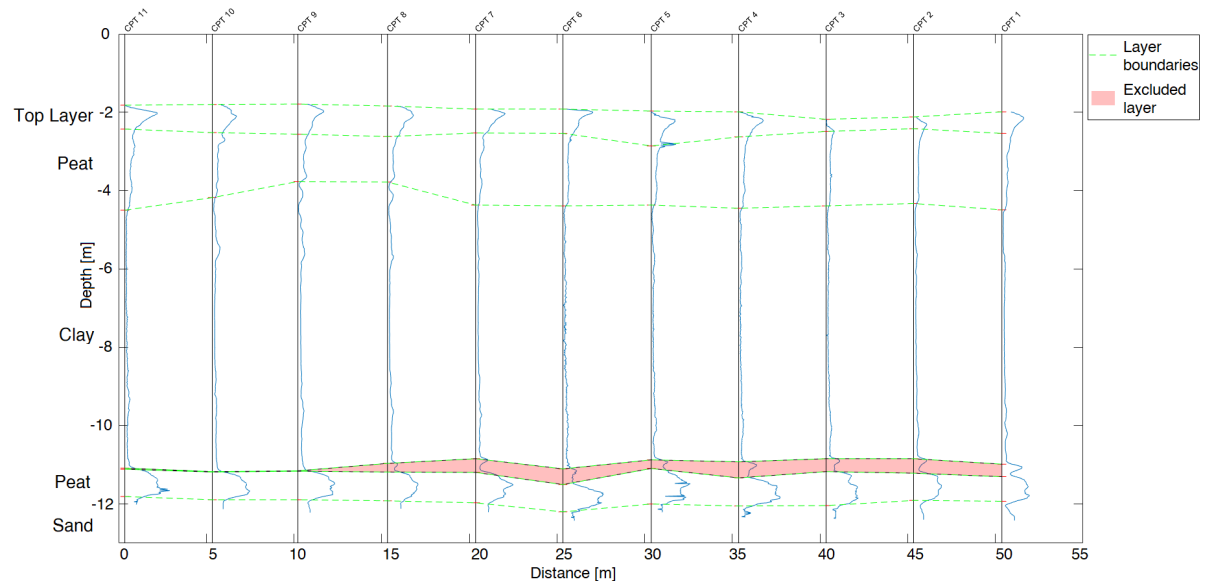


Figure 4.6: Analysis of the first line of CPTs, located in the polder, furthest away from the dyke

The features that define the layer boundaries are based on patterns such as the patterns defined in Section 4.1.2. An example of the results of the following patterns is shown in Figure 4.6 for the first line of CPTs.

- Boundary between top layer and first peat layer: After the first peak of the sleeve friction, where $f_s < 0.02\text{MPa}$;
- Boundary between first peat layer and clay layer: Where $f_s < 0.006\text{MPa}$ for the first time;
- Boundary between clay layer and second peat layer: Where $f_s > 0.017\text{MPa}$ for the first time;
- Boundary between second peat layer and sand layer: Where $f_s < 0.026\text{MPa}$ for the first time;
- Two small layers can be found between the clay and the second peat layer. The first is a peat layer and the second a clay layer, but since these layers are too small to be analysed for their correlations, these are excluded from the analyses in this thesis.

4.1.6. Layer Boundaries

Currently the layers are separated by a *meet-in-the-middle* method, which means that the layer separation has been chosen halfway through the transition between layers. However, in order to find the correlations specific to one soil layer, the data cannot be polluted by measurements from the other layers. This is achieved by applying a certain margin to the boundaries to exclude data points which are in the transition zone. The margin is set to 10 centimetres from both sides of the meet-in-the-middle line to create an exclusion zone of 20 centimetres. Figure 4.7 shows the result of the soil layers with margins for the first line of cone penetration tests. The layer depths at every CPT location are included in Appendix C.

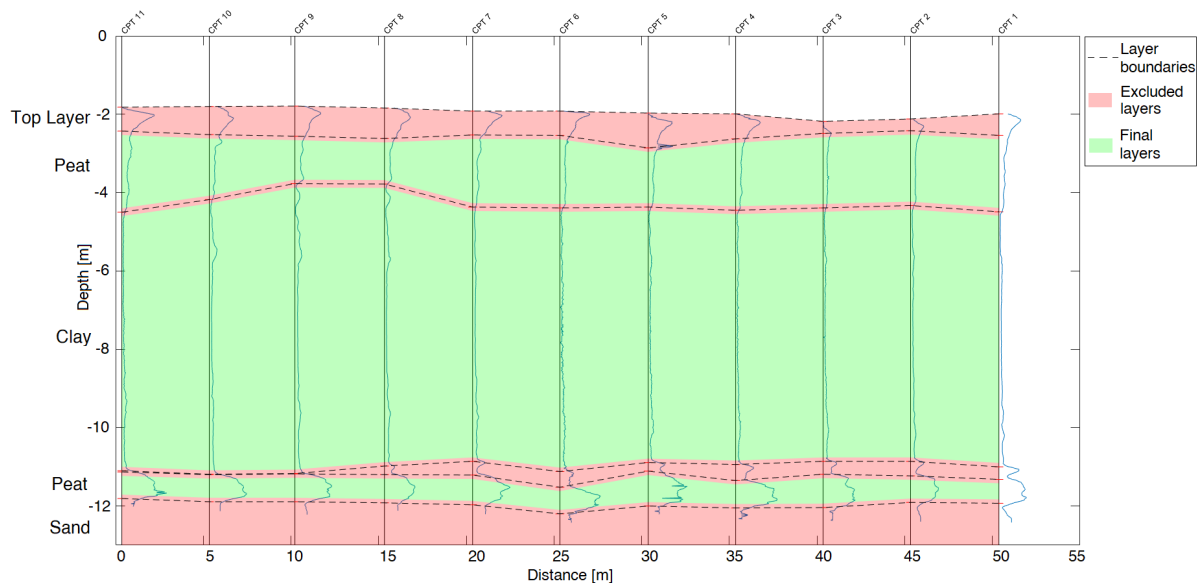


Figure 4.7: Soil layers indentified at the first line of CPTs by making use of the sleeve friction and margins

4.1.7. Deviations and Abnormalities

While most of the CPTs follow the defined soil layer boundaries, some deviations and abnormalities are observed and discussed in this section.

Drainage Canal

On the aerial photos shown in Figure A.2, it can be seen that canals are present in the polder. Even though the cone penetration tests have been aligned in such a way that the least amount of tests were performed in the canal, CPT 13 had to be taken in a drainage canal. This can be seen in the cross-section of figure C.3 by the dipping ground level at that location. From the sleeve friction it is clear that there is little to no top layer of soil, especially when taking the margin of the layers into account. At CPT 13 the first soil layer encountered is the top peat layer.

Dyke Material

Due to the dyke, the ground level increases from approximately -2.0 m+NAP in the polder to approximately -1.3 m+NAP for the CPTs taken in the slope of the dyke (line 6) and finally to approximately -0.4 m+NAP at the dyke crest (line 7). It is noted from Figure C.8 that the first layer of peat and the layer of clay have been compressed under influence of the dyke, but the second layer of peat seems to be less influenced as its top and bottom are located at the same depth under the dyke as in the polder.

Regarding CPT line 7, shown in Figure C.7, the compression of the first peat layer seems to be larger at certain locations. It is expected that this happened due to the dyke material that has been deposited on top, which likely consists of soil with different local densities and might even contain debris. This causes differences in the overburden pressure of the dyke on the soil layers underneath it, explaining the differential settlements. At the surface of the dyke the locations that settled faster than other locations have probably been refilled with additional material to maintain an even surface of the dyke.

Because this thesis focusses on the influence of the dyke on the correlations of the soft soils underneath, the spatial variability of the dyke material will not be analysed.

4.2. Removing the Depth Trends

In order to retrieve the spatial variability of the Leendert de Boerspolder from the soil data, the trend of the cone resistance data has to be removed for every soil layer. This section will show the necessary steps to remove the trend of the soil data and conclude with the resulting trends.

4.2.1. Groups of CPTs

Removing the depth trend of the cone penetration test data has to be performed on each of the one hundred CPTs. However, removing the trend of each of the cone penetration tests individually could cause the wrong trend to be identified and therefore cause part of the fluctuation of the data to be removed as well. Since the fluctuation is the part that is necessary for a proper analysis of the correlations, the solution is to select groups of CPTs which have experienced a similar stress history and identify a trend for all of the cone resistance data, such that the average trend of those measurements will be removed.

One way of combining the cone penetration tests with a similar stress history is by dividing them into CPTs taken in the polder, in the slope of the dyke and in the dyke crest. Within these groups, the soil has experienced a similar overburden pressure, which makes it likely that a combined trend can be found for the CPTs in those groups. However, due to the overburden pressure of the dyke, additional settlements near the toe of the dyke could have occurred. Therefore the choice is made to add an additional group at this location.

The overburden pressure of the dyke is not only responsible for the consolidation of the soil underneath it, there is a possibility that a small amount of macro instability occurred. Macro instability is defined as the sliding of the soil body of the dyke along a slip surface. Stability is obtained from the resistance against sliding along the slip surface. Figure 3.1 shows an example of such a slip circle. In order to take macro instability into account when creating groups of CPTs with similar stress history, it is necessary to group the CPTs as parallel lines to the dyke, since macro instability is a process that occurs perpendicular to the dyke. It is assumed that if a small macro instability occurred at the Leendert de Boerspolder, it occurred over the complete length of the dyke, therefore creating zones parallel to the dyke that show an equal amount of rotation.

In order to obtain groups of cone penetration tests with exactly the same stress history, the groups of CPTs have been chosen to be equal to the lines of CPTs presented in Figure 1.5 and the trend of the soil layers will be identified for each of the seven lines of CPTs.

CPTs between the Lines

The cone penetration tests 88, 89, 91, 92 and 94 are not located on any of the seven lines of CPTs, but are situated halfway in between lines. Because the other CPTs will have their trend removed according to the lines parallel to the dyke, the solution for the CPTs in between is to remove the average trend of the lines that are directly next to the CPT in between. In case a linear trend is identified for a soil layer, this will come down to $(\frac{a_1+a_2}{2}) \cdot z + \frac{b_1+b_2}{2}$, where $\{a_1, b_1\}$ are respectively the slope and intercept of the first line next to the CPT and $\{a_2, b_2\}$ are the slope and intercept of the second line.

4.2.2. Identifying the Depth Trend

In order to identify the depth trend for each of the lines of CPTs and each of the soil layers, a plot of the corrected cone resistance (q_t) against the depth will be made for the cone penetration tests on a line. An example of the first peat layer of the line of CPTs in the crest of the dyke (line 7) is shown in Figure 4.10 and an example of the clay layer of the same line of CPTs is shown in Figure 4.11.

Linear Trends

Using the corrected cone resistance data, it is possible to calculate linear and higher order polynomial trends that fit the data of a line of CPTs. A first order polynomial (*linear*) trend is a common trend found in soil mechanics as it describes the increase of the vertical stress with depth according to $\sigma = \gamma \cdot d$, where γ is the volumetric weight of the soil, which is constant within a homogeneous soil layer, and d is the depth.

As explained in Section 2.1.2, two linear trend estimators can be used: the ordinary least squares (LS) estimator and the Theil-Sen (TS) estimator. Figure 4.10 shows both of the estimators for the corrected cone resistance data of the first peat layer of the CPTs in the crest of the dyke. As will become clear in Section 4.2.3, the Theil-Sen estimator will be used to identify outliers in the soil data, after which the ordinary least squares estimator will be used to identify the trend of the soil data from which the outliers have been removed.

Both peat layers at the Leendert de Boerspolder show a linear trend in the soil data.

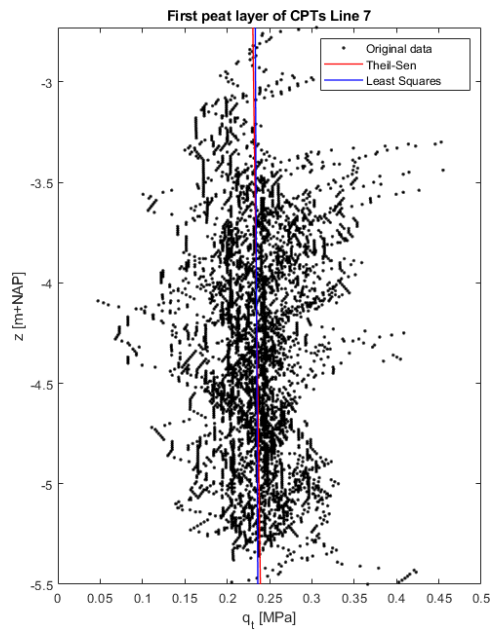


Figure 4.10: The linear trend identified for the corrected cone resistance data for the first peat layer of the CPTs located in the crest of the dyke

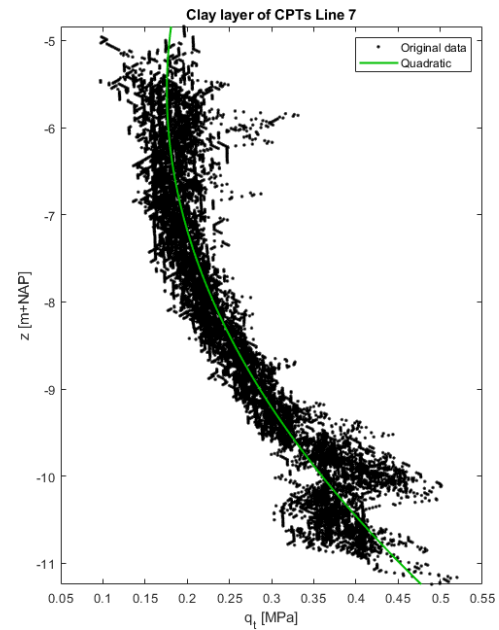


Figure 4.11: The Quadratic trend identified for the corrected cone resistance data for the clay layer of the CPTs located in the crest of the dyke

Quadratic Trends

When a quadratic trend is observed in the data, the linear ordinary least squares and Theil-Sen estimators cannot be used to identify the trend. A second order polynomial will be used to fit the data:

$$\text{polyfit} = a \cdot z^2 + b \cdot z + c \quad (4.1)$$

In case of a higher order polynomial trend, the reason for each additional order will have to be found in the layer under investigation. The clay layer in the Leendert de Boerspolder shows a quadratic trend, as can be seen from Figure 4.11, due to a gradual change in clay type. The top of the clay layer consists of a more organic clay, which slowly transitions to a silty clay at the bottom of the layer. By reviewing the Robertson soil behaviour type graphs in Figures 4.4 and 4.5 the gradual change in soil type can be seen between approximately -4.50m+NAP and -11.00m+NAP.

4.2.3. Outliers in the Cone Resistance Data

In Section 4.1 an effort is made to find the homogeneous soil layers of the Leendert de Boerspolder. But since the subsurface is not made up of perfect homogeneous soils, some irregularities or outliers can be encountered in the measured cone resistance. Some examples of outliers that can be found are roots, small patches of sand within non-sandy layers or gravel. These outliers will cause a peak in the cone resistance over a small depth and bias the outcome of the correlation function, leading to an incorrect estimation of the scales of fluctuation. Therefore it is necessary to remove the measurement outliers from the data.

Outliers of the Peat Layers

As discussed in Section 2.1.3, three methods are available to identify and remove outliers from data. From literature it became clear that the most robust method to detect outliers in the data makes use of the median and the median absolute deviation. This method will be used.

Before the outliers can be identified, the data should follow a normal distribution. This is achieved by removing the linear trend of the data with the robust Theil-Sen estimator. After identification and removal of the Theil-Sen trend, the Matlab function `isoutlier` will be used with the median method. An example of the results is shown in Figure 4.12. By investigating the histogram of the corrected cone resistance data before and after the outlier removal, of which an example is shown in Figure 4.13, it can be seen that a better fit with the normal distribution is achieved since no data falls outside the fit.

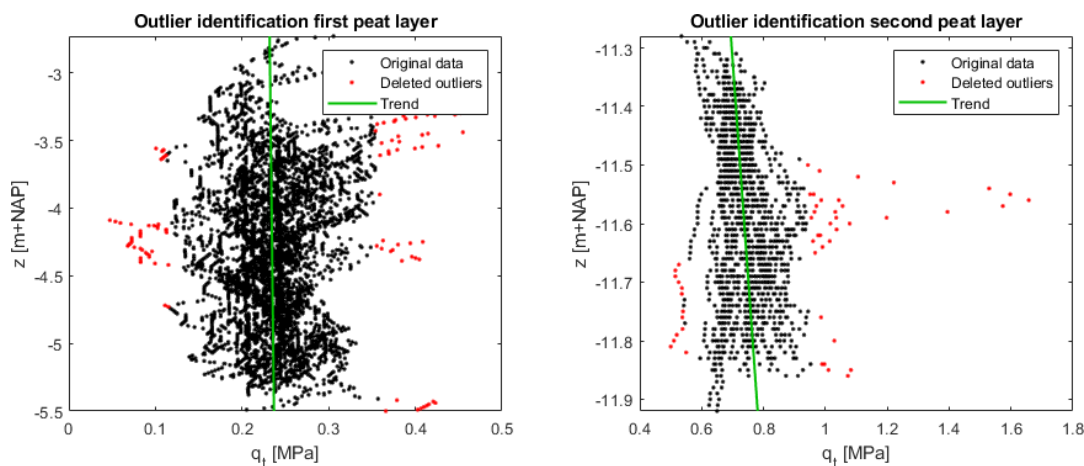


Figure 4.12: The results for the outlier removal of the first and second peat layers underneath the crest of the dyke

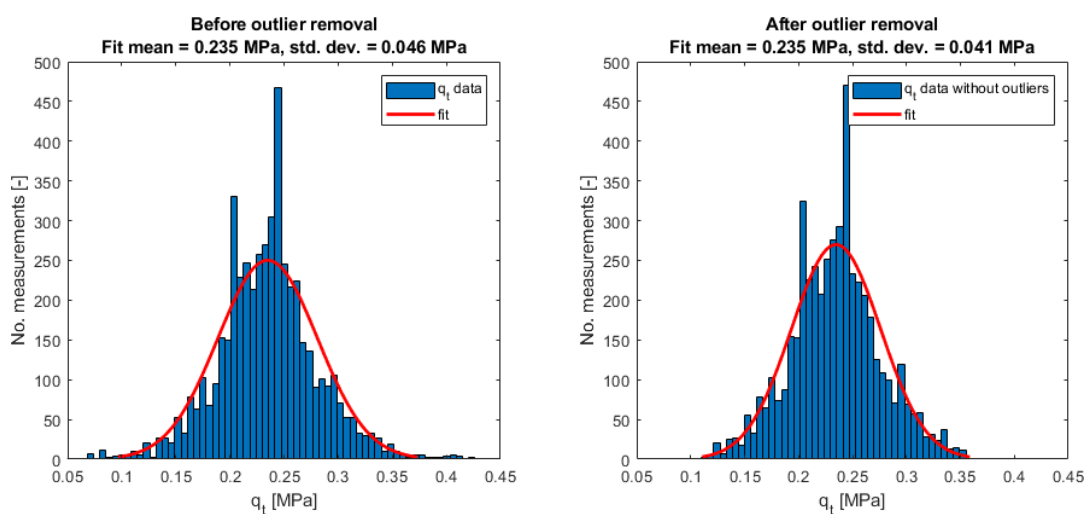


Figure 4.13: The histogram of the q_t data of the first peat layer underneath the crest of the dyke before and after outlier removal

Outliers of the Clay Layer

As explained in Section 4.2.2, the clay layer follows a quadratic trend due to the gradual change in soil type with depth. When the quadratic trend is removed from the q_t data, the resulting data does not follow a normal distribution, but a log-normal distribution, as shown in Figure 4.14. It is required that the data follows an approximately normal distribution in order to identify the outliers by the proposed methods, which is why the mean plus or minus three standard deviations, the interquartile range and the median plus or minus three median absolute deviations cannot be used.

While investigating the data, only one major outlier was found within the clay layer at CPT line 3, which is the peak in Figure 4.14 at approximately -9.90m+NAP. The choice has been made to remove this outlier from the soil data manually. The additional layer at the top of the clay layer, identified in Section 4.1.7, will be removed manually as well when calculating the spatial variability for the clay layer without the additional layer.

4.2.4. Trend Removal of the Lines of CPTs

After the outliers have been identified and removed for each of the three soil layers at every line of CPTs, the depth trend will have to be removed by making use of the simple method described in Section 2.1.2. After trend removal, the detrended soil data should result in normally or log-normally distributed data with a mean equal to zero. Since the trend has been identified for the lines parallel to the dyke, the mean of the data in that direction will be zero. However, when the correlations in other directions have to be calculated, for example perpendicular to the dyke, the data on that line of CPTs will not necessarily have an average mean equal to

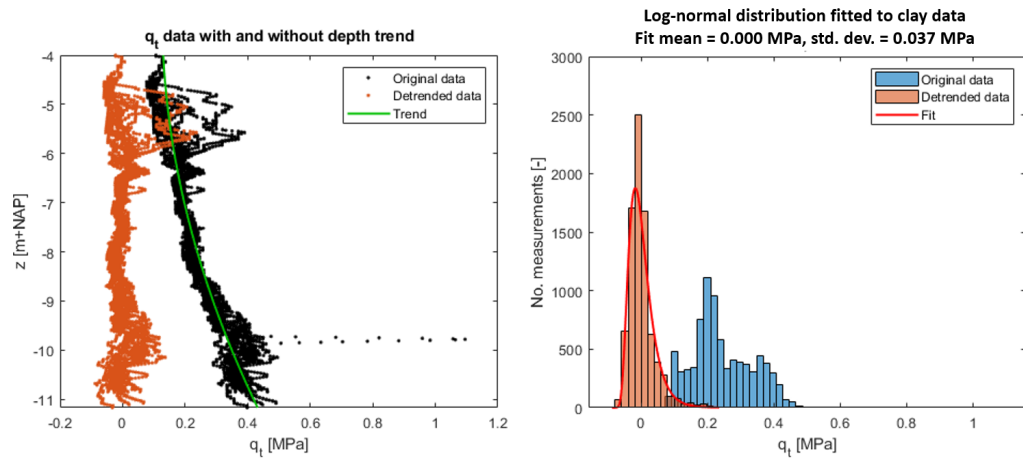


Figure 4.14: The detrended clay data, in this example of CPT line 3, follows a log-normal distribution

zero. In order to cope with this problem, the average mean of the detrended data will be removed.

Figure 4.15 shows an example of the trend removal for the first peat layer of CPT line 5, where the original data is presented in black and the detrended data in orange. By investigating the histogram of the original and detrended data, it is seen that after trend removal the data follows a normal distribution with a mean equal to zero.

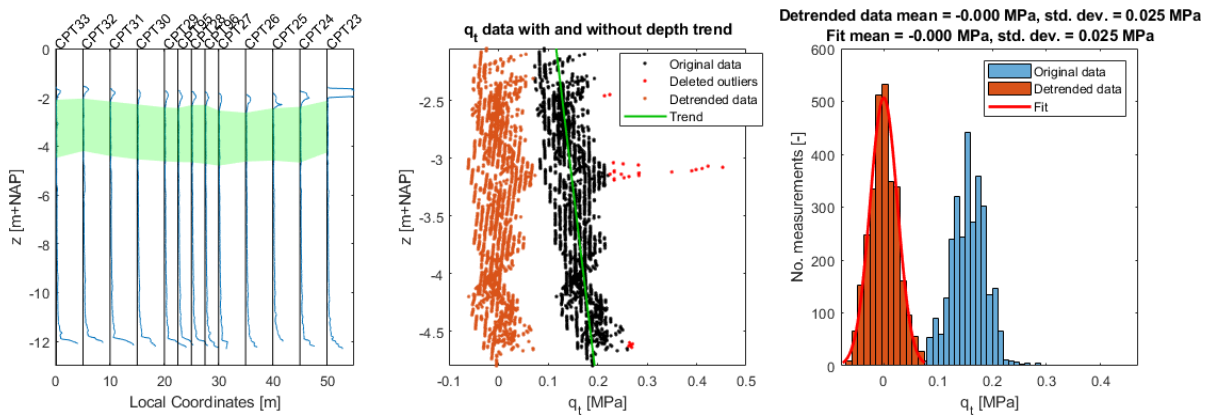


Figure 4.15: Trend removal for the first peat layer of CPT line 5: after trend removal the data is normally distributed

4.2.5. Results of the Trend Removal

The trends for every line of CPTs and for the individual CPTs in between the lines can be found in the figures in Appendix D.

Depth Trends of the First Peat Layer

Figure 4.16 shows the results of the trend removal of the first peat layer for all 100 CPTs in the Leendert de Boerspolder. The outliers are not shown in this figure for clarity. Appendix D contains the results of the individual lines of CPTs and shows the outliers.

The trends of the first peat layer are summarised in Table 4.1. There are two trendlines that stand out from the others. The first of which is the trendline of CPT line 6 with the largest slope, and the second of which is the trendline of CPT line 7 with the largest intercept value and almost no slope. The five left-most trends that show some similarity are the trendlines for CPT lines 1 to 5, for which the slope increases as the lines get closer to the dyke.

After trend removal, the detrended data follows a normal distribution with a mean equal to zero. In order to compare the degree of dispersion between the results of the different CPT lines, the coefficient of variation is calculated by using the standard deviation of the data after trend removal and the mean of the data before

trend removal without the outliers, because outliers are not actually part of the data. The COV lines show good agreement between the lines, with the standard deviation ranging between 13.5% to 18.5% of the mean.

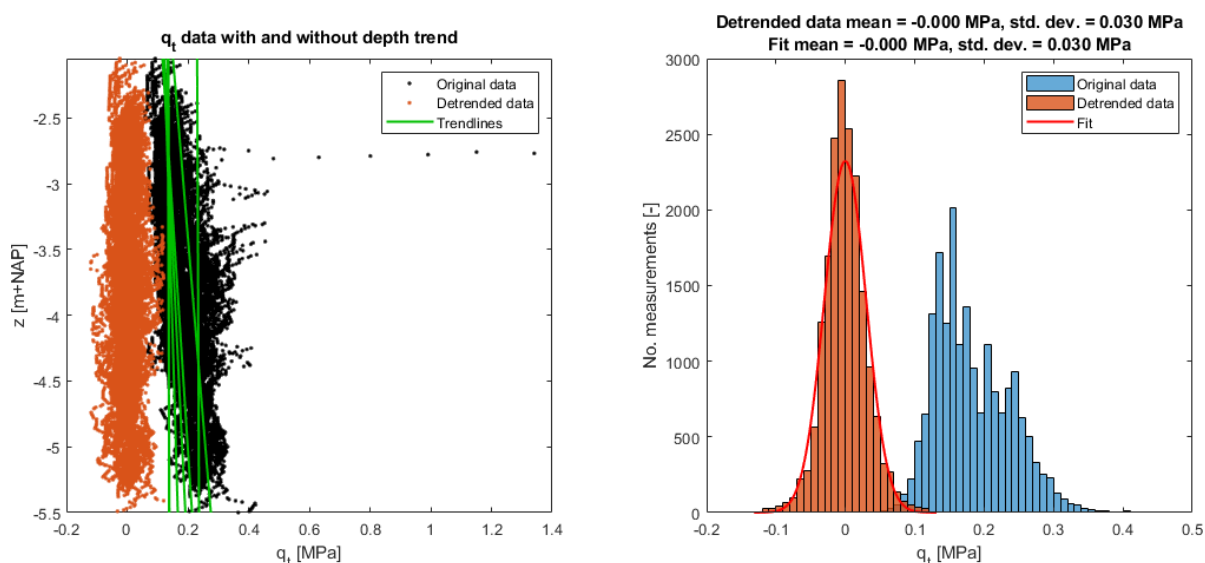


Figure 4.16: Summary of the trends that have been removed from the first peat layer. The detrended data follows a normal distribution.

Table 4.1: The statistical properties of the first peat layer for the CPT lines

CPT Line	1	2	3	4
Trend	$-0.0004 \cdot z + 0.1357$	$-0.0017 \cdot z + 0.1298$	$-0.0126 \cdot z + 0.0976$	$-0.0212 \cdot z + 0.0753$
σ [MPa]	0.0244	0.0251	0.0196	0.0242
μ [MPa]	0.1372	0.1359	0.1415	0.1485
COV [-]	0.1778	0.1847	0.1385	0.1630

CPT Line	5	6	7
Trend	$-0.0282 \cdot z + 0.0586$	$-0.0361 \cdot z + 0.0771$	$-0.0018 \cdot z + 0.2269$
σ [MPa]	0.0252	0.0297	0.0413
μ [MPa]	0.1558	0.2192	0.2347
COV [-]	0.1617	0.1355	0.1760

Depth Trends of the Clay Layer

Figure 4.17 shows the results of the trend removal of the clay layer for all 100 CPTs in the Leendert de Boerspolder. Appendix D contains the results of the individual lines of CPTs.

The trends of the clay layer are summarised in Table 4.2. The trendlines show similar results for the different lines of CPTs, but the trends for CPT line 6 and 7 appear to make wrong estimations of the top section of the clay layer. However, the top of the clay layer underneath CPT line 6 is equal to approximately -5.15m+NAP and underneath line 7 the top of the clay layer is found at approximately -5.39m+NAP , while at the other CPT lines the top of the clay layer is situated between approximately -4.37m+NAP to -4.76m+NAP . The trend estimate of CPT lines 6 and 7 at the top of the clay layer is therefore an extrapolation and not used to remove the trend of any q_t data.

After trend removal, the detrended data follows a log-normal distribution with a mean equal to zero. The coefficient of variation shows good agreement between the CPT lines with the standard deviation ranging between 10.1% and 18.0% of the mean.

As discussed in Section 4.1.7, the corrected cone resistance of the top section of the clay layer, from approximately -4.75m+NAP to -6.00m+NAP , shows that there might be an additional layer present within the clay layer at several cone penetration test locations. The CPTs at which this layer is found can be found in Figure 4.8. When the correlations of the clay layer are determined, the choice can be made to include or exclude that additional layer. A summary of the identified trends of the clay layer without the additional layer is shown in Figure 4.18.

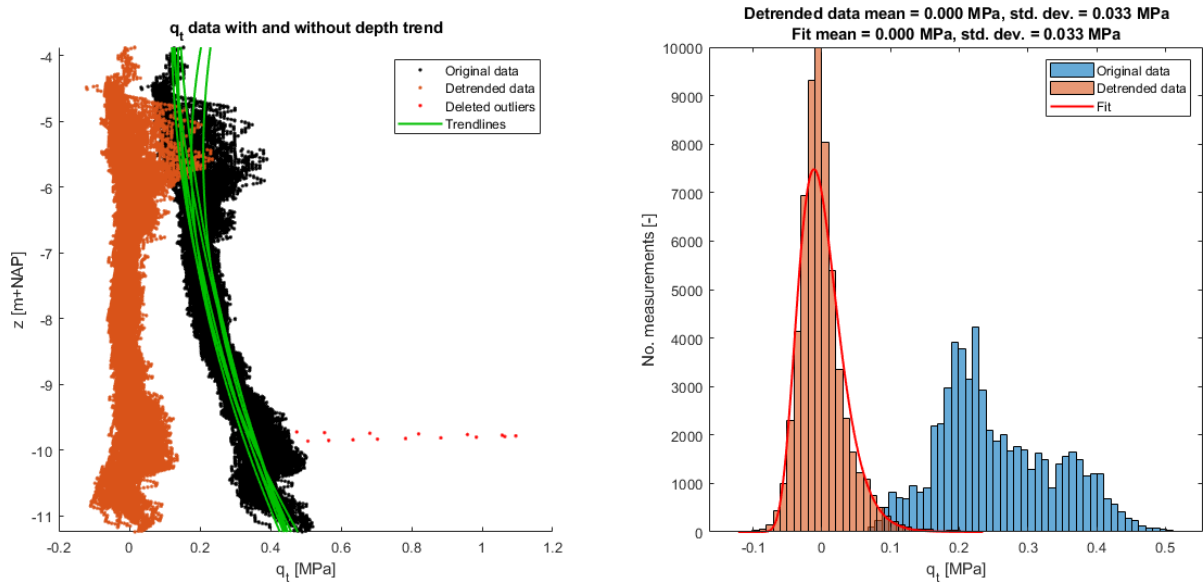


Figure 4.17: Summary of the trends that have been removed from the clay layer. The detrended data follows a log-normal distribution.

Table 4.2: The statistical properties of the clay layer for the CPT lines

CPT Line	1	2	3
Trend	$0.0056 \cdot z^2 + 0.0455 \cdot z + 0.2308$	$0.0055 \cdot z^2 + 0.0389 \cdot z + 0.1890$	$0.0047 \cdot z^2 + 0.0292 \cdot z + 0.1713$
σ [MPa]	0.0417	0.0318	0.0382
μ [MPa]	0.2321	0.2325	0.2427
COV [-]	0.1797	0.1368	0.1574
CPT Line	4	5	6
Trend	$0.0036 \cdot z^2 + 0.0103 \cdot z + 0.1100$	$0.0036 \cdot z^2 + 0.0143 \cdot z + 0.1474$	$0.0076 \cdot z^2 + 0.0838 \cdot z + 0.4406$
σ [MPa]	0.0336	0.0339	0.0284
μ [MPa]	0.2545	0.2640	0.2808
COV [-]	0.1320	0.1284	0.1011
CPT Line	7		
Trend	$0.0094 \cdot z^2 + 0.1048 \cdot z + 0.4679$		
σ [MPa]	0.0283		
μ [MPa]	0.2583		
COV [-]	0.1096		

The trends of the clay layer without the additional layer are shown in Table 4.3. For the same reason as before the removal of the additional layer, the trendlines of CPT lines 6 and 7 stand out at the top of the clay layer. Comparing the results with the results of the complete clay layer, it is found that the top section of the detrended soil data shifts to higher q_t values, because the trends estimate a lower q_t at the top of the clay layer without the additional layer.

Without the additional layer the detrended data still follows a log-normal distribution with a mean equal to zero. The COV shows better agreement between the CPT lines than without the removal of the additional layer, with the current standard deviation ranging between 9.83% and 14.45% of the mean.

Depth Trends of the Second Peat Layer

Figure 4.19 shows the results of the trend removal of the second peat layer for all 100 CPTs in the Leendert de Boerspolder. The outliers are not shown in this figure for clarity. The results of the individual lines of CPTs with the outliers identified can be found in Appendix D.

A summary of the trends is shown in Table 4.4. One trend stands out, which is the almost vertical trendline, with just a small slope, of CPT line 3. It might be that CPT 13, located on CPT line 3, of which the peat layer continues until -12.28m+NAP, causes a slight bias in the slope, but upon inspection of the trend identification of line 3 in Figure D.24 it is observed that all CPTs on line 3 show an approximately vertical trend for the second peat layer.

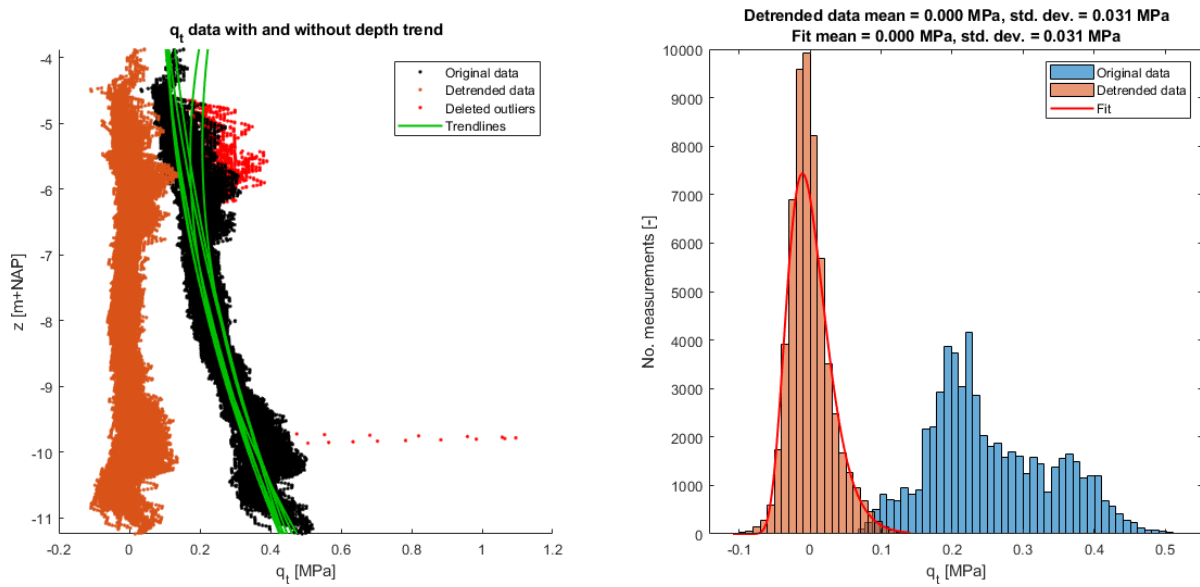


Figure 4.18: Summary of the trends that have been removed from the clay layer when the additional layer is removed from the data. The detrended data follows a log-normal distribution.

Table 4.3: The statistical properties of the clay layer without the additional layer for the CPT lines

CPT Line	1	2	3
Trend	$0.0047 \cdot z^2 + 0.0282 \cdot z + 0.1491$	$0.0051 \cdot z^2 + 0.0323 \cdot z + 0.1569$	$0.0038 \cdot z^2 + 0.0131 \cdot z + 0.0970$
σ [MPa]	0.0334	0.0280	0.0297
μ [MPa]	0.2312	0.2325	0.2417
COV [-]	0.1445	0.1204	0.1229

CPT Line	4	5	6
Trend	$0.0031 \cdot z^2 + 0.0014 \cdot z + 0.0713$	$0.0029 \cdot z^2 + 0.0022 \cdot z + 0.0944$	$0.0073 \cdot z^2 + 0.0778 \cdot z + 0.4143$
σ [MPa]	0.0319	0.0314	0.0276
μ [MPa]	0.2549	0.2643	0.2807
COV [-]	0.1251	0.1188	0.0983

CPT Line	7
Trend	$0.0092 \cdot z^2 + 0.1013 \cdot z + 0.4517$
σ [MPa]	0.0274
μ [MPa]	0.2582
COV [-]	0.1061

After trend removal, the detrended data follow a normal distribution with a mean equal to zero. The COV shows good agreement between the CPT lines, with the standard deviation ranging from 8.2% to 11.5% of the mean.

Table 4.4: The statistical properties of the second peat layer for the CPT lines

CPT Line	1	2	3	4
Trend	$-0.2611 \cdot z - 2.2975$	$-0.2422 \cdot z - 2.0984$	$-0.0166 \cdot z + 0.5693$	$-0.2515 \cdot z - 2.1751$
σ [MPa]	0.0843	0.0592	0.0856	0.0768
μ [MPa]	0.7287	0.7162	0.7622	0.7463
COV [-]	0.1157	0.0827	0.1123	0.1029

CPT Line	5	6	7
Trend	$-0.2635 \cdot z - 2.3055$	$-0.2007 \cdot z - 1.5812$	$-0.1352 \cdot z - 0.8306$
σ [MPa]	0.0871	0.0661	0.0728
μ [MPa]	0.7549	0.7543	0.7368
COV [-]	0.1154	0.0876	0.0988

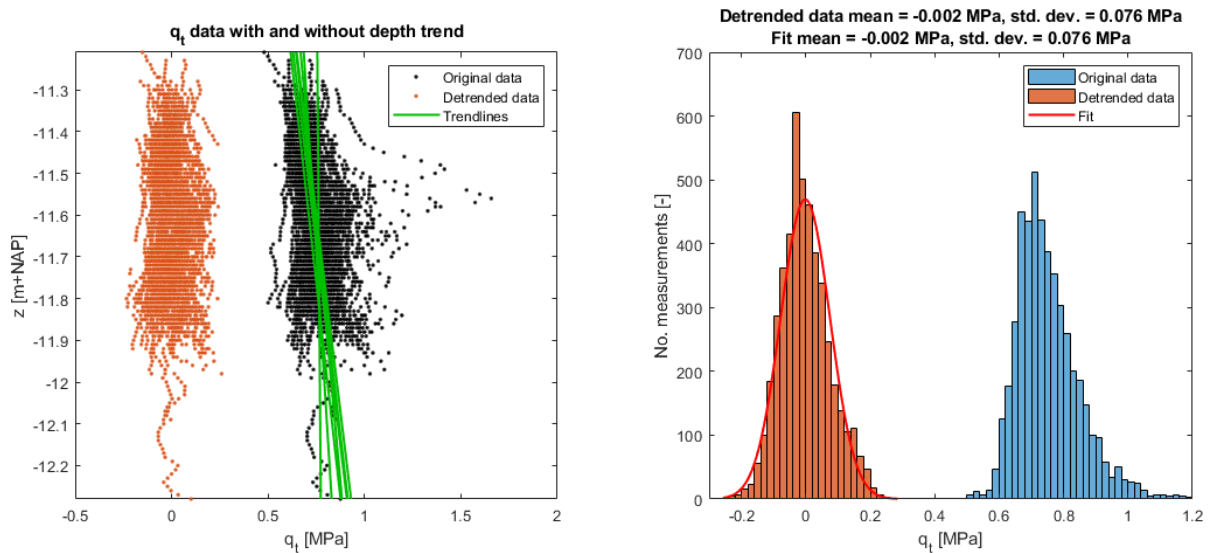


Figure 4.19: Summary of the trends that have been removed from the second peat layer. The detrended data can be described by a normal distribution.

4.3. Calculating the Scales of Fluctuation

With the soil layers identified and the trend of the data removed, the scales of fluctuation can be calculated from the CPT data by using the method described in Section 2.1.5.

The scales of fluctuation of the Leendert de Boerspolder are calculated in both horizontal and vertical directions by using a line of cone penetration tests. Regarding the spatial variability of lines of CPTs parallel to the dyke, the stress history is expected to be more or less similar over the whole line. Another possibility is to calculate the correlations of lines of CPTs perpendicular or in other orientations. This way it can be checked whether the field is symmetric in certain directions and it allows a comparison of the influence of the deformations to be made in different directions. For example, settlement of the field has likely occurred mostly underneath the dyke, so the CPTs underneath the dyke can be compared with those in the polder from perpendicular lines of CPTs to the dyke. On the other hand, rotation should be checked by comparing the spatial variability of each of the parallel lines of CPTs.

The lines of CPTs that will be analysed for the purpose of this thesis are presented in Figure 4.20. As explained in Section 2.1.5, the minimum amount of autocorrelation function datapoints required to create a good fit of the autocorrelation model is three datapoints which are larger than the Bartlett limit. This implies that in order to be able to calculate the horizontal scale of fluctuation, a minimum amount of three CPTs are needed. Therefore it is possible to calculate the horizontal scale of fluctuation in the polder between CPT 59 (line 4) and CPT 66 (line 2), but it is not possible to do the same between CPT 60 (line 4) and CPT 67 (line 2).

Some of the perpendicular lines can be split into a section of three or more CPTs under the dyke or into a section in the polder. The perpendicular lines of CPTs underneath the dyke that can be analysed for their horizontal and vertical scales of fluctuation are CPTs: {40 to 29}, {74 to 95}, {39 to 91}, {73 to 96} and {38 to 27}. The same can be done for the following three lines in the polder: {59 to 66}, {90 to 6} and {58 to 65}.

Finally, the vertical correlations of the individual cone penetration tests will be calculated and compared as well.

4.3.1. Matlab Code

The calculation of the correlations is performed in Matlab. This section will go through the code and discuss the main input parameters that are necessary. A flowchart of the code is shown in Figure 4.21.

At the initialisation step, the CPT data and the soil layer depth data are imported. The depths of the soil layer have been determined as discussed in Section 4.1. From the CPT data a plot of the CPT grid of the Leendert de Boerspolder is made, as seen in Figure 4.22.

The next step requires user input two times: once for the choice of CPTs to be analysed, and once for the layer that should be analysed. With this final input, the corrected cone resistance data is extracted for the CPTs and layer to be analysed. Figure 4.23 shows a plot of the line of CPTs that is made.

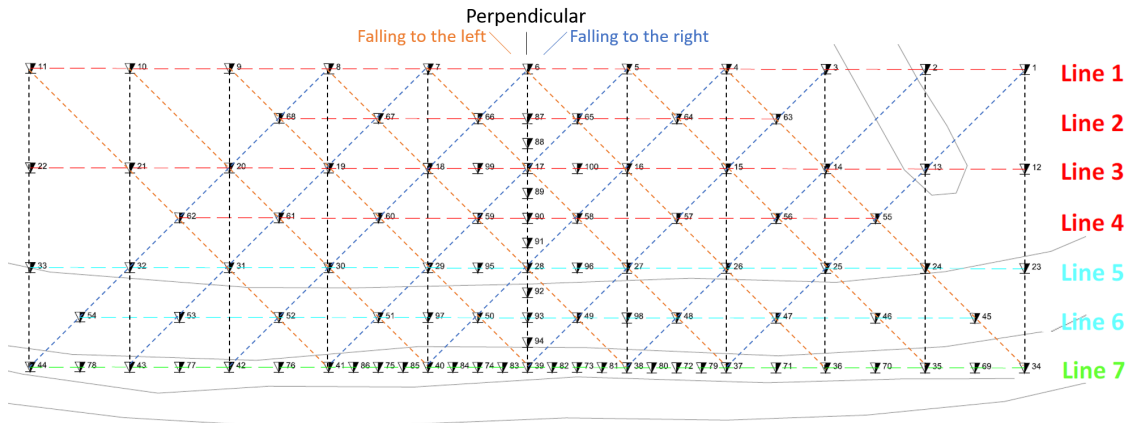


Figure 4.20: Besides the parallel lines, it is possible to analyse (part of) the perpendicular lines of CPTs and the lines under 45 degrees angles to the dyke

The trend removal step follows the steps set out in Section 4.2, identifying and removing the outliers first and then identifying and removing the trend. From the original q_t data and the detrended q_t data a plot over the depth is generated, shown in Figure 4.24, and a plot of the histograms with a distribution fit is made, shown in Figure 4.25. Since the lines of CPTs are analysed in different directions, the results of the detrended soil data are saved in a Matlab save file for every CPT. This makes it possible to call the save file and use the detrended soil data, saving time and reducing the chance of errors in the code.

Finally, the spatial variability is calculated. For both horizontal and vertical directions the same steps have to be taken, but for the horizontal autocorrelation function the calculation is looped over the depth for every CPT, while for the vertical ACF the calculation is looped the other way around. In order to cope with data points without data, for example removed outliers, the data is set to be equal to zero and is not accounted for in the t-matrix. Data equal to zero does not add to the sum made for the calculation of the ACF, making this a proper work-around. The autocorrelation model (ACM) code includes two `fit` functions. The fit is only made to the initial part of the ACF that is larger than the Barlett's limit, explained in Section 2.1.5. For the ACM, the best fit of the θ_{avg} for a single Markov exponential is calculated first. The average scale of fluctuation is then used to create a range of smaller θ_1 , which are smaller than the single scale of fluctuation, accompanied by a range of weighting factors c_1 and c_2 . All possible combinations of θ_2 are calculated by

$$\theta_2 = (\theta_{avg} - c_1) / c_2 \tag{4.2}$$

with all possible combinations for the range of c_1 and c_2 . The ACM code is concluded by combining all possibilities of weighting factors and small and large scales of fluctuation into one matrix, of which the lowest error to the ACF is calculated by means of the root mean squared error (RMSE). The lowest RMSE gives the combination of weighting factors and scales of fluctuation that best fit the ACF. A plot of the results of the horizontal ACF and ACM is made, of which an example is shown in Figure 4.26, and the same is done for the vertical ACF and ACM, of which an example is shown in Figure 4.27.

The output of the horizontal and vertical spatial variability is saved and can be analysed and compared.

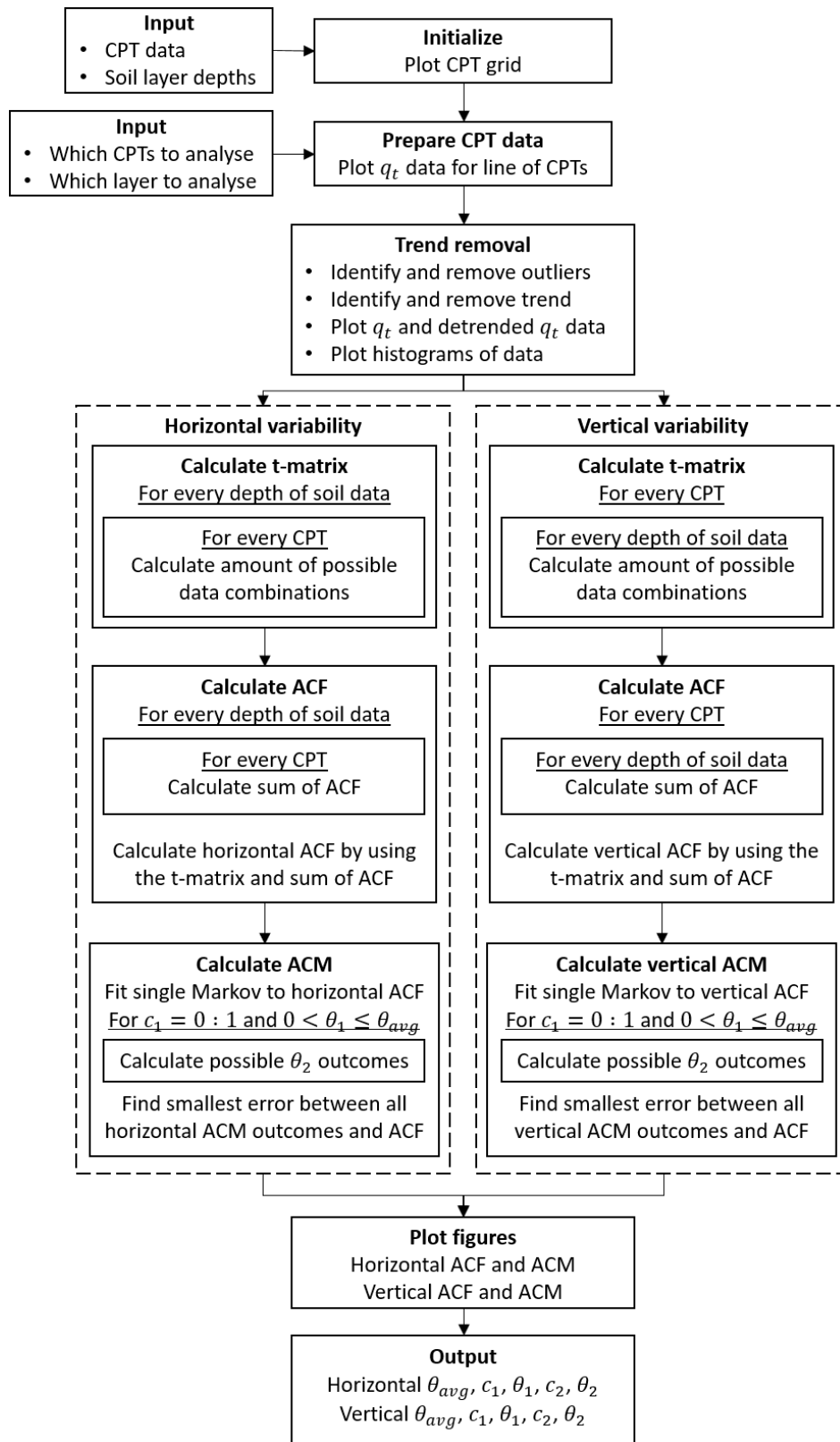


Figure 4.21: A flowchart summarising the code that has been used to estimate the scales of fluctuation. The explanation of the t-matrix, autocorrelation function (ACF) and autocorrelation model (ACM) can be found in Section 2.1.5.

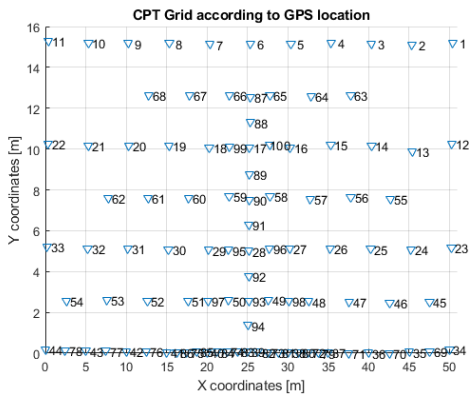


Figure 4.22: Example of the CPT grid output of Matlab

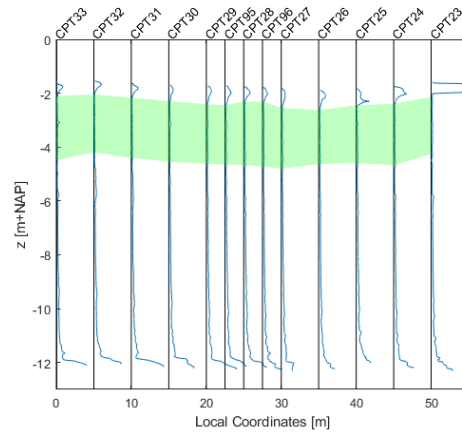


Figure 4.23: Example of the CPT line output of Matlab

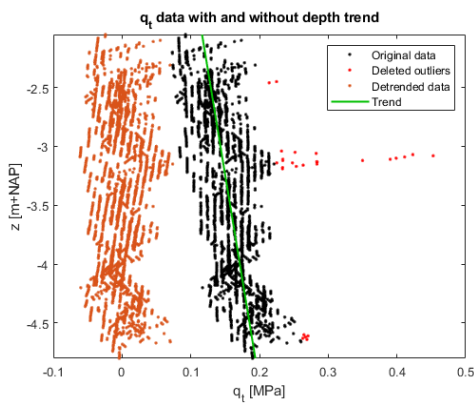


Figure 4.24: Example of the trend removal output of Matlab

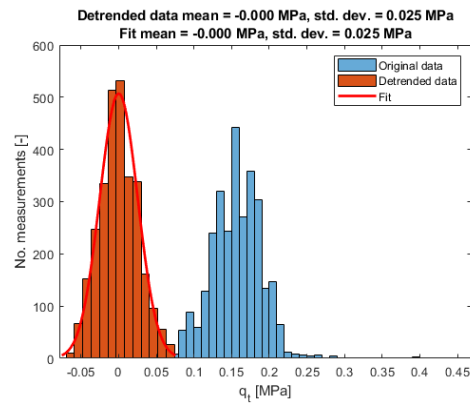


Figure 4.25: Example of the histogram output of Matlab

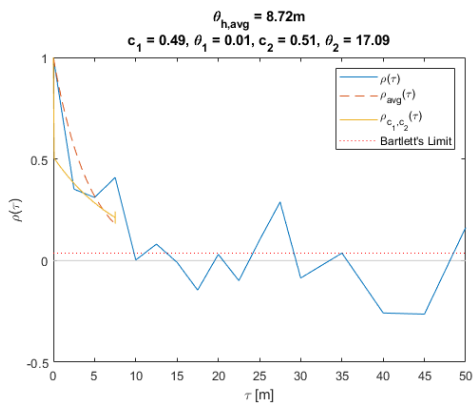


Figure 4.26: Example of the horizontal spatial variability output of Matlab

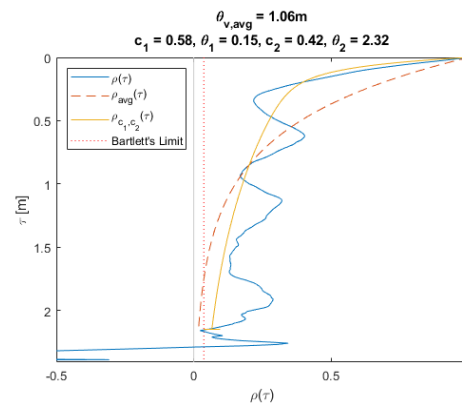


Figure 4.27: Example of the vertical spatial variability output of Matlab

4.4. Results

The results of the spatial variability of the Leendert de Boerspolder will be discussed in this section for every soil layer. The complete results can be found in Appendix E. This section will present the main findings.

For every cone penetration test the vertical scale of fluctuation per layer has been calculated. After trend removal, the mean of the q_t data of individual CPTs is not always equal to zero. Since this is required in order to calculate the scales of fluctuation, the mean of the detrended soil data will be subtracted from that data. This also applies to the lines perpendicular to the dyke and those diagonal to the dyke.

4.4.1. Spatial Variability of the First Peat Layer

The spatial variability of the first peat layer is first investigated for the individual CPTs. For the individual CPTs it is only possible to calculate the vertical scale of fluctuation (θ_v). Afterwards, the results of the spatial variability in horizontal and vertical direction will be calculated for the lines of CPTs shown in Figure 4.20.

Individual CPTs

The results for the first peat layer of the vertical scales of fluctuation of individual CPTs are summarised in Figure E.1 and Table E.1. A more comprehensive summary is shown in the histograms of Figure 4.28, of which the bin width has been set to 0.05m.

It is observed that the lowest and highest median are both found in the polder, at the two CPT lines furthest from the dyke. The median vertical scales of fluctuation of the other lines are almost identical. By investigating the mean, it is found that the average θ_v underneath the dyke is the largest.

Figure E.1 was investigated to find out whether the bimodal distribution of vertical scales of fluctuation underneath the crest of the dyke (line 7) can be explained by zoning of the larger and smaller values. However, it was found that the high and low values of θ_v are spread out and are not found in certain zones underneath the dyke.

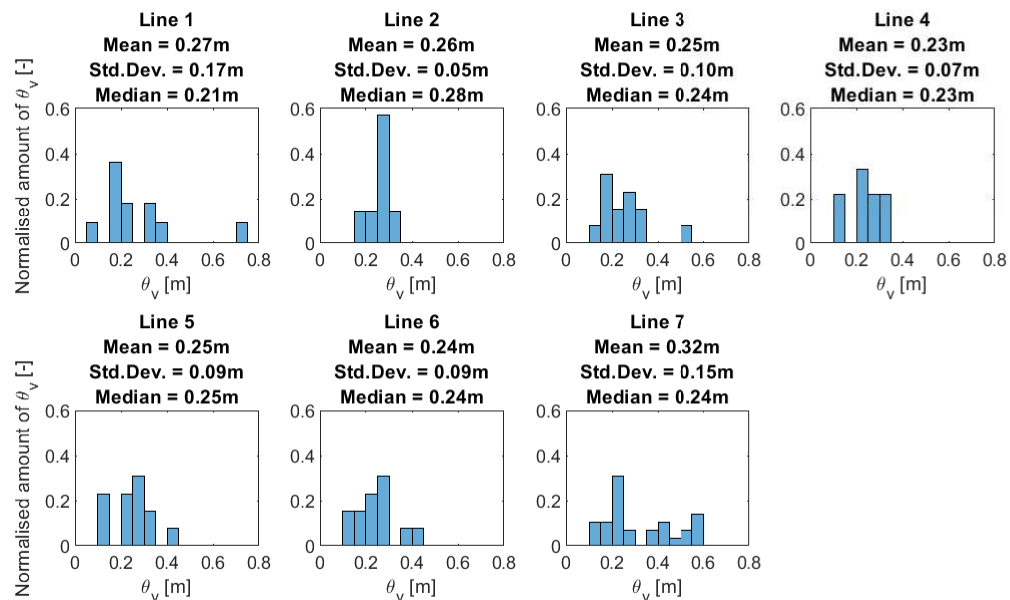


Figure 4.28: The vertical scales of fluctuation of the single CPTs for the first peat layer, per line

Lines of CPTs

After the assessment of the vertical scales of fluctuation for the individual CPTs, the evaluation of the lines of CPTs was made. By using lines of CPTs it is possible to calculate the horizontal and vertical scales of fluctuation. It has to be noted that some horizontal correlation lengths could not be calculated, because the autocorrelation function decreased to a value below the Bartlett limit within three lag distances. As explained in Section 2.1.5, in order to fit the correlation model to the correlation function, at least three autocorrelation function values larger than the Bartlett limit are necessary. The summary of the results of the spatial variability of the first peat layer can be found in Table E.2 and Figure E.5.

Parallel Lines

The scales of fluctuation of the parallel lines are shown in Table 4.5. The horizontal correlation lengths for the single Markov exponential fall within the range of 7.95m to 8.72m, but at CPT line 3 the θ_h is approximately twice as long and at CPT line 7 the θ_h is approximately three times smaller. By using the double Markov exponential it is found that each line of CPTs shows a $\theta_{h,1}$ smaller than the shortest lag distance for that line. The results of $\theta_{h,2}$ show spread in the polder and decrease near the dyke from the toe to the crest.

The single vertical scales of fluctuation show two correlation lengths: a short correlation length with a range of 0.28 to 0.46m for lines 2, 3 and 7, and a large correlation length larger than 1.00m. When investigating the double Markov exponential it is seen that the larger vertical scales of fluctuation are divided into a small and large component, while the small vertical scales of fluctuation cannot be described by a double scale of fluctuation. The general trend of the small $\theta_{v,1}$ is that it decreases towards the crest of the dyke, while the larger $\theta_{v,2}$ fluctuates between 2.32m and 3.12m.

Table 4.5: The scales of fluctuation for the parallel lines of the first peat layer

CPT Line		1		2		3		4		5		6		7	
$\theta_h[m]$		7.95		8.57		19.10		-		8.72		8.49		2.77	
c_1	c_2	0.65	0.35	0.48	0.52	0.64	0.36	-	-	0.49	0.51	0.33	0.67	0.38	0.62
$\theta_{h,1}[m]$	$\theta_{h,2}[m]$	0.01	22.70	0.01	16.47	0.01	53.04	-	-	0.01	17.09	0.01	12.67	0.22	4.33
$\theta_v[m]$		1.20		0.36		0.28		1.22		1.06		1.49		0.46	
c_1	c_2	0.60	0.40	1.00	-	1.00	-	0.64	0.36	0.58	0.42	0.46	0.54	0.06	0.94
$\theta_{v,1}[m]$	$\theta_{v,2}[m]$	0.17	2.75	0.36	-	0.28	-	0.15	3.12	0.15	2.32	0.14	2.64	0.10	0.48

The vertical scales of fluctuation of the first peat layer of the Leendert de Boerspolder have also been calculated by de Gast et al. (2017) over the parallel lines of CPTs. The results are summarised in Table 4.6. Compared to the findings of this research (Table 4.5), the contributions of the small vertical scales of fluctuation, c_1 , as well as the correlation length $\theta_{v,1}$ are larger, except for line 2. In contrast to this research, the $\theta_{v,2}$ are much larger, ranging from 1.60m to as much as 143.30m. By investigating the average θ_v , it is seen that from the toe of the dyke (line 5) to the crest of the dyke (line 7), the vertical scale of fluctuation decreases. The vertical scales of fluctuation of the lines in the polder show a large range in the results. The conclusions that can be made are similar to the results of this research, albeit with different values.

Table 4.6: The vertical scales of fluctuation for the parallel lines of the first peat layer, calculated by de Gast et al. (2017). The average θ_v is calculated from the weighting factors and the double vertical scales of fluctuation.

CPT Line		1		2		3		4		5		6		7	
$\theta_v[m]$		2.79		0.13		0.32		28.80		2.04		1.83		0.36	
c_1	c_2	0.90	0.10	0.95	0.05	1.00	-	0.80	0.20	0.80	0.20	0.60	0.40	1.00	-
$\theta_{v,1}[m]$	$\theta_{v,2}[m]$	0.38	24.50	0.05	1.60	0.32	-	0.18	143.30	0.25	9.20	0.18	4.30	0.36	-

Perpendicular Lines

The perpendicular lines have been investigated as complete lines from CPT line 1 to 7, and as sections that are only in the polder or only underneath the dyke. The sections are mentioned in Section 4.3.

For the complete perpendicular lines it was almost impossible to calculate any horizontal correlation length, because the ACF dropped below the Barlett limit within three lag distances. Only one correlation length could be calculated, which is not enough information to draw conclusions from. From the sections in the polder and underneath the dyke it was equally impossible to calculate the horizontal correlations, with both sections giving results for a single line of CPTs each. The first peat layer shows little to no correlation in the horizontal direction perpendicular to the dyke.

In the vertical direction the complete lines show mostly two scales of fluctuation. The smaller $\theta_{v,1}$ is on average equal to approximately 0.16m with a standard deviation of 0.11m, indicating quite some variability of the results. The mean of the larger $\theta_{v,2}$ is equal to 1.18m with a standard deviation of 1.51m, indicating very high variability. The high standard deviation of the $\theta_{v,2}$ is caused by one larger outlier of 5.15m. Without the outlier the mean and standard deviation would be 0.68m and 0.29m respectively. The vertical scales of fluctuation of the perpendicular sections show a mean θ_v underneath the dyke which is approximately 10% larger than the mean θ_v in the polder. Regardless of the exclusions of the outlier of the complete lines, the sections show smaller average vertical scales of fluctuation than the complete lines.

Diagonal Lines

Similar to the perpendicular lines, the horizontal correlations of the diagonal lines could hardly be determined. Two out of eight correlations lengths could be calculated for the angle to the right, and three out of eight for the angle to the left. Four of those results showed a $\theta_{h,1}$ smaller than the shortest lag distance.

The vertical scales of fluctuation for the angle to the right show one outlier θ_v of 1.76m. Without that outlier, the results for both diagonal directions are similar, resulting in an average of 0.39m and 0.38m with

standard deviations of 0.07m and 0.10m for the angle to the right and the angle to the left respectively. These mean vertical scales of fluctuation are slightly lower than what was found in the perpendicular direction.

4.4.2. Spatial Variability of the Clay Layer

The spatial variability of the clay layer is investigated in the same steps as the first peat layer. However, since the clay layer has also been analysed without the additional layer, those results are presented as well to ease the comparison. First the θ_v of the individual CPTs will be analysed. Afterwards, the results of the spatial variability in horizontal and vertical direction will be estimated for the lines of CPTs shown in Figure 4.20.

Individual CPTs

The results for the clay layer can be found in Figure E.2 and Table E.4. A more comprehensive summary is shown in the histograms of Figure 4.29, of which the bin width has been set to 0.05m.

It was observed that the mean θ_v decreases when moving closer towards the crest of the dyke. The spread of the vertical scales of fluctuation is larger in the polder than underneath the crest. Regarding the median θ_v , the values found in the polder at lines 1 to 3 are larger than those found at the other lines. The median values at lines 4 to 7 are almost identical to each other with the largest difference being just 5 centimetres.

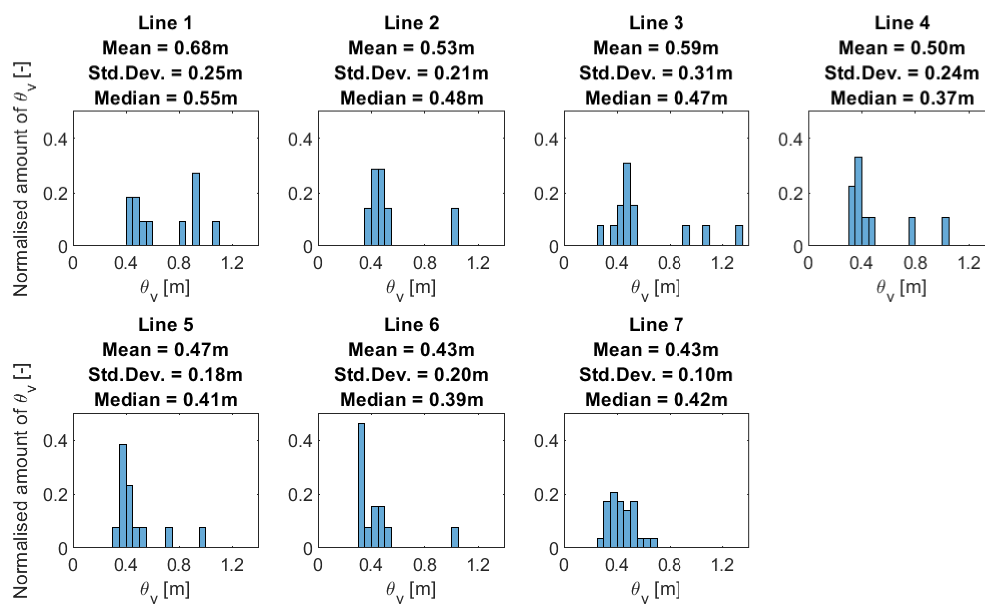


Figure 4.29: The vertical scales of fluctuation of the single CPTs for the clay layer, per line

The results after removal of the additional organic layer near the top of the complete clay layer can be found in Figure E.3 and Table E.7. The comprehensive summary is shown in the histograms of Figure 4.30, of which the bin width has been set to 0.05m.

The results without the additional layer show that the same trends as the results of the complete clay layer, except that the spread of the data has been reduced. In general the correlation length has been decreased by removing the additional layer. The largest decrease of the mean θ_v is found in the polder. By investigating the results of the complete clay layer it was found that the outliers at the complete clay layer were caused by the CPTs where the additional layer was present. Due to the removal of the additional layer the values of θ_v at those CPTs were approximately halved in the polder. In the proximity of the dyke the removal of the additional layer had less influence on the vertical scales of fluctuation.

Lines of CPTs

The summary of the results of the spatial variability of the clay layer can be found in Table E.5 and Figure E.6. The summary of the clay layer without the additional layer is given in Table E.8 and Figure E.7.

Parallel Lines

For the entire clay layer the scales of fluctuation are shown in Table 4.7 and without the additional layer the

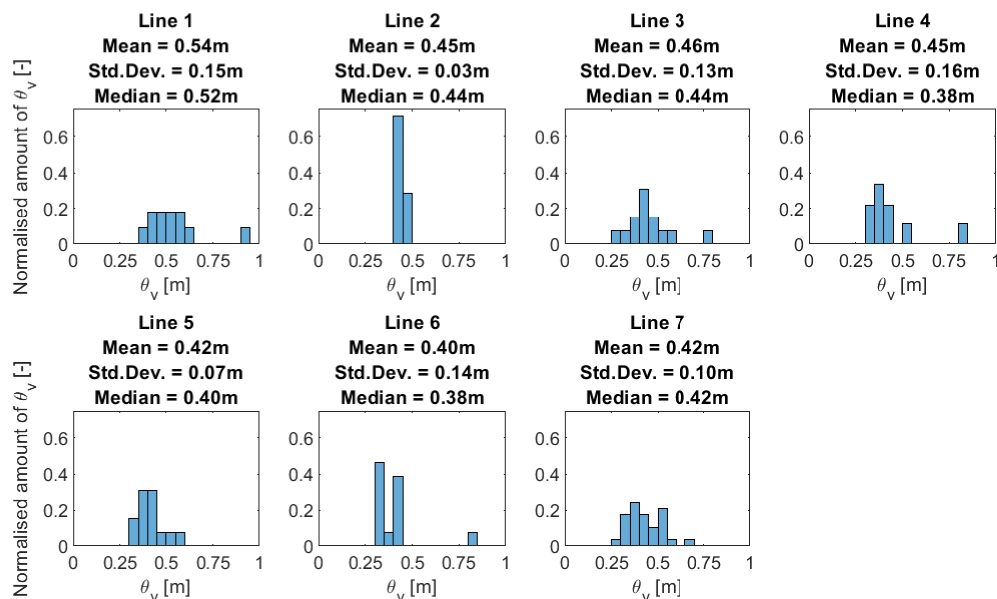


Figure 4.30: The vertical scales of fluctuation of the single CPTs for the clay layer without the additional layer, per line

scales of fluctuation can be found in Table 4.8. When ‘the clay layers’ are mentioned, this refers to both the complete clay layer and the clay layer without the additional layer.

In contrast with the first peat layer, all horizontal correlations could be calculated for the clay layers. The complete clay layer will be analysed first. It was found that all lines except CPT line 1 show a $\theta_{h,1}$ smaller than the shortest lag distance. At CPT line 1 a $\theta_{h,1}$ of 12.30m was found. The $\theta_{h,2}$ decreases from line 1 to line 4 and then increases drastically towards the crest. The large horizontal scale of fluctuation underneath the crest of the dyke is approximately twice as large as the average found in the polder. Without the additional layer, all CPT lines show a $\theta_{h,1}$ smaller than the shortest lag distance, of which the weighting factor is larger closer to the dyke. The $\theta_{h,2}$ for the clay layer without the additional layer in the polder is approximately 1.6 times larger than for the complete layer, 1.8 times larger at the toe of the dyke, 1.2 times larger underneath the slope and underneath the crest of the dyke the results are approximately the same. The general trend is that without the additional layer, the horizontal correlation length is larger, especially near the toe of the dyke.

For both clay layers the vertical scales of fluctuation are described only by single θ_v . For the complete clay layer the results in the polder fluctuate between 0.60m and 0.90m, and from the polder to underneath the slope the θ_v decreases. Underneath the crest it slightly increases compared to the slope. Without the additional layer, the vertical scales of fluctuation in the polder are on average slightly larger than those underneath the dyke. Comparing the results of the clay layers, it was found that without the additional layer the θ_v is lower, except for CPT line 7, where almost no reduction was found.

Table 4.7: The scales of fluctuation for the parallel lines of the clay layer

CPT Line		1		2		3		4		5		6		7	
$\theta_h[m]$		21.15		19.47		12.43		17.60		15.62		23.43		28.79	
c_1	c_2	0.64	0.36	0.41	0.59	0.53	0.47	0.32	0.68	0.58	0.42	0.54	0.46	0.53	0.47
$\theta_{h,1}[m]$	$\theta_{h,2}[m]$	12.30	36.88	0.01	32.99	0.01	26.44	0.01	25.88	0.01	37.18	0.01	50.92	0.01	61.24
$\theta_v[m]$		0.89		0.64		0.90		0.60		0.58		0.48		0.52	
c_1	c_2	1.00	-	1.00	-	1.00	-	1.00	-	1.00	-	1.00	-	1.00	-
$\theta_{v,1}[m]$	$\theta_{v,2}[m]$	0.89	-	0.64	-	0.90	-	0.60	-	0.58	-	0.48	-	0.52	-

Perpendicular Lines

Both clay layers have been analysed for their spatial variability in the perpendicular direction, with calculations made for the complete lines and the two sections: one underneath the dyke and one in the polder.

For both clay layers the horizontal correlation of only one section underneath the dyke could not be calculated, which was the CPT line from 74 to 95. The results for the complete perpendicular lines of the complete

Table 4.8: The scales of fluctuation for the parallel lines of the clay layer without the additional layer

CPT Line		1		2		3		4		5		6		7	
$\theta_h[m]$		41.29		33.67		25.37		26.74		31.79		28.26		30.15	
c_1	c_2	0.28	0.72	0.34	0.66	0.41	0.59	0.39	0.61	0.53	0.47	0.53	0.47	0.52	0.48
$\theta_{h,1}[m]$	$\theta_{h,2}[m]$	0.01	57.34	0.01	51.01	0.01	42.99	0.01	43.83	0.01	67.63	0.01	60.12	0.01	62.80
$\theta_v[m]$		0.57		0.48		0.53		0.57		0.50		0.43		0.51	
c_1	c_2	1.00	-	1.00	-	1.00	-	1.00	-	1.00	-	1.00	-	1.00	-
$\theta_{v,1}[m]$	$\theta_{v,2}[m]$	0.57	-	0.48	-	0.53	-	0.57	-	0.50	-	0.43	-	0.51	-

clay layer show a larger correlation length for three lines at which the additional layer is identified than at the other lines. Except for two of these largest θ_h , all other horizontal correlations can be divided into a smaller and larger horizontal scale of fluctuation, of which the $\theta_{h,1}$ is smaller than the shortest lag distance for all lines. For the clay layer without the additional layer, most results are almost identical to the complete clay layer, because the trend removal is only changed slightly without the additional layer. One difference is that the lines at which the additional layer has been removed now show double horizontal scales of fluctuation with $\theta_{h,1}$ smaller than the shortest lag distance.

The horizontal correlations of the sections show almost no difference between both clay layers, because the additional layer did not occur at these sections. The small difference is due to a slightly different trend removal. Most horizontal scales of fluctuation show a single θ_h or small weighting factor $c_1 \leq 0.06$, except for the centre lines (39 to 91 and 90 to 6) at which c_1 is larger. The general trend is that underneath the dyke the horizontal correlation lengths are shorter.

For the complete perpendicular lines of the complete clay layer, the two largest θ_v are found at the lines where the additional layer is identified. Without the additional layer the vertical correlation lengths at those lines are reduced by approximately 40%. For both clay layers there is just one line that shows double vertical scales of fluctuation. Without the results of the lines at which two large vertical correlation lengths were found, the average θ_v for the complete layer is equal to 0.50m and for the clay layer without the additional layer to 0.48m. This shows that the difference in trends causes marginal change in the vertical scales of fluctuation, while the removal of the additional layer itself caused large changes in the results.

For the perpendicular sections under the dyke and in the polder the differences between vertical scales of fluctuation for both clay layers are irrelevant, since the only difference is a slight change in trends that have been removed. Most correlations are single θ_v , with little difference between the polder, with a mean of 0.46m for the complete clay layer and of 0.43m for the clay layer without the additional layer, and the dyke, with a mean of 0.43m for the complete clay layer and of 0.44m for the clay layer without the additional layer.

Diagonal Lines

The diagonal lines under an angle to the right show similar horizontal correlation results for both clay layers, with all but one result indicating that the values of $\theta_{h,1}$ are smaller than the shortest lag distance. The single line that goes through the zone with the additional layer shows the single correlation length, and after removal of the additional layer this layer shows a double correlation length of which the average θ_h is lower. Similar observations are made for the vertical correlation lengths. Both layers show mostly single vertical scales of fluctuation with almost no difference between the clay layers, except for the single line that crosses the additional layer. For that layer the θ_v is halved after removing the additional layer.

Under an angle to the left the diagonal lines show a notable difference in horizontal correlation length after removing the additional layer, compared to the complete clay layer. In all but one cases the $\theta_{h,1}$ is smaller than the shortest lag distance, but c_1 increased after removing the additional layer for the three lines that cut through the additional layer. This results in larger $\theta_{h,2}$ values for two of those lines, but for one it becomes smaller after removing the additional layer. Regarding the vertical scales of fluctuation, the three lines crossing the additional layer show a reduction in θ_v after removing the additional layer, while the other lines remain almost unchanged.

4.4.3. Spatial Variability of the Second Peat Layer

The spatial variability of the clay layer is investigated in the same steps as the other layers. First the θ_v of the individual CPTs will be analysed. Afterwards, the results of the spatial variability in horizontal and vertical direction will be shown for the lines of CPTs shown in Figure 4.20.

Individual CPTs

The results for the second peat layer can be found in Figure E.4 and Table E.10. A more comprehensive summary is shown in the histograms of Figure 4.31, of which the bin width has been set to 0.05m.

The first observation from the results of the second peat layer is that the correlation lengths are approximately half those found at the first peat layer. The second observation is that there is almost no difference in results of the polder and those in the proximity of the dyke. It is expected that either the amount of data available was too little to calculate the actual correlation length, since the layer has a thickness of just 40 to 60 centimetres, or that the overburden pressure of the soil layers on top of the second peat layer compressed the peat layer, causing a decrease of the vertical correlation length.

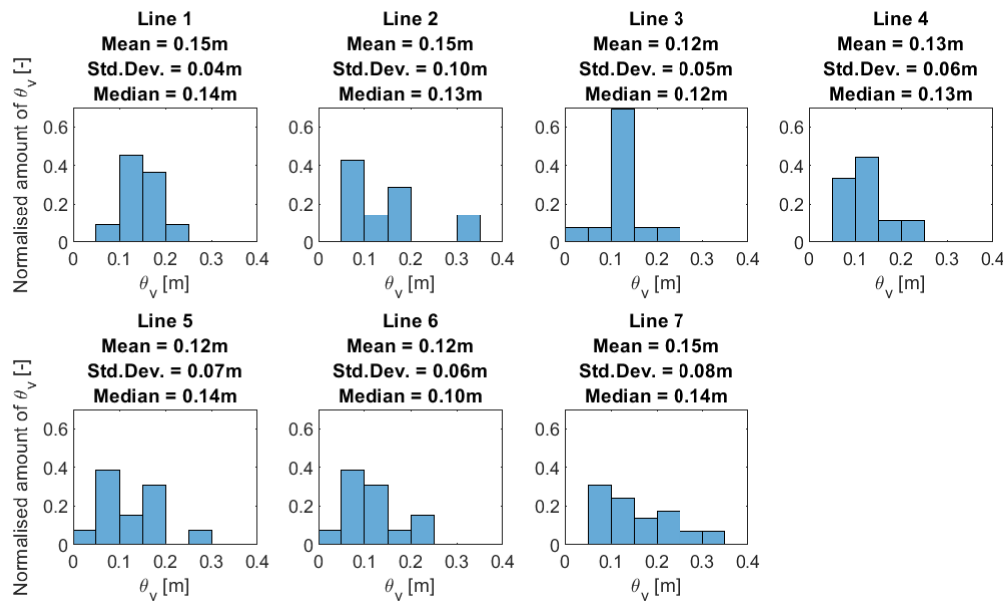


Figure 4.31: The vertical scales of fluctuation of the single CPTs for the second peat layer, per line

Lines of CPTs

The results of the spatial variability of the first peat layer can be found in Table E.11 and Figure E.8.

Table 4.9: The scales of fluctuation for the parallel lines of the second peat layer

CPT Line		1		2		3		4		5		6		7	
$\theta_h [m]$		-		-		-		3.51		-		-		-	
c_1	c_2	-	-	-	-	-	-	0.76	0.24	-	-	-	-	-	-
$\theta_{h,1} [m]$	$\theta_{h,2} [m]$	-	-	-	-	-	-	0.01	14.59	-	-	-	-	-	-
$\theta_v [m]$		0.55		0.25		0.67		0.15		0.37		0.17		0.34	
c_1	c_2	0.24	0.76	0.55	0.45	0.26	0.74	1.00	-	0.25	0.75	1.00	-	1.00	-
$\theta_{v,1} [m]$	$\theta_{v,2} [m]$	0.07	0.70	0.15	0.37	0.05	0.89	0.15	-	0.08	0.47	0.17	-	0.34	-

Parallel Lines

For the lines parallel to the dyke the scales of fluctuation are shown in Table 4.9. It is observed that for the second peat layer the horizontal ACF dropped below Bartlett's limit within three data points for all lines except CPT line 4. The results of the horizontal correlation length of that line show that the θ_h is lower at that location than the horizontal scales of fluctuation in the polder of other soil layers, due to a large weighting factor of the $\theta_{h,1}$, which is once again smaller than the shortest lag distance.

Most of the vertical scales of fluctuation are smaller than those found at the first peat layer. This is true for the single θ_v that were found, but the values of $\theta_{v,2}$ are smaller at the second peat layer as well. There is not a clear difference between the vertical scales of fluctuation found in the polder and underneath the dyke, similar to the results of the individual CPTs of the second peat layer.

Perpendicular Lines

The second peat layer has been analysed for its spatial variability in the perpendicular direction over the entire domain, but also for the sections underneath the dyke and in the polder.

Just two horizontal correlation lengths could be calculated. Over the entire domain this resulted in an approximately single vertical scale of fluctuation of 5.19m. The other horizontal scale of fluctuation was found at the centre section of the polder, and could be split into a $\theta_{h,1}$ smaller than the shortest lag distance and a $\theta_{h,2}$ of 8.89m. For the sections underneath the dyke it was not possible to calculate a horizontal correlation length.

The vertical scales of fluctuation in the perpendicular direction show two θ_v values that are more than three times as large as the third-largest vertical scale of fluctuation. Without the large values, the mean θ_v is equal to 0.19m, three times smaller than the average of the first peat layer in perpendicular direction. For the sections in the polder one larger θ_v is found of 0.99m and a large θ_v of 0.57m is also found underneath the dyke. Without the large values, the mean in the polder is equal to 0.13m and underneath the dyke the mean is 0.18m.

Diagonal Lines

For the diagonal lines to the left it was not possible to calculate a horizontal scale of fluctuation. For the diagonal lines in the other direction it was possible to calculate it at two locations. Both lines resulted in a $\theta_{v,1}$ smaller than the shortest lag distance with a relatively large weighting factor. The values of $\theta_{v,2}$ were found to be 14.20m and 18.14m.

When double vertical scales of fluctuation were found, the lines in both diagonal directions showed a $\theta_{v,1}$ of 0.01m to 0.09m, much smaller than the results of other layers. The range of $\theta_{v,2}$ and the single θ_v show no clear trend for both diagonal directions.

4.5. Discussion

Outlier and trend removal of the clay layer

For the linear trends of the peat layers, a robust method of identifying and removing both the outliers and the trends has been used. This is a reproducible method and not influenced by any engineering judgement. The clay layer did not follow a normal distribution, but a log-normal distribution after quadratic trend removal. Since the methods to identify the outliers of the peat layers are applicable to normally distributed data, they could not be applied to the clay layer. The outlier identification and removal of the clay layer was done manually, based on engineering judgement. In order to create a reproducible method, a robust non-linear regression method should be applied to the clay layer.

Spatial variability of the Leendert de Boerspolder

A general trend that is observed for almost all horizontal scales of fluctuation is that when the average θ_h can be split into two scales of fluctuation, the $\theta_{h,1}$ is smaller than the shortest lag distance. This minimum lag distance (τ_{min}) is different for each line of CPTs, but underneath the crest of the dyke, where $\tau_{min} = 1.25m$, this trend was found as well. It appeared that in order to determine the horizontal scales of fluctuation in the Leendert de Boerspolder exactly, the cone penetration tests should have been made in a denser grid.

The first peat layer

The results of the first peat layer showed a decrease of the parallel θ_h and θ_v from the toe of the dyke to the crest of the dyke. The reduction in scales of fluctuation from CPT line 6 to line 7 was more than 60%. Underneath the crest of the dyke this reduction is likely caused by vertical compression of the peat layer due to the overburden pressure of the dyke. Underneath the slope and at the toe of the dyke it is expected that the change is due to this compression as well, but an additional influence of rotation at these locations caused a slight increase of the vertical scales of fluctuation. In the direction perpendicular to the dyke, it was hardly possible to calculate any horizontal scale of fluctuation. It is hypothesised that this is due to the difference in stress history between the dyke and polder zones or due to deposition history of the peat, since different types of plants could have grown at different distances from the water. For the vertical scales of fluctuation perpendicular to the dyke, it was found that the θ_v in the polder were slightly lower than underneath the dyke, possibly indicating an increase under the dyke due to slight rotation. From the diagonal lines no clear conclusions could be drawn.

The clay layer

The results of the complete clay layer showed lower values of θ_v underneath the dyke than in the polder for the individual CPTs. Parallel to the dyke it was found that the horizontal scales of fluctuation decrease from line 1 to 4 and then drastically increase from the toe to the crest of the dyke. The overburden pressure of the dyke may have compressed the dyke to a more horizontally uniform layer. The θ_v parallel to the dyke show lower values underneath the dyke than in the polder, possibly due to vertical compression from the dyke. Underneath the crest the values are higher than underneath the slope, likely caused by slight rotation. In the perpendicular direction the θ_h underneath the dyke is lower, due to rotation, but on the other hand the horizontal scales of fluctuation show almost no difference between the dyke and the polder. From the diagonal lines no clear conclusions could be drawn.

The clay layer without the additional layer

When removing the additional layer from the clay layer, most of the overall findings are the same. However, the main difference is that much of the spread in the results is reduced. Without the additional layer, the parallel lines show a larger θ_h , especially at the toe of the dyke, and the θ_v at all CPT lines 1 to 6 are reduced. In the perpendicular direction most results are almost identical to the complete clay layer, because the trends that have been removed from the CPTs are changed just slightly. At the perpendicular lines where the additional layer was removed, the vertical correlation length is shorter and the horizontal correlation length is longer. From the diagonal lines no clear conclusions could be drawn.

The second peat layer

The results of the second peat layer show that the horizontal scales of fluctuation can hardly be calculated. This might be due to the deposition history of the peat layer, but also due to the little data that is available from the thin peat layer. The vertical scales of fluctuation showed no notable difference over the area, but compared to the first peat layer the θ_v of the second peat layer are much smaller.

Influence of the Dyke on the Spatial Variability

The spatial variability of the Leendert de Boerspolder has been influenced by the man-made structure. From the assumed deformations it is expected that vertical compression of the soft soil layers leads to a decrease of the vertical scale of fluctuation. No clear conclusion can be made regarding the change in horizontal scale of fluctuation due to vertical compression, since the results for the clay layer with and without the additional layer are different. Rotation is expected to lead to an increase of the vertical scale of fluctuation and a decrease of the horizontal scale of fluctuation. Even though rotation does not influence the scales of fluctuation of the peat layer underneath the crest, it is expected that it does influence the scales of fluctuation of the clay layer underneath the crest. Finally, it is expected that there is no influence of the man-made structure on the spatial variability of the second peat layer.

In Chapter 5 a finite element analysis of the Leendert de Boerspolder will result in the deformations that occur in the area. These findings will confirm or deny the expectations that have been given here.

Layout of the CPT grid

For the purpose of this research a more efficient grid of CPTs could have been used. Some interesting observations may be made by comparing the perpendicular sections underneath the dyke with those in the polder. Currently, the findings for the perpendicular sections in this research are based on just three sections of CPTs in the polder, and five underneath the dyke, because at all other locations there were just two CPTs available. It would have been favourable if there were more perpendicular lines of three or more CPTs in the polder and underneath the dyke.

5

Linking Theory and Practice

Two studies have been undertaken so far. In Chapter 3 the change in spatial variability due to deformations of random fields was calculated, resulting in expected changes in the spatial variability for the different deformations that occur in the proximity of a dyke. Chapter 4 continued with the investigation of the scales of fluctuation of the Leendert de Boerspolder and resulted in the conclusion that the influence of the dyke on the spatial variability of the soft soil layers could be seen. This chapter will continue with a third study, making use of the finite element software Plaxis. A two-dimensional plane strain analysis of the dyke at the Leendert de Boerspolder will be made in order to find the deformations that have taken place in the soft soils of the Leendert de Boerspolder. The resulting deformations will be linked with the results of the random fields and the results of the spatial variability of the Leendert de Boerspolder to draw the final conclusions of this research.

5.1. Deformations from a Finite Element Analysis

Before it is possible to obtain the deformations from the finite element analysis in Plaxis, the input parameters of the soil layers have to be defined. Afterwards, the finite element model should be set up in such a way that it represents the stress history of the Leendert de Boerspolder. When everything is defined properly, the finite element analysis can be run in Plaxis to determine the deformations. The main steps will be discussed in this section.

5.1.1. Input Parameters

The first step of setting up the finite element model in Plaxis is to define the soil parameters. Lab tests have been carried out for the research of de Gast (2019). From this research it is known that failure of the dyke would occur through the first peat layer and the (organic) top part of the clay layer, which is the reason that only these soil layers will be modelled. The soil parameters are summarised in Table 5.1.

In order to retrieve the correct deformations in the soft soil layers, a more advanced soil model than the Mohr-Coulomb model has to be used for these layers. The choice is made for the Soft Soil model, which requires two additional parameters: the one-dimensional swelling index (C_s) and the one-dimensional compression index (C_c) of the soil. Since no test data is available to base the values of the parameters on, Table 2.b of Eurocode 7 (2016) will be used to obtain reasonable parameters. Assuming an initial void ratio (e_0) equal to 0.5, the Soft Soil parameters of the peat layer are taken from the soft peat, being $C_c = 0.69$ and $C_s = 0.23$. The Soft Soil parameters of the organic clay layer are taken from the organic, moderate clay, being $C_c = 0.35$ and $C_s = 0.12$.

For the dyke material the Mohr-Coulomb soil model will be sufficient, since the dyke is only responsible for the overburden pressure on top of the soft soil layers.

5.1.2. The Finite Element Model

The set up of the finite element model can be found in Appendix F. This section will treat the results of the finite element analysis.

The results of the total displacements $|u|$ are shown in Figure 5.1. The results of the vertical deformations from the FEM are compared with the depth at which the layers are found in the polder in Table 5.2. It is

Table 5.1: The soil parameters for the Plaxis soil model, after de Gast (2019) and Eurocode 7 (2016)

	γ_d [kN/m ³]	γ_{sat} [kN/m ³]	c' [kPa]	ϕ' [deg]	E [kPa]	ν [-]	$k_{x,y}$ [m/day]	C_c [-]	C_s [-]
Dyke material	13.0	18.0	5.0	33.0	5600	0.30	$3.46 \cdot 10^{-1}$	-	-
Peat	9.0	10.0	2.5	28.8	1700	0.30	$4.10 \cdot 10^{-2}$	0.69	0.23
Organic clay	14.5	15.0	4.4	29.5	5200	0.35	$7.52 \cdot 10^{-4}$	0.35	0.12

found that the finite element analysis underestimated the vertical settlement of the layers. This is attributed to the soil model that is used for the peat and clay layers, since the Soft Soil model does not take secondary consolidation or creep into account. It is expected that the Soft Soil Creep model will estimate settlements that resemble the situation in the Leendert de Boerspolder with more accuracy. However, the results of the finite element analysis will not be used quantitatively, but a qualitative analysis of the deformations will be made in order to compare the results of the random fields and the results of the finite element analysis with the results of the spatial variability of the Leendert de Boerspolder. Therefore the results that are currently found are deemed good enough.

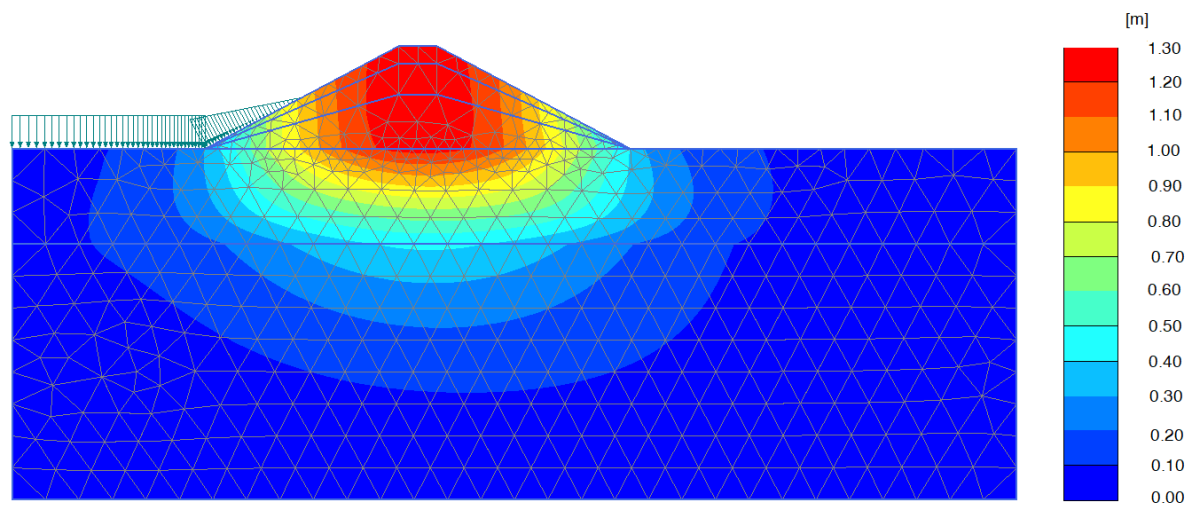


Figure 5.1: The results of the total displacements after the final analysis stage in Plaxis

Table 5.2: The resulting layer depths of the FE analysis compared to the depths found at the Leendert de Boerspolder

	Crest		Slope		Toe	
	Polder	FEM	Polder	FEM	Polder	FEM
Top peat [m+NAP]	-3.47	-3.12	-2.94	-2.84	-2.33	-2.12
Top clay [m+NAP]	-5.29	-4.81	-5.05	-4.72	-4.76	-4.51

In order to retrieve the deformations that occurred at the different layers, the total displacements can be visualised as arrows that point in the direction of the displacement. The results of the analysis are shown in Figure 5.2. The results show that due to the water pressure on the dyke, the total displacements of the peat and the organic clay layer underneath the crest of the dyke show not only vertical displacement, but also some horizontal displacement. Underneath the slope of the dyke the contribution of the horizontal displacement to the total displacement is larger than underneath the crest, and at the toe of the dyke it is larger than underneath the slope. In the polder at approximately 5 meters from the toe the influence of the dyke is almost reduced to nothing.

5.2. Results of the Peat Layer

The deformations of the finite element analysis can be combined with the results of the random fields and the calculated spatial variability of the Leendert de Boerspolder to give more insight into the influence of the man-made structure on the spatial variability of the soft soil layers of the Leendert de Boerspolder. The comparison will be made for three zones: the crest, the slope and the toe. The FE analysis showed little to no

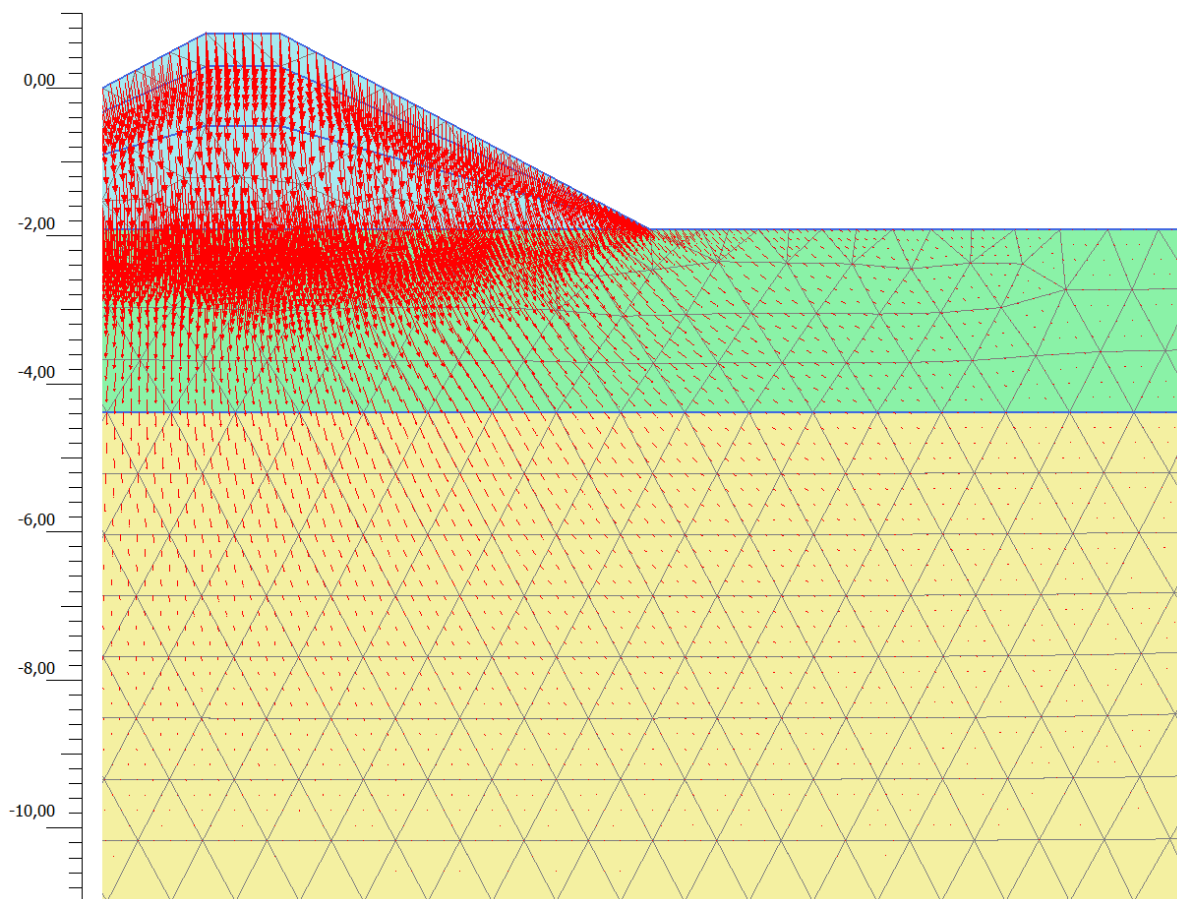


Figure 5.2: The results of the total displacements after the final analysis stage in Plaxis, with the displacements visualised by arrows

deformations in the polder for both soil layers, suggesting that the spatial variability that has been calculated in the polder can be interpreted as the original spatial variability before the dyke was constructed.

5.2.1. Underneath the Crest

Figure 5.3 summarises the deformations of the FE analysis underneath the crest of the dyke. The results showed a vertical displacement (u_y) equal to -1.23m at the top of the peat layer and equal to -0.41m at the bottom of the peat layer. The difference in settlement indicates a vertical compression of the peat layer, which is expected to lead to a decrease of the vertical scale of fluctuation, as shown by the deformation of random fields in Section 3.3. The results of the spatial variability of the Leendert de Boerspolder indicated that the vertical scale of fluctuation in the polder varied for the parallel lines that have been investigated. Comparing the average θ_v of the polder area, which is equal to 0.77m , to the θ_v found underneath the crest of the dyke, equal to 0.46m , it is concluded that the FE analysis confirms the findings that the overburden pressure of the dyke decreased the vertical scale of fluctuation underneath the crest of the dyke.

The horizontal displacements (u_x) of the FE analysis show that the contribution of the horizontal displacement to the total displacements is smaller than the contribution of the vertical displacement. Almost all horizontal displacement occurs due to the water pressure on one side of the dyke, as seen from the increase of u_x at the end of the analysis. Nonetheless, the horizontal displacement at the top of the peat layer is equal to 0.10m and at the bottom of the peat layer equal to 0.07m , showing a small amount of shear between the top and bottom of the peat layer. By applying simple shear deformation to the random fields, it was found that the horizontal scale of fluctuation decreases slightly. By comparing the horizontal deformations at the crest with those at the slope of the dyke, shown in Figure 5.4, it was found that the horizontal displacement at the slope was larger than underneath the crest of the dyke, indicating some extension of the peat layer. Since horizontal compression led to a decrease of the horizontal scale of fluctuation in the random fields, it is expected that extension leads to an increase of the horizontal correlation length. From the spatial variability

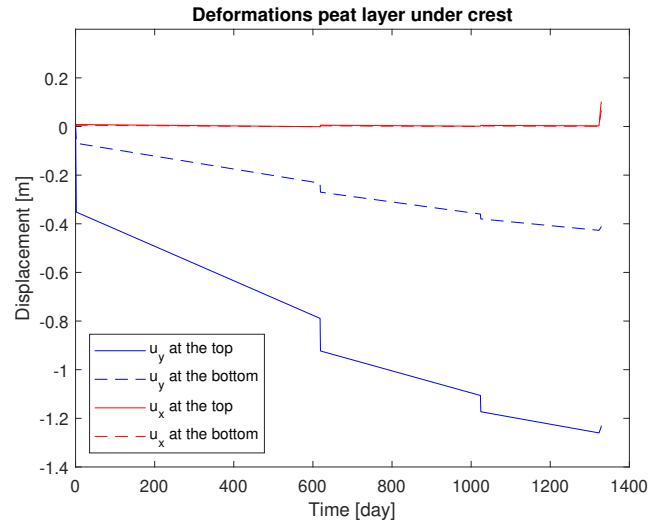


Figure 5.3: The results of the displacements in the peat layer underneath the crest of the dyke

of the Leendert de Boerspolder it is known that the θ_h underneath the crest of the dyke is smaller than in the polder. Since the simple shear mechanism would decrease θ_h and extension would increase it, the correlation length should remain more or less unchanged. However, the vertical compression of the random fields resulted in a decrease of θ_h as well, tipping the scale in favour of a lower θ_h underneath the crest than in the polder. It is concluded that the influence of the dyke results in a low θ_h underneath the crest of the dyke.

5.2.2. Underneath the Slope

The resulting FE deformations of the peat layer underneath the slope of the dyke are summarised in Figure 5.4. Compared to the deformations underneath the crest, it is found that the contribution to the total deformations of u_y decreased and the contribution of u_x increased.

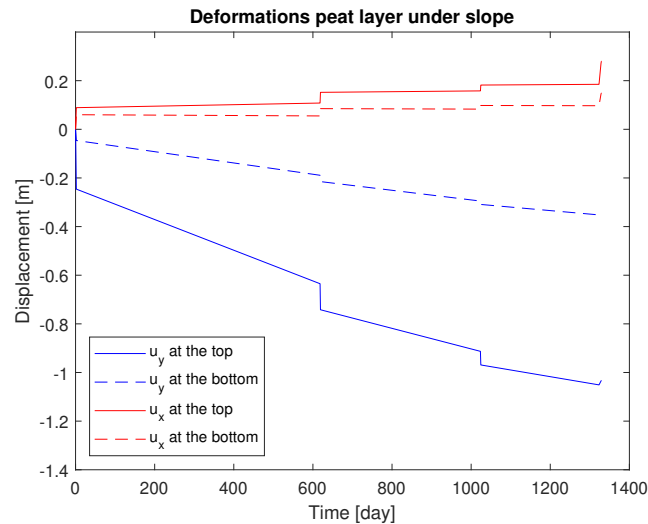


Figure 5.4: The results of the displacements in the peat layer underneath the slope of the dyke

The vertical displacements of the peat layer underneath the slope of the dyke are equal to -1.03m at the top and -0.34m at the bottom of the layer. According to the change in spatial variability due to vertical compression of random fields, the compression should show a lower vertical scale of fluctuation underneath the slope than in the polder. However, the amount of vertical compression is less than underneath the crest, so the θ_v underneath the slope should be larger than underneath the crest of the dyke. From the spatial variability of the Leendert de Boerspolder it was found that θ_v underneath the slope is larger than underneath the

crest of the dyke, but it is also larger than the values found in the polder, due to a relatively large contribution of $\theta_{v,2}$ underneath the slope. For the values of $\theta_{v,1}$ the theory confirms the influence of the vertical compression due to the dyke. The larger $\theta_{v,2}$ value can likely be attributed to rotation, which is found by investigating the direction of the total displacement ($|u|$) underneath the slope of the dyke.

The horizontal deformations at the top of the peat layer are equal to 0.28m and at the bottom equal to 0.15m according to the FE analysis. Approximately 33% of the total horizontal displacement is caused by the increase of water level at the end of the analysis. Similar to the situation underneath the crest, shear is found underneath the slope, but a larger amount of it. By investigating the horizontal displacement underneath the crest and at the toe of the dyke, it is found that the section of the peat layer underneath the slope also extended. The direction of the total displacements indicates rotation underneath the slope of the dyke. From the spatial variability of the Leendert de Boerspolder it was found that the θ_h underneath the slope was similar to the horizontal correlation length in the polder. However, the $\theta_{h,2}$ underneath the slope is smaller than all other values, except for the one underneath the crest of the dyke. It is concluded that the influence of the dyke decreased the $\theta_{h,2}$, but increased its weighting factor in the overall θ_h underneath the slope of the dyke.

5.2.3. Underneath the Toe

At the toe the finite element analysis resulted in deformations in the peat layer that have been summarised in Figure 5.5. Compared to the results underneath the crest and slope of the dyke, the vertical deformations have decreased to -0.45m at the top of the peat layer and -0.19m at the bottom, and the horizontal deformations at the top have increased to 0.32m while at the bottom it remained equal to underneath the slope, which was 0.15m. Nonetheless, this indicates that the relative horizontal contribution to the total deformations has increased in comparison to underneath the crest and slope of the dyke.

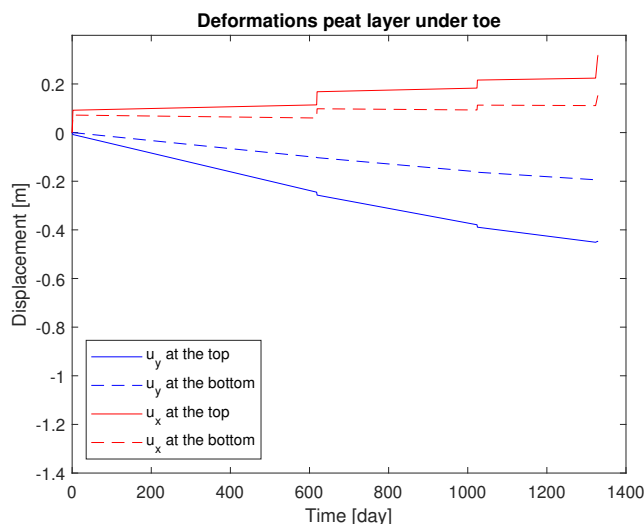


Figure 5.5: The results of the displacements in the peat layer underneath the toe of the dyke

The difference in vertical settlement at the top and bottom indicates once more that a certain amount of vertical compression took place. Due to the small ratio of vertical displacement compared to the horizontal displacement, it is likely that rotation plays a larger role at the toe than underneath the crest and slope of the dyke. From the random field deformations it is expected that the vertical compression reduced the vertical correlation length and rotation increased it. The vertical scales of fluctuation at the Leendert de Boerspolder show that compared to the results underneath the slope, the $\theta_{v,1}$ has increased and $\theta_{v,2}$ has decreased, due to the rotation and compression respectively. Compared to the results in the polder, both the small and large vertical scales of fluctuation at the toe are somewhat smaller. It is concluded that influence of the dyke decreased the θ_v in relation to the polder, but in relation to the slope and crest the decreased vertical influence of the dyke let the θ_v be larger.

At the toe of the dyke, approximately 28% of the horizontal displacement is due to the increased water level at the end of the analysis. The difference in horizontal displacement at the toe for the top and bottom of the peat layer shows more shear than at the other investigated locations. Combined with the ratio of vertical to horizontal displacements, it is once more expected that rotation plays a role at the toe. Taking into account

that the horizontal displacement at the toe of the dyke is such that towards the side of the dyke it is extended and towards the side of the polder it is compressed, the horizontal scale of fluctuation is expected to increase as well as decrease from the results of the random field deformations. In the Leendert de Boerspolder the results showed that the weighting factor of $\theta_{h,1}$ (where $\theta_{h,1} < \tau_{min}$) increased, and that the length of $\theta_{h,2}$ increased. However, the results were comparable to the horizontal scales of fluctuation calculated in the polder, leading to the conclusion that the dyke has a small influence on the horizontal results at the toe.

5.3. Results of the Organic Clay Layer

A similar analysis can be made for the organic clay layer. In the Leendert de Boerspolder the clay layer is found between -4.37m+NAP and -10.81m+NAP, with an average thickness throughout the area of approximately six meters. Since the change from an organic clay layer at the top to a silty clay at the bottom is a gradual change, the assumption is made that the organic clay layer ends halfway through the clay layer. Therefore, the deformations of the top three meters of the organic clay layer of the FE analysis will be used for the comparison.

5.3.1. Underneath the Crest

The results of the finite element analysis are summarised in Figure 5.6. Compared to the results of the peat layer, the displacements are much smaller, indicating less influence of the dyke on the clay layer than on the peat layer. The vertical displacement at the top of the clay layer is equal to -0.41m and three meters in the clay layer u_y is equal to -0.14m. In the horizontal direction a displacement of 0.07m is found at the top and a horizontal displacement of 0.04m is found at the bottom.

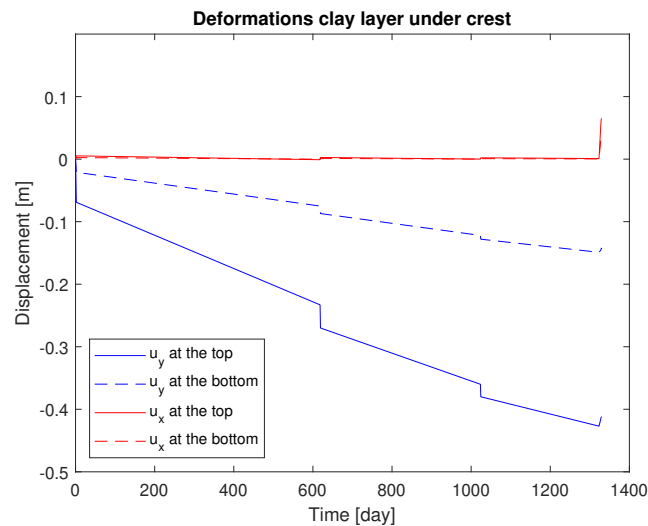


Figure 5.6: The results of the displacements in the clay layer underneath the crest of the dyke

The difference in vertical deformations indicates that the top of the clay layer is compressed under influence of the dyke, which should lead to reduced vertical scales of fluctuation according to the random field deformations. The relatively large ratio between the vertical and horizontal displacements indicates that it is likely that rotation has had no to little influence on the clay layer underneath the crest. From the vertical scales of fluctuation of the entire clay layer of the Leendert de Boerspolder, it becomes clear that in comparison to the polder, the θ_v underneath the crest is lower, confirming the findings from the FE analysis and the random field deformations. However, when the additional layer is removed from the clay layer of the Leendert de Boerspolder, the vertical correlation lengths in the polder decrease. In the latter case, the difference in θ_v between the polder and the crest is less, but the average of the polder is slightly larger. It is concluded that the overburden pressure of the dyke reduced the vertical scale of fluctuation underneath the crest of the dyke, but the influence of the dyke is less than it was in the peat layer.

The horizontal displacements are almost entirely caused by the increase in water level at the end of the FE analysis. By investigating the horizontal displacement in the clay layer at the slope, it is found that the clay underneath the crest is extended, since the horizontal displacement at the slope is larger than underneath the

crest. The slight extension is expected to cause an increase in the horizontal scale of fluctuation, according to the random field deformations. From the horizontal correlations in the Leendert de Boerspolder for the entire clay layer it becomes clear that this minor extension may have lead to a larger θ_h under the crest than in the polder. For the clay layer without the additional layer the same conclusion can be drawn for the larger $\theta_{h,2}$, but for the average θ_h the correlation length underneath the crest of the dyke is smaller than the average of the polder. It is concluded that the influence of the dyke in the clay layer underneath the crest is only due to the change in water pressure, and has almost no effects on the horizontal scale of fluctuation for the clay layer without the additional layer.

5.3.2. Underneath the Slope

Figure 5.7 shows a summary of the displacements retrieved from the FE analysis of the clay layer underneath the slope of the dyke. The displacements in the vertical direction resulted in -0.34m at the top and -0.12m three meters in the organic clay layer. The horizontal displacements resulted in 0.15m and 0.07m respectively.

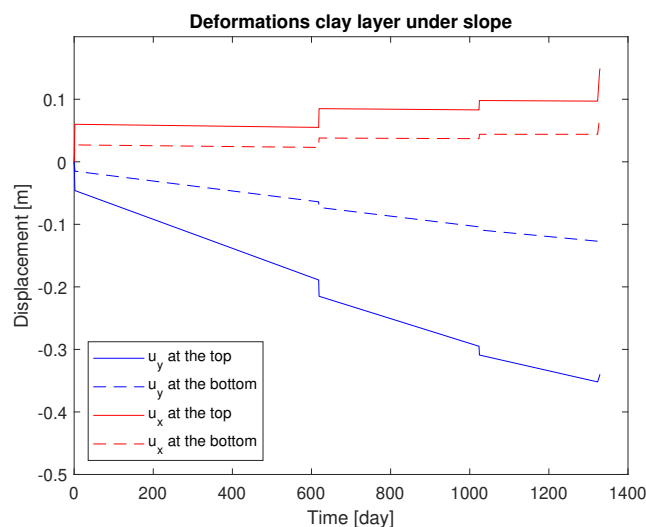


Figure 5.7: The results of the displacements in the clay layer underneath the slope of the dyke

The vertical displacement of the clay layer underneath the slope shows a compression of the layer, but the vertical compression is less than underneath the crest of the dyke. However, the results of the vertical scale of fluctuation in the Leendert de Boerspolder show that underneath the slope of the dyke both the clay layer with and without the additional layer show the shortest correlation length. It was hypothesised that rotation underneath the crest would be the cause of the difference, but this has not been found from the FE analysis. An explanation may be found in the fact that the clay layer of the Leendert de Boerspolder has been analysed over the complete depth, while the FE analysis only analysed the top part of the clay layer. Another cause for the difference in results underneath the crest and slope may be found from local abnormalities that occurred over the history in the soil which have not been taken into account.

The increase of the water level is responsible for approximately 40% of the total horizontal displacement. The total horizontal displacement shows no compression or extension relative to the soil at the toe, but there is some extension at the side of the crest. Furthermore, a small amount of shear is found from the difference between the top and bottom of the investigated section of organic clay. From the random field deformations it is expected that, relative to the polder, the horizontal scale of fluctuation is larger underneath the slope due to extension, although the shear may have reduced the θ_h . The horizontal scale of fluctuation found underneath the slope for the entire clay layer of the Leendert de Boerspolder is larger than the θ_h in the polder, but without the additional layer the results underneath the slope are comparable with the polder area. It is concluded that it is likely that another mechanism, such as rotation, caused a decrease in the horizontal correlation length in relation to the θ_h underneath the crest. Compared to the polder, no clear conclusion can be made, since with or without the additional layer creates a large difference in the analyses and results.

5.3.3. Underneath the Toe

The horizontal and vertical displacements of the clay layer at the toe of the dyke are summarised in Figure 5.8. The vertical displacement at the top is equal to -0.19m and at three meters deep into the clay layer the vertical displacement is equal to -0.08m. In the horizontal direction the top of the clay layer displaced by 0.15m and three meters deep in the clay layer the horizontal displacement is equal to 0.08m.

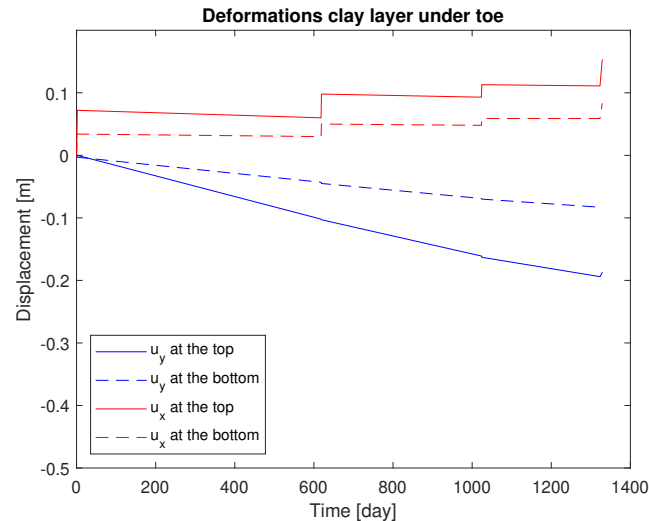


Figure 5.8: The results of the displacements in the clay layer underneath the toe of the dyke

The organic clay layer shows some vertical compression, as seen from the difference between the vertical displacement at the top and bottom of the investigated section, resulting in a lower vertical scale of fluctuation relative to the polder. However, the horizontal and vertical displacement are almost identical, hinting that some rotation occurred at this location, causing an increase in the vertical scale of fluctuation. From the results of the Leendert de Boerspolder it is found that for both the entire clay layer and the clay layer without the additional layer, the θ_v is smaller at the toe than in the polder, but larger or equal to the vertical correlation length underneath the crest. It is concluded that the dyke influences the vertical scale of fluctuation in the clay layer by a decrease due to the vertical compression and an increase due to rotation.

The increase of the water level is responsible for approximately 29% of the total horizontal displacement. Since the soil in the polder is hardly displaced at all, the soil at the toe is horizontally compressed. Combined with the rotation, this leads to a decreased θ_h compared to the polder, which is confirmed by the average horizontal scale of fluctuation underneath the toe and those in the polder. However, the spatial variability of Leendert de Boerspolder showed a $\theta_{h,2}$ that is larger than the values in the polder for both the entire clay layer and the clay layer without the additional layer. It appears that the deformations that occur at the toe in the clay layer increase the weighting factor of the small horizontal scale of fluctuation, thereby reducing the average θ_h , but increase the length of $\theta_{h,2}$. These findings cannot be confirmed from the deformations of the random fields. It is concluded that the influence of the dyke in the clay layer underneath the toe results in rotation and compression of the soil, thereby increasing c_1 and $\theta_{h,2}$, but decreasing the overall θ_h .

5.4. Account for Changes in Spatial Variability within the RFEM

The research into the influence of man-made structures on the spatial variability of soft soils has led to the conclusion that at different locations near the dyke its influence causes a changes in the spatial variability of the soft soil layers. The differences in spatial variability should be taken into account when assessing the man-made structure for its safety in order to obtain the most realistic outcome of the analysis. This section will discuss two methods by which the influence of the dyke on the spatial variability could be taken into account in the random finite element method. This can be used as a starting point for future research in order to point out what the difference in reliability of the structure is when accounting for the change in spatial variability.

The first method creates a finite element model in which the soil layers are modelled at the depth at which they were found at the time of the soil investigation. For each of the soil layers the spatial variability that has

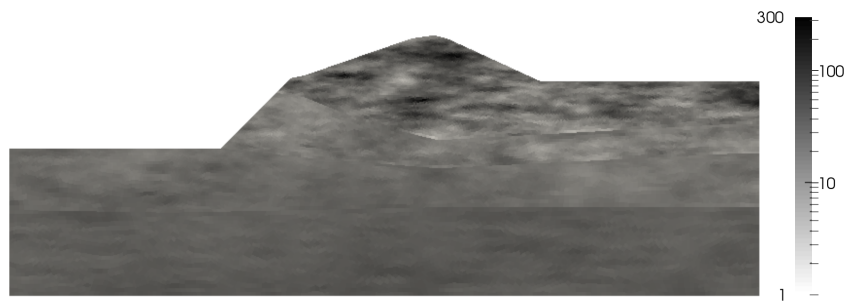


Figure 5.9: An example of an RFEM realisation of the dyke at the Leendert de Boerspolder, with the undrained shear strength as spatially random parameter on a logarithmic scale in kPa, after de Gast et al. (2018a)

been estimated from the soil investigations is used to generate random fields of the material properties of the soil layers. Research by de Gast et al. (2018a) analysed a case study at the Leendert de Boerspolder by using the RFEM. The researchers assumed that the undrained shear strength was the only spatially random parameter. One of the RFEM realisations is shown in Figure 5.9. However, the spatial variability of the soil layers was assumed not to change under influence of the dyke, resulting in a single spatial variability per soil layer. By dividing the soil layers in different zones, for example a zone where the dyke influences the spatial variability of the soil and a zone where the dyke has not influenced the spatial variability, a more accurate representation of the reality is obtained which can be used to analyse the change in reliability of the structure due to a difference in spatial variability. There are, however, several downsides to this method. The spatial variability of a random field is not exactly equal to the input spatial variability from which the field is generated. The difference between the random field spatial variability of the zones of a soil layer could result in a bias in the results, since the failure may pass through one zone within the soil layer more easily than through the other, or because the strong and weak regions of soil at the boundary of the zones do not align. Another downside is that there would still be averaging of the spatial variability over the zones and that the location of the zones has to be determined by the person using the RFEM.

The second method should be able to cope with the downsides of the previous method. The model will be based on the stress history of the soil. At the start of the analysis, the finite element model will consist of the soil layers without the man-made structure. The spatial variability of each of the soil layers is estimated from the soil investigation in the polder, sufficiently far from the dyke such that the structure has had no influence on the spatial variability. The next steps in the FE analysis construct the dyke, allowing it to influence the spatial variability of the soft soil layers in the proximity of the dyke, until the soil layers in the model are at the depth at which they were found in the site investigation. The average spatial variability of the soft soils in the proximity of the dyke after construction of the dyke over all realisations is expected to be similar to the spatial variability estimated from the site investigation. Research is necessary to figure out whether this method results in the correct spatial variability. A downside of the second method is that the computation time in comparison to the first method is expected to be longer, due to the additional steps that need to be analysed before the actual safety of the dyke against failure can be calculated.

5.5. Discussion

Deformations of the finite element analysis

The results of the FE analysis were in line with the assumed deformations in Chapters 3 and 4. Underneath the crest of the dyke mainly vertical deformation was found, underneath the slope vertical deformation and rotation were found and underneath the toe the horizontal deformation became more significant, with vertical deformation and rotation being present as well. Approximately five meters from the dyke there was no influence on the polder, showing that CPT lines 1 to 4 of Figure 1.5 were not influenced by the dyke and can therefore be used as the baseline spatial variability of the polder.

However, the amount of deformation that occurred in the FE analysis was too little compared to the deformation of the soil layers found in the Leendert de Boerspolder, as shown in Table 5.2. This is caused by the Soft Soil model not taking creep or secondary consolidation into account. For future research it is advised to make use of the Soft Soil Creep model, which does take creep into account and should lead to more accurate deformations of the subsurface in the FE analysis. Since the results have been used qualitatively in this research, it is expected that the similar qualitative results will be obtained from an analysis that makes use of

the Soft Soil Creep model.

A significant amount of the horizontal displacement was caused by the water pressure of the increased water level. This horizontal deformation is not expected at all man-made structures, for example at a road embankment this water pressure will not be present, but since this research focussed on a dyke, the water pressure has had an influence on the horizontal displacement and therefore the horizontal scales of fluctuation.

The finite element model was set up without the presence of the silty clay layer and the second peat layer, because research by de Gast (2019) showed that the failure of the dyke only passed through those soil layers. At three meters depth in the organic clay layer of the FE analysis the vertical displacements were equal to -0.14m underneath the crest and -0.08m underneath the toe. The horizontal displacements were equal to 0.04m and 0.08m respectively. The deformations of the silty clay layer of the Leendert de Boerspolder have not been modelled and analysed, but from the results it is expected that small deformations due to the dyke could be present in the top of the silty clay layer.

Agreement between results

A comparison between the theoretical analyses and the estimated scales of fluctuation of the Leendert de Boerspolder was made to investigate the agreement between the results. Since the dyke hardly influenced the polder, the spatial variability of the polder was used as the baseline spatial variability to which the results were compared.

The peat layer showed good agreement between the different results. The vertical scales of fluctuation were found to decrease due to vertical compression and increase due to rotation. The influence of rotation was found to be less substantial in the peat layer than the vertical compression of the dyke, since the increase in $\theta_{v,2}$ due to rotation was countered by a decrease of its weighting factor c_2 , resulting in a decrease of the average θ_v . For the horizontal scales of fluctuation it was found that rotation leads to a decreased $\theta_{h,2}$ and an increase of its weighting factor c_2 . The horizontal deformation showed that extension of the peat layer occurred underneath the dyke, which was expected to lead to an increase of the horizontal scales of fluctuation. A third contribution to a change in the horizontal scales of fluctuation is that vertical compression is responsible for a decrease of the horizontal correlation length. Especially underneath the crest of the dyke the vertical compression has led to a decrease of the θ_h . The three mechanisms combined resulted in hardly any change of the θ_h underneath the slope and toe of the dyke compared to the polder, leading to the conclusion that the extension contributed to a larger change in horizontal scale of fluctuation than the rotation and vertical compression did at those locations.

The dyke caused less deformations in the organic clay layer than it did in the peat layer. Underneath the crest and toe reasonable agreement between the results of the investigations was found. A difference with the results of the peat layer was that the reduced influence of the dyke underneath the crest resulted in no change in the horizontal scale of fluctuation, because little vertical compression or horizontal deformation took place.

Underneath the slope of the dyke it was found that there was little agreement between the theoretical studies and the estimated horizontal and vertical scales of fluctuation of the organic clay layer. Since the spatial variability of the clay layer has been calculated over the entire depth of the clay layer, the resulting spatial variability is an average over the organic and silty clay within the clay layer. From the finite element analysis it was found that the influence of the dyke at the bottom of the organic clay layer would be small, leading to the assumption that in the silty clay layer almost no influence of the dyke would be present. It is possible that the spatial variability of the slightly different clay layers influenced the results in such a way that the influence of the dyke on the spatial variability at this location could not be determined correctly. In order to find out whether this is the case, the clay layer should be analysed as two layers, where one is the organic clay layer at the top half and the other is the silty clay at the bottom half.

Future research

The effect of the changes in spatial variability on the reliability analysis of the random finite element method are subject for future research. This research has presented a method by which the changes in spatial variability due to the influence of a man-made structure can be modelled in a random finite element analysis. The proposed method should be investigated for its effectiveness in modelling the spatial variability that is estimated from the field data. This could be done by extracting the soil data of the layers after the dyke has deformed the mesh and analysing that soil data for its spatial variability. By comparing those results to the spatial variability of the soil layers of the Leendert de Boerspolder a conclusion can be made about the effectiveness of the method.

6

Conclusions and Recommendations

The aim of this thesis was to research how the spatial variability of soft soils under a man-made structure is influenced by that man-made structure. Throughout this thesis several aspects of the subject have been researched and discussed. By combining the conclusions from the previous chapters, an answer to the research questions can be given. The overall conclusion will be given as well. The final section of this chapter gives several recommendations that could be used to improve this research, and it presents several recommendations for future research into this topic.

6.1. Conclusions per Research Question

How can the spatial correlations be estimated from CPTs?

In the random finite element method, the spatial variability of a soil property can be represented by its statistics, which are the mean, standard deviation and the scales of fluctuation in both horizontal and vertical directions. Before the spatial variability can be determined, it is necessary to determine the soil layers that can be found in the area under investigation. Due to the unique properties of each soil type, an estimation of the depth of the soil layers can be made by analysing plots of cone resistance, sleeve friction and pore pressure measurements of the cone penetration test data against the depth for each of the CPTs.

In order to determine the spatial variability, the soil data has to be normalised by removing its depth trend. To prevent removal of part of the fluctuation of the soil data, the normalisation of the soil data begins by grouping the CPTs that experienced a similar stress history. The next step is to identify and remove outliers in the soil data that are present due to irregularities in the soil, an example is roots, to prevent bias in the outcome of the spatial variability. Then the average depth trend of each of the groups of CPTs is identified for every soil layer, which is at most a quadratic trend, and removed from the soil data. This results in normalised soil data of which the mean is equal to zero and does not change over the depth, and of which the correlation between CPTs only depends on the lag distance. By calculating the autocorrelation function (ACF) of the data and fitting an autocorrelation model (ACM) to the ACF, an estimate of the horizontal and vertical scales of fluctuation can be made. Since the reliability of the ACF drops with increasing lag distance, fitting the ACM to the ACF should only be done for the initial part of the ACF, which is larger than the Bartlett's limit.

The trends of the data that have been removed were identified along the lines of CPTs parallel to the dyke. When combining the normalised data of different parallel lines of CPTs to estimate the spatial variability in the perpendicular or diagonal direction, it was found that the mean would not always be equal to zero. Since the mean of the data is required to be equal to zero in order to estimate the scales of fluctuation, the mean of the soil data of the lines of CPTs perpendicular or diagonal has to be subtracted from the data.

How do deformations caused by man-made structures on soft soils influence the spatial correlations of the soft soil layers?

This research question has been investigated in three parts. In Chapter 3 the influence of deformations on the spatial variability of random fields was researched. Four main deformations that occur in the soil under influence of the dyke have been identified and applied to three resolutions of random fields. However, no actual soil properties were assigned to the random fields, so the results of the change in spatial variability can only be interpreted qualitatively. The changes in spatial variability that have been observed show that vertical

compression leads to a decrease of the vertical scale of fluctuation and a slight decrease of the horizontal scale of fluctuation. Horizontal compression of the random fields results in only a decrease of the horizontal scale of fluctuation and simple shear shows a slight decrease of only the horizontal scale of fluctuation. The change in spatial variability due to rotation has resulted in an increase of the vertical scale of fluctuation and a decrease of the horizontal scale of fluctuation.

In Chapter 4 the CPTs at the Leendert de Boerspolder were used to estimate the actual spatial variability in the area for each of the soil layers and to compare the results. From the difference in spatial variability, it has been found that the influence of man-made structures can be found from the horizontal and vertical scales of fluctuation in the first peat layer and in the clay layer. Underneath the crest the vertical scale of fluctuation decreases compared to the other lines of CPTs, likely due to the overburden pressure. The horizontal scale of fluctuation underneath the crest decreases in the peat layer, while it increases in the clay layer. Underneath the slope and toe of the dyke the results show vertical scales of fluctuation smaller than those in the polder, but larger than those underneath the crest, likely due to the reduced influence of the overburden pressure and the added influence of rotation. The horizontal scales of fluctuation underneath the slope and toe of the dyke increase towards the polder for the peat layer. In the clay layer more influence of rotation is expected underneath the slope than underneath the crest, because the horizontal scale of fluctuation is lower. Underneath the toe the horizontal scale of fluctuation for the entire clay layer is at its lowest and without the additional layer it is at its largest, indicating that most influence may be found in the organic top part of the clay layer where rotation reduces the horizontal scale of fluctuation. The spatial variability of the second peat layer does not show any influence of the dyke, because the spatial variability at all locations is similar.

Finally, the results have been combined with a finite element analysis in Chapter 5 to link the conclusions of the first two parts with the deformations that have taken place in the Leendert de Boerspolder. The displacements have confirmed the assumed deformations and showed that at five meters from the dyke the influence of the dyke hardly causes displacements. This led to the conclusion that all parallel CPT lines in the polder can be used as a baseline of spatial variability to which the change of the spatial variability under influence of the dyke can be compared. In the peat layer the deformations confirmed that vertical compression has decreased the vertical and increased the horizontal scales of fluctuation. Rotation was found to mainly influence the larger second scales of fluctuation, indicated by an increase of $\theta_{v,2}$ with a decrease of its weighting factor, and by a decrease of $\theta_{h,2}$ with an increase of its weighting factor. The little change in horizontal scale of fluctuation underneath the slope and toe of the dyke can be attributed to horizontal extension of the peat layer, which increased the horizontal scale of fluctuation. In the organic clay layer there is less influence of the dyke, resulting in no change in horizontal scale of fluctuation underneath the crest of the dyke due to vertical compression. Aside from this difference, the conclusions underneath the crest and toe are equal to the conclusions of the peat layer. Underneath the slope the difference in results can be attributed to the analysis of the spatial variability of the Leendert de Boerspolder, where the combined analysis of the organic and silty clay layer gives different results than the deformations of the organic clay layer have shown. A separate analysis of the spatial variability of the organic and silty clay layer is recommended for more accurate conclusions on the influence of the man-made structure on the spatial variability of the clay layer.

How can the influence of spatial changes in spatial variability due to deformations caused by man-made structures on soft soils be taken into account in the RFEM?

The random finite element analysis should start with the soil layers as they were before the man-made structure was constructed. Therefore, the random fields should use the spatial variability that is estimated from cone penetration tests that have not been influenced by the man-made structure. For the case study of the Leendert de Boerspolder, no influence of the man-made structure on the spatial variability was found at CPT lines 1 to 4. Then by step-wise construction of the man-made structure and by allowing the finite element mesh to deform, the random fields in the proximity of the man-made structure should result in an approximation of the spatial variability that was estimated from CPTs at those locations. Additional research is necessary to test this method for its accuracy in obtaining the measured spatial variability after construction of the man-made structure.

6.2. General Conclusion

The overall conclusion of this research is that the influence of man-made structures on the spatial variability of soft soils can be estimated from cone penetration test data. Specific deformations cause corresponding changes in the spatial variability of the soft soil layers. Further investigations have to be made using the

random finite element method to research how well the proposed method accounts for the changes in spatial variability in the RFEM.

6.3. Recommendations

In an effort to improve the reproducibility of this research, a robust method for the linear outlier removal was used. However, for the clay layer it was decided to manually remove the single outlier of the soil data, because the identified methods were not suited for log-normal data. It is recommended that a robust outlier detection method is applied to any log-normal soil data to improve the reproducibility.

Regarding the site investigation, the cone penetration tests have been executed in a grid such that the spatial variability could be estimated in different directions relative to the dyke. In order to estimate the spatial variability, at least three values of the autocorrelation function have to be larger than the Bartlett's limit. When investigating the horizontal scale of fluctuation perpendicular or diagonal to the dyke for the polder and the zone in the proximity of the dyke, many lines consisted of less than three CPTs. A more effective site investigation would ensure that in the perpendicular direction at least three CPTs are taken in the dyke and at least three CPTs are taken in the polder, such that a proper comparison can be made between the θ_h underneath the dyke and in the polder in the perpendicular direction.

From the spatial variability of the Leendert de Boerspolder it was found that the small horizontal scale of fluctuation is often smaller than the shortest lag distance ($\theta_{h,1} < \tau_{min}$). In order to find the value of this small correlation length, several CPTs should be taken in a closer proximity than the current minimum lag distance of 1.25m. Another option is to perform a horizontal cone penetration test, effectively decreasing the minimum lag distance to the measurement interval of 1 centimetre. It has to be investigated whether a horizontal CPT is a feasible method.

The change in spatial variability due to the deformation of random fields has been analysed qualitatively, because no soil properties had been mapped on the random fields. In order to calculate the actual change in spatial variability, soil properties should be given to the random fields and the fields should be deformed in a finite element analysis. This way, better predictions can be made of the influence of the different deformations on the change in spatial variability. It is advised to estimate the spatial variability at different stages during the deformation to be sure what happens during deformation.

From the deformations of the finite element analysis it has been concluded that most of the influence of the dyke is found in the organic clay layer and not in the silty clay layer. The spatial variability of the clay layer has been calculated over its entire depth and showed some inconsistencies between the expected influence of the dyke and the actual influence of the dyke on the spatial variability. It is recommended to analyse the spatial variability of the organic and silty clay layers individually to figure out whether the discrepancy is caused by the averaging over the two layers or by something else.

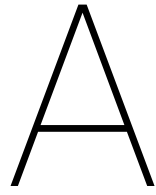
Finally, this thesis has shown that the influence of a man-made structure changes the spatial variability of the soft soil layers in the proximity of that man-made structure. Future research should investigate the following question: How does the man-made structure influence its reliability due to its influence on the spatial variability of the soft soil layers on which it has been constructed?

Bibliography

- [1] Almeida, M. and Marques, M. E. S. (2013). *Design and performance of embankments on very soft soils*. CRC Press.
- [2] Bjerrum, L. (1973). Problems of soil mechanics and construction on soft clays and structurally unstable soils. In *Proc. 8th ICSMFE*, volume 3, pages 111–159.
- [3] Campanella, R. G., Robertson, P. K., and Gillespie, D. (1983). Cone penetration testing in deltaic soils. *Canadian Geotechnical Journal*, 20(1):23–35.
- [4] Campbell, J. B. (1979). Spatial variability of soils. *Annals of the Association of American Geographers*, 69(4):544–556.
- [5] Davis, M. W. (1987). Production of conditional simulations via the lu triangular decomposition of the covariance matrix. *Mathematical geology*, 19(2):91–98.
- [6] de Gast, T. (2019). Dykes and embankments: a geostatistical analysis of soft terrain. PhD Thesis unpublished at time of writing this thesis.
- [7] de Gast, T., Hicks, M. A., Vardon, P. J., and van den Eijnden, A. P. (2018a). A practical case study of slope stability analysis using the random finite element method.
- [8] de Gast, T., Vardon, P. J., and Hicks, M. A. (2017). Estimating spatial correlations under man-made structures on soft soils. *Geo-Risk*, pages 382–389.
- [9] de Gast, T., Vardon, P. J., and Hicks, M. A. (2018b). Detection of soil variability using CPTs. In *Proceedings of the 4th International Symposium on Cone Penetration Testing (CPT'18), 21-22 June, 2018, Delft, The Netherlands*, pages 289–294, London. CRC Press.
- [10] Donoho, D. L. and Huber, P. J. (1983). The notion of breakdown point. *A festschrift for Erich L. Lehmann*.
- [11] Eurocode 7 (2016). Geotechnisch ontwerp - deel 1: Algemene regels. standard, NEN.
- [12] Fang, J. and Tacher, L. (2003). An efficient and accurate algorithm for generating spatially-correlated random fields. *Communications in numerical methods in engineering*, 19(10):801–808.
- [13] Fenton, G. A. and Vanmarcke, E. H. (1990). Simulation of random fields via local average subdivision. *Journal of Engineering Mechanics*, 116(8):1733–1749.
- [14] Hampel, F. R. (1973). Robust estimation: A condensed partial survey. *Zeitschrift für Wahrscheinlichkeitstheorie und verwandte Gebiete*, 27(2):87–104.
- [15] Hicks, M. A. (2005). Risk and variability in geotechnical engineering. *Géotechnique*, 55(1):1–2.
- [16] Hicks, M. A. (2014). Application of the random finite element method. *ALERT Doctoral School*, page 181.
- [17] Hicks, M. A. and Onisiphorou, C. (2007). Stochastic evaluation of static liquefaction in a predominantly dilative sand fill. In *Risk and Variability in Geotechnical Engineering*, pages 68–79. Thomas Telford Publishing.
- [18] Hicks, M. A. and Samy, K. (2002a). Influence of heterogeneity on undrained clay slope stability. *Quarterly Journal of Engineering Geology and Hydrogeology*, 35(1):41–49.
- [19] Hicks, M. A. and Samy, K. (2002b). Reliability-based characteristic values: a stochastic approach to eurocode 7. *Ground Engineering*, 35(12).
- [20] Huber, P. J. and Ronchetti, E. M. (2009). *Robust statistics*. Wiley.

- [21] Jaksa, M. B., Kaggwa, W. S., and Brooker, P. I. (1999). Experimental evaluation of the scale of fluctuation of a stiff clay. In *Proceedings of the 8th International Conference on Applications of Statistics and Probability in Civil Engineering*, volume 1, pages 415–422, Rotterdam. AA Balkema.
- [22] Leys, C., Ley, C., Klein, O., Bernard, P., and Licata, L. (2013). Detecting outliers: Do not use standard deviation around the mean, use absolute deviation around the median. *Journal of Experimental Social Psychology*, 49(4):764–766.
- [23] Lloret-Cabot, M., Fenton, G. A., and Hicks, M. A. (2014). On the estimation of scale of fluctuation in geostatistics. *Georisk: Assessment and Management of Risk for Engineered Systems and Geohazards*, 8(2):129–140.
- [24] Lloret-Cabot, M., Hicks, M. A., and van den Eijnden, A. P. (2012). Investigation of the reduction in uncertainty due to soil variability when conditioning a random field using kriging. *Géotechnique letters*, 2:123–127.
- [25] Ohlson, J. A. and Kim, S. (2014). Linear valuation without ols: the theil-sen estimation approach. *Review of Accounting Studies*, 20(1):395–435.
- [26] Phoon, K. K. and Kulhawy, F. H. (1999). Characterization of geotechnical variability. *Canadian Geotechnical Journal*, 36(4):612–624.
- [27] Robertson, P. K. (1990). Soil classification using the cone penetration test. *Canadian Geotechnical Journal*, 27(1):151–158.
- [28] Robertson, P. K. (2010). Soil behaviour type from the cpt: an update. In *2nd international symposium on cone penetration testing*, pages 9–11, USA.
- [29] Robertson, P. K. and Wride, C. E. (1998). Evaluating the cyclic liquefaction potential using the cone penetration test. *Canadian Geotechnical Journal*, 35(3):442–459.
- [30] Sen, P. K. (1968). Estimates of the regression coefficient based on kendall's tau. *Journal of the American statistical association*, 63(324):1379–1389.
- [31] 't Hart, R., de Bruijn, H., and de Vries, G. (2016). Fenomenologische beschrijving faalmechanismen wti. Technical report, Deltares.
- [32] Tukey, J. W. (1977). *Exploratory data analysis*, volume 2. Reading, Mass.
- [33] Uzielli, M., Vannucchi, G., and Phoon, K. K. (2005). Random field characterisation of stress-normalised cone penetration testing parameters. *Géotechnique*, 55(1):3–20.
- [34] van den Eijnden, A. P. and Hicks, M. A. (2011). Conditional simulation for characterizing the spatial variability of sand state. In *Proc. 2nd Int. Symp. Comp. Geomech., Croatia*, pages 288–296.
- [35] Vanmarcke, E., Shinozuka, M., Nakagiri, S., Schuëller, G. I., and Grigoriu, M. (1986). Random fields and stochastic finite elements. *Structural Safety*, 3(3-4):143–166.
- [36] Vanmarcke, E. H. (1983). *Random fields, analysis and synthesis*. The MIT Press, Cambridge, Massachusetts.
- [37] Verruijt, A. (2012). *Soil Mechanics*. Delft University of Technology.

Appendices



Leendert de Boerspolder

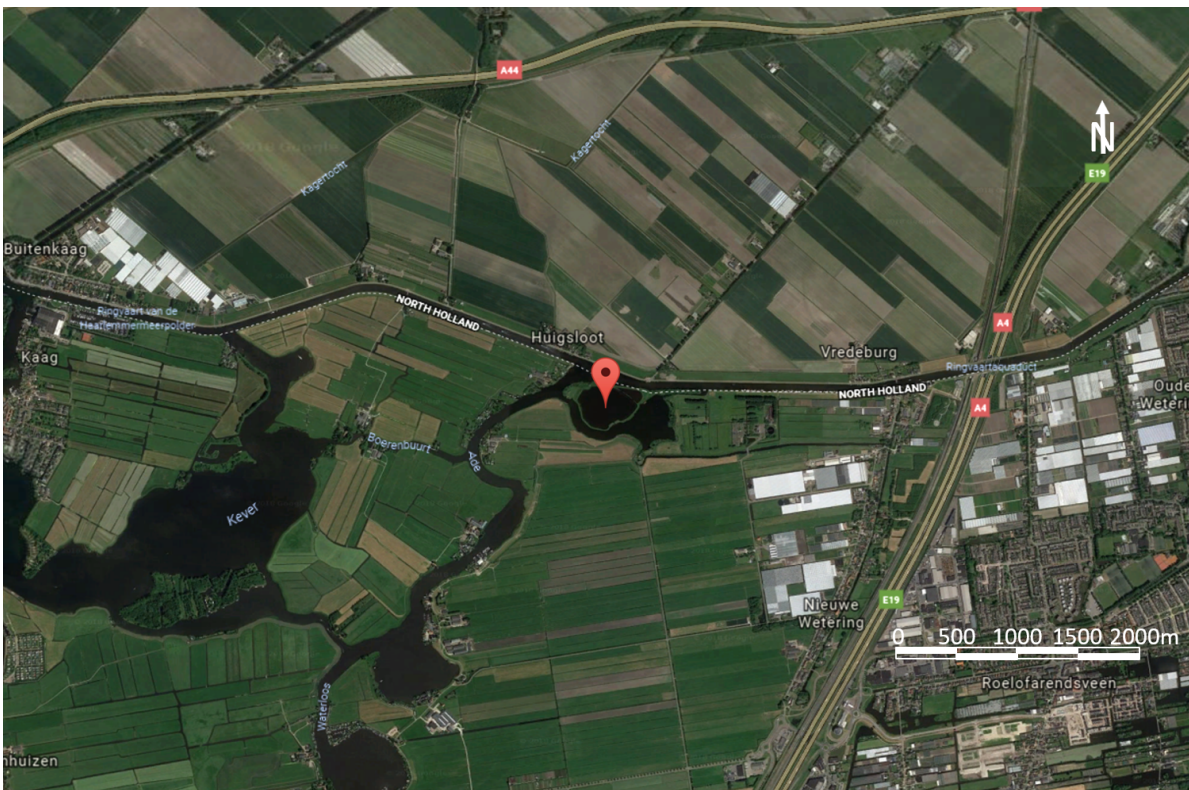


Figure A.1: The location of the Leendert de Boerspolder, taken from Google Earth



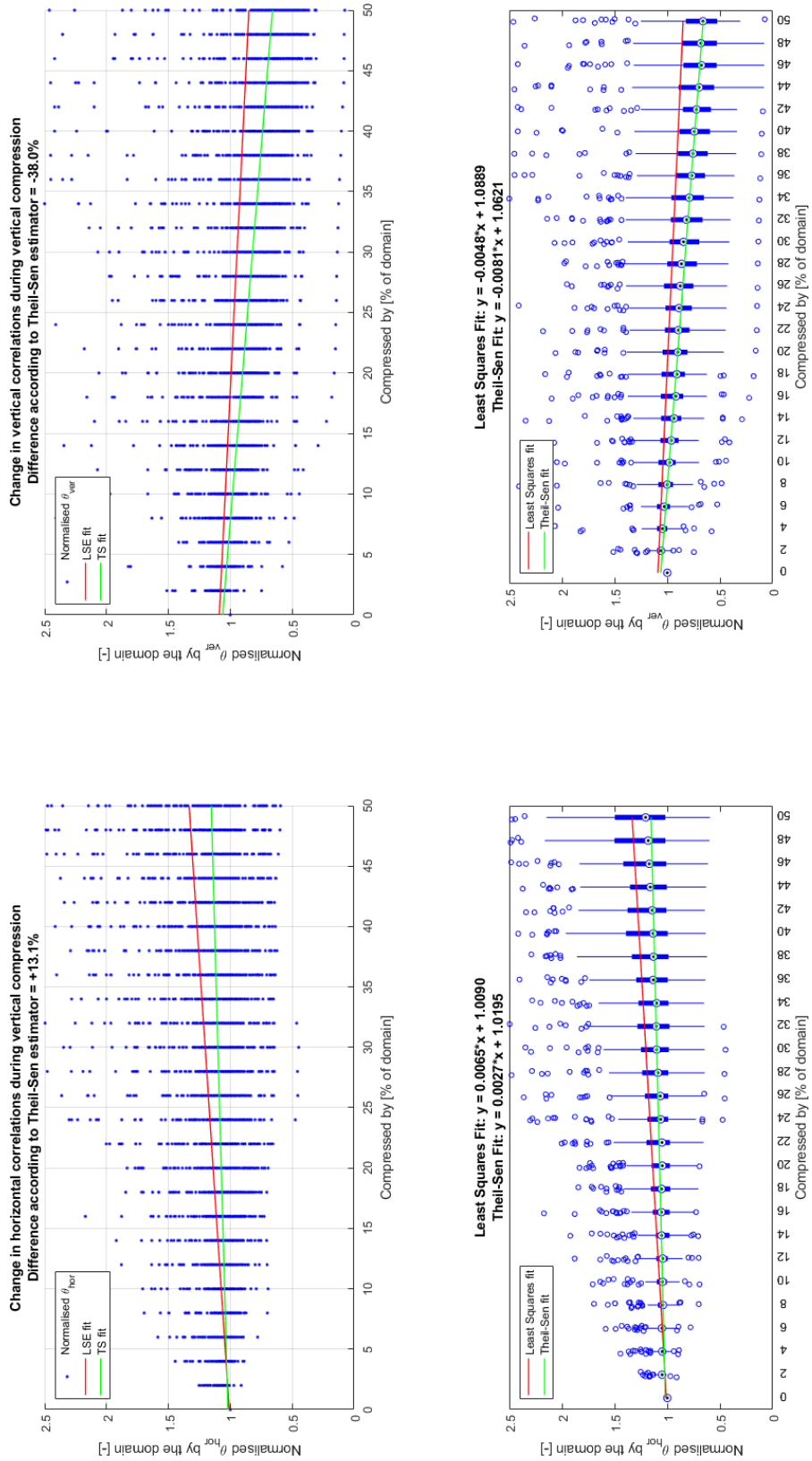
Figure A.2: The Leendert de Boerspolder before it was flooded, taken from Google Earth



Figure A.3: The Leendert de Boerspolder after it has been flooded, taken from Google Earth

B

Change in Spatial Variability when Deforming Random Fields

Figure B.1: Change in θ_h and θ_v due to vertical compression of low resolution random fields, compared to the domain spatial variability

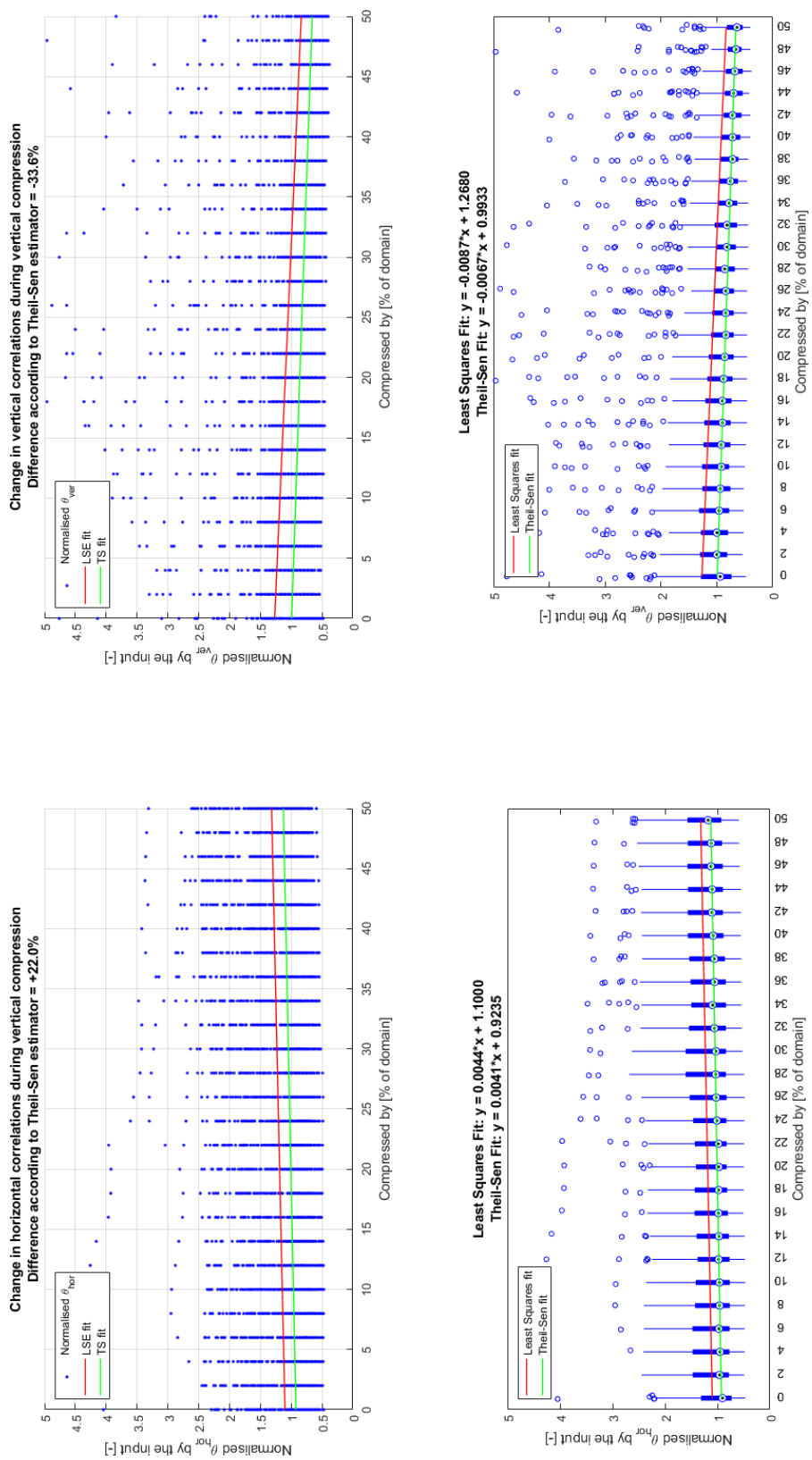


Figure B.2: Change in θ_h and θ_v due to vertical compression of low resolution random fields, compared to the input spatial variability

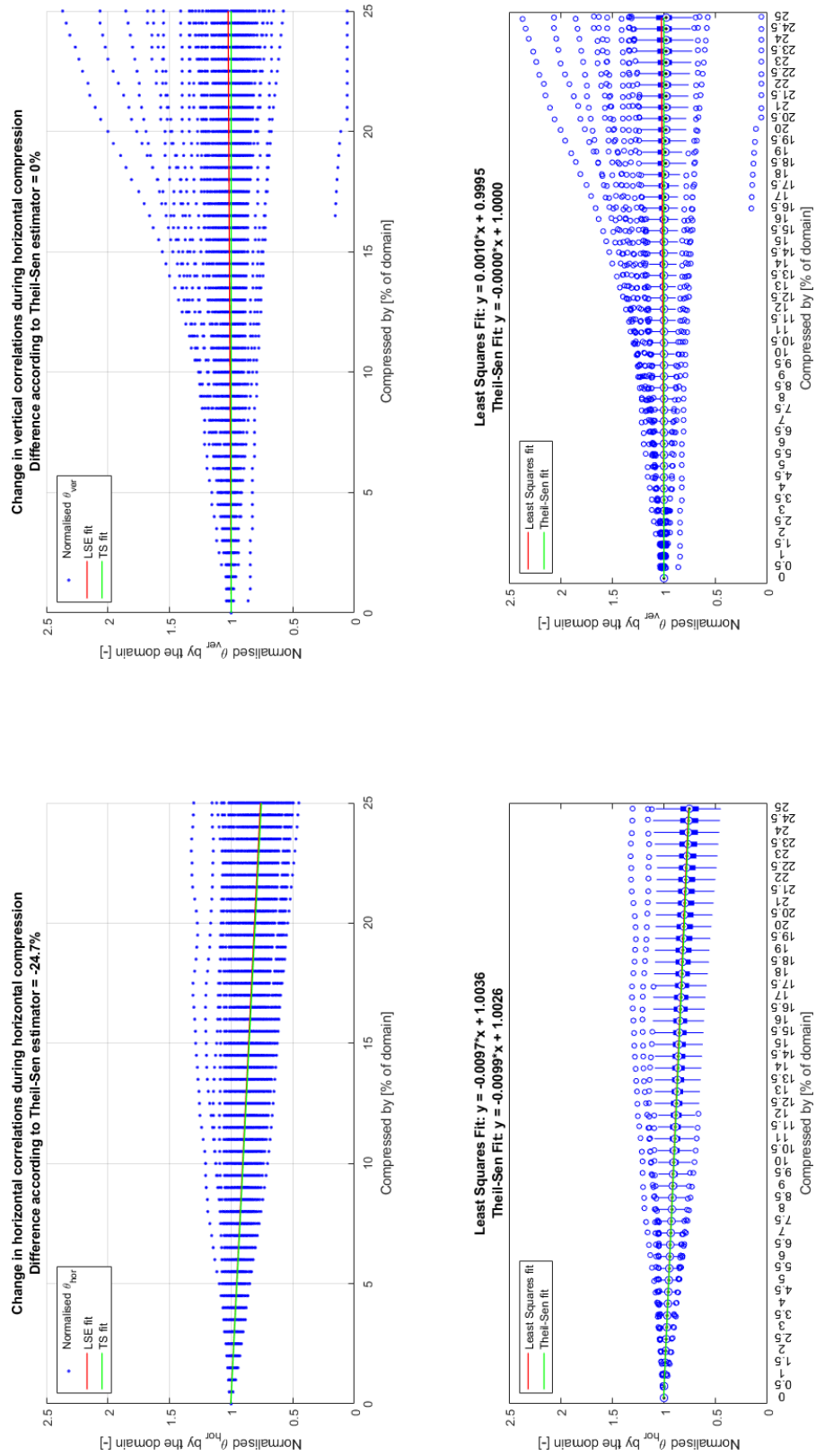


Figure B.3: Change in θ_h and θ_v due to horizontal compression of low resolution random fields, compared to the domain spatial variability

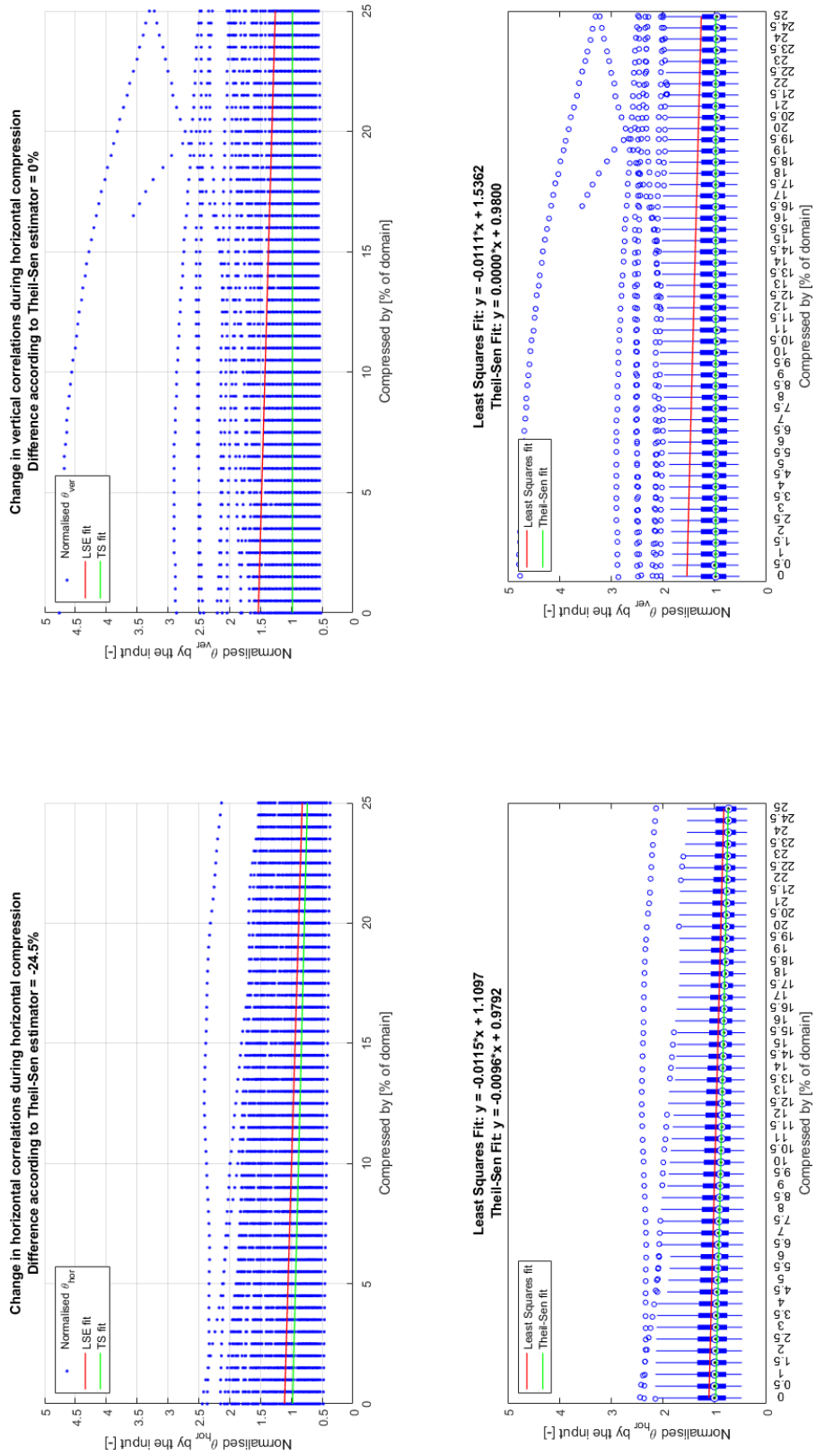
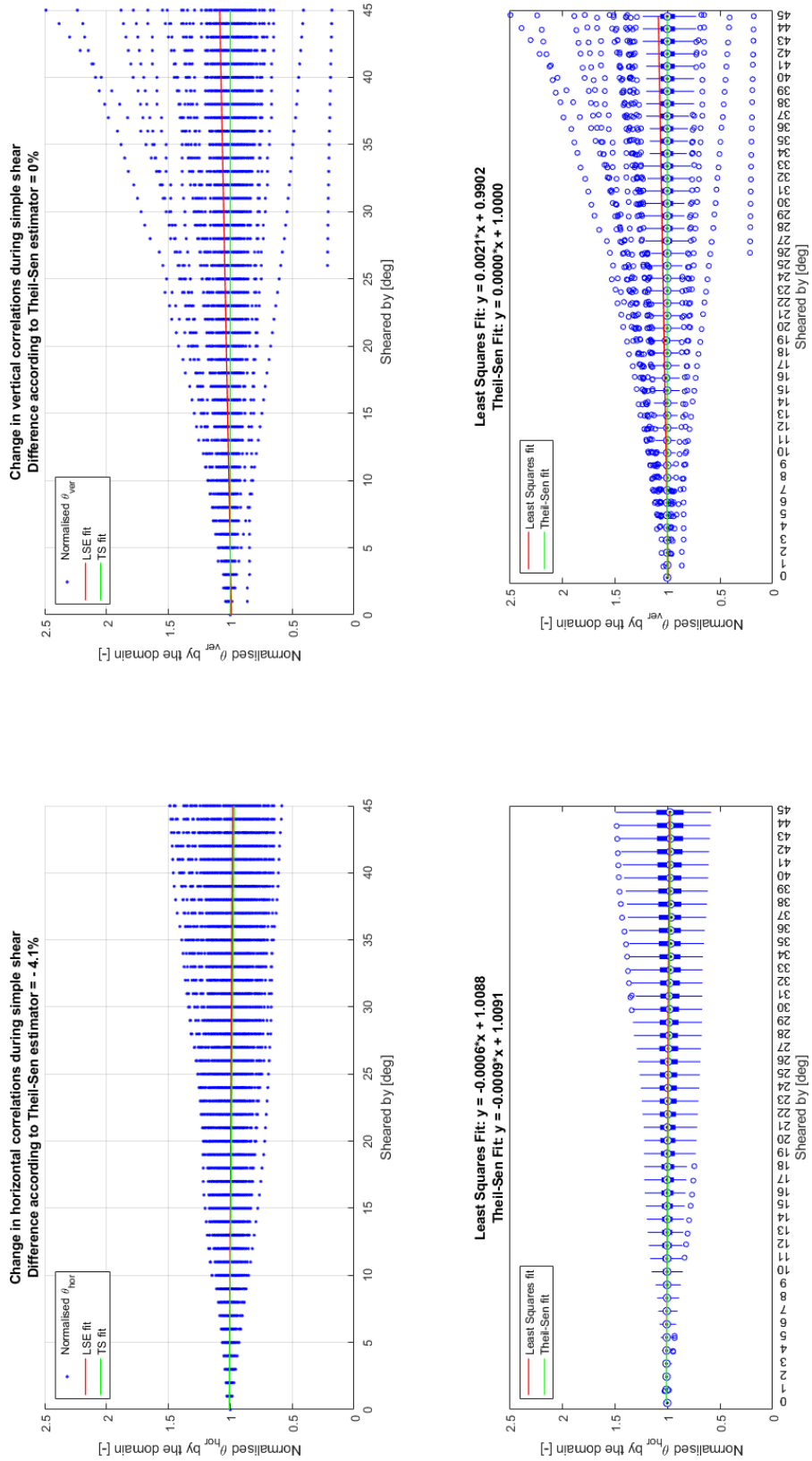


Figure B.4: Change in θ_h and θ_v due to horizontal compression of low resolution random fields, compared to the input spatial variability

Figure B.5: Change in θ_h and θ_v due to simple shear of low resolution random fields, compared to the domain spatial variability

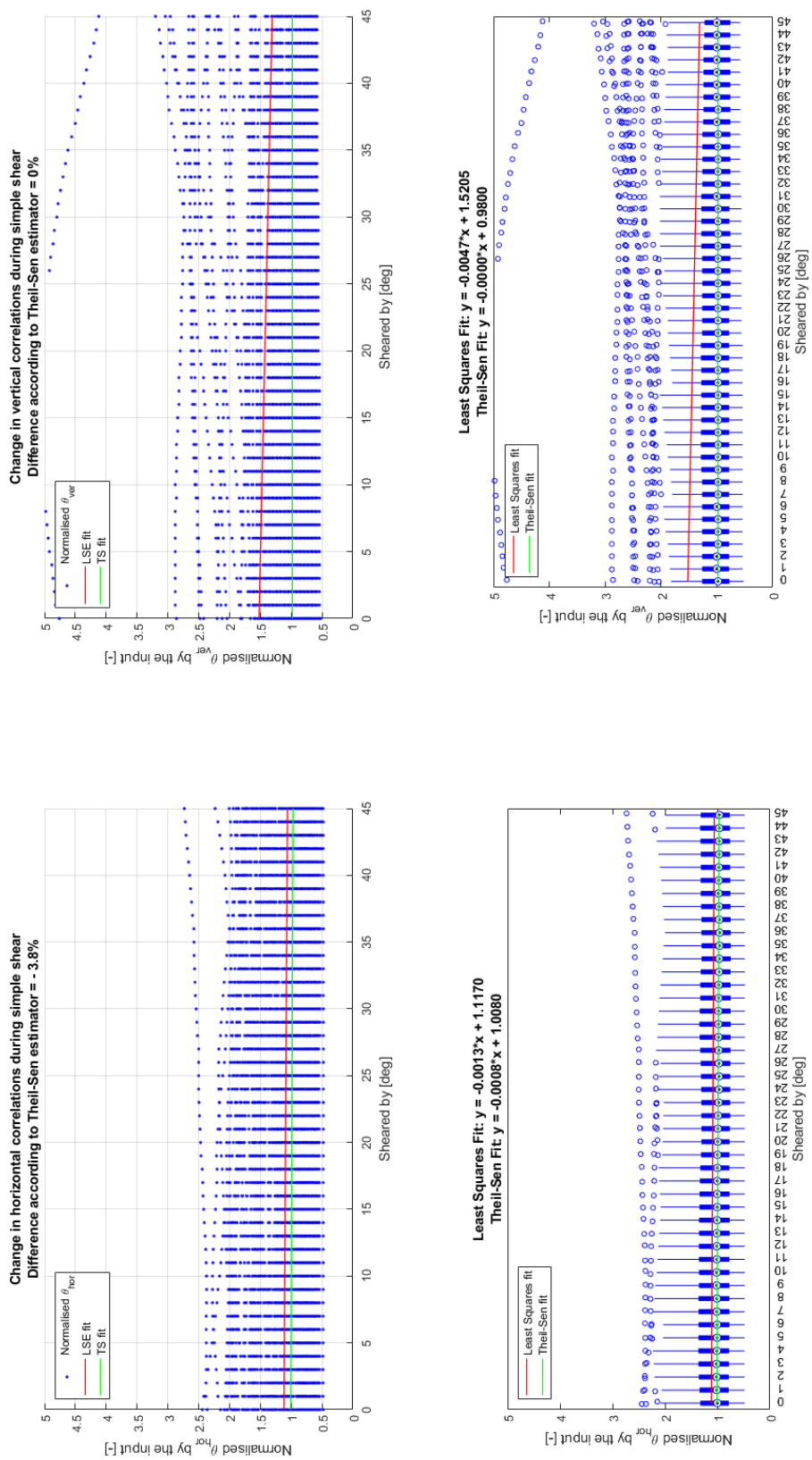


Figure B.6: Change in θ_h and θ_v due to simple shear of low resolution random fields, compared to the input spatial variability

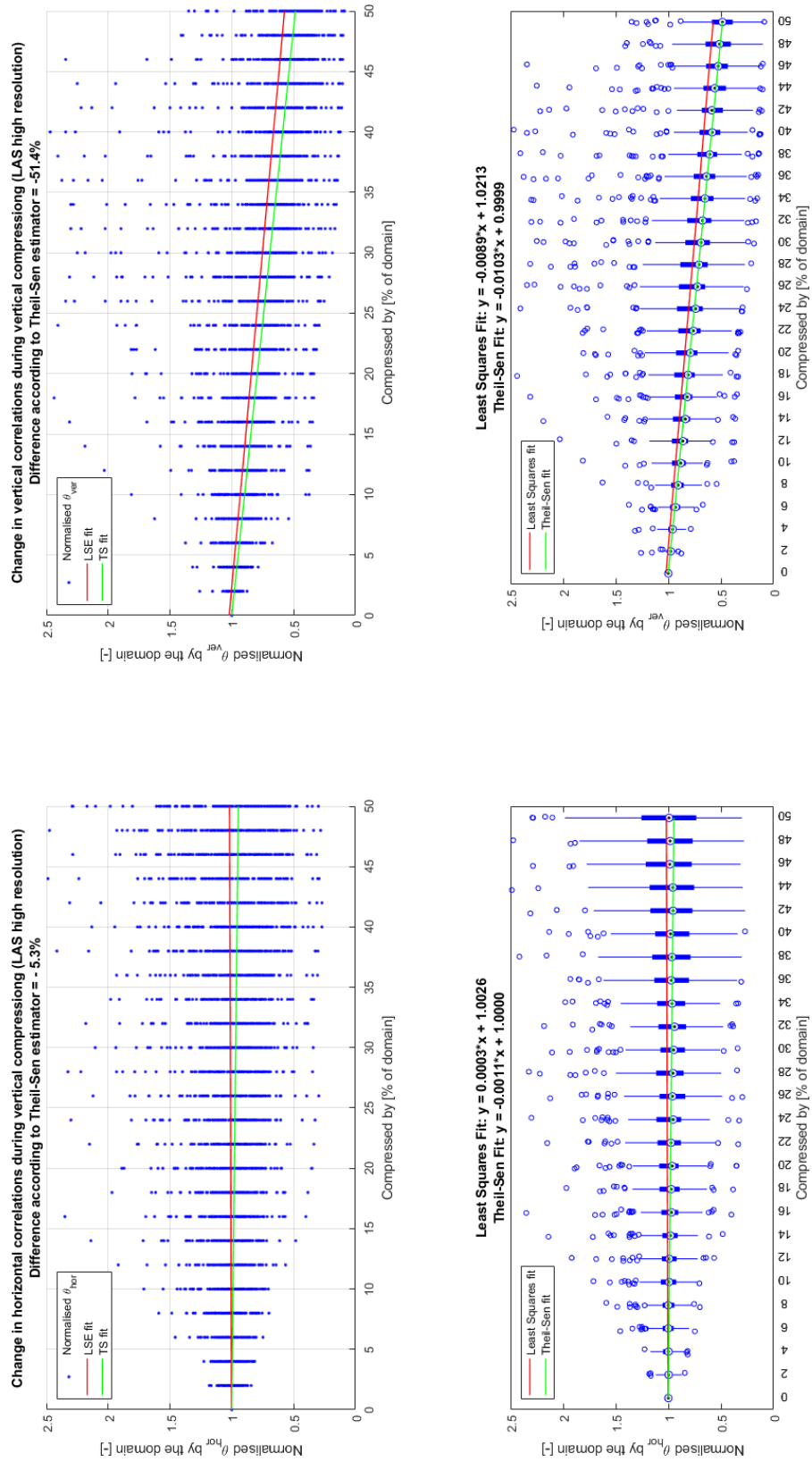


Figure B.7: Change in θ_h and θ_v due to vertical compression of high resolution random fields, compared to the domain spatial variability

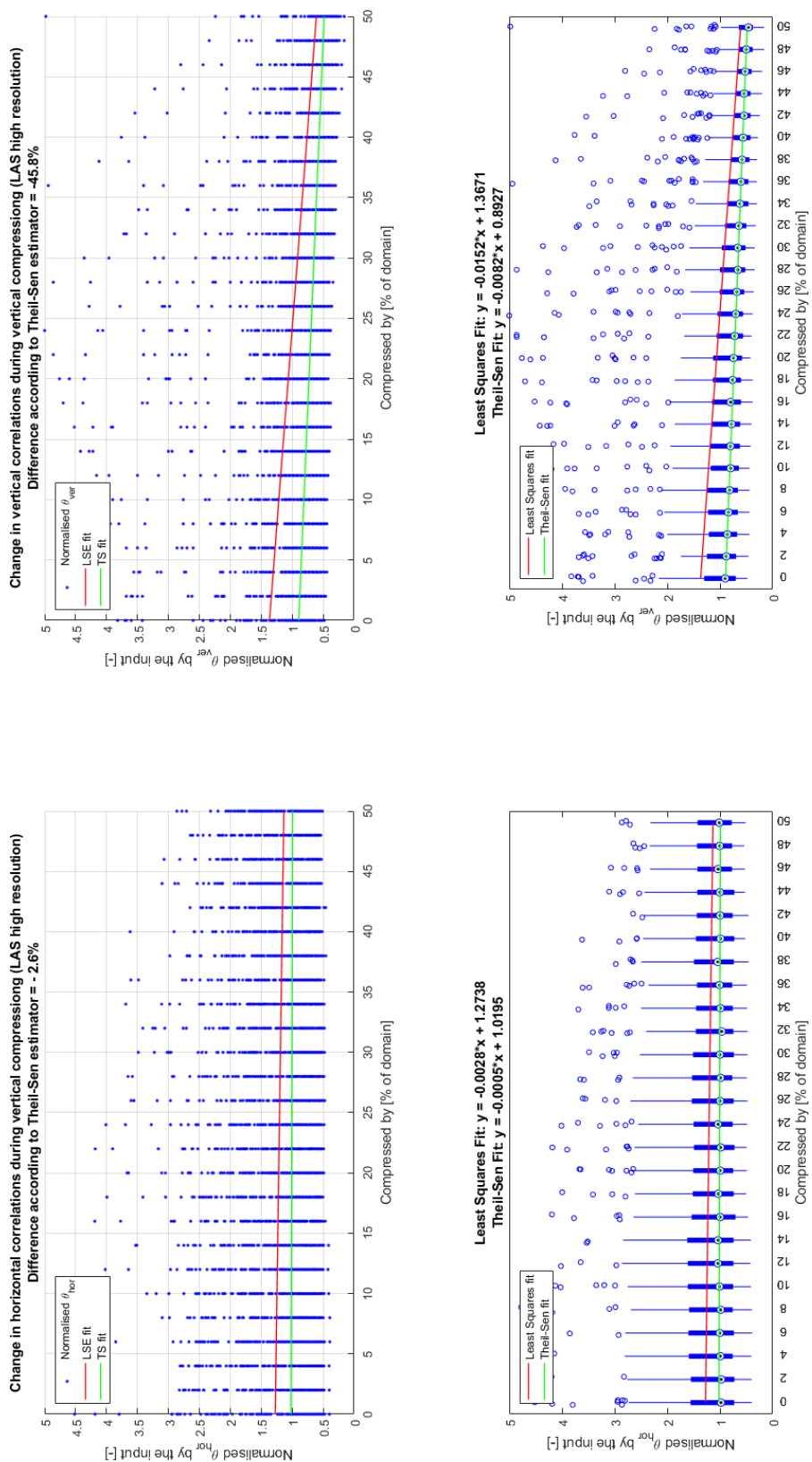


Figure B.8: Change in θ_h and θ_v due to vertical compression of high resolution random fields, compared to the input spatial variability

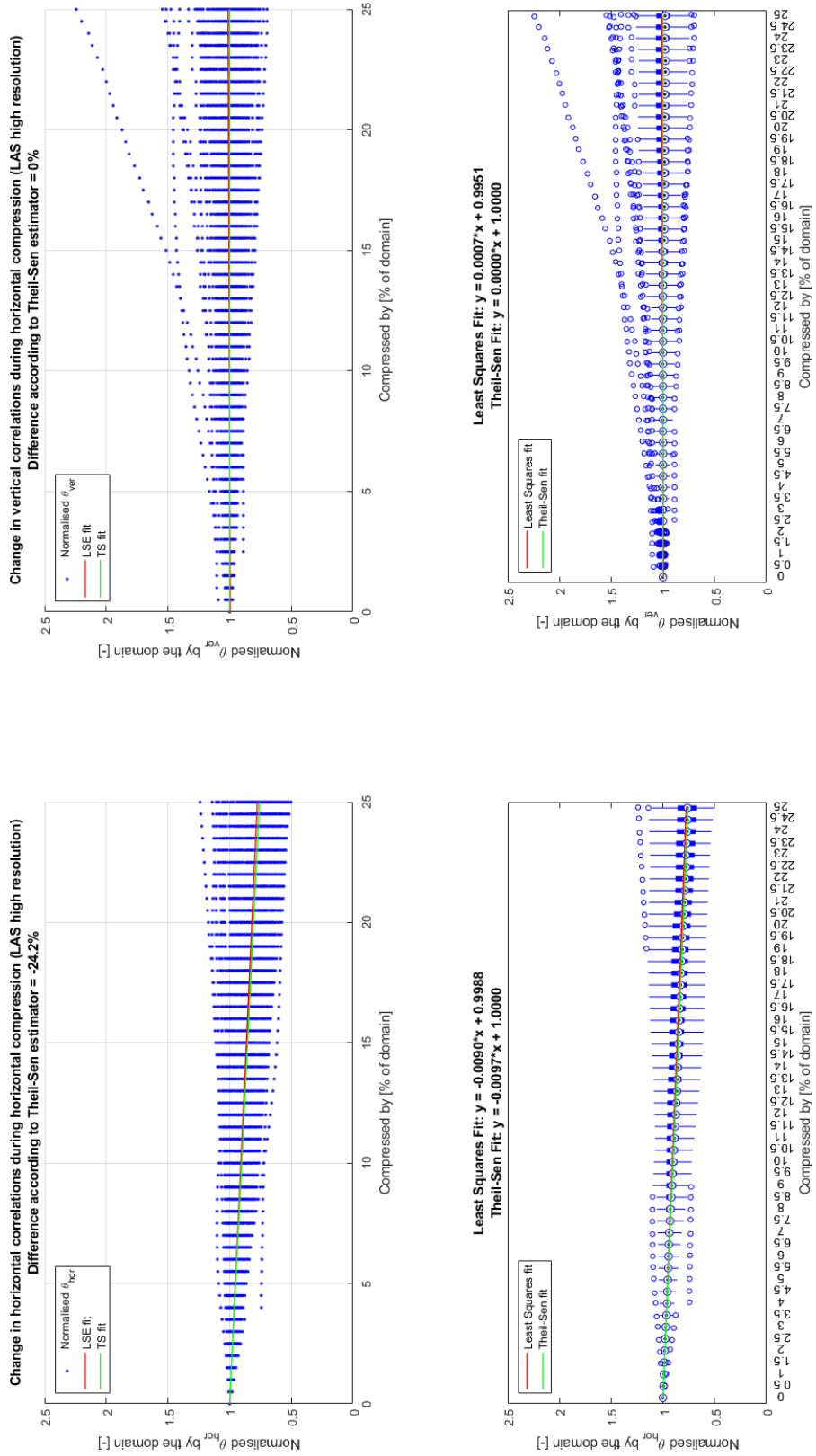


Figure B.9: Change in θ_h and θ_v due to horizontal compression of high resolution random fields, compared to the domain spatial variability

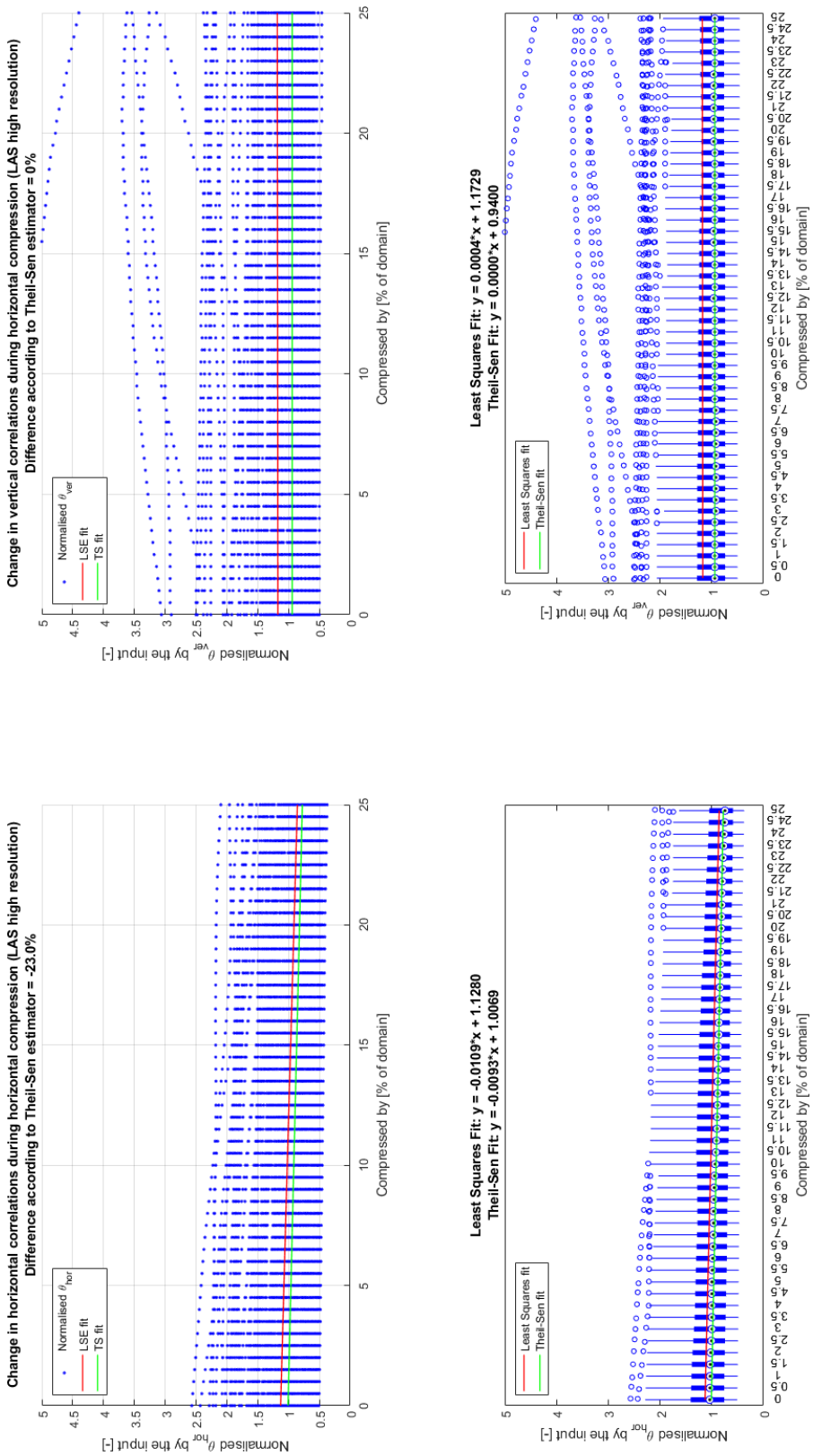


Figure B.10: Change in θ_h and θ_v due to horizontal compression of high resolution random fields, compared to the input spatial variability

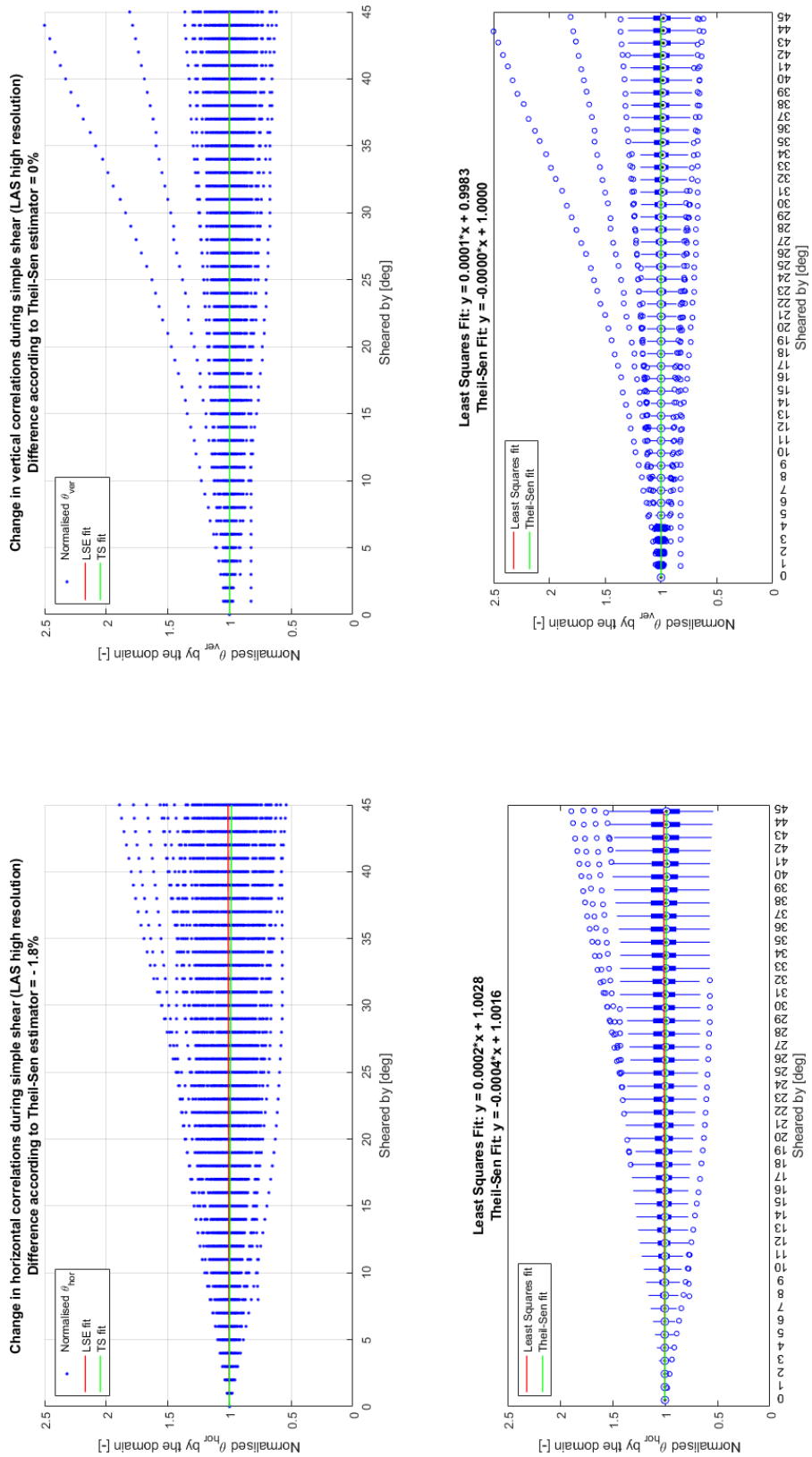


Figure B.11: Change in θ_h and θ_v due to simple shear of high resolution random fields, compared to the domain spatial variability

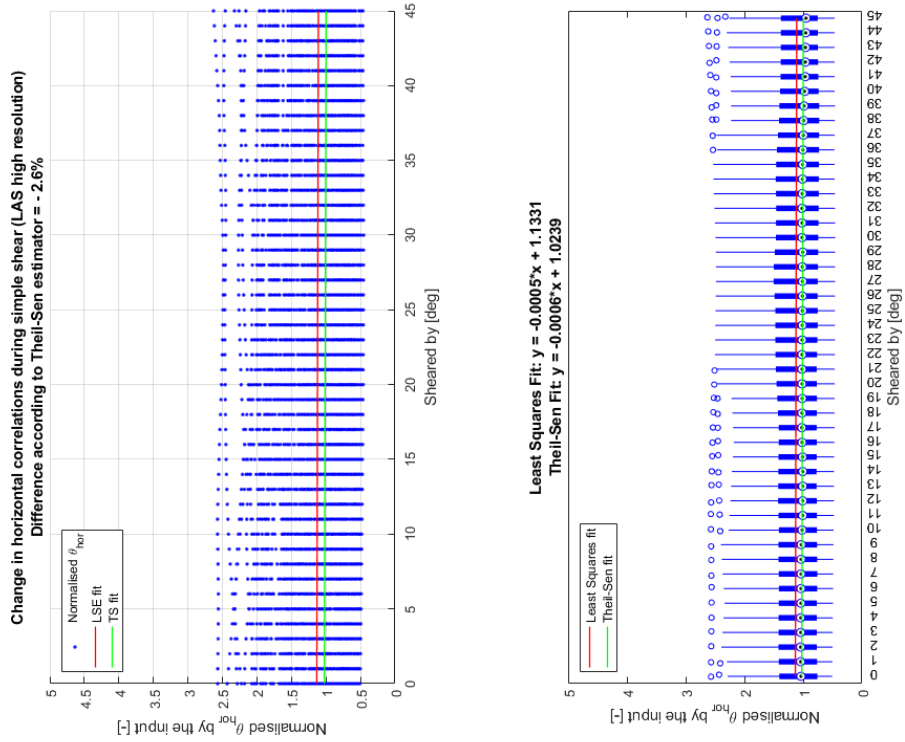
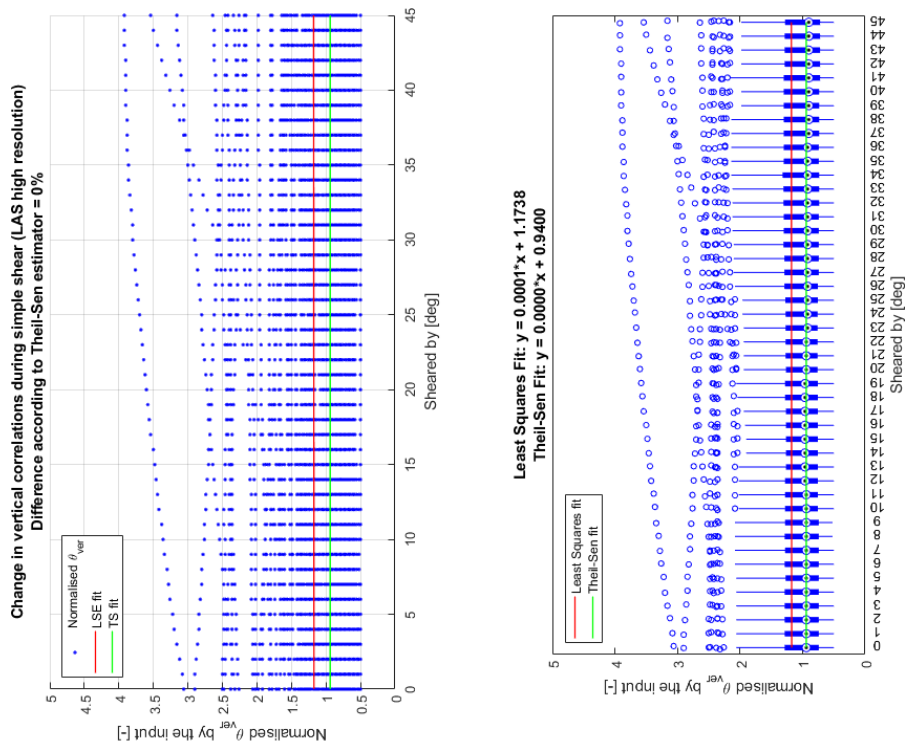


Figure B.12: Change in θ_h and θ_v due to simple shear of high resolution random fields, compared to the input spatial variability

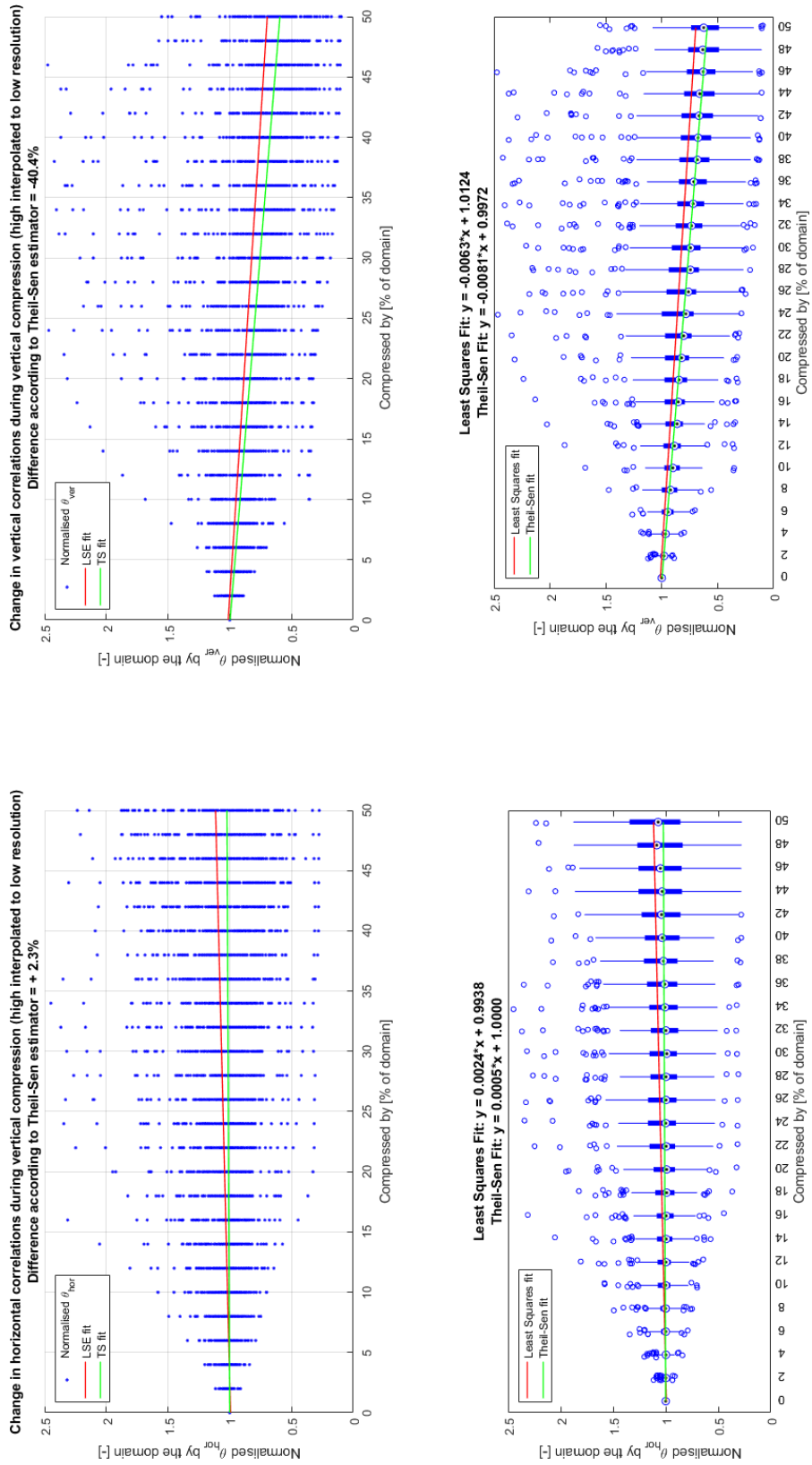


Figure B.13: Change in θ_h and θ_v due to vertical compression of high to low resolution random fields, compared to the domain spatial variability

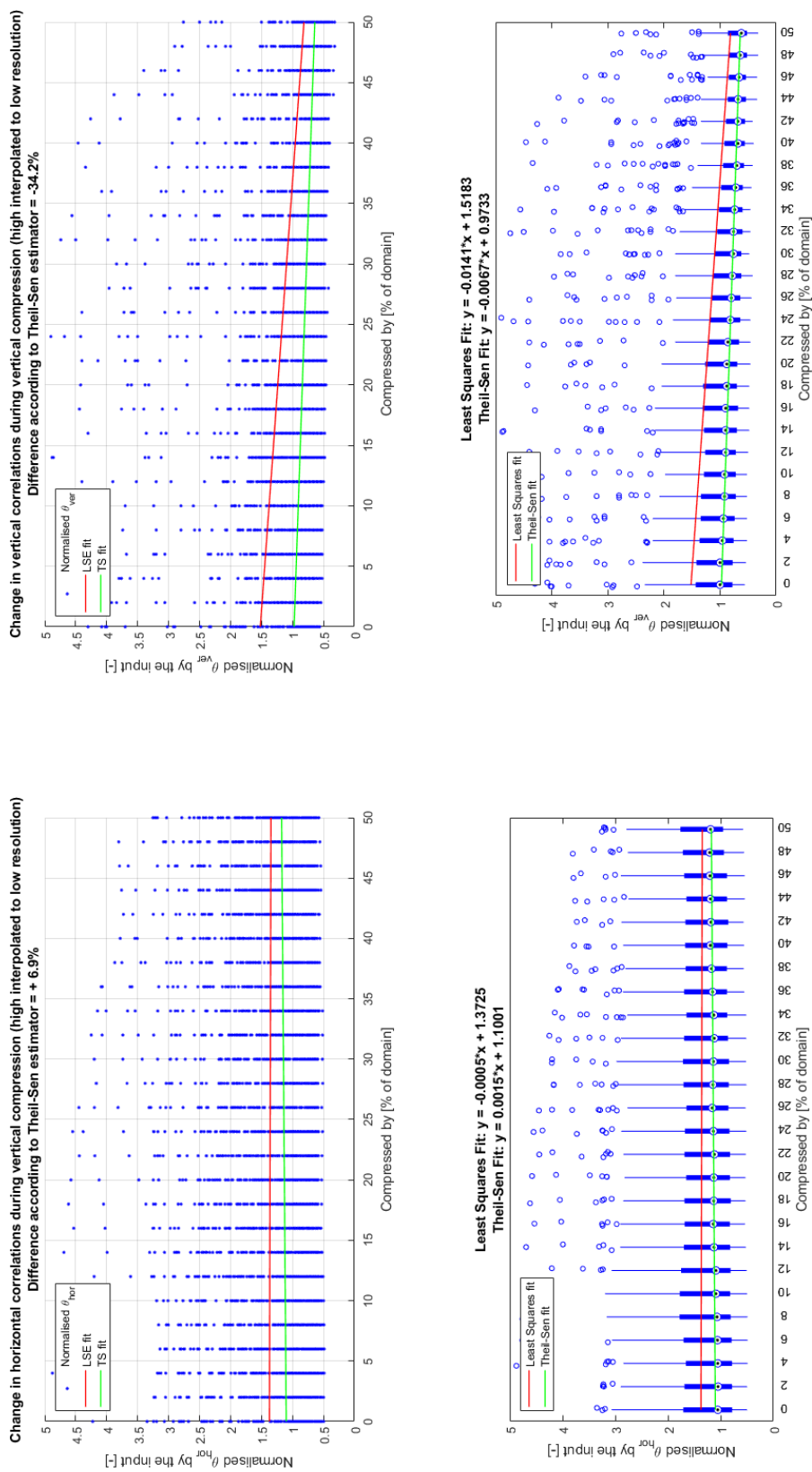


Figure B.14: Change in θ_h and θ_v due to vertical compression of high to low resolution random fields, compared to the input spatial variability

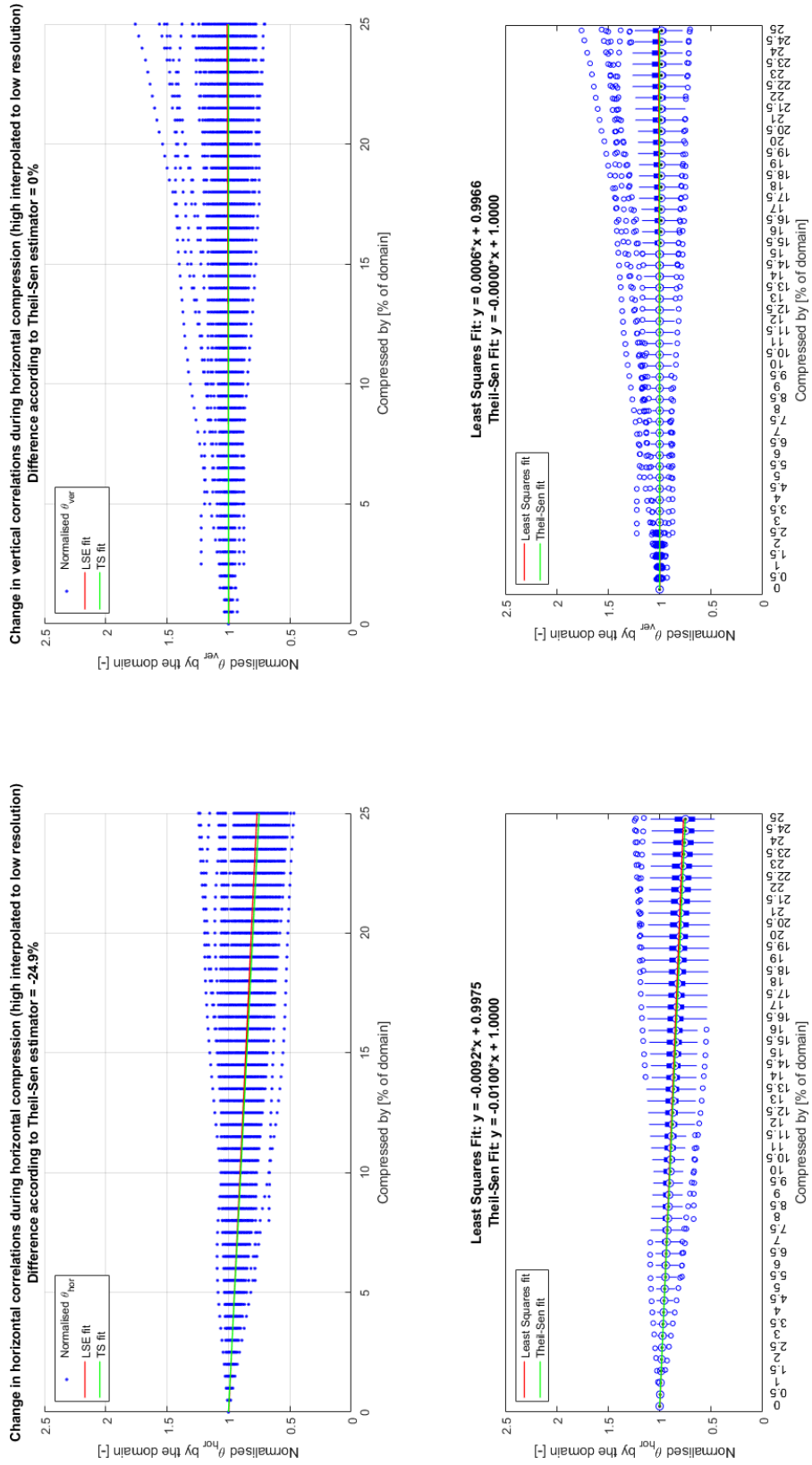


Figure B.15: Change in θ_h and θ_v due to horizontal compression of high to low resolution random fields, compared to the domain spatial variability

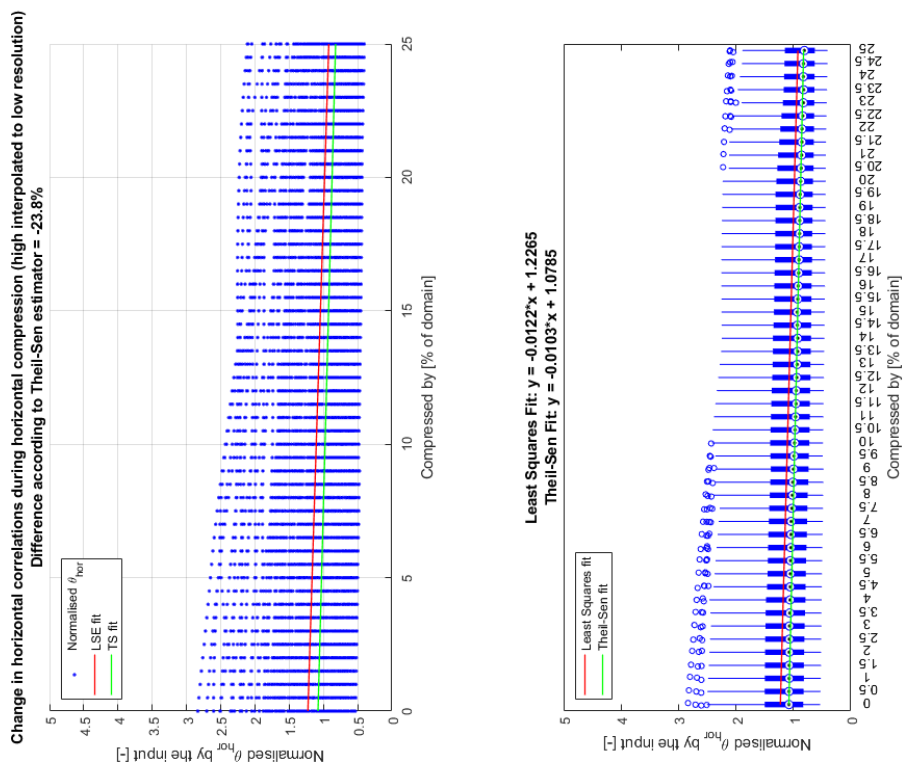
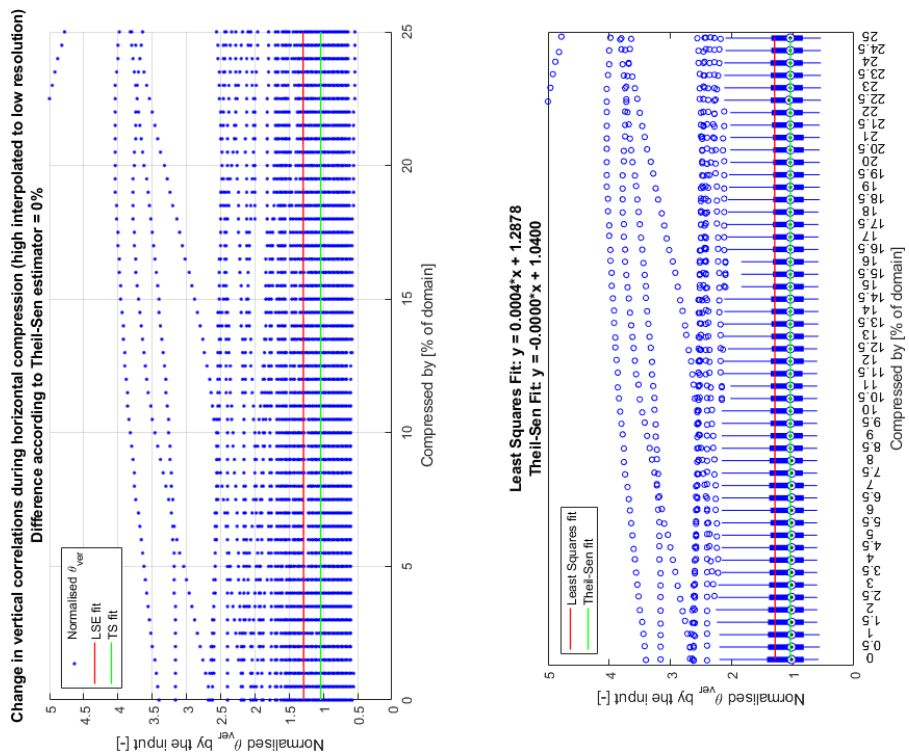


Figure B.16: Change in θ_h and θ_v due to horizontal compression of high to low resolution random fields, compared to the input spatial variability

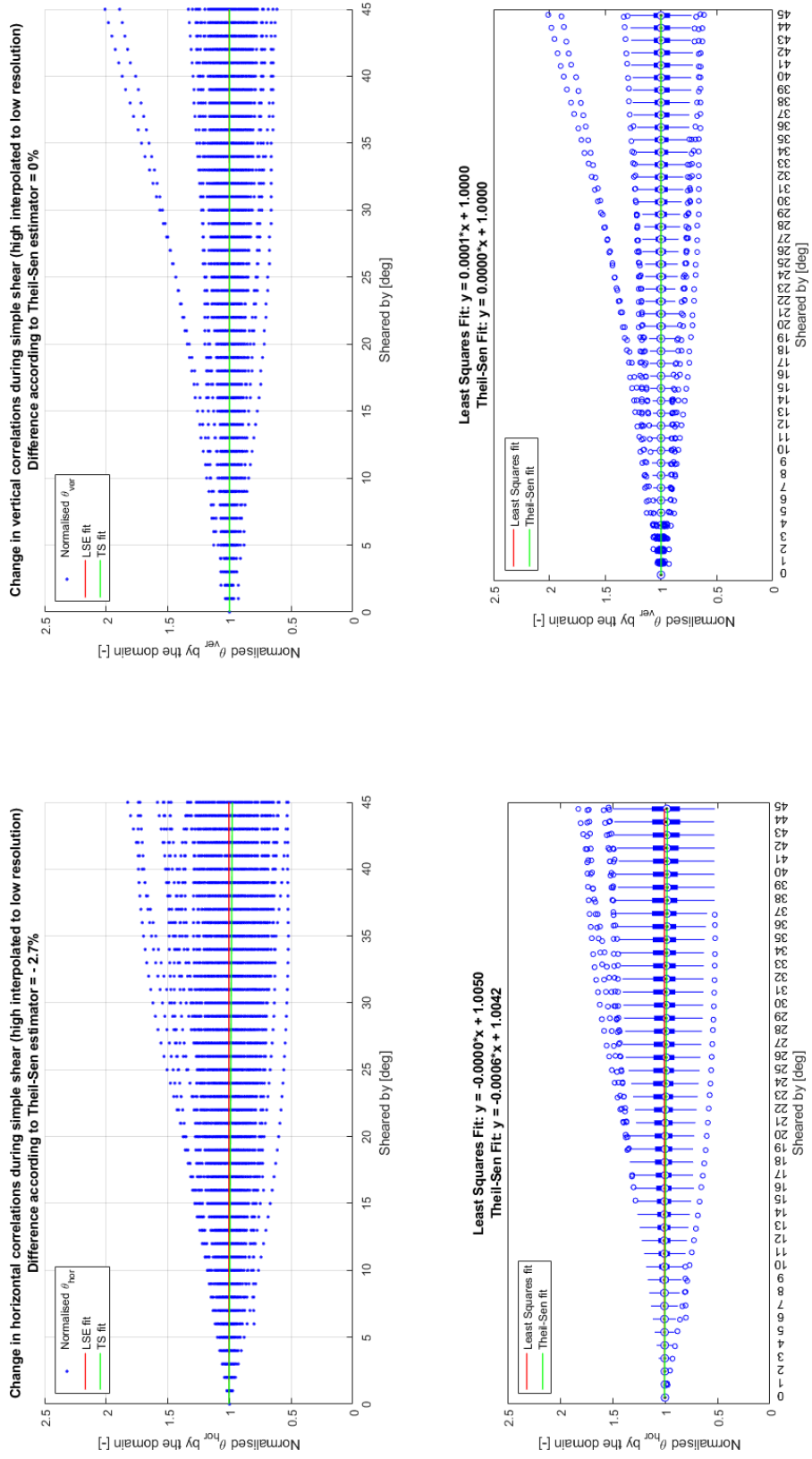


Figure B.17: Change in θ_h and θ_v due to simple shear of high to low resolution random fields, compared to the domain spatial variability

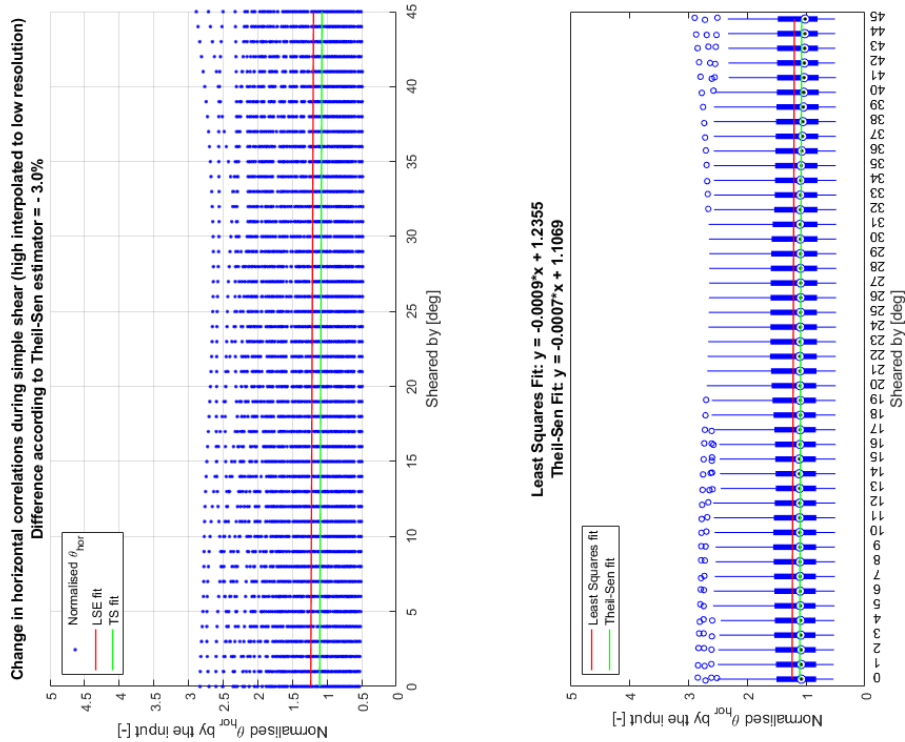
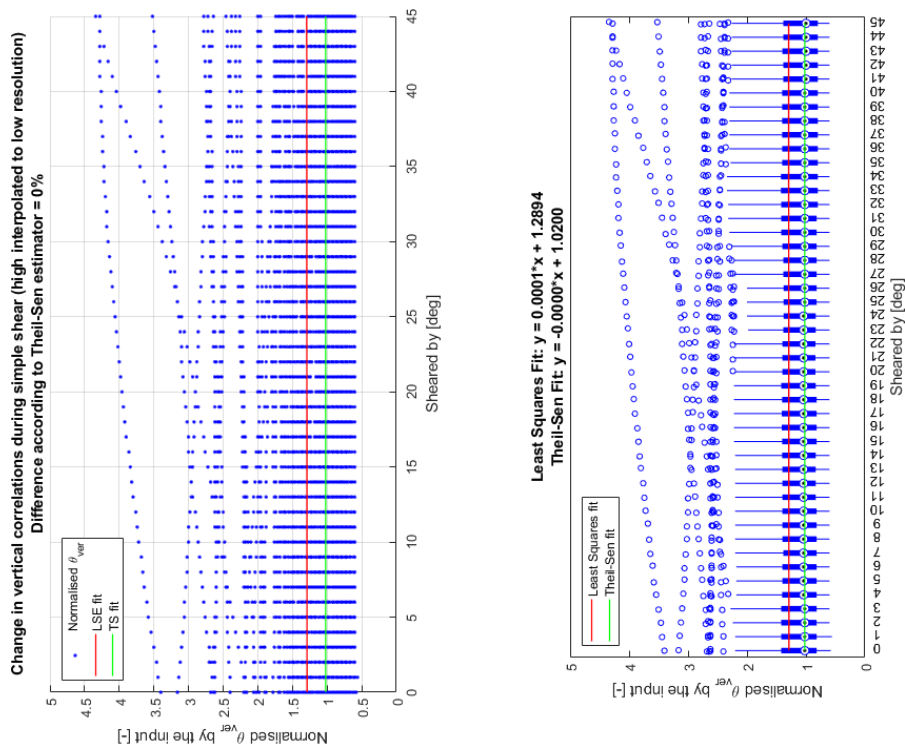


Figure B.18: Change in θ_h and θ_v due to simple shear of high to low resolution random fields, compared to the input spatial variability



Soil Layer Depth per CPT

Table C.1: The depth of the soil layers at the Leendert de Boerspolder. Peat₁ is the top peat layer and Peat₂ is the bottom peat layer.

CPT	Surface [m+NAP]	Top peat ₁ [m+NAP]	Bottom peat ₁ [m+NAP]	Top clay [m+NAP]	Bottom clay [m+NAP]	Top peat ₂ [m+NAP]	Bottom peat ₂ [m+NAP]
1	-1.99	-2.64	-4.39	-4.59	-10.90	-11.42	-11.83
2	-2.12	-2.52	-4.23	-4.43	-10.76	-11.33	-11.81
3	-2.18	-2.59	-4.29	-4.49	-10.76	-11.29	-11.91
4	-1.99	-2.73	-4.35	-4.55	-10.84	-11.45	-11.90
5	-1.97	-2.96	-4.27	-4.47	-10.79	-11.21	-11.89
6	-1.92	-2.64	-4.29	-4.49	-11.02	-11.62	-12.09
7	-1.92	-2.63	-4.27	-4.47	-10.76	-11.31	-11.85
8	-1.84	-2.72	-3.68	-3.88	-10.88	-11.30	-11.82
9	-1.79	-2.66	-3.67	-3.87	-11.07	-11.28	-11.78
10	-1.80	-2.62	-4.08	-4.28	-11.09	-11.30	-11.79
11	-1.82	-2.53	-4.40	-4.60	-11.00	-11.23	-11.71
12	-1.75	-2.39	-4.49	-4.69	-10.85	-11.38	-11.80
13	-2.94	-3.18	-4.87	-5.07	-11.17	-11.74	-12.28
14	-1.98	-2.77	-4.53	-4.73	-10.79	-11.40	-11.98
15	-1.92	-2.69	-4.55	-4.75	-10.84	-11.46	-11.99
16	-1.90	-2.53	-4.39	-4.59	-10.85	-11.39	-11.86
17	-1.90	-2.55	-4.16	-4.36	-10.81	-11.43	-11.83
18	-1.84	-2.54	-4.40	-4.60	-10.85	-11.39	-11.86
19	-1.81	-2.52	-4.27	-4.47	-10.81	-11.36	-11.76
20	-1.72	-2.43	-3.80	-4.00	-10.94	-11.27	-11.80
21	-1.67	-2.37	-4.17	-4.37	-11.08	-11.30	-11.80
22	-1.68	-2.44	-4.47	-4.67	-11.11	-11.33	-11.72
23	-1.58	-2.14	-4.26	-4.46	-10.89	-11.43	-11.88
24	-1.75	-2.39	-4.67	-4.87	-10.79	-11.35	-11.86
25	-1.83	-2.45	-4.59	-4.79	-10.69	-11.34	-11.77
26	-1.88	-2.63	-4.63	-4.83	-10.63	-11.41	-11.93
27	-1.83	-2.54	-4.80	-5.00	-10.82	-11.40	-11.92
28	-1.75	-2.32	-4.66	-4.86	-10.85	-11.38	-11.88
29	-1.73	-2.41	-4.62	-4.82	-10.89	-11.44	-11.84
30	-1.69	-2.29	-4.54	-4.74	-10.90	-11.35	-11.78
31	-1.64	-2.17	-4.40	-4.60	-10.85	-11.31	-11.80
32	-1.53	-2.05	-4.20	-4.40	-11.11	-11.34	-11.76
33	-1.56	-2.10	-4.48	-4.68	-11.17	-11.38	-11.90

CPT	Surface [m+NAP]	Top peat₁ [m+NAP]	Bottom peat₁ [m+NAP]	Top clay [m+NAP]	Bottom clay [m+NAP]	Top peat₂ [m+NAP]	Bottom peat₂ [m+NAP]
34	-0.34	-3.44	-5.24	-5.44	-10.84	-11.38	-11.86
35	-0.43	-3.31	-5.35	-5.55	-10.93	-11.38	-11.83
36	-0.46	-3.45	-5.50	-5.70	-10.76	-11.40	-11.86
37	-0.47	-3.54	-5.19	-5.39	-10.88	-11.41	-11.86
38	-0.47	-3.49	-5.33	-5.53	-10.78	-11.28	-11.81
39	-0.49	-3.61	-5.38	-5.58	-10.89	-11.35	-11.80
40	-0.44	-3.35	-5.30	-5.50	-10.94	-11.34	-11.78
41	-0.43	-3.29	-5.13	-5.33	-10.72	-11.32	-11.85
42	-0.43	-2.95	-4.88	-5.08	-10.83	-11.29	-11.77
43	-0.41	-2.73	-4.64	-4.84	-10.69	-11.31	-11.77
44	-0.31	-2.98	-4.83	-5.03	-11.15	-11.37	-11.81
45	-1.12	-2.76	-5.07	-5.27	-10.86	-11.41	-11.85
46	-1.39	-3.21	-5.07	-5.27	-10.75	-11.39	-11.84
47	-1.41	-3.18	-4.98	-5.18	-10.65	-11.43	-11.97
48	-1.37	-3.40	-5.21	-5.41	-11.21	-11.43	-11.88
49	-1.36	-3.37	-5.04	-5.24	-11.21	-11.43	-11.80
50	-1.36	-2.86	-5.01	-5.21	-10.89	-11.46	-11.90
51	-1.35	-2.74	-4.97	-5.17	-10.80	-11.40	-11.90
52	-1.37	-2.58	-4.74	-4.94	-10.74	-11.39	-11.76
53	-1.36	-2.58	-4.59	-4.79	-10.79	-11.36	-11.77
54	-1.26	-2.39	-4.52	-4.72	-11.18	-11.39	-11.93
55	-1.86	-2.59	-4.60	-4.80	-10.79	-11.39	-11.89
56	-1.88	-2.67	-4.57	-4.77	-10.73	-11.41	-11.93
57	-1.90	-2.61	-4.63	-4.83	-10.86	-11.45	-11.93
58	-1.83	-2.42	-4.54	-4.74	-10.86	-11.43	-11.94
59	-1.80	-2.53	-4.47	-4.67	-10.91	-11.40	-11.86
60	-1.78	-2.45	-4.46	-4.66	-10.79	-11.36	-11.84
61	-1.69	-2.29	-4.25	-4.45	-10.77	-11.23	-11.71
62	-1.63	-2.08	-4.08	-4.28	-10.81	-11.30	-11.75
63	-2.01	-2.67	-4.41	-4.61	-10.83	-11.35	-11.88
64	-1.97	-2.65	-4.40	-4.60	-10.80	-11.43	-11.90
65	-1.95	-2.63	-4.37	-4.57	-11.23	-11.46	-11.86
66	-1.88	-2.58	-4.30	-4.50	-10.78	-11.33	-11.86
67	-1.86	-2.62	-4.34	-4.54	-10.80	-11.33	-11.80
68	-1.85	-2.70	-3.86	-4.06	-10.99	-11.41	-11.91
69	-0.32	-3.30	-5.31	-5.51	-10.82	-11.37	-11.82
70	-0.47	-3.51	-5.26	-5.46	-10.76	-11.39	-11.83
71	-0.48	-3.59	-5.49	-5.69	-10.83	-11.42	-11.85
72	-0.51	-3.92	-5.25	-5.45	-10.84	-11.41	-11.92
73	-0.45	-3.68	-5.14	-5.34	-10.87	-11.35	-11.80
74	-0.48	-4.00	-5.28	-5.48	-10.83	-11.37	-11.76
75	-0.39	-3.59	-5.17	-5.37	-10.76	-11.31	-11.85
76	-0.41	-3.52	-5.03	-5.23	-10.77	-11.31	-11.77
77	-0.45	-3.23	-4.80	-5.00	-10.79	-11.40	-11.85
78	-0.35	-3.07	-4.76	-4.96	-10.92	-11.38	-11.74
79	-0.47	-3.81	-5.25	-5.45	-11.24	-11.47	-11.91
80	-0.47	-3.67	-5.34	-5.54	-10.81	-11.42	-11.86
81	-0.46	-3.49	-5.25	-5.45	-10.84	-11.34	-11.80
82	-0.44	-3.57	-5.22	-5.42	-10.82	-11.39	-11.85
83	-0.50	-3.76	-5.37	-5.57	-10.90	-11.45	-11.84

CPT	Surface [m+NAP]	Top peat₁ [m+NAP]	Bottom peat₁ [m+NAP]	Top clay [m+NAP]	Bottom clay [m+NAP]	Top peat₂ [m+NAP]	Bottom peat₂ [m+NAP]
84	-0.46	-3.40	-5.29	-5.49	-10.88	-11.29	-11.81
85	-0.41	-3.42	-5.26	-5.46	-10.81	-11.38	-11.83
86	-0.43	-4.09	-5.28	-5.48	-10.74	-11.36	-11.81
87	-1.93	-2.58	-4.35	-4.55	-10.80	-11.37	-11.86
88	-1.92	-2.52	-4.38	-4.58	-10.80	-11.42	-11.95
89	-1.87	-2.42	-4.41	-4.61	-10.92	-11.41	-11.83
90	-1.83	-2.35	-4.46	-4.66	-10.81	-11.37	-11.88
91	-1.76	-2.35	-4.62	-4.82	-10.84	-11.46	-11.86
92	-1.70	-2.47	-4.82	-5.02	-10.85	-11.38	-11.89
93	-1.40	-3.00	-4.93	-5.13	-10.95	-11.40	-11.84
94	-0.93	-2.88	-5.07	-5.27	-10.85	-11.33	-11.77
95	-1.72	-2.44	-4.65	-4.85	-10.73	-11.41	-11.84
96	-1.78	-2.31	-4.72	-4.92	-10.87	-11.40	-11.91
97	-1.34	-2.81	-4.92	-5.12	-10.88	-11.33	-11.81
98	-1.41	-3.40	-5.25	-5.45	-10.89	-11.45	-11.93
99	-1.86	-2.54	-4.44	-4.64	-10.87	-11.41	-11.90
100	-1.89	-2.50	-4.40	-4.60	-10.86	-11.41	-11.89

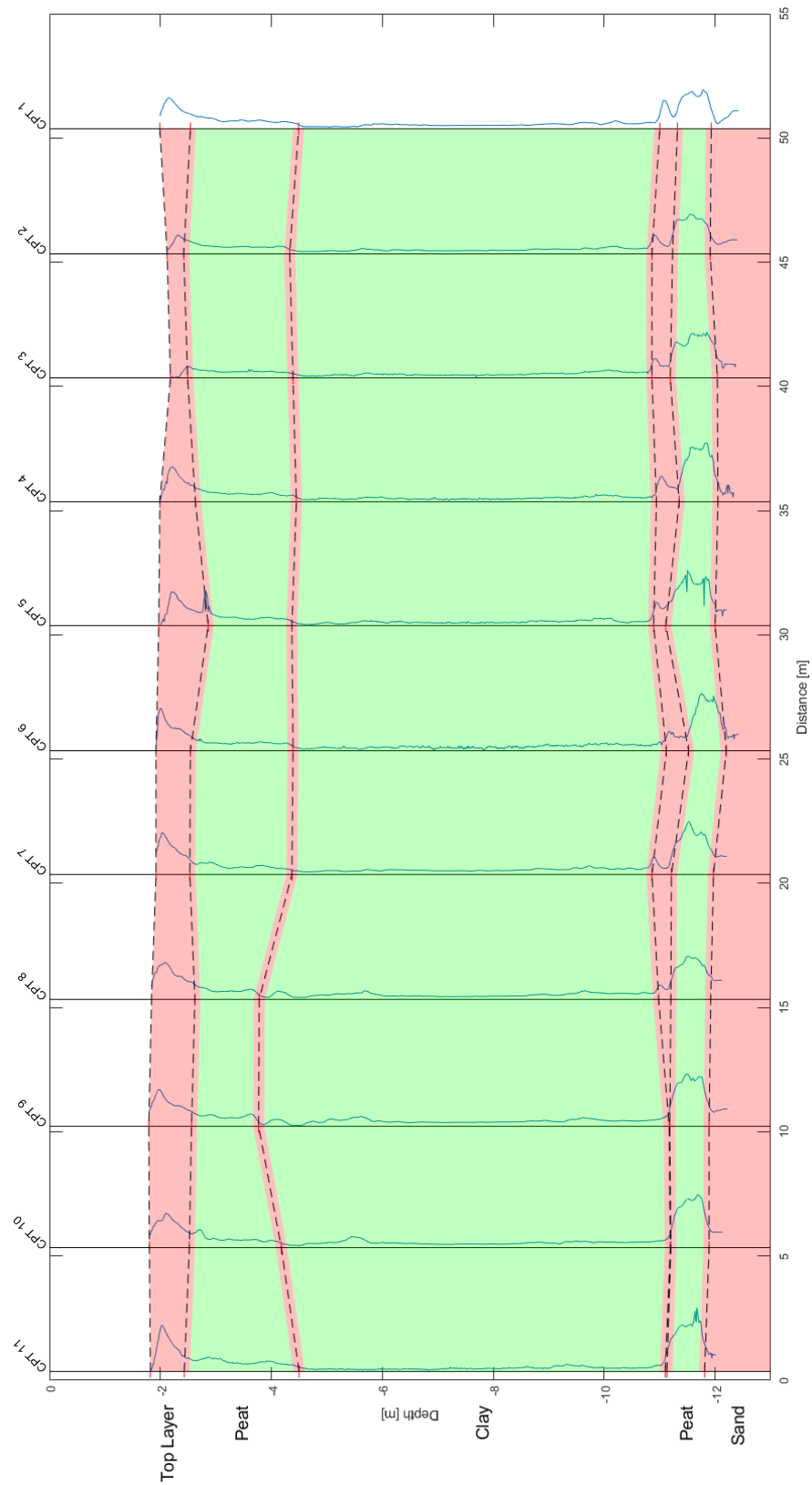


Figure C.1: Soil layer identification for line 1

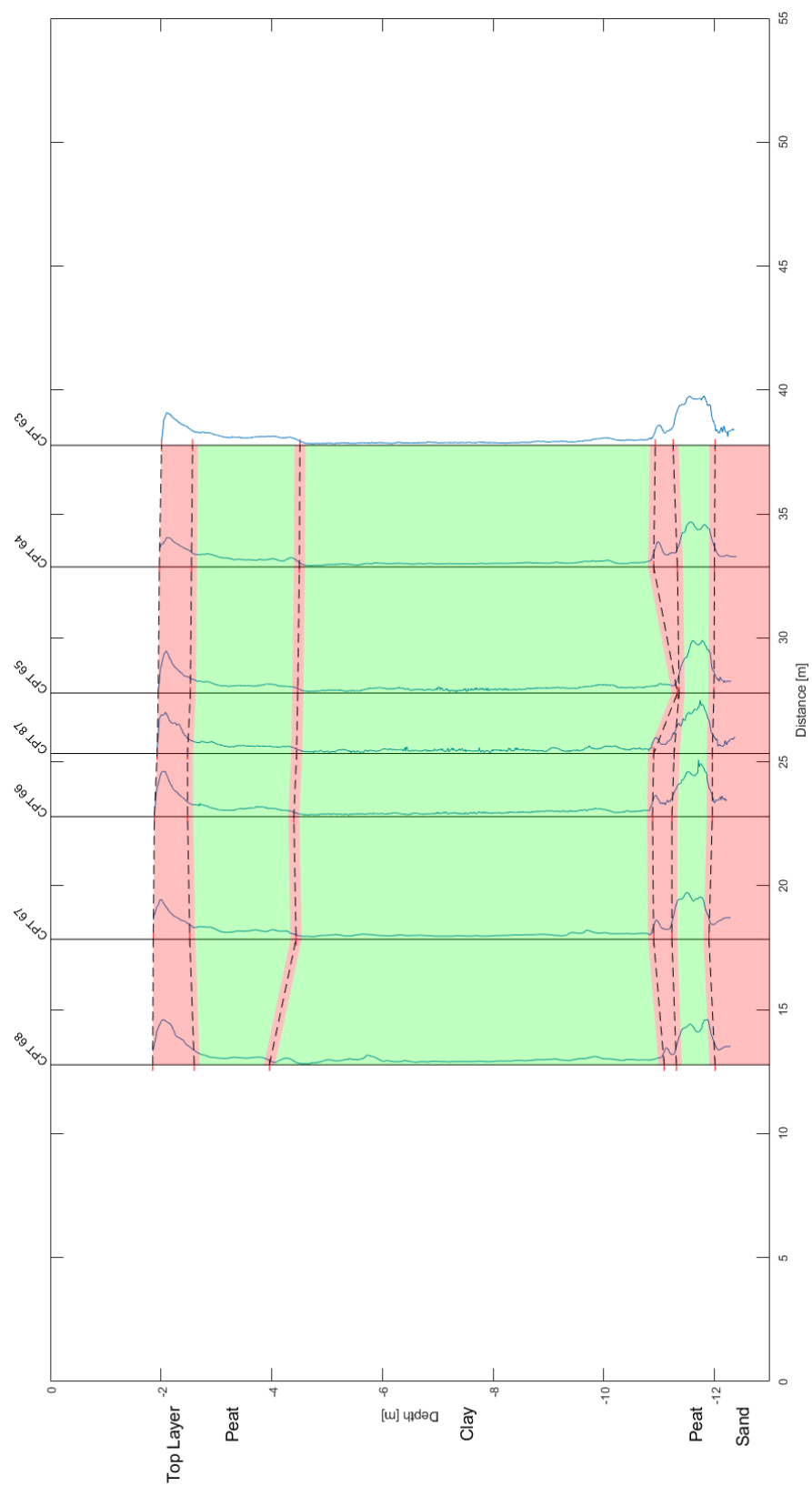


Figure C.2: Soil layer identification for line 2

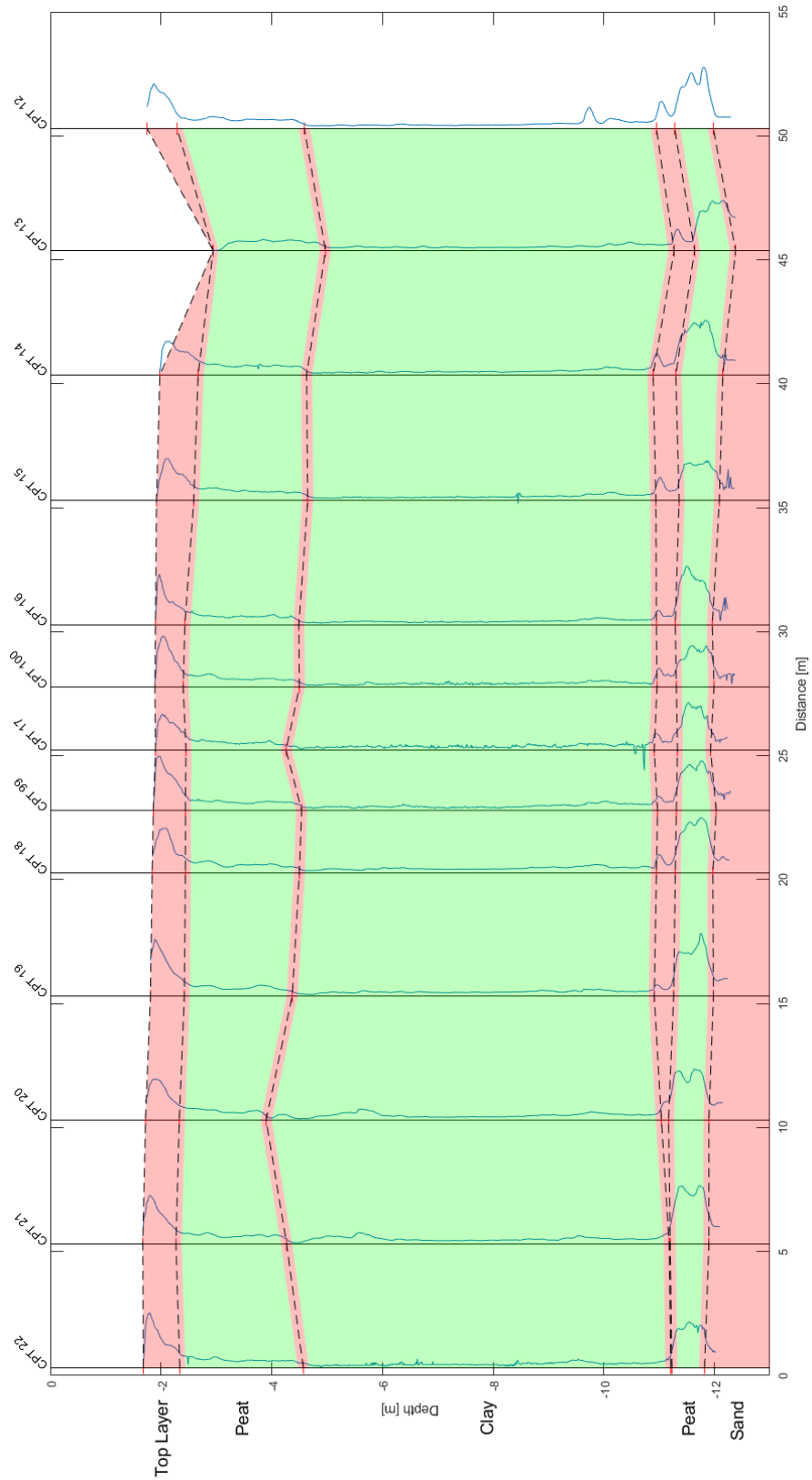


Figure C.3: Soil layer identification for line 3

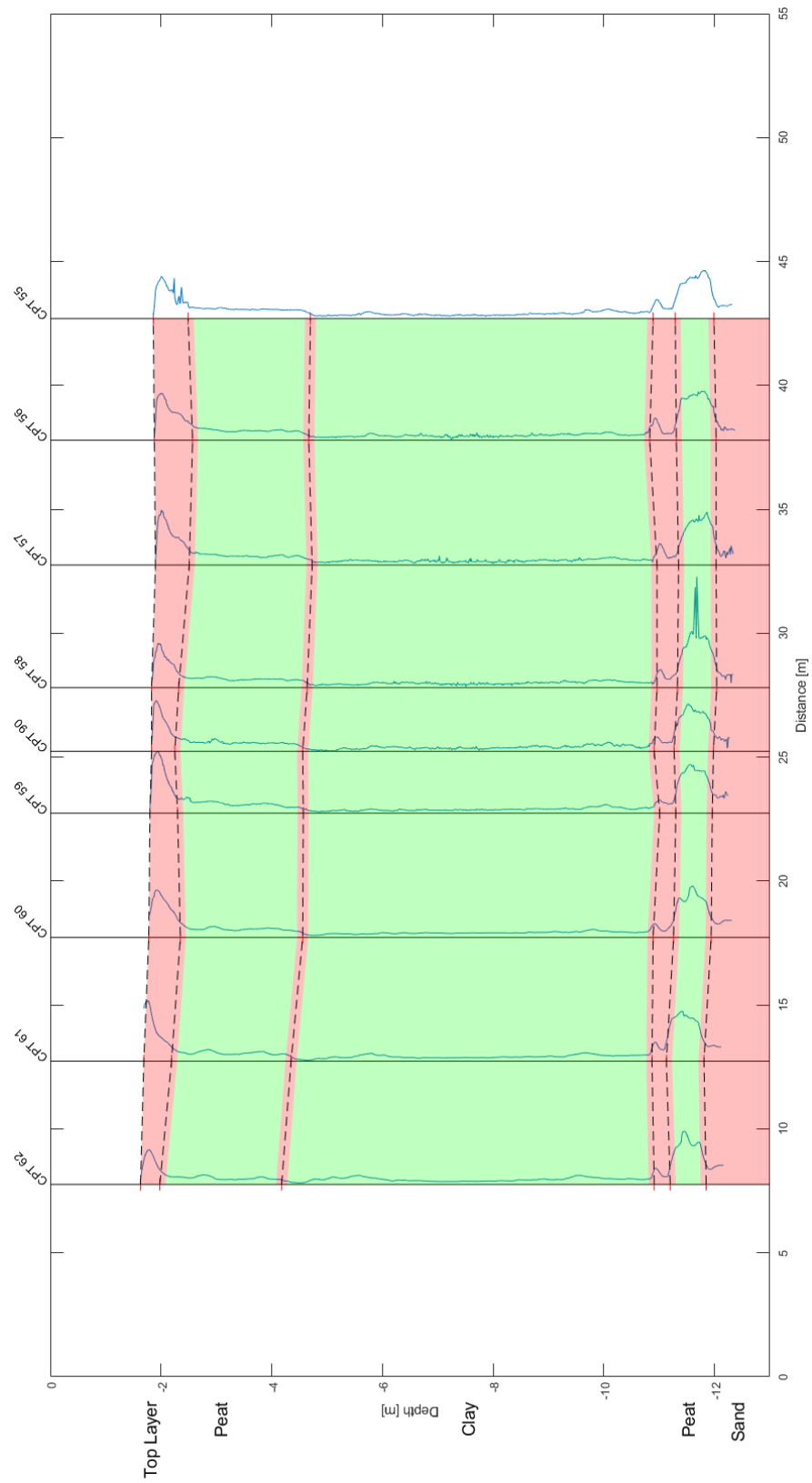


Figure C.4: Soil layer identification for line 4

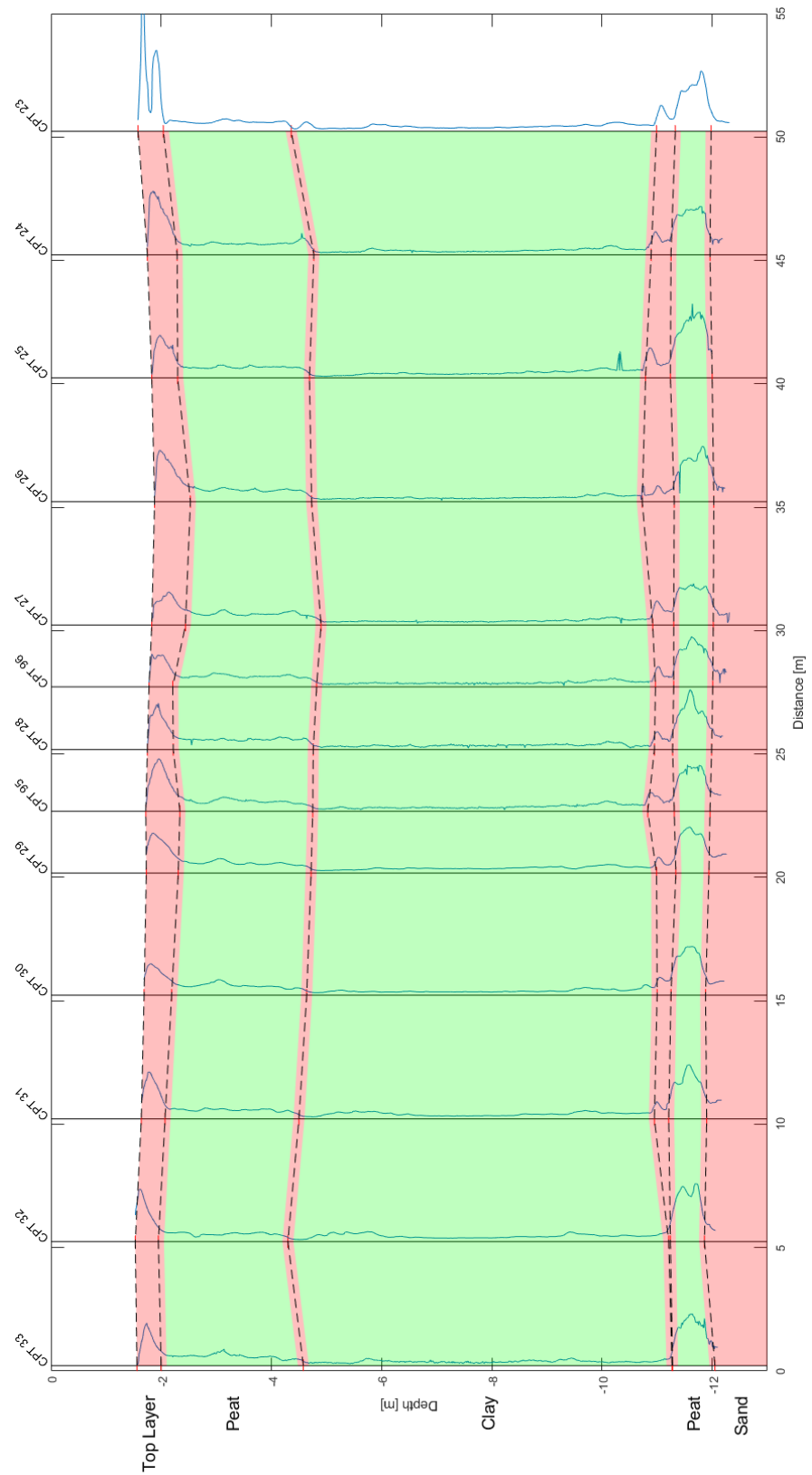


Figure C.5: Soil layer identification for line 5

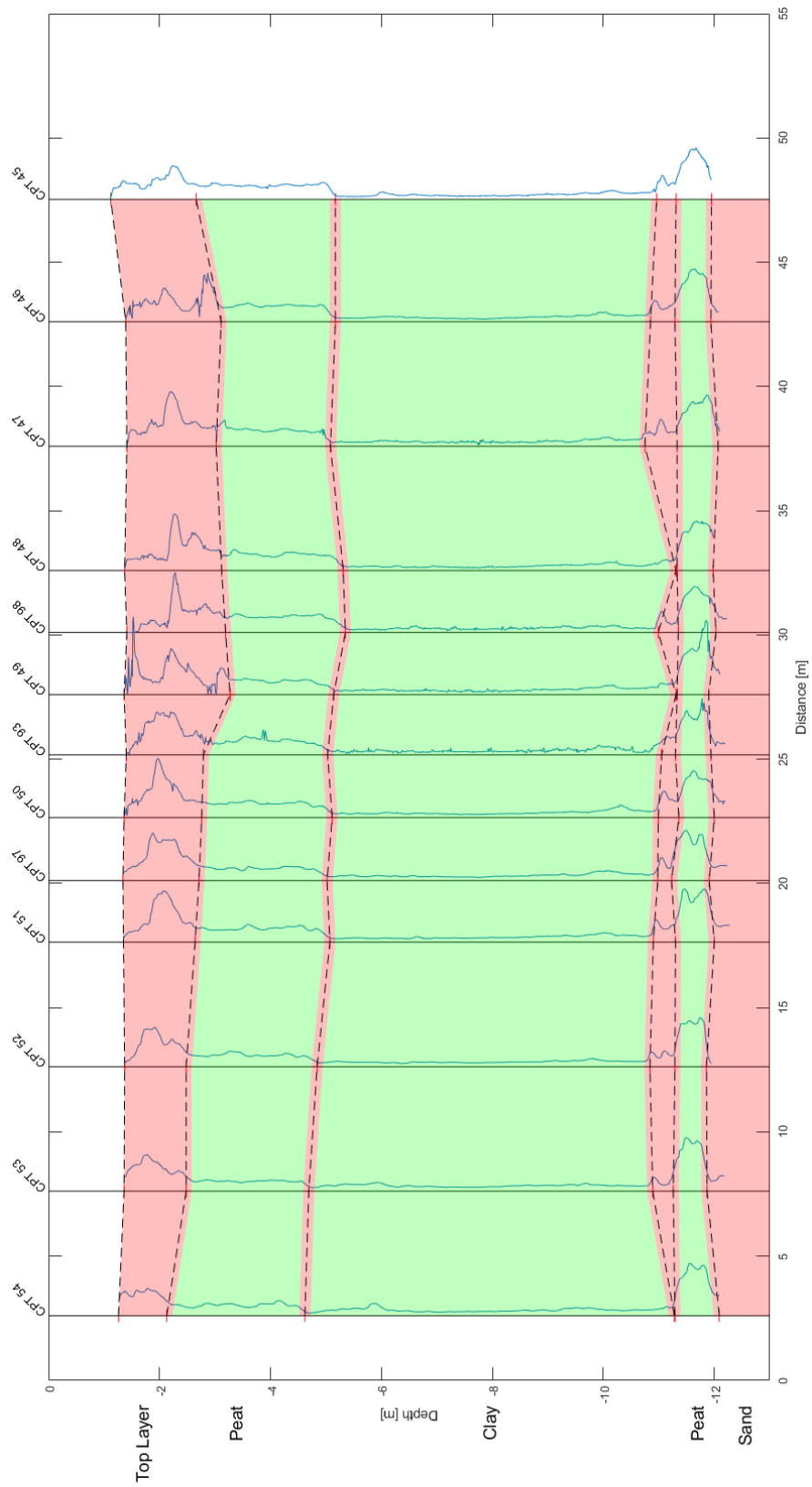


Figure C.6: Soil layer identification for line 6

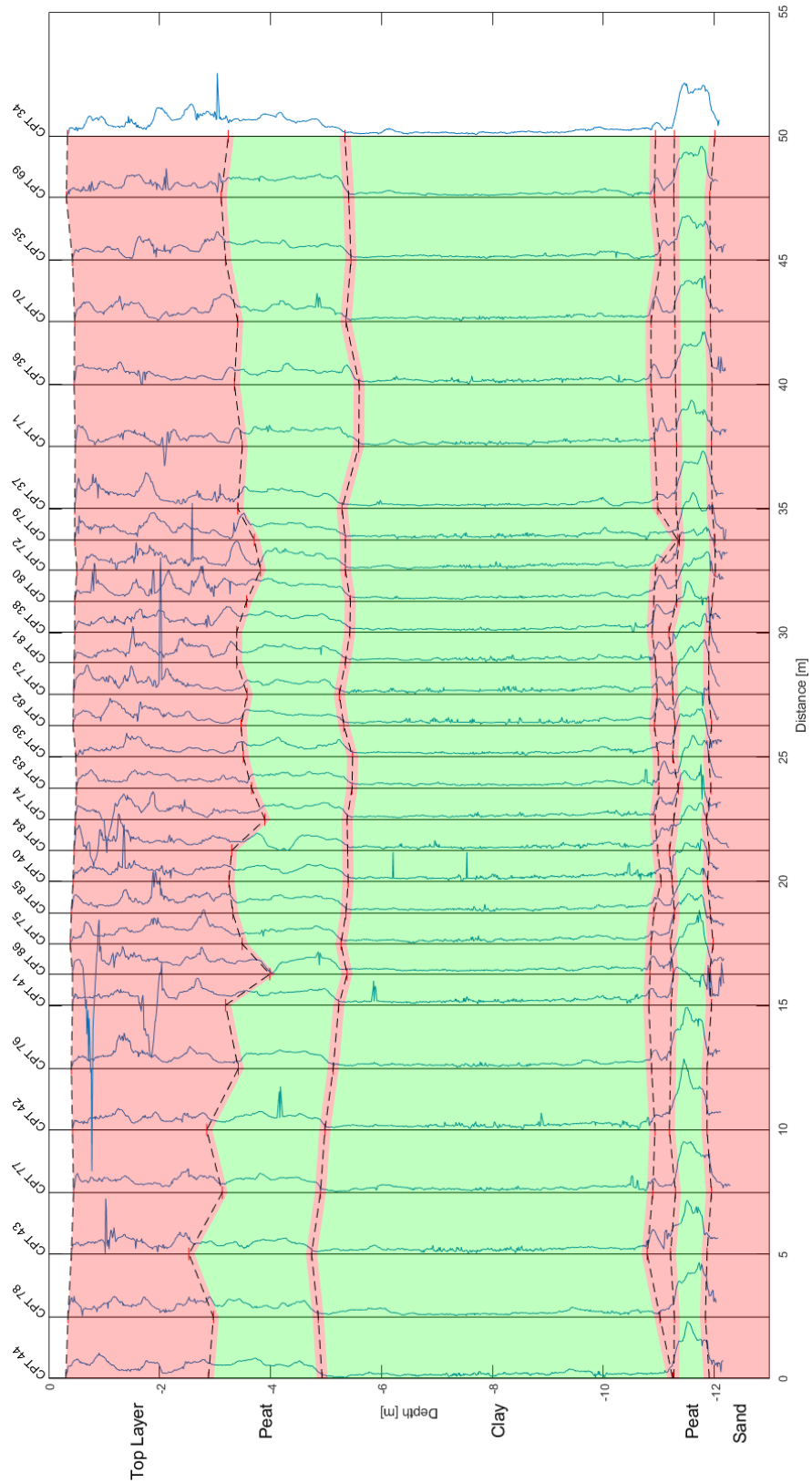


Figure C.7: Soil layer identification for line 7

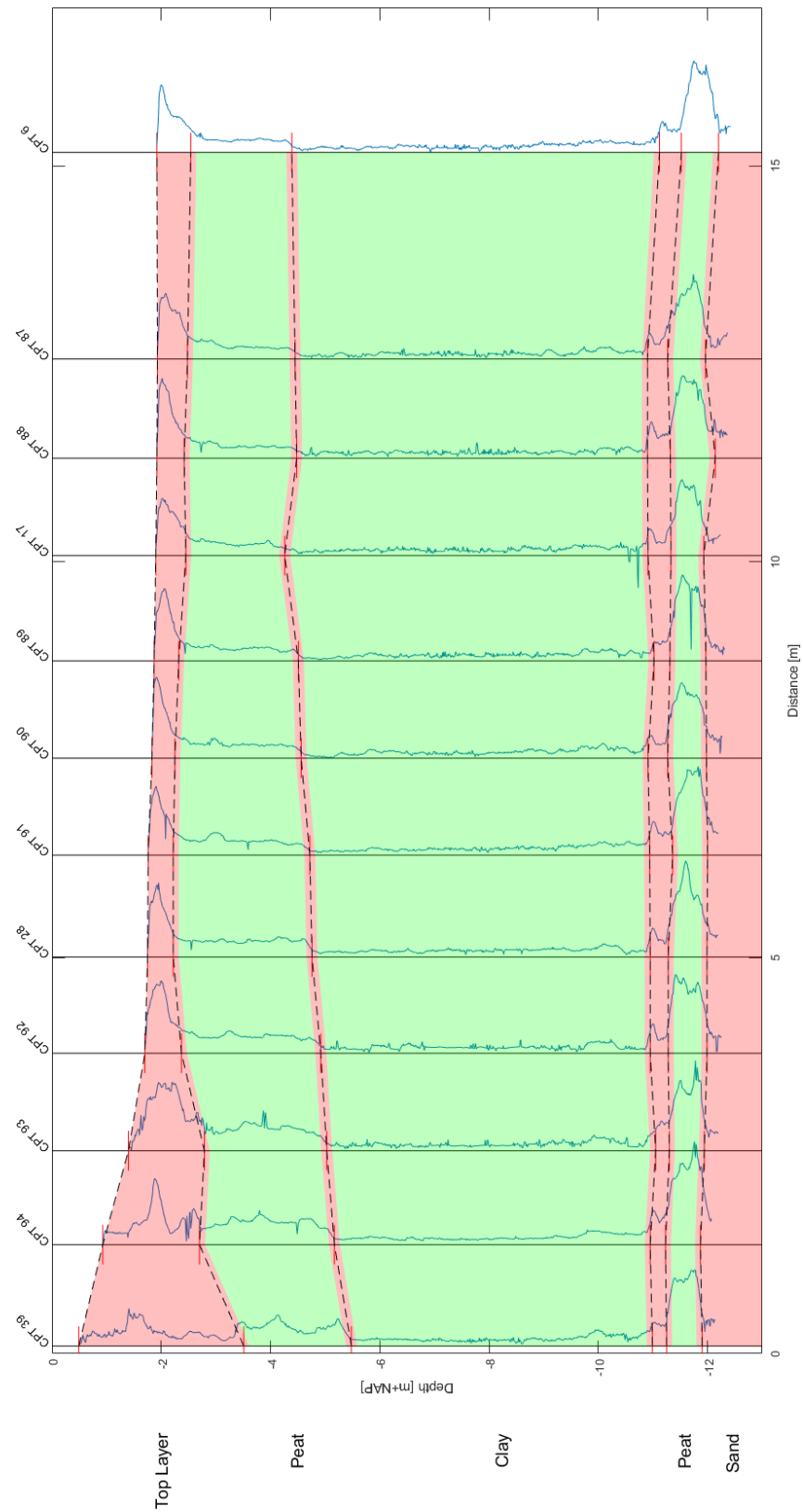


Figure C.8: Soil layer identification for line 8, which is perpendicular to the dyke

D

Trend Identification and Removal

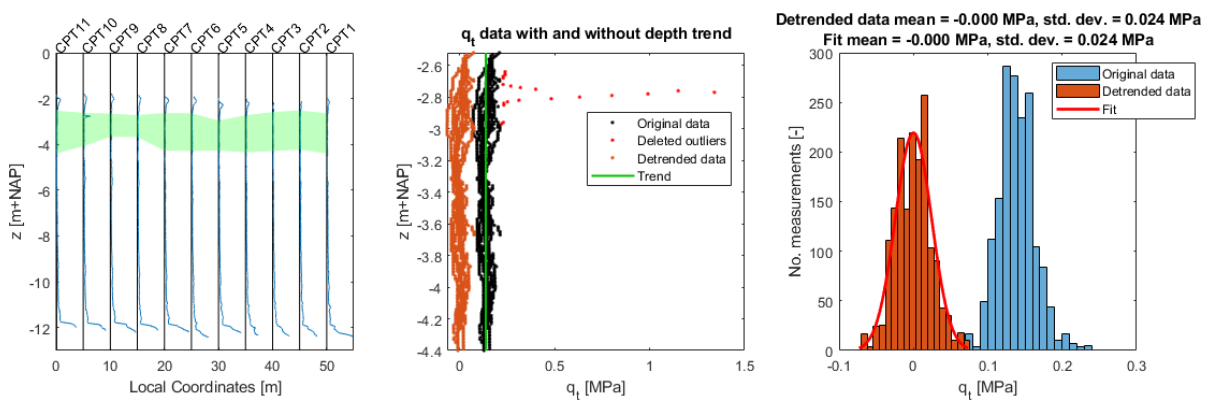


Figure D.1: Trend identification and removal for the first peat layer at CPT line 1

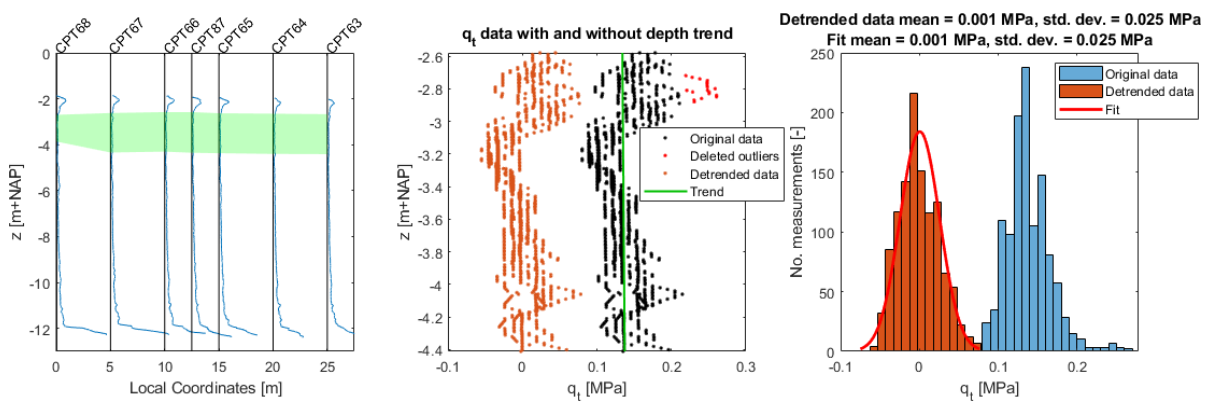


Figure D.2: Trend identification and removal for the first peat layer at CPT line 2

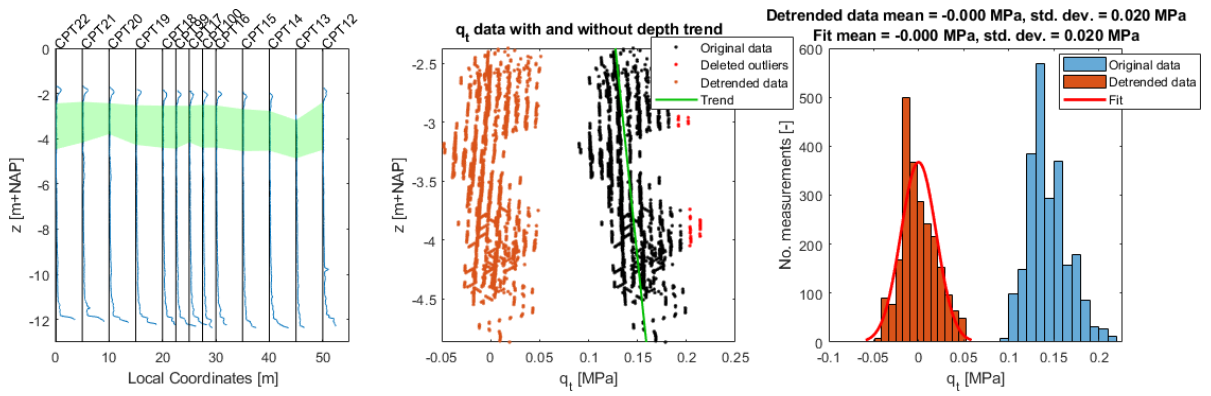


Figure D.3: Trend identification and removal for the first peat layer at CPT line 3

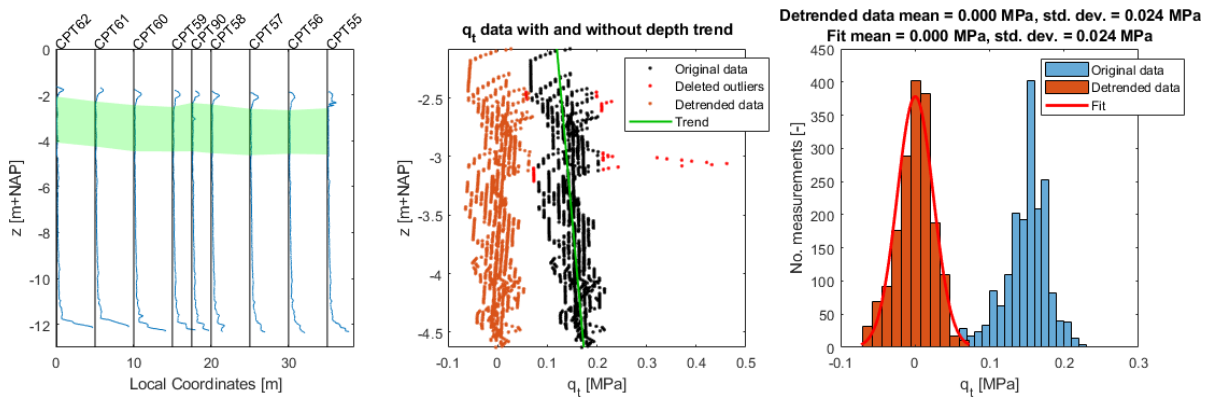


Figure D.4: Trend identification and removal for the first peat layer at CPT line 4

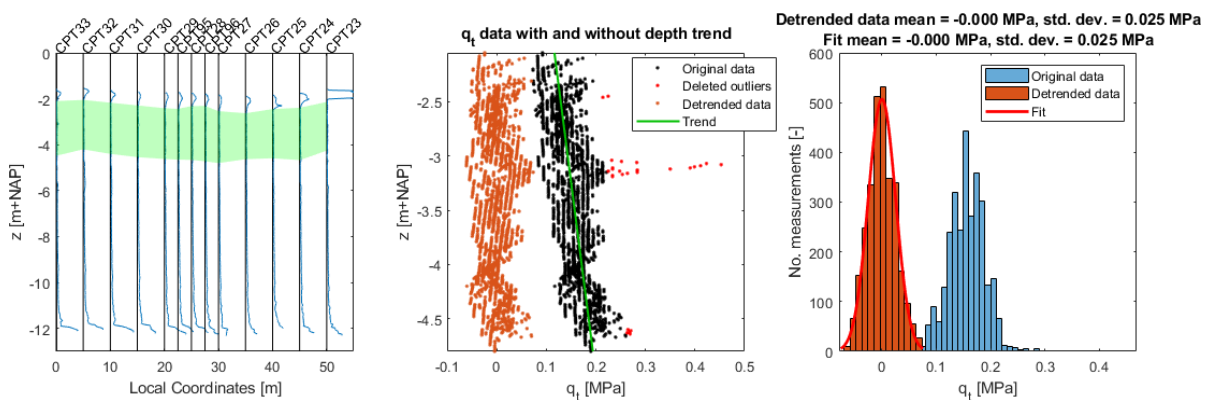


Figure D.5: Trend identification and removal for the first peat layer at CPT line 5

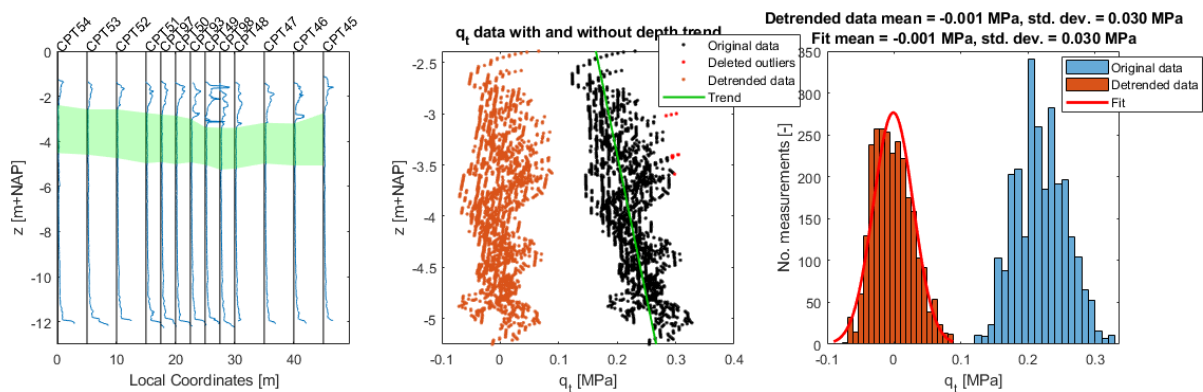


Figure D.6: Trend identification and removal for the first peat layer at CPT line 6

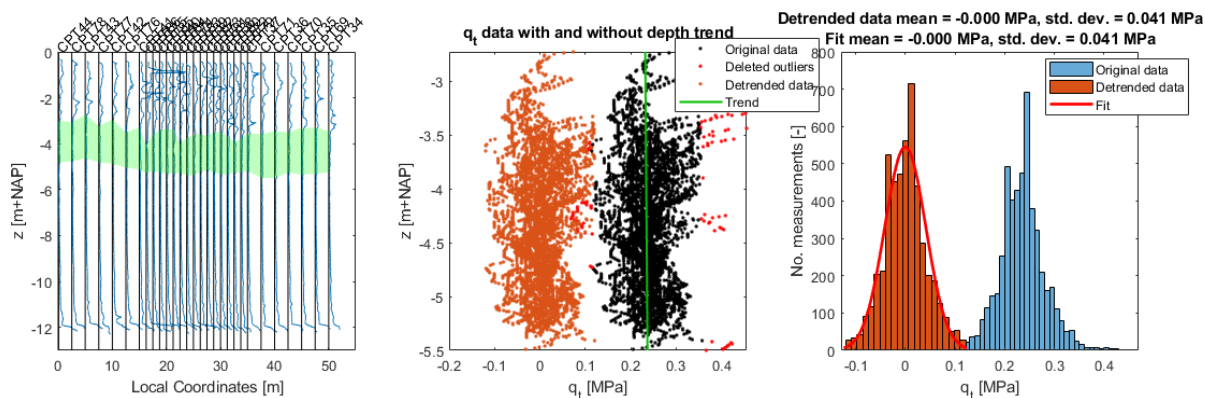


Figure D.7: Trend identification and removal for the first peat layer at CPT line 7

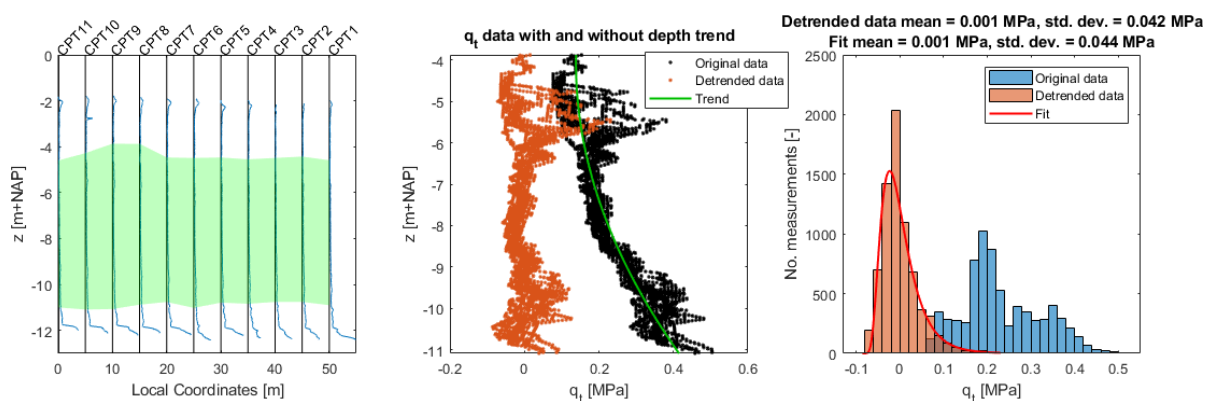


Figure D.8: Trend identification and removal for the clay layer at CPT line 1

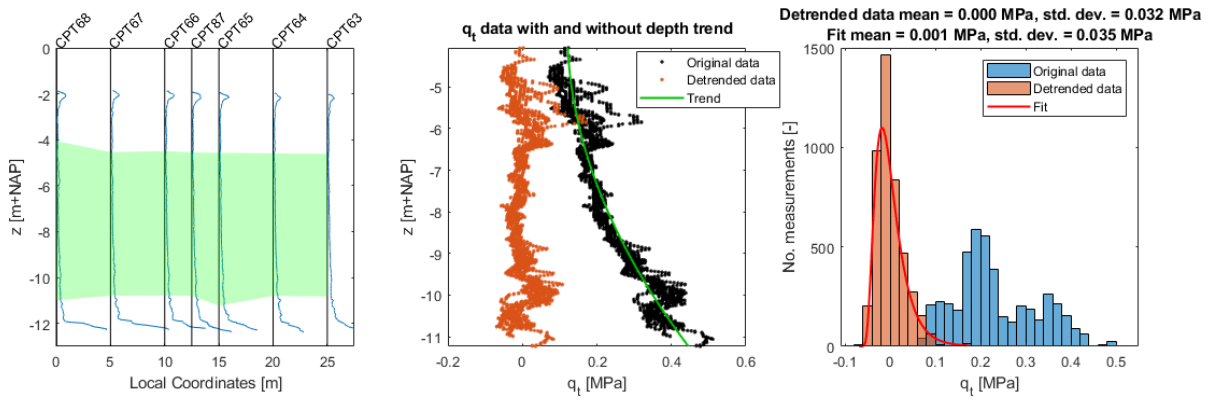


Figure D.9: Trend identification and removal for the clay layer at CPT line 2

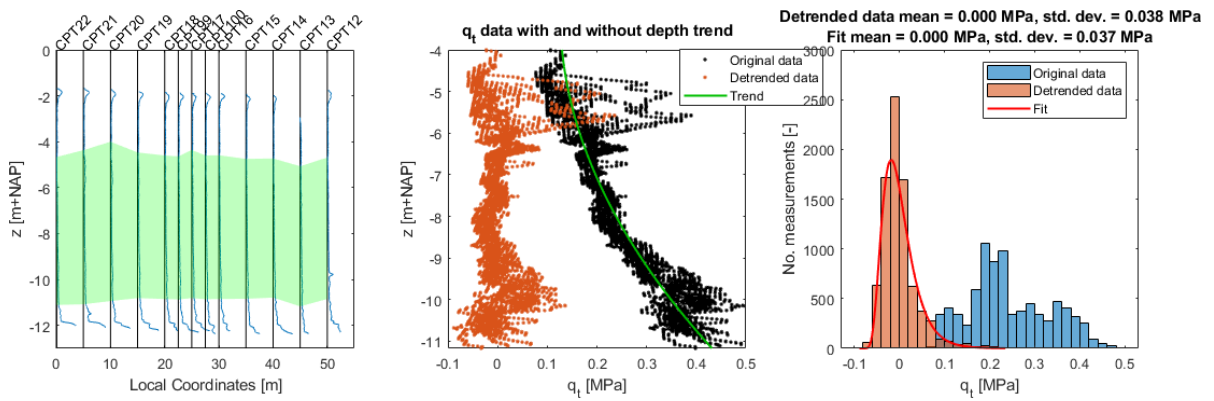


Figure D.10: Trend identification and removal for the clay layer at CPT line 3

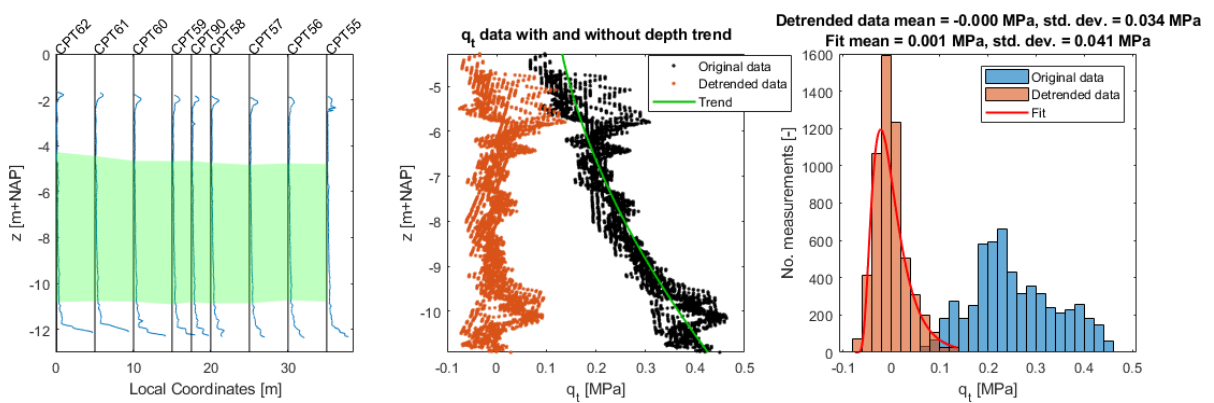


Figure D.11: Trend identification and removal for the clay layer at CPT line 4

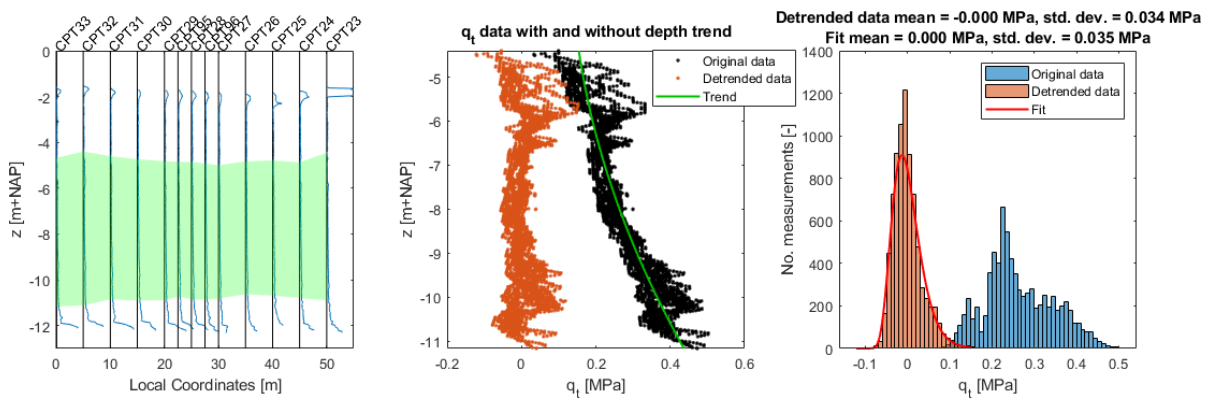


Figure D.12: Trend identification and removal for the clay layer at CPT line 5

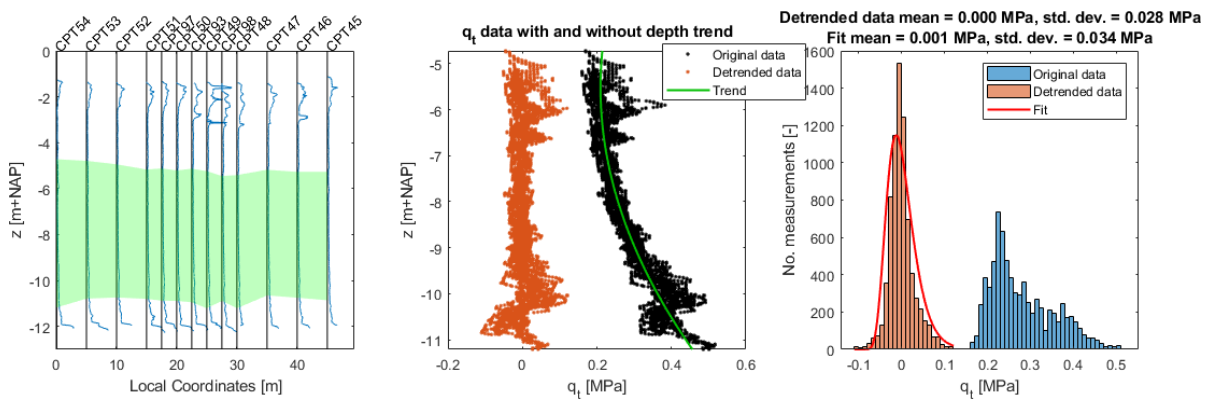


Figure D.13: Trend identification and removal for the clay layer at CPT line 6

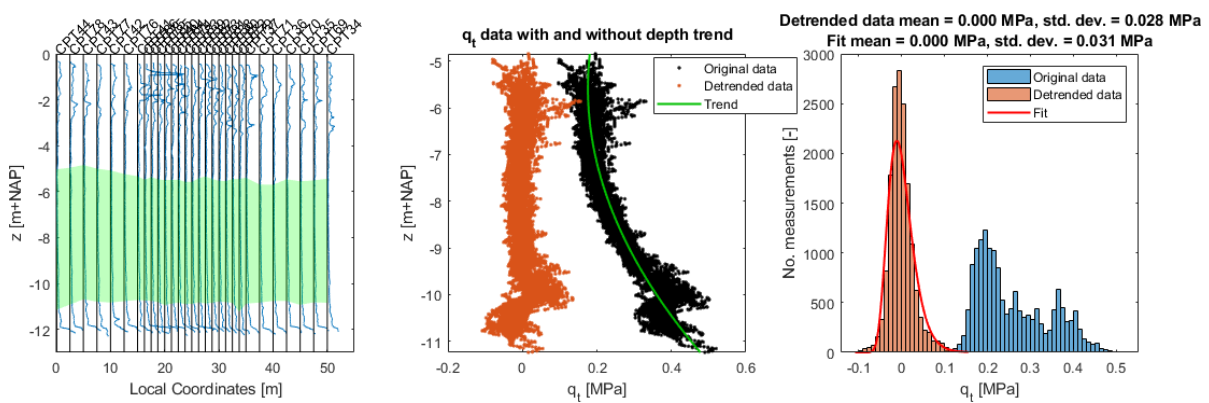


Figure D.14: Trend identification and removal for the clay layer at CPT line 7

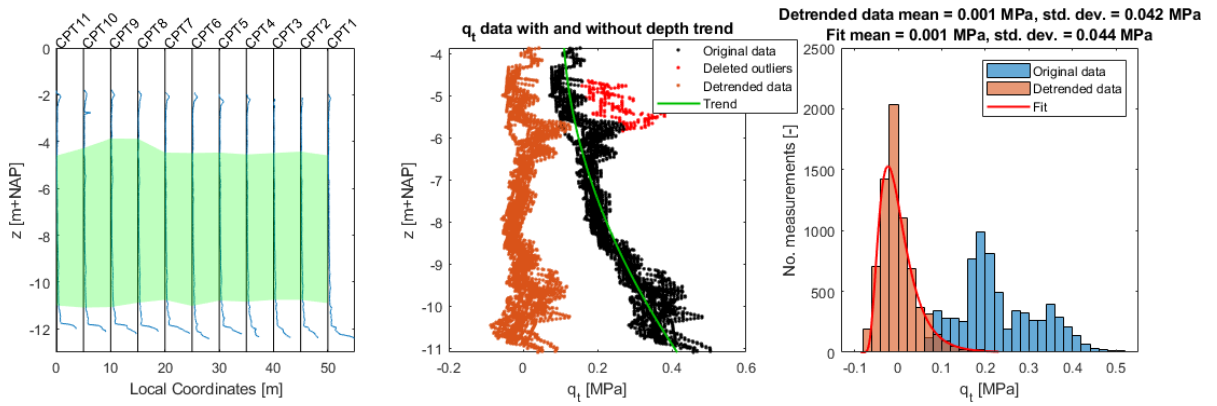


Figure D.15: Trend identification and removal for the clay layer without the additional layer at CPT line 1

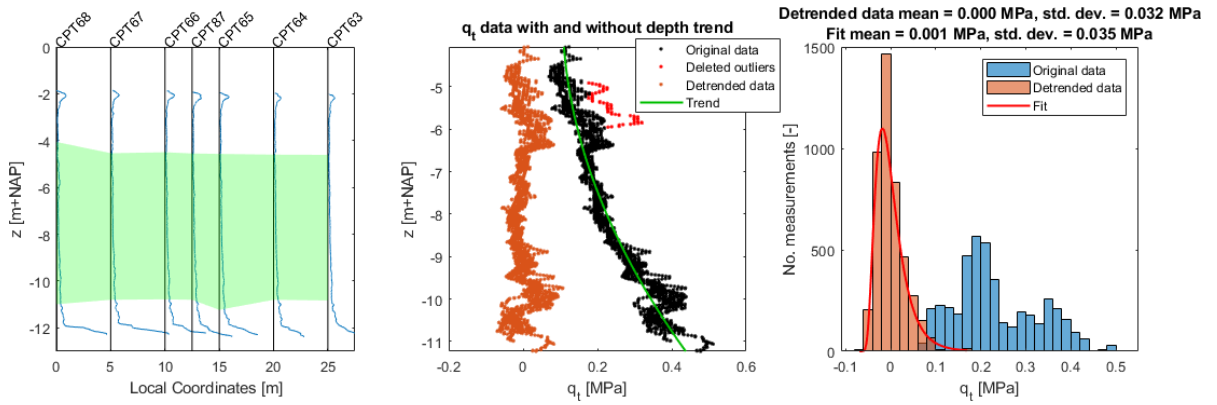


Figure D.16: Trend identification and removal for the clay layer without the additional layer at CPT line 2

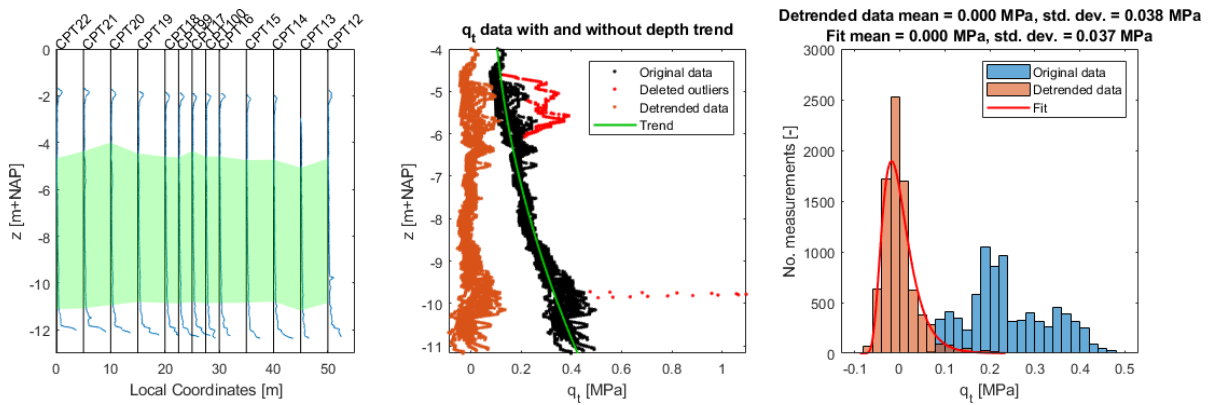


Figure D.17: Trend identification and removal for the clay layer without the additional layer at CPT line 3

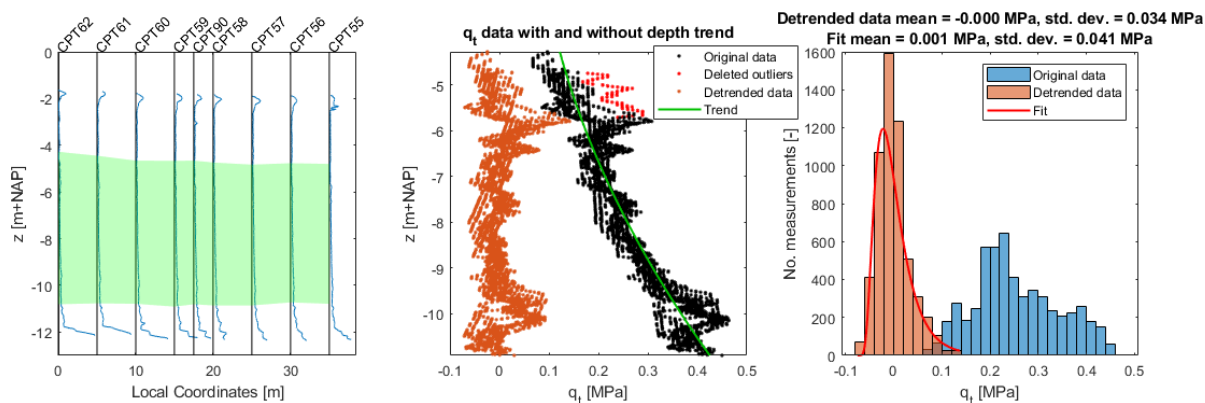


Figure D.18: Trend identification and removal for the clay layer without the additional layer at CPT line 4

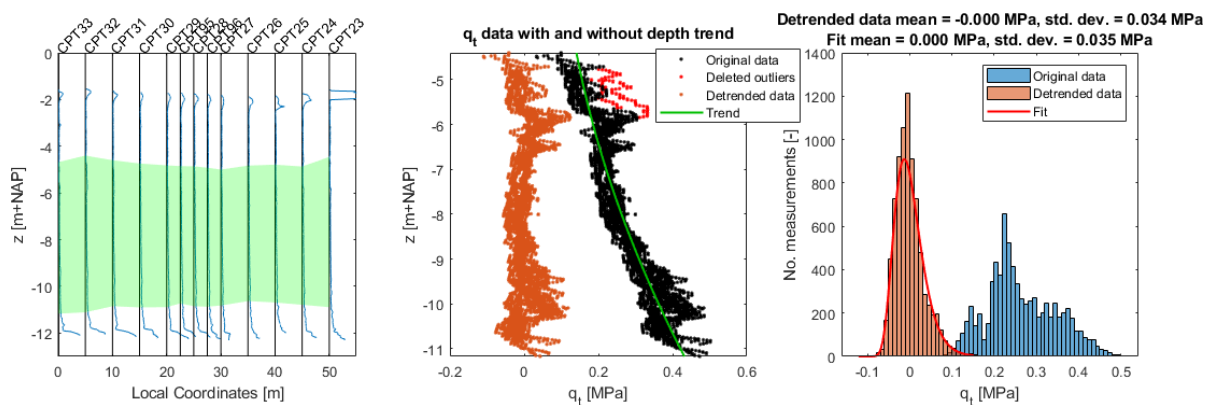


Figure D.19: Trend identification and removal for the clay layer without the additional layer at CPT line 5

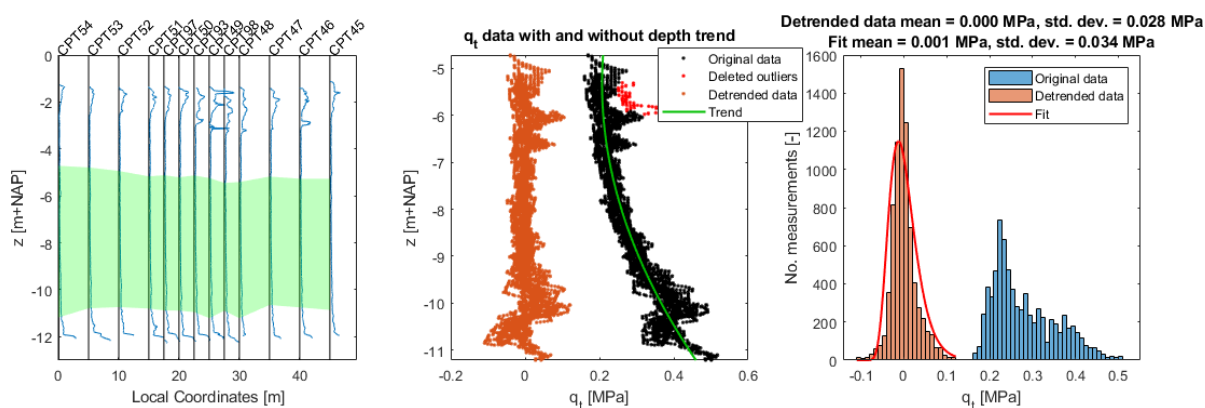


Figure D.20: Trend identification and removal for the clay layer without the additional layer at CPT line 6

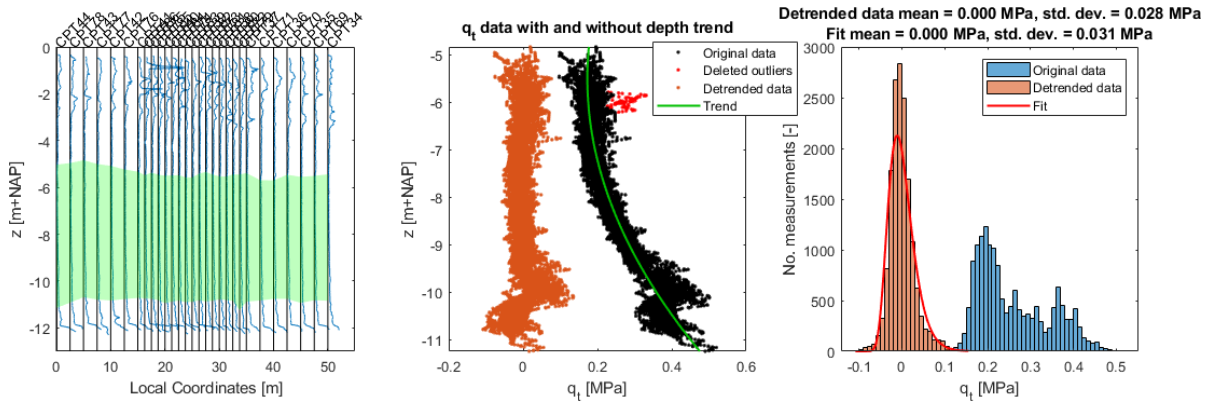


Figure D.21: Trend identification and removal for the clay layer without the additional layer at CPT line 7

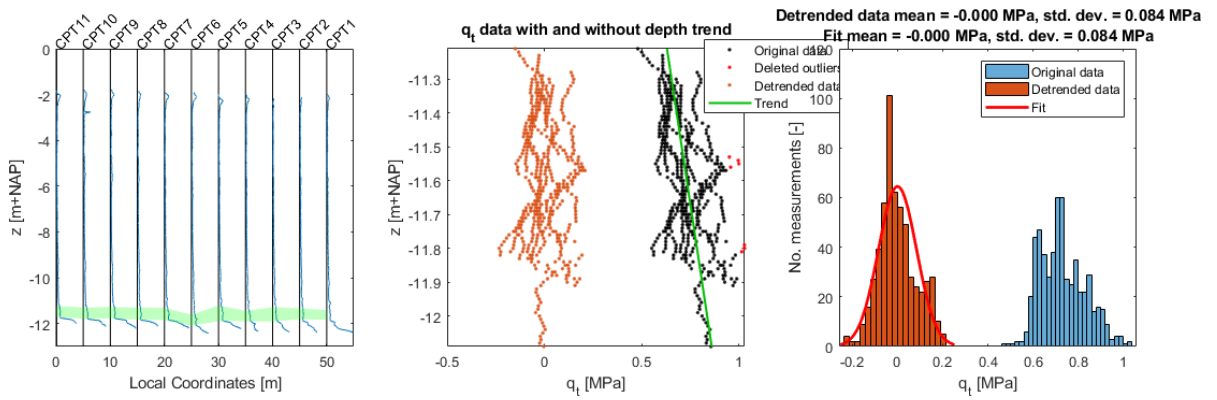


Figure D.22: Trend identification and removal for the second peat layer at CPT line 1

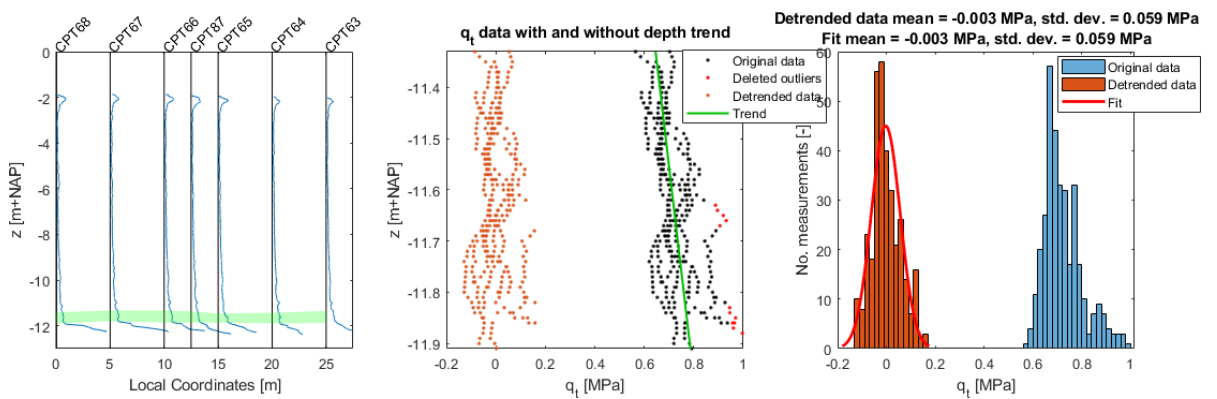


Figure D.23: Trend identification and removal for the second peat layer at CPT line 2

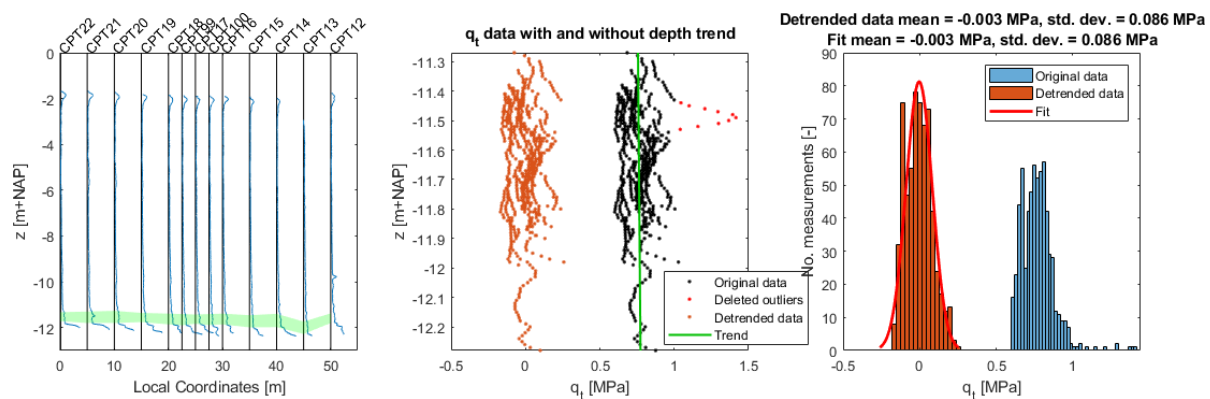


Figure D.24: Trend identification and removal for the second peat layer at CPT line 3

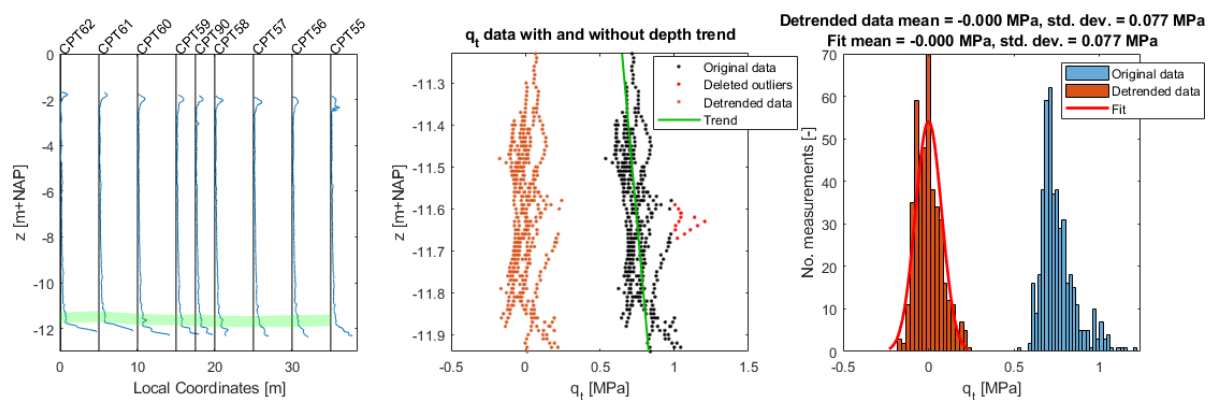


Figure D.25: Trend identification and removal for the second peat layer at CPT line 4

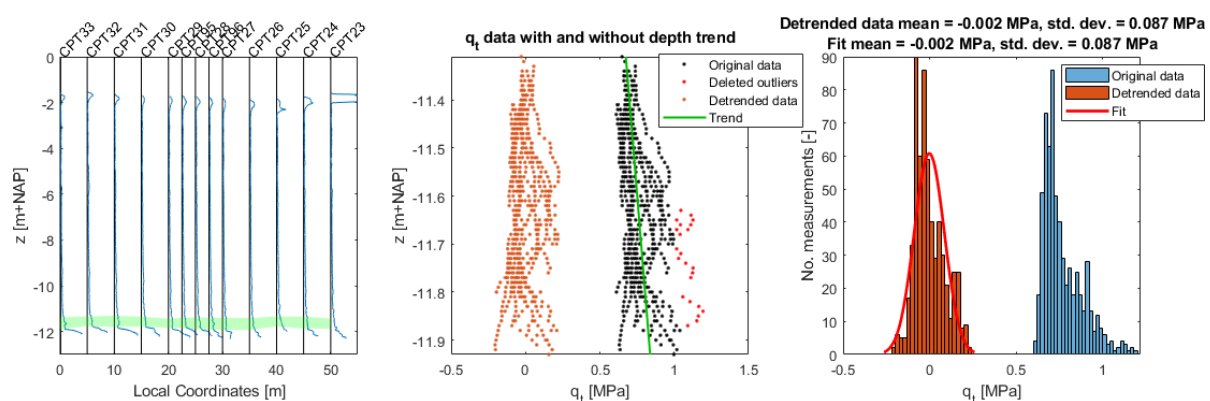


Figure D.26: Trend identification and removal for the second peat layer at CPT line 5

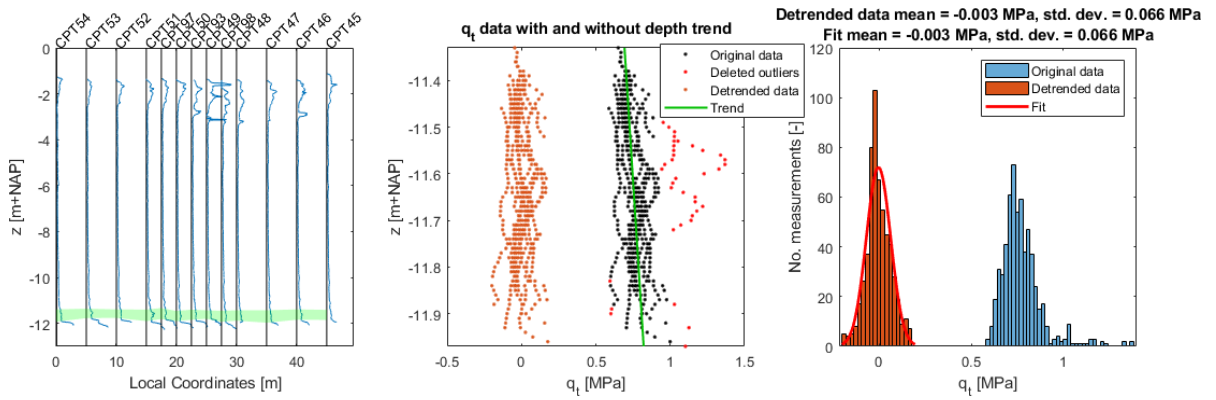


Figure D.27: Trend identification and removal for the second peat layer at CPT line 6

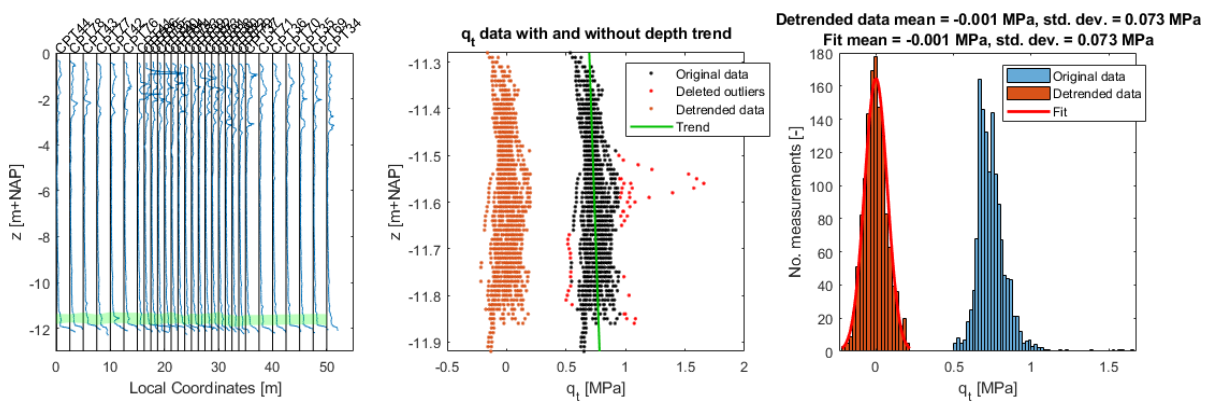


Figure D.28: Trend identification and removal for the second peat layer at CPT line 7

E

The Scales of Fluctuation

Table E.1: The vertical scales of fluctuation of the first peat layer for the individual CPTs

CPT	θ_v [m]	c_1 c_2	$\theta_{v,1}$ [m] $\theta_{v,1}$ [m]	CPT	θ_v [m]	c_1 c_2	$\theta_{v,1}$ [m] $\theta_{v,1}$ [m]	CPT	θ_v [m]	c_1 c_2	$\theta_{v,1}$ [m] $\theta_{v,1}$ [m]	CPT	θ_v [m]	c_1 c_2	$\theta_{v,1}$ [m] $\theta_{v,1}$ [m]
1	0.21	0.10 0.90	0.02 0.23	26	0.20	1.00 -	0.20 -	51	0.17	1.00 -	0.17 -	76	0.10	1.00 -	0.10 -
2	0.24	1.00 -	0.24 -	27	0.25	1.00 -	0.25 -	52	0.28	1.00 -	0.28 -	77	0.24	1.00 -	0.24 -
3	0.31	1.00 -	0.31 -	28	0.13	1.00 -	0.13 -	53	0.12	1.00 -	0.12 -	78	0.40	1.00 -	0.40 -
4	0.19	1.00 -	0.19 -	29	0.25	1.00 -	0.25 -	54	0.22	1.00 -	0.22 -	79	0.44	0.28 0.72	0.13 0.56
5	0.16	1.00 -	0.16 -	30	0.43	0.04 0.96	0.01 0.45	55	0.12	1.00 -	0.12 -	80	0.58	0.06 0.94	0.10 0.61
6	0.71	1.00 -	0.71 -	31	0.12	1.00 -	0.12 -	56	0.23	0.06 0.94	0.03 0.24	81	0.18	1.00 -	0.18 -
7	0.36	1.00 -	0.36 -	32	0.14	1.00 -	0.14 -	57	0.20	1.00 -	0.20 -	82	0.51	1.00 -	0.51 -
8	0.18	1.00 -	0.18 -	33	0.30	0.41 0.59	0.08 0.45	58	0.23	1.00 -	0.23 -	83	0.20	1.00 -	0.20 -
9	0.16	1.00 -	0.16 -	34	0.55	0.18 0.82	0.29 0.61	59	0.29	1.00 -	0.29 -	84	0.35	1.00 -	0.35 -
10	0.07	1.00 -	0.07 -	35	0.57	0.36 0.64	0.07 0.85	60	0.15	1.00 -	0.15 -	85	0.21	1.00 -	0.21 -
11	0.34	1.00 -	0.34 -	36	0.18	1.00 -	0.18 -	61	0.31	1.00 -	0.31 -	86	0.42	1.00 -	0.42 -
12	0.19	1.00 -	0.19 -	37	0.52	0.04 0.96	0.06 0.54	62	0.31	1.00 -	0.31 -	87	0.16	1.00 -	0.16 -
13	0.52	0.10 0.90	0.05 0.57	38	0.29	1.00 -	0.29 -	63	0.24	0.11 0.89	0.04 0.26	88	0.15	1.00 -	0.15 -
14	0.16	1.00 -	0.16 -	39	0.24	0.41 0.59	0.12 0.32	64	0.32	1.00 -	0.32 -	89	0.10	1.00 -	0.10 -
15	0.29	0.12 0.88	0.06 0.32	40	0.49	1.00 -	0.49 -	65	0.28	1.00 -	0.28 -	90	0.26	0.09 0.91	0.03 0.28
16	0.22	1.00 -	0.22 -	41	0.58	0.02 0.98	0.08 0.59	66	0.30	1.00 -	0.30 -	91	0.26	1.00 -	0.26 -
17	0.12	1.00 -	0.12 -	42	0.37	1.00 -	0.37 -	67	0.26	1.00 -	0.26 -	92	0.14	1.00 -	0.14 -
18	0.26	1.00 -	0.26 -	43	0.21	0.24 0.76	0.03 0.27	68	0.28	1.00 -	0.28 -	93	0.35	1.00 -	0.35 -
19	0.18	0.90 0.10	0.17 0.27	44	0.25	1.00 -	0.25 -	69	0.24	1.00 -	0.24 -	94	0.24	1.00 -	0.24 -
20	0.31	0.15 0.85	0.10 0.35	45	0.44	1.00 -	0.44 -	70	0.22	1.00 -	0.22 -	95	0.31	1.00 -	0.31 -
21	0.31	0.10 0.90	0.31 0.31	46	0.26	1.00 -	0.26 -	71	0.16	1.00 -	0.16 -	96	0.24	1.00 -	0.24 -
22	0.17	1.00 -	0.17 -	47	0.25	1.00 -	0.25 -	72	0.14	1.00 -	0.14 -	97	0.14	1.00 -	0.14 -
23	0.30	1.00 -	0.30 -	48	0.24	1.00 -	0.24 -	73	0.15	1.00 -	0.15 -	98	0.18	1.00 -	0.18 -
24	0.21	1.00 -	0.21 -	49	0.26	1.00 -	0.26 -	74	0.24	1.00 -	0.24 -	99	0.28	0.14 0.86	0.06 0.32
25	0.33	0.01 0.99	0.10 0.33	50	0.22	1.00 -	0.22 -	75	0.20	1.00 -	0.20 -	100	0.24	0.12 0.88	0.04 0.27

Table E.2: The horizontal and vertical scales of fluctuation of the first peat layer for different lines of CPTs

Parallel Lines							Perpendicular Lines						
Line	θ_h [m]	c_1 c_2	$\theta_{h,1}$ [m] $\theta_{h,2}$ [m]	θ_v [m]	c_1 c_2	$\theta_{v,1}$ [m] $\theta_{v,2}$ [m]	Line	θ_h [m]	c_1 c_2	$\theta_{h,1}$ [m] $\theta_{h,2}$ [m]	θ_v [m]	c_1 c_2	$\theta_{v,1}$ [m] $\theta_{v,2}$ [m]
1	7.95	0.65 0.35	0.01 22.70	1.20	0.60 0.40	0.17 2.75	44 : 11	-	-	-	0.29	1.00	0.29
2	8.57	0.48 0.52	0.01 16.47	0.36	1.00 -	0.36 -	43 : 10	-	-	-	2.17	0.59 0.41	0.10 5.15
3	19.10	0.64 0.36	0.01 53.04	0.28	1.00 -	0.28 -	42 : 9	-	-	-	0.49	0.07 0.93	0.07 0.52
4	-	-	-	1.22	0.64 0.36	0.15 3.12	41 : 8	-	-	-	0.54	0.05 0.95	0.04 0.57
5	8.72	0.49 0.51	0.01 17.09	1.06	0.58 0.42	0.15 2.32	40 : 7	3.64	0.60 0.40	0.38 8.53	0.38	1.00	0.38
6	8.49	0.33 0.67	0.01 12.67	1.49	0.46 0.54	0.14 2.64	39 : 6	-	-	-	0.35	0.44 0.56	0.14 0.52
7	2.77	0.38 0.62	0.22 4.33	0.46	0.06 0.94	0.10 0.48	38 : 5	-	-	-	0.35	0.70 0.30	0.18 0.75
							37 : 4	-	-	-	0.41	0.25 0.75	0.19 0.48
							36 : 3	-	-	-	0.61	0.61 0.39	0.15 1.33
							35 : 2	-	-	-	0.36	0.33 0.67	0.13 0.47
							34 : 1	-	-	-	0.44	0.95 0.05	0.42 0.82

Diagonal Lines							Diagonal Lines						
Line	θ_h [m]	c_1 c_2	$\theta_{h,1}$ [m] $\theta_{h,2}$ [m]	θ_v [m]	c_1 c_2	$\theta_{v,1}$ [m] $\theta_{v,2}$ [m]	Line	θ_h [m]	c_1 c_2	$\theta_{h,1}$ [m] $\theta_{h,2}$ [m]	θ_v [m]	c_1 c_2	$\theta_{v,1}$ [m] $\theta_{v,2}$ [m]
44 : 8	-	-	-	0.29	1.00	0.29	41 : 11	5.53	0.52 0.48	1.00 10.44	0.56	1.00	0.56
43 : 7	9.42	1.00	9.42	1.76	0.60 0.40	0.14 4.19	40 : 10	-	-	-	0.46	1.00	0.46
42 : 6	-	-	-	0.41	1.00	0.41	39 : 9	-	-	-	0.34	0.16 0.84	0.10 0.39
41 : 5	4.43	0.65 0.35	1.06 10.69	0.46	0.27 0.73	0.18 0.56	38 : 8	-	-	-	0.25	1.00	0.25
40 : 4	-	-	-	0.32	1.00	0.32	37 : 7	-	-	-	0.30	1.00	0.30
39 : 3	-	-	-	0.35	1.00	0.35	36 : 6	5.07	0.48 0.52	1.35 8.50	0.33	0.76 0.24	0.27 0.52
38 : 2	-	-	-	0.44	0.68 0.32	0.21 0.93	35 : 5	3.50	0.84 0.16	0.01 21.82	0.37	0.39 0.61	0.15 0.51
37 : 1	-	-	-	0.46	0.08 0.92	0.08 0.49	34 : 4	-	-	-	0.44	0.47 0.53	0.28 0.58

Table E.3: The scales of fluctuation for the sections of perpendicular lines of the first peat layer, where CPT lines 39 to 91 and 90 to 6 mark the centre of the area under investigation

CPT Line under dyke		40 to 29		74 to 95		39 to 91		73 to 96		38 to 27	
$\theta_h[m]$		-		3.17		-		-		-	
c_1	c_2	-	-	0.77	0.23	-	-	-	-	-	-
$\theta_{h,1}[m]$	$\theta_{h,2}[m]$	-	-	0.01	13.75	-	-	-	-	-	-
$\theta_v[m]$		0.43		0.25		0.33		0.33		0.26	
c_1	c_2	0.07	0.93	1.00	-	0.36	0.64	0.71	0.29	1.00	-
$\theta_{v,1}[m]$	$\theta_{v,2}[m]$	0.14	0.45	0.25	-	0.14	0.44	0.27	0.48	0.26	-

CPT Line in polder		59 to 66		90 to 6		58 to 65	
$\theta_h[m]$		6.14		-		-	
c_1	c_2	0.54	0.46	-	-	-	-
$\theta_{h,1}[m]$	$\theta_{h,2}[m]$	0.01	13.34	-	-	-	-
$\theta_v[m]$		0.28		0.35		0.25	
c_1	c_2	1.00	-	0.49	0.51	1.00	-
$\theta_{v,1}[m]$	$\theta_{v,2}[m]$	0.28	-	0.12	0.57	0.25	-

Table E.4: The vertical scales of fluctuation of the clay layer for the individual CPTs, without the removal of the additional layer

CPT	θ_v [m]	c_1	$\theta_{v,1}$ [m]	CPT	θ_v [m]	c_1	$\theta_{v,1}$ [m]	CPT	θ_v [m]	c_1	$\theta_{v,1}$ [m]	CPT	θ_v [m]	c_1	$\theta_{v,1}$ [m]
		c_2	$\theta_{v,1}$ [m]												
1	0.44	1.00	0.44	26	0.38	1.00	0.38	51	0.31	1.00	0.31	76	0.47	1.00	0.47
		-	-			-	-			-	-			-	-
2	0.40	1.00	0.40	27	0.38	1.00	0.38	52	0.45	1.00	0.45	77	0.60	1.00	0.60
		-	-			-	-			-	-			-	-
3	0.46	1.00	0.46	28	0.43	1.00	0.43	53	0.53	1.00	0.53	78	0.61	1.00	0.61
		-	-			-	-			-	-			-	-
4	0.49	1.00	0.49	29	0.51	1.00	0.51	54	1.04	0.09	0.04	79	0.32	1.00	0.32
		-	-			-	-			0.91	1.14			-	-
5	0.55	1.00	0.55	30	0.31	1.00	0.31	55	0.37	1.00	0.37	80	0.33	1.00	0.33
		-	-			-	-			-	-			-	-
6	0.91	0.16	0.17	31	0.74	1.00	0.74	56	0.46	1.00	0.46	81	0.40	0.36	0.24
		0.84	1.05			-	-			-	-			0.64	0.49
7	0.51	1.00	0.51	32	0.96	1.00	0.96	57	0.37	1.00	0.37	82	0.38	1.00	0.38
		-	-			-	-			-	-			-	-
8	0.91	1.00	0.91	33	0.46	1.00	0.46	58	0.35	1.00	0.35	83	0.68	0.12	0.08
		-	-			-	-			-	-			0.88	0.76
9	1.10	1.00	1.10	34	0.36	1.00	0.36	59	0.41	1.00	0.41	84	0.37	1.00	0.37
		-	-			-	-			-	-			-	-
10	0.81	1.00	0.81	35	0.43	1.00	0.43	60	0.37	1.00	0.37	85	0.42	1.00	0.42
		-	-			-	-			-	-			-	-
11	0.94	0.15	0.40	36	0.50	1.00	0.50	61	0.78	1.00	0.78	86	0.31	1.00	0.31
		0.85	1.04			-	-			-	-			-	-
12	0.36	1.00	0.36	37	0.31	1.00	0.31	62	1.04	1.00	1.04	87	0.48	1.00	0.48
		-	-			-	-			-	-			-	-
13	0.28	1.00	0.28	38	0.50	1.00	0.50	63	0.50	1.00	0.50	88	0.43	0.60	0.24
		-	-			-	-			-	-			0.40	0.72
14	0.52	0.08	0.48	39	0.51	1.00	0.51	64	0.39	1.00	0.39	89	0.37	1.00	0.37
		0.92	0.52			-	-			-	-			-	-
15	0.44	1.00	0.44	40	0.43	1.00	0.43	65	0.45	1.00	0.45	90	0.35	1.00	0.35
		-	-			-	-			-	-			-	-
16	0.50	1.00	0.50	41	0.51	1.00	0.51	66	0.49	1.00	0.49	91	0.47	1.00	0.47
		-	-			-	-			-	-			-	-
17	0.49	0.35	0.23	42	0.49	1.00	0.49	67	0.41	1.00	0.41	92	0.37	1.00	0.37
		0.65	0.63			-	-			-	-			-	-
18	0.40	1.00	0.40	43	0.48	1.00	0.48	68	1.01	1.00	1.01	93	0.39	1.00	0.39
		-	-			-	-			-	-			-	-
19	0.47	1.00	0.47	44	0.53	1.00	0.53	69	0.39	1.00	0.39	94	0.35	0.99	0.34
		-	-			-	-			-	-			0.01	1.34
20	1.05	1.00	1.05	45	0.34	1.00	0.34	70	0.45	1.00	0.45	95	0.36	1.00	0.36
		-	-			-	-			-	-			-	-
21	1.33	1.00	1.33	46	0.30	1.00	0.30	71	0.31	1.00	0.31	96	0.42	1.00	0.42
		-	-			-	-			-	-			-	-
22	0.91	1.00	0.91	47	0.32	1.00	0.32	72	0.36	1.00	0.36	97	0.40	1.00	0.40
		-	-			-	-			-	-			-	-
23	0.37	0.93	0.33	48	0.32	1.00	0.32	73	0.35	1.00	0.35	98	0.47	1.00	0.47
		0.07	0.90			-	-			-	-			-	-
24	0.41	1.00	0.41	49	0.40	1.00	0.40	74	0.26	1.00	0.26	99	0.45	1.00	0.45
		-	-			-	-			-	-			-	-
25	0.37	1.00	0.37	50	0.31	1.00	0.31	75	0.41	1.00	0.41	100	0.46	1.00	0.46
		-	-			-	-			-	-			-	-

Table E.5: The horizontal and vertical scales of fluctuation of the clay layer without additional layer removal for different lines of CPTs

Parallel Lines							Perpendicular Lines						
Line	θ_h [m]	c_1 c_2	$\theta_{h,1}$ [m] $\theta_{h,2}$ [m]	θ_v [m]	c_1 c_2	$\theta_{v,1}$ [m] $\theta_{v,2}$ [m]	Line	θ_h [m]	c_1 c_2	$\theta_{h,1}$ [m] $\theta_{h,2}$ [m]	θ_v [m]	c_1 c_2	$\theta_{v,1}$ [m] $\theta_{v,2}$ [m]
1	21.15	0.64 0.36	12.30 36.88	0.89	1.00 -	0.89 -	44 : 11	28.93	0.20 0.80	0.01 36.16	0.64	1.00 -	0.64 -
2	19.47	0.41 0.59	0.01 32.99	0.64	1.00 -	0.64 -	43 : 10	24.37	1.00 -	24.37 -	1.02	1.00 -	1.02 -
3	12.43	0.53 0.47	0.01 26.44	0.90	1.00 -	0.90 -	42 : 9	24.07	1.00 -	24.07 -	1.03	1.00 -	1.03 -
4	17.60	0.32 0.68	0.01 25.88	0.60	1.00 -	0.60 -	41 : 8	19.69	0.32 0.68	0.01 28.95	0.59	1.00 -	0.59 -
5	15.62	0.58 0.42	0.01 37.18	0.58	1.00 -	0.58 -	40 : 7	14.69	0.35 0.65	0.01 22.59	0.45	1.00 -	0.45 -
6	23.43	0.54 0.46	0.01 50.92	0.48	1.00 -	0.48 -	39 : 6	20.08	0.30 0.70	0.01 28.68	0.49	1.00 -	0.49 -
7	28.79	0.53 0.47	0.01 61.24	0.52	1.00 -	0.52 -	38 : 5	14.27	0.49 0.51	0.01 27.97	0.49	1.00 -	0.49 -
							37 : 4	16.60	0.43 0.57	0.01 29.12	0.43	1.00 -	0.43 -
							36 : 3	18.49	0.21 0.79	0.01 23.40	0.60	1.00 -	0.60 -
							35 : 2	16.23	0.61 0.39	0.01 41.60	0.36	1.00 -	0.36 -
							34 : 1	11.54	0.32 0.68	0.58 16.70	0.48	0.63 0.37	0.37 0.67

Diagonal Lines							Diagonal Lines						
Line	θ_h [m]	c_1 c_2	$\theta_{h,1}$ [m] $\theta_{h,2}$ [m]	θ_v [m]	c_1 c_2	$\theta_{v,1}$ [m] $\theta_{v,2}$ [m]	Line	θ_h [m]	c_1 c_2	$\theta_{h,1}$ [m] $\theta_{h,2}$ [m]	θ_v [m]	c_1 c_2	$\theta_{v,1}$ [m] $\theta_{v,2}$ [m]
44 : 8	34.43	1.00 -	34.43 -	0.96	1.00 -	0.96 -	41 : 11	9.06	1.00 -	9.06 -	1.10	1.00 -	1.10 -
43 : 7	45.10	0.10 0.90	0.01 50.11	0.61	1.00 -	0.61 -	40 : 10	17.45	0.37 0.63	0.01 27.69	0.79	1.00 -	0.79 -
42 : 6	25.44	0.22 0.78	0.01 32.61	0.47	1.00 -	0.47 -	39 : 9	10.17	0.10 0.90	0.52 11.24	0.89	1.00 -	0.89 -
41 : 5	28.55	0.39 0.61	0.01 46.80	0.50	1.00 -	0.50 -	38 : 8	8.68	0.45 0.55	0.01 15.77	0.59	1.00 -	0.59 -
40 : 4	19.82	0.53 0.47	0.01 42.16	0.49	0.93 0.07	0.42 1.42	37 : 7	15.09	0.40 0.60	0.01 25.14	0.39	1.00 -	0.39 -
39 : 3	32.75	0.33 0.67	0.01 48.88	0.52	1.00 -	0.52 -	36 : 6	33.37	0.35 0.65	0.01 51.33	0.60	0.58 0.42	0.47 0.78
38 : 2	14.66	0.48 0.52	0.01 28.18	0.51	1.00 -	0.51 -	35 : 5	28.44	0.42 0.58	0.01 49.03	0.50	1.00 -	0.50 -
37 : 1	9.10	0.68 0.32	0.01 28.42	0.42	1.00 -	0.42 -	34 : 4	24.52	0.28 0.72	0.01 34.05	0.43	1.00 -	0.43 -

Table E.6: The scales of fluctuation for the sections of perpendicular lines of the clay layer, where CPT lines 39 to 91 and 90 to 6 mark the centre of the area under investigation

CPT Line under dyke		40 to 29		74 to 95		39 to 91		73 to 96		38 to 27	
$\theta_h[m]$		11.44		-		9.32		5.21		6.09	
c_1	c_2	0.06	0.94	-	-	0.22	0.78	1.00	-	1.00	-
$\theta_{h,1}[m]$	$\theta_{h,2}[m]$	0.01	12.17	-	-	0.01	11.95	5.21	-	6.09	-
$\theta_v[m]$		0.44		0.41		0.44		0.39		0.48	
c_1	c_2	1.00	-	0.94	0.06	1.00	-	1.00	-	1.00	-
$\theta_{v,1}[m]$	$\theta_{v,2}[m]$	0.44	-	0.23	3.23	0.44	-	0.39	-	0.48	-

CPT Line in polder		59 to 66		90 to 6		58 to 65	
$\theta_h[m]$		15.25		25.64		11.82	
c_1	c_2	0.01	0.99	0.19	0.81	0.01	0.99
$\theta_{h,1}[m]$	$\theta_{h,2}[m]$	0.01	15.40	0.01	31.65	0.01	11.94
$\theta_v[m]$		0.44		0.50		0.43	
c_1	c_2	1.00	-	0.42	0.58	1.00	-
$\theta_{v,1}[m]$	$\theta_{v,2}[m]$	0.44	-	0.32	0.63	0.43	-

Table E.7: The vertical scales of fluctuation of the clay layer for the individual CPTs, with the removal of the additional layer

CPT	θ_v [m]	c_1	$\theta_{v,1}$ [m]	CPT	θ_v [m]	c_1	$\theta_{v,1}$ [m]	CPT	θ_v [m]	c_1	$\theta_{v,1}$ [m]	CPT	θ_v [m]	c_1	$\theta_{v,1}$ [m]
		c_2	$\theta_{v,1}$ [m]												
1	0.41	1.00	0.41	26	0.42	0.99	0.41	51	0.31	1.00	0.31	76	0.48	1.00	0.48
		-	-			0.01	1.41			-	-			-	-
2	0.39	1.00	0.39	27	0.38	1.00	0.38	52	0.44	1.00	0.44	77	0.44	0.60	0.36
		-	-			-	-			-	-			0.40	0.56
3	0.45	1.00	0.45	28	0.37	1.00	0.37	53	0.40	1.00	0.40	78	0.51	1.00	0.51
		-	-			-	-			-	-			-	-
4	0.52	1.00	0.52	29	0.50	1.00	0.50	54	0.85	0.26	0.14	79	0.32	1.00	0.32
		-	-			-	-			0.74	1.10			-	-
5	0.56	1.00	0.56	30	0.32	1.00	0.32	55	0.38	1.00	0.38	80	0.33	1.00	0.33
		-	-			-	-			-	-			-	-
6	0.93	0.17	0.17	31	0.60	1.00	0.60	56	0.45	1.00	0.45	81	0.38	0.35	0.25
		0.83	1.09			-	-			-	-			0.65	0.45
7	0.53	1.00	0.53	32	0.45	0.58	0.38	57	0.37	1.00	0.37	82	0.38	1.00	0.38
		-	-			0.42	0.55			-	-			-	-
8	0.48	0.77	0.41	33	0.48	1.00	0.48	58	0.33	1.00	0.33	83	0.68	0.13	0.09
		0.23	0.71			-	-			-	-			0.87	0.77
9	0.60	1.00	0.60	34	0.35	1.00	0.35	59	0.41	1.00	0.41	84	0.37	1.00	0.37
		-	-			-	-			-	-			-	-
10	0.49	1.00	0.49	35	0.43	1.00	0.43	60	0.38	1.00	0.38	85	0.42	1.00	0.42
		-	-			-	-			-	-			-	-
11	0.63	1.00	0.63	36	0.50	1.00	0.50	61	0.85	1.00	0.85	86	0.32	1.00	0.32
		-	-			-	-			-	-			-	-
12	0.34	1.00	0.34	37	0.31	1.00	0.31	62	0.51	1.00	0.51	87	0.44	1.00	0.44
		-	-			-	-			-	-			-	-
13	0.29	1.00	0.29	38	0.49	1.00	0.49	63	0.50	1.00	0.50	88	0.43	0.63	0.24
		-	-			-	-			-	-			0.37	0.75
14	0.45	1.00	0.45	39	0.51	1.00	0.51	64	0.41	1.00	0.41	89	0.37	1.00	0.37
		-	-			-	-			-	-			-	-
15	0.36	1.00	0.36	40	0.43	1.00	0.43	65	0.44	1.00	0.44	90	0.34	1.00	0.34
		-	-			-	-			-	-			-	-
16	0.48	1.00	0.48	41	0.51	1.00	0.51	66	0.49	1.00	0.49	91	0.45	1.00	0.45
		-	-			-	-			-	-			-	-
17	0.43	0.46	0.24	42	0.50	1.00	0.50	67	0.42	1.00	0.42	92	0.36	1.00	0.36
		0.54	0.59			-	-			-	-			-	-
18	0.38	1.00	0.38	43	0.59	1.00	0.59	68	0.43	1.00	0.43	93	0.38	1.00	0.38
		-	-			-	-			-	-			-	-
19	0.56	0.92	0.53	44	0.53	1.00	0.53	69	0.39	1.00	0.39	94	0.37	1.00	0.37
		0.08	0.91			-	-			-	-			-	-
20	0.54	1.00	0.54	45	0.34	1.00	0.34	70	0.45	1.00	0.45	95	0.35	1.00	0.35
		-	-			-	-			-	-			-	-
21	0.44	1.00	0.44	46	0.31	1.00	0.31	71	0.31	1.00	0.31	96	0.42	1.00	0.42
		-	-			-	-			-	-			-	-
22	0.80	1.00	0.80	47	0.33	1.00	0.33	72	0.36	1.00	0.36	97	0.40	1.00	0.40
		-	-			-	-			-	-			-	-
23	0.39	0.79	0.31	48	0.31	1.00	0.31	73	0.35	1.00	0.35	98	0.45	1.00	0.45
		0.21	0.69			-	-			-	-			-	-
24	0.40	1.00	0.40	49	0.41	1.00	0.41	74	0.26	1.00	0.26	99	0.43	1.00	0.43
		-	-			-	-			-	-			-	-
25	0.36	1.00	0.36	50	0.31	1.00	0.31	75	0.41	1.00	0.41	100	0.44	1.00	0.44
		-	-			-	-			-	-			-	-

Table E.8: The horizontal and vertical scales of fluctuation of the clay layer with additional layer removal for different lines of CPTs

Parallel Lines							Perpendicular Lines						
Line	θ_h [m]	c_1 c_2	$\theta_{h,1}$ [m] $\theta_{h,2}$ [m]	θ_v [m]	c_1 c_2	$\theta_{v,1}$ [m] $\theta_{v,2}$ [m]	Line	θ_h [m]	c_1 c_2	$\theta_{h,1}$ [m] $\theta_{h,2}$ [m]	θ_v [m]	c_1 c_2	$\theta_{v,1}$ [m] $\theta_{v,2}$ [m]
1	41.29	0.28 0.72	0.01 57.34	0.57	1.00 -	0.57 -	44 : 11	29.14	0.22 0.78	0.01 37.36	0.55	1.00 -	0.55 -
2	33.67	0.34 0.66	0.01 51.01	0.48	1.00 -	0.48 -	43 : 10	23.93	0.26 0.74	0.01 32.33	0.59	1.00 -	0.59 -
3	25.37	0.41 0.59	0.01 42.99	0.53	1.00 -	0.53 -	42 : 9	24.48	0.34 0.66	0.01 37.09	0.65	0.95 0.05	0.60 1.60
4	26.74	0.39 0.61	0.01 43.83	0.57	1.00 -	0.57 -	41 : 8	21.72	0.33 0.67	0.01 32.41	0.53	1.00 -	0.53 -
5	31.79	0.53 0.47	0.01 67.63	0.50	1.00 -	0.50 -	40 : 7	14.34	0.36 0.64	0.01 22.40	0.45	1.00 -	0.45 -
6	28.26	0.53 0.47	0.01 60.12	0.43	1.00 -	0.43 -	39 : 6	20.71	0.33 0.67	0.01 30.91	0.47	1.00 -	0.47 -
7	30.15	0.52 0.48	0.01 62.80	0.51	1.00 -	0.51 -	38 : 5	8.39	0.37 0.63	0.01 13.31	0.50	1.00 -	0.50 -
							37 : 4	16.04	0.43 0.57	0.01 28.13	0.42	1.00 -	0.42 -
							36 : 3	20.52	0.27 0.73	0.01 28.11	0.55	1.00 -	0.55 -
							35 : 2	17.13	0.58 0.42	0.01 40.77	0.38	1.00 -	0.38 -
							34 : 1	11.35	0.38 0.62	0.01 18.30	0.48	0.60 0.40	0.35 0.68

Diagonal Lines							Diagonal Lines						
Line	θ_h [m]	c_1 c_2	$\theta_{h,1}$ [m] $\theta_{h,2}$ [m]	θ_v [m]	c_1 c_2	$\theta_{v,1}$ [m] $\theta_{v,2}$ [m]	Line	θ_h [m]	c_1 c_2	$\theta_{h,1}$ [m] $\theta_{h,2}$ [m]	θ_v [m]	c_1 c_2	$\theta_{v,1}$ [m] $\theta_{v,2}$ [m]
44 : 8	26.76	0.32 0.68	0.01 39.35	0.50	1.00 -	0.50 -	41 : 11	11.61	0.05 0.95	0.01 12.22	0.58	1.00 -	0.58 -
43 : 7	40.34	0.11 0.89	0.01 45.32	0.63	1.00 -	0.63 -	40 : 10	9.82	0.51 0.49	0.01 20.03	0.50	1.00 -	0.50 -
42 : 6	24.73	0.19 0.81	0.01 30.53	0.46	1.00 -	0.46 -	39 : 9	13.01	0.54 0.46	0.01 28.27	0.60	0.91 0.09	0.52 1.41
41 : 5	28.45	0.41 0.59	0.01 48.21	0.51	1.00 -	0.51 -	38 : 8	10.52	0.48 0.52	0.01 20.22	0.53	0.86 0.14	0.43 1.14
40 : 4	20.52	0.54 0.46	0.01 44.60	0.49	0.89 0.11	0.39 1.30	37 : 7	13.72	0.39 0.61	0.01 22.49	0.39	1.00 -	0.39 -
39 : 3	38.17	0.32 0.68	0.01 56.13	0.49	1.00 -	0.49 -	36 : 6	39.42	0.32 0.68	0.01 57.97	0.57	0.77 0.23	0.49 0.84
38 : 2	14.65	0.50 0.50	0.01 29.29	0.51	1.00 -	0.51 -	35 : 5	31.35	0.41 0.59	0.01 53.13	0.49	1.00 -	0.49 -
37 : 1	9.07	0.68 0.32	0.01 28.32	0.42	0.99 0.01	0.41 1.41	34 : 4	24.60	0.28 0.72	0.01 34.16	0.42	1.00 -	0.42 -

Table E.9: The scales of fluctuation for the sections of perpendicular lines of the clay layer without the additional layer, where CPT lines 39 to 91 and 90 to 6 mark the centre of the area under investigation

CPT Line under dyke		40 to 29		74 to 95		39 to 91		73 to 96		38 to 27	
$\theta_h[m]$		11.46		-		9.35		5.12		5.76	
c_1	c_2	0.06	0.94	-	-	0.25	0.75	1.00	-	1.00	-
$\theta_{h,1}[m]$	$\theta_{h,2}[m]$	0.01	12.19	-	-	0.01	12.46	5.12	-	5.76	-
$\theta_v[m]$		0.44		0.45		0.43		0.39		0.48	
c_1	c_2	1.00	-	0.93	0.07	1.00	-	1.00	-	1.00	-
$\theta_{v,1}[m]$	$\theta_{v,2}[m]$	0.44	-	0.22	3.51	0.43	-	0.39	-	0.48	-

CPT Line in polder		59 to 66		90 to 6		58 to 65	
$\theta_h[m]$		14.81		23.64		11.24	
c_1	c_2	0.01	0.99	0.21	0.79	0.02	0.98
$\theta_{h,1}[m]$	$\theta_{h,2}[m]$	0.01	14.96	0.01	29.92	0.01	11.47
$\theta_v[m]$		0.43		0.47		0.40	
c_1	c_2	1.00	-	0.51	0.49	1.00	-
$\theta_{v,1}[m]$	$\theta_{v,2}[m]$	0.43	-	0.33	0.62	0.40	-

Table E.10: The vertical scales of fluctuation of the second peat layer for the individual CPTs

CPT	θ_v [m]	c_1	$\theta_{v,1}$ [m]	CPT	θ_v [m]	c_1	$\theta_{v,1}$ [m]	CPT	θ_v [m]	c_1	$\theta_{v,1}$ [m]	CPT	θ_v [m]	c_1	$\theta_{v,1}$ [m]
		c_2	$\theta_{v,1}$ [m]												
1	0.14	1.00	0.14	26	0.16	1.00	0.16	51	0.06	0.67	0.05	76	0.05	1.00	0.05
		-	-			-	-			0.33	0.08			-	-
2	0.14	1.00	0.14	27	0.19	0.89	0.18	52	0.09	1.00	0.09	77	0.19	0.11	0.01
		-	-			0.11	0.27			-	-			0.89	0.21
3	0.11	0.89	0.10	28	0.16	1.00	0.16	53	0.05	1.00	0.05	78	0.05	1.00	0.05
		0.11	0.19			-	-			-	-			-	-
4	0.19	1.00	0.19	29	0.14	1.00	0.14	54	0.14	1.00	0.14	79	0.27	1.00	0.27
		-	-			-	-			-	-			-	-
5	0.07	1.00	0.07	30	0.09	1.00	0.09	55	0.08	0.55	0.07	80	0.10	1.00	0.10
		-	-			-	-			0.45	0.09			-	-
6	0.10	0.11	0.01	31	0.16	1.00	0.16	56	0.09	1.00	0.09	81	0.14	1.00	0.14
		0.89	0.11			-	-			-	-			-	-
7	0.18	1.00	0.18	32	0.15	1.00	0.15	57	0.13	1.00	0.13	82	0.20	1.00	0.20
		-	-			-	-			-	-			-	-
8	0.18	1.00	0.18	33	0.06	0.81	0.05	58	0.12	0.75	0.11	83	0.21	1.00	0.21
		-	-			0.19	0.10			0.25	0.15			-	-
9	0.20	1.00	0.20	34	0.15	1.00	0.15	59	0.15	1.00	0.15	84	0.28	1.00	0.28
		-	-			-	-			-	-			-	-
10	0.14	0.94	0.13	35	0.16	1.00	0.16	60	0.05	1.00	0.05	85	0.18	1.00	0.18
		0.06	0.30			-	-			-	-			-	-
11	0.19	1.00	0.19	36	0.06	1.00	0.06	61	0.24	1.00	0.24	86	0.31	1.00	0.31
		-	-			-	-			-	-			-	-
12	0.05	0.78	0.04	37	0.08	1.00	0.08	62	0.18	1.00	0.18	87	0.09	0.14	0.03
		0.22	0.09			-	-			-	-			0.86	0.10
13	0.11	1.00	0.11	38	0.14	1.00	0.14	63	0.09	0.11	0.02	88	0.15	1.00	0.15
		-	-			-	-			0.89	0.10			-	-
14	0.15	0.09	0.01	39	0.07	1.00	0.07	64	0.17	1.00	0.17	89	0.06	0.86	0.05
		0.91	0.16			-	-			-	-			0.14	0.12
15	0.11	0.06	0.01	40	0.18	1.00	0.18	65	0.35	1.00	0.35	90	0.13	1.00	0.13
		0.94	0.12			-	-			-	-			-	-
16	0.15	1.00	0.15	41	0.22	1.00	0.22	66	0.06	0.54	0.05	91	0.22	1.00	0.22
		-	-			-	-			0.46	0.07			-	-
17	0.10	0.87	0.09	42	0.06	1.00	0.06	67	0.19	1.00	0.19	92	0.23	0.17	0.01
		0.13	0.17			-	-			-	-			0.83	0.28
18	0.18	1.00	0.18	43	0.31	1.00	0.31	68	0.13	1.00	0.13	93	0.14	1.00	0.14
		-	-			-	-			-	-			-	-
19	0.04	0.25	0.01	44	0.08	1.00	0.08	69	0.07	1.00	0.07	94	0.11	0.85	0.10
		0.75	0.05			-	-			-	-			0.15	0.17
20	0.12	1.00	0.12	45	0.07	1.00	0.07	70	0.10	1.00	0.10	95	0.05	0.35	0.04
		-	-			-	-			-	-			0.65	0.06
21	0.12	1.00	0.12	46	0.17	1.00	0.17	71	0.13	1.00	0.13	96	0.05	1.00	0.05
		-	-			-	-			-	-			-	-
22	0.15	1.00	0.15	47	0.10	0.12	0.01	72	0.23	1.00	0.23	97	0.21	1.00	0.21
		-	-			0.88	0.11			-	-			-	-
23	0.03	0.37	0.01	48	0.03	0.11	0.01	73	0.20	1.00	0.20	98	0.23	1.00	0.23
		0.63	0.04			0.89	0.03			-	-			-	-
24	0.09	0.86	0.08	49	0.07	1.00	0.07	74	0.13	0.93	0.12	99	0.22	1.00	0.22
		0.14	0.15			-	-			0.07	0.26			-	-
25	0.28	1.00	0.28	50	0.14	0.96	0.13	75	0.08	1.00	0.08	100	0.11	1.00	0.11
		-	-			0.04	0.38			-	-			-	-

Table E.11: The horizontal and vertical scales of fluctuation of the second peat layer for different lines of CPTs

Parallel Lines						
Line	θ_h [m]	c_1 c_2	$\theta_{h,1}$ [m] $\theta_{h,2}$ [m]	θ_v [m]	c_1 c_2	$\theta_{v,1}$ [m] $\theta_{v,2}$ [m]
1	-	-	-	0.55	0.24 0.76	0.07 0.70
2	-	-	-	0.25	0.55 0.45	0.15 0.37
3	-	-	-	0.67	0.26 0.74	0.05 0.89
4	3.51	0.76 0.24	0.01 14.59	0.15	1.00 -	0.15 -
5	-	-	-	0.37	0.25 0.75	0.08 0.47
6	-	-	-	0.17	1.00 -	0.17 -
7	-	-	-	0.34	1.00 -	0.34 -

Perpendicular Lines						
Line	θ_h [m]	c_1 c_2	$\theta_{h,1}$ [m] $\theta_{h,2}$ [m]	θ_v [m]	c_1 c_2	$\theta_{v,1}$ [m] $\theta_{v,2}$ [m]
44 : 11	-	-	-	0.11	0.23 0.77	0.02 0.14
43 : 10	-	-	-	0.20	1.00 -	0.20 -
42 : 9	-	-	-	0.17	1.00 -	0.17 -
41 : 8	-	-	-	0.27	0.03 0.97	0.01 0.28
40 : 7	5.10	0.02 0.98	0.65 5.19	0.20	1.00 -	0.20 -
39 : 6	-	-	-	0.13	1.00 -	0.13 -
38 : 5	-	-	-	0.23	0.51 0.49	0.11 0.35
37 : 4	-	-	-	0.80	1.00 -	0.80 -
36 : 3	-	-	-	0.30	1.00 -	0.30 -
35 : 2	-	-	-	0.13	1.00 -	0.13 -
34 : 1	-	-	-	0.74	0.11 0.89	0.02 0.83

Diagonal Lines						
Line	θ_h [m]	c_1 c_2	$\theta_{h,1}$ [m] $\theta_{h,2}$ [m]	θ_v [m]	c_1 c_2	$\theta_{v,1}$ [m] $\theta_{v,2}$ [m]
44 : 8	6.82	0.52 0.48	0.01 14.20	1.12	0.28 0.72	0.06 1.53
43 : 7	-	-	-	0.18	1.00 -	0.18 -
42 : 6	-	-	-	0.10	1.00 -	0.10 -
41 : 5	-	-	-	0.17	0.05 0.95	0.01 0.18
40 : 4	-	-	-	0.51	0.29 0.71	0.06 0.69
39 : 3	-	-	-	0.72	0.15 0.85	0.03 0.84
38 : 2	4.18	0.77 0.23	0.01 18.14	0.14	1.00 -	0.14 -
37 : 1	-	-	-	0.38	0.27 0.73	0.08 0.49

Diagonal Lines						
Line	θ_h [m]	c_1 c_2	$\theta_{h,1}$ [m] $\theta_{h,2}$ [m]	θ_v [m]	c_1 c_2	$\theta_{v,1}$ [m] $\theta_{v,2}$ [m]
41 : 11	-	-	-	0.92	0.42 0.58	0.05 1.55
40 : 10	-	-	-	0.25	1.00 -	0.25 -
39 : 9	-	-	-	1.18	0.21 0.79	0.03 1.49
38 : 8	-	-	-	0.17	1.00 -	0.17 -
37 : 7	-	-	-	0.55	0.42 0.58	0.06 0.90
36 : 6	-	-	-	0.17	1.00 -	0.17 -
35 : 5	-	-	-	0.52	0.47 0.53	0.09 0.90
34 : 4	-	-	-	0.49	0.14 0.86	0.04 0.56

Table E.12: The scales of fluctuation for the sections of perpendicular lines of the second peat layer, where CPT lines 39 to 91 and 90 to 6 mark the centre of the area under investigation

CPT Line under dyke		40 to 29		74 to 95		39 to 91		73 to 96		38 to 27	
$\theta_h[m]$		-		-		-		-		-	
c_1	c_2	-	-	-	-	-	-	-	-	-	-
$\theta_{h,1}[m]$	$\theta_{h,2}[m]$	-	-	-	-	-	-	-	-	-	-
$\theta_v[m]$		0.17		0.57		0.18		0.13		0.22	
c_1	c_2	1.00	-	0.32	0.68	1.00	-	0.02	0.98	1.00	-
$\theta_{v,1}[m]$	$\theta_{v,2}[m]$	0.17	-	0.05	0.81	0.18	-	0.01	0.13	0.22	-

CPT Line in polder		59 to 66		90 to 6		58 to 65	
$\theta_h[m]$		-		2.85		-	
c_1	c_2	-	-	0.68	0.32	-	-
$\theta_{h,1}[m]$	$\theta_{h,2}[m]$	-	-	0.01	8.89	-	-
$\theta_v[m]$		0.14		0.11		0.99	
c_1	c_2	1.00	-	1.00	-	0.03	0.97
$\theta_{v,1}[m]$	$\theta_{v,2}[m]$	0.14	-	0.11	-	0.01	1.02

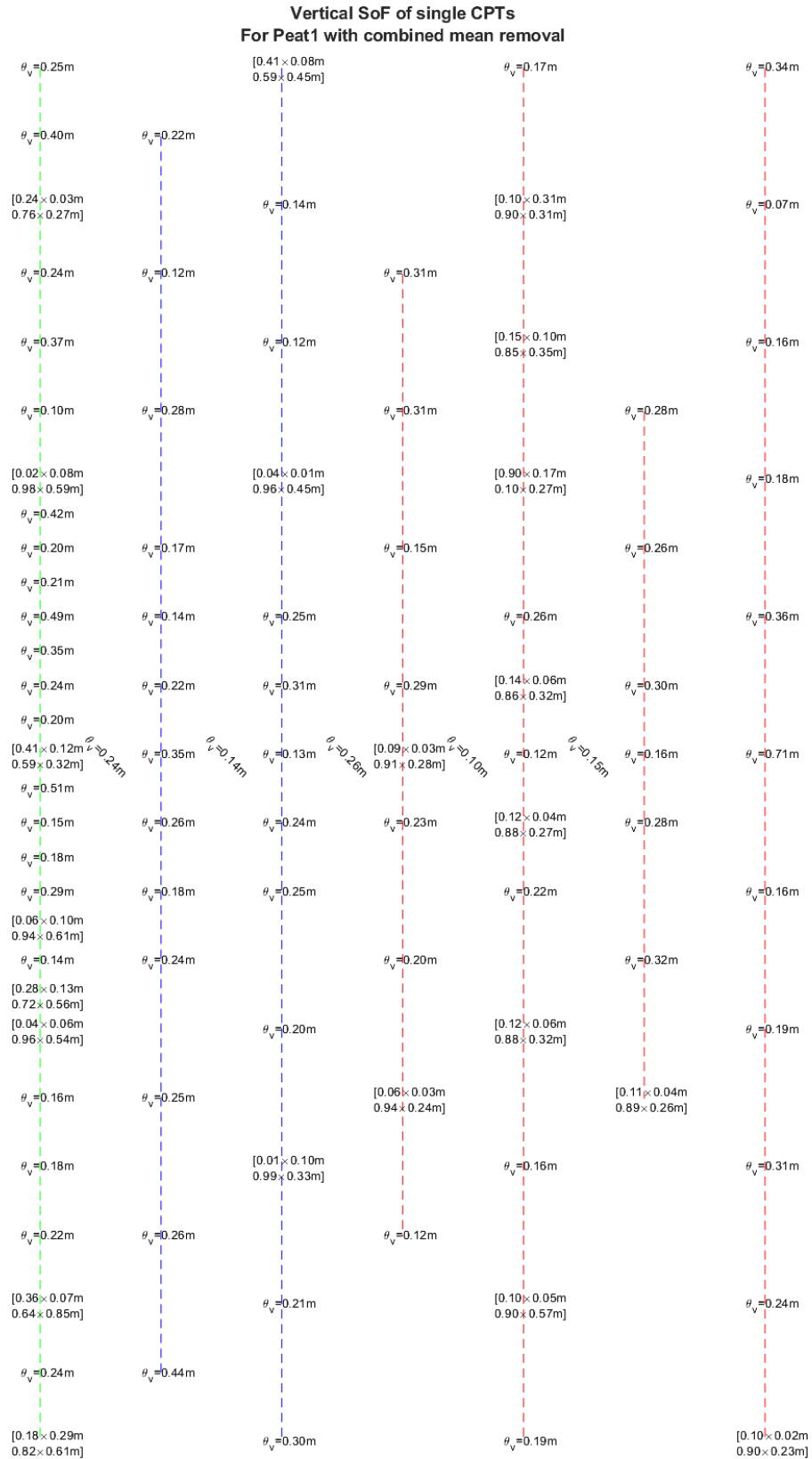


Figure E.1: The vertical scales of fluctuation of the first peat layer for every individual CPT

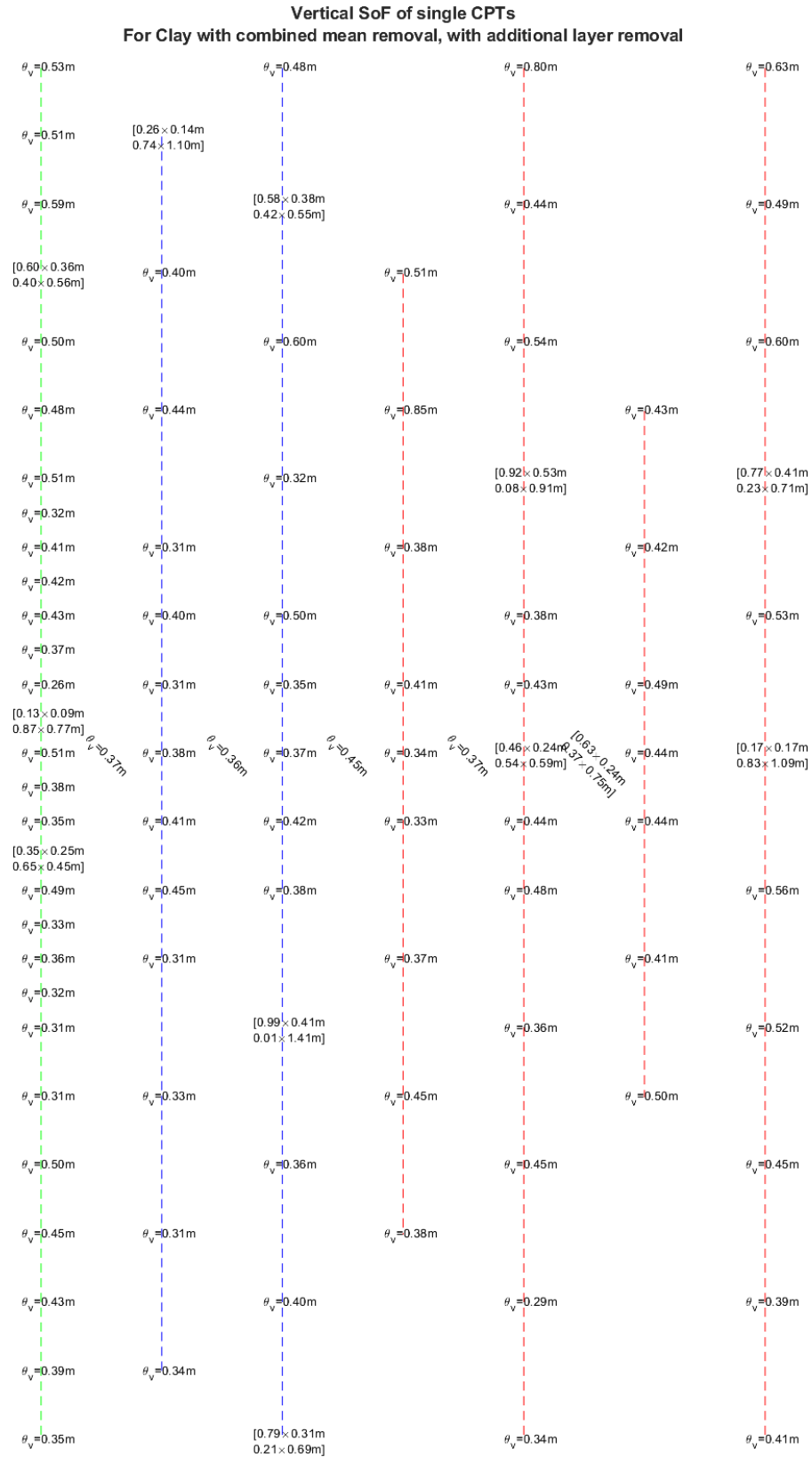


Figure E.3: The vertical scales of fluctuation of the clay layer for every individual CPT, with the removal of the additional layer

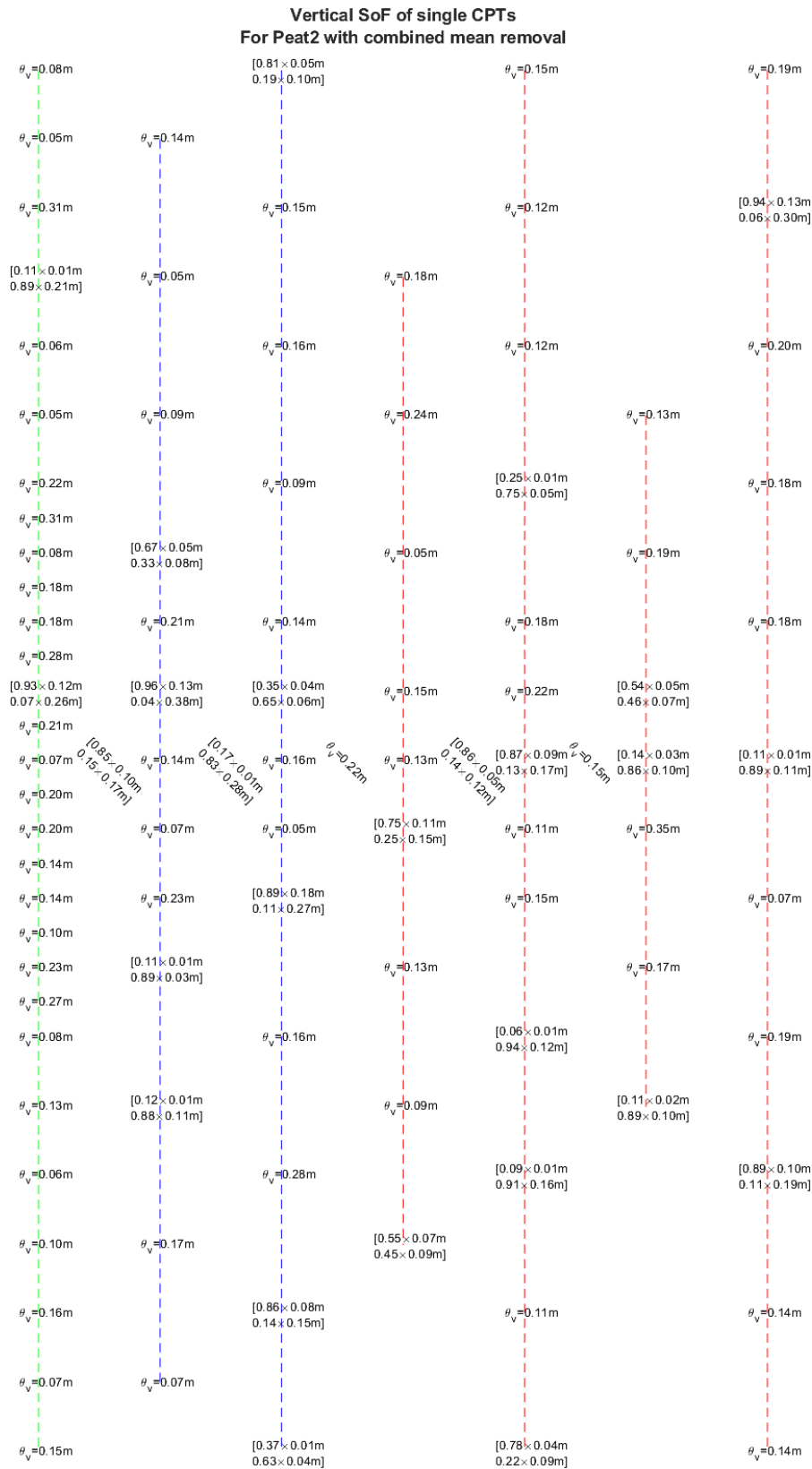


Figure E.4: The vertical scales of fluctuation of the second peat layer for every individual CPT

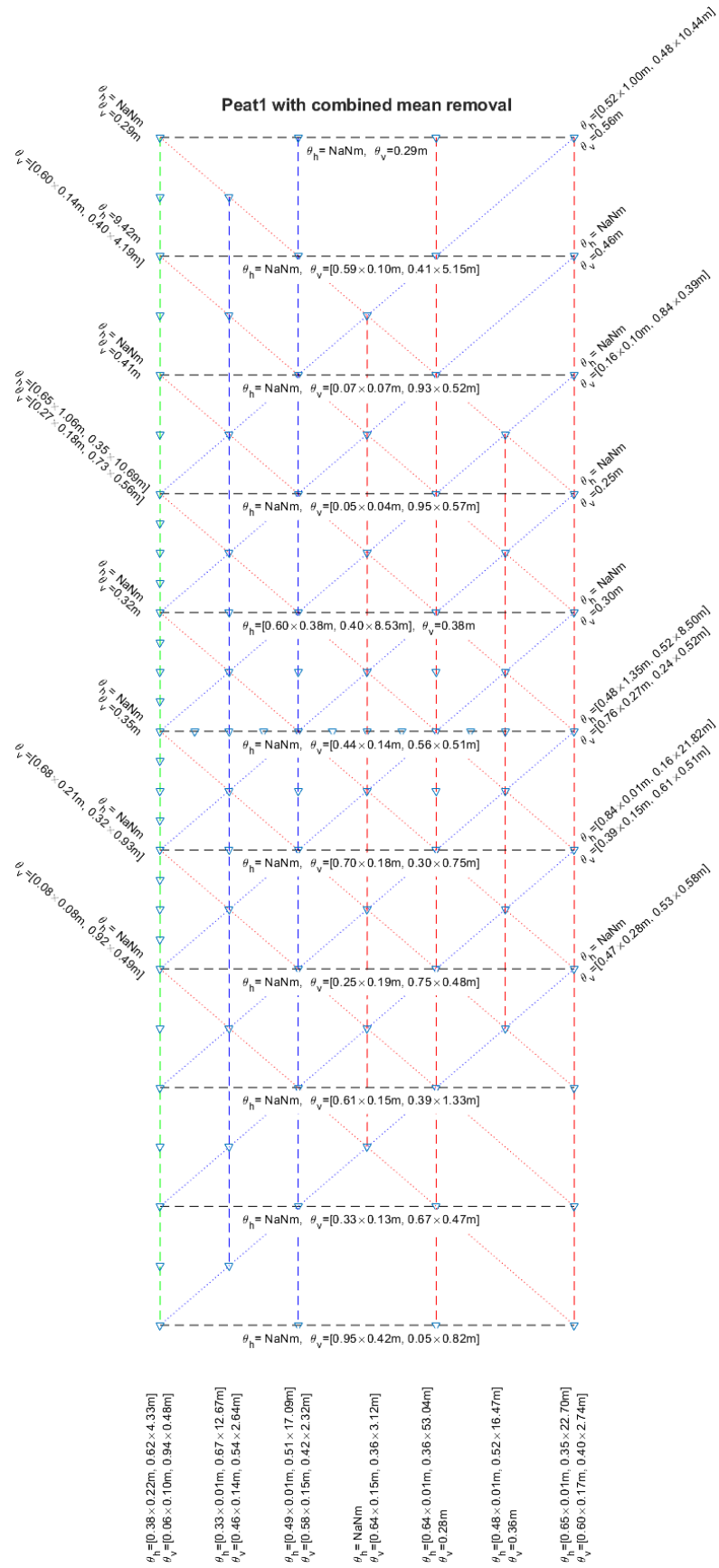


Figure E.5: The horizontal and vertical scales of fluctuation of the first peat layer

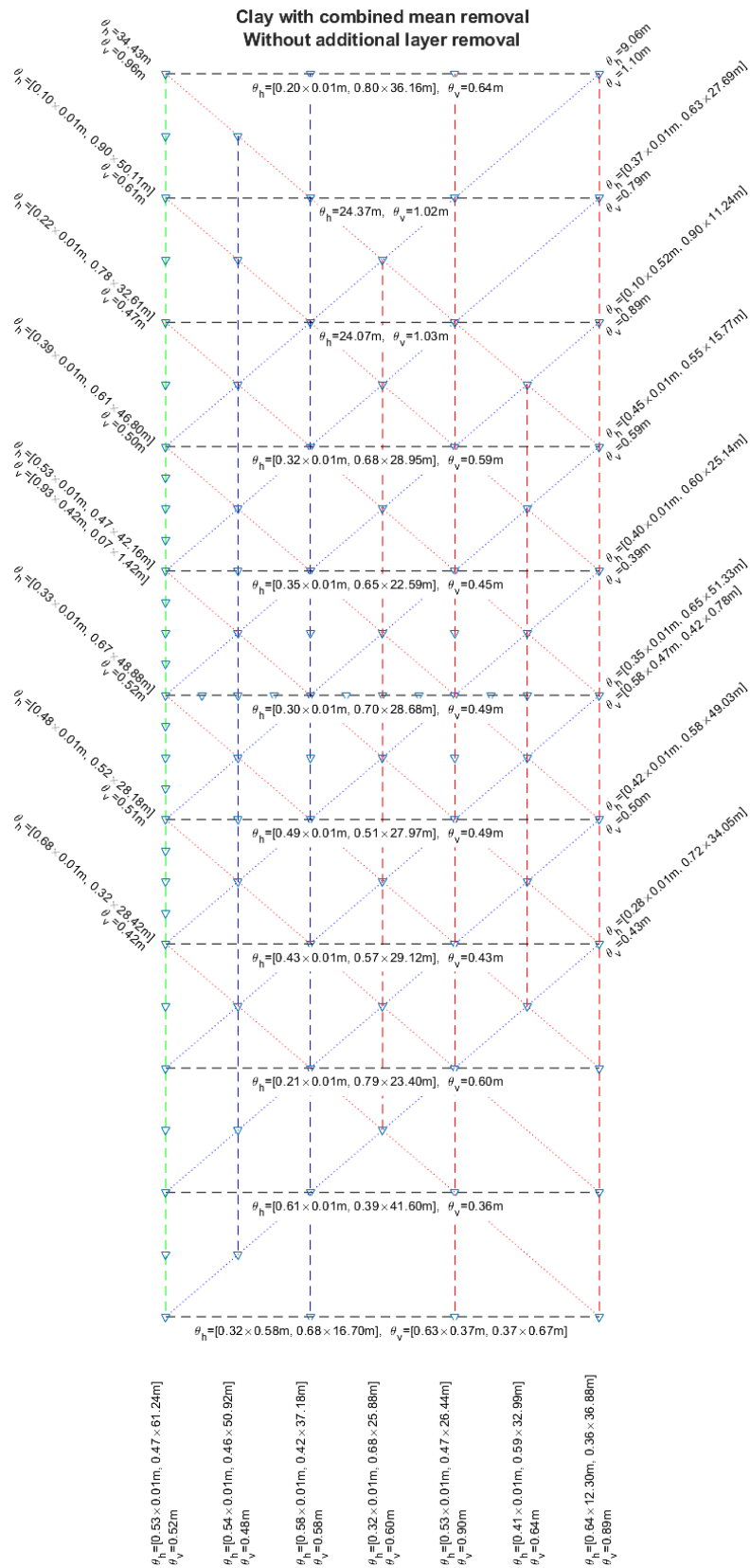


Figure E.6: The horizontal and vertical scales of fluctuation of the clay layer, without the removal of the additional layer

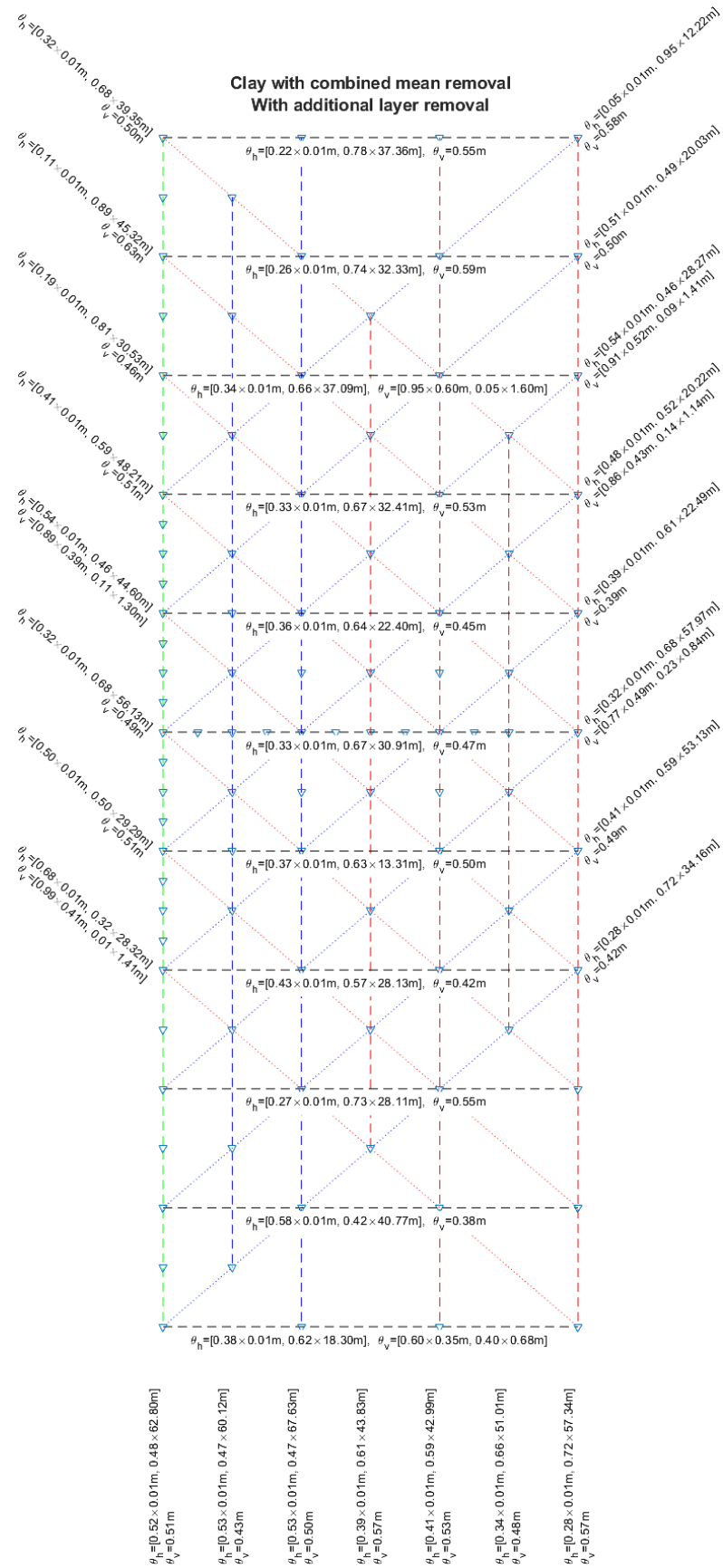


Figure E.7: The horizontal and vertical scales of fluctuation of the clay layer, with the removal of the additional layer

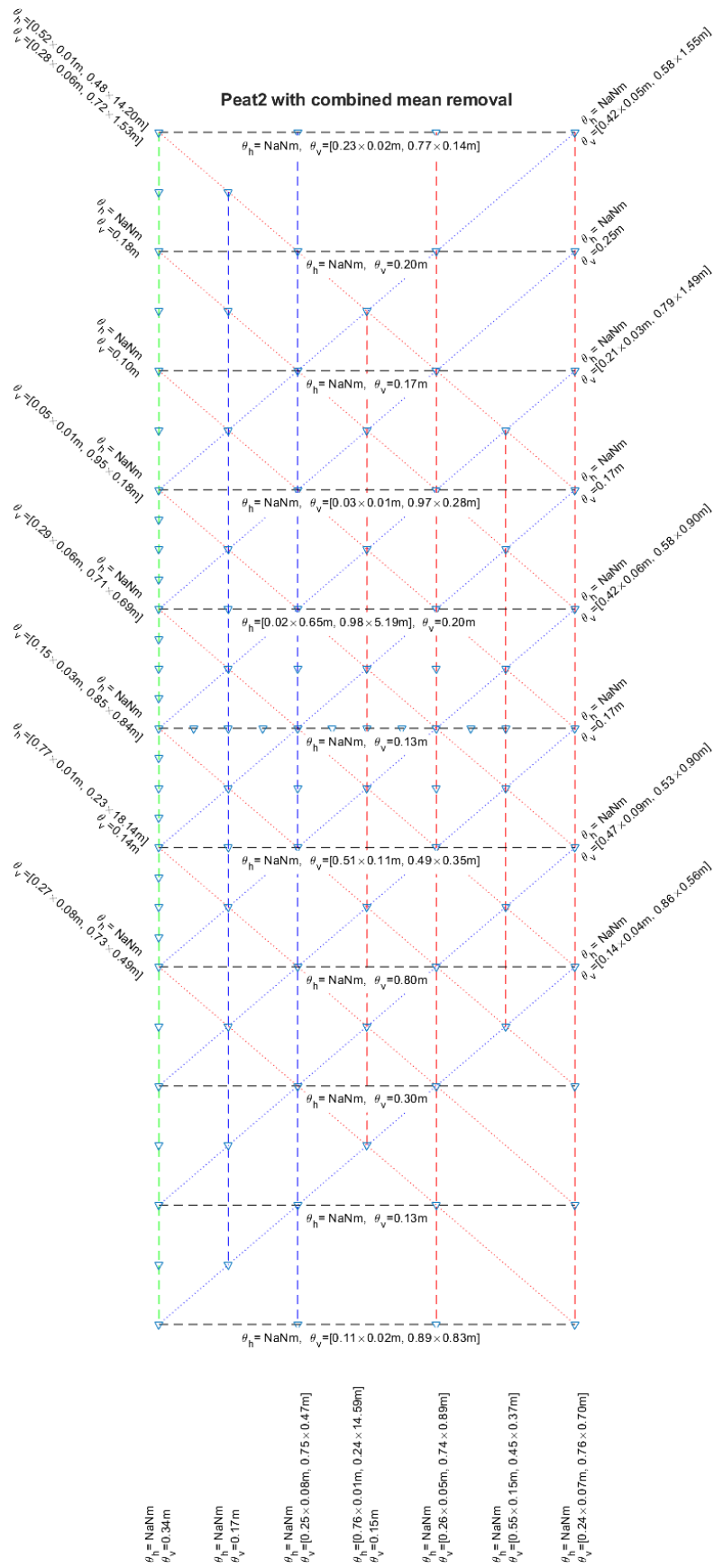
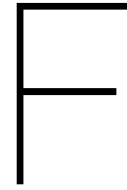


Figure E.8: The horizontal and vertical scales of fluctuation of the second peat layer



The Finite Element Model

The first step to defining the finite element model is to define the soil layer depths and the domain. Since the goal is to determine the deformations that occurred in the soft soils near the dyke, the peat and organic clay layers are defined without any deformations. The top of the peat layer is horizontal and set to the height at which the top of the soil of the Leendert de Boerspolder is found, which is $-1.92\text{m}+\text{NAP}$ at the polder. The depth of the peat layer is set at the depth at which it is found in the polder as well, which is $-4.39\text{m}+\text{NAP}$. The top of the organic clay layer is set at $-4.39\text{m}+\text{NAP}$, but in order to minimise boundary effects of the model, the bottom of the organic clay layer is not set at the depth found at the Leendert de Boerspolder. Instead, it is set to $-11.00\text{m}+\text{NAP}$. The initial groundwater level is set to $-2.67\text{m}+\text{NAP}$, similar to what was found in the polder.

The domain size has to be large enough to prevent any influence of the boundaries on the finite element analysis. From the cone penetration tests in the Leendert de Boerspolder it is estimated that the slope of the dyke has a footprint of 5 meters and the crest is approximately 1 meter. Assuming the footprint of the dyke on the waterside is 5 meters as well, the total width of the dyke is equal to 11 meters. The choice is made to add 5 meters domain width to the waterside of the dyke and 10 meters domain width to the polderside of the dyke, resulting in a total domain width of 26 meters.

The dyke at the Leendert de Boerspolder has been constructed in approximately the year 1600 (de Gast et al., 2017) and has likely been maintained several times since then. Therefore, the structure that will be defined in Plaxis will be constructed in multiple stages until the crest of the structure after the deformations is at the same height as found currently in the Leendert de Boerspolder, which is at approximately $-0.50\text{m}+\text{NAP}$. The resulting finite element model is shown in Figure F.1.

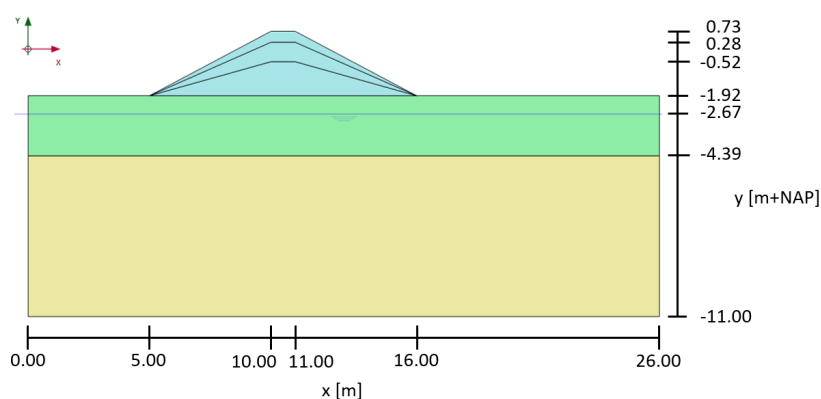


Figure F.1: The finite element model in Plaxis

Finite Element Mesh

When the finite element model is defined, Plaxis calculates the optimal grid based on a single user input: the element distribution. Since the finite element model used for this research is not a complex model, the

element distribution will be set to very fine. In case the analysis takes a long time to analyse, it will be possible to set the element distribution to a coarser distribution. The resulting finite element mesh is shown in Figure E2.

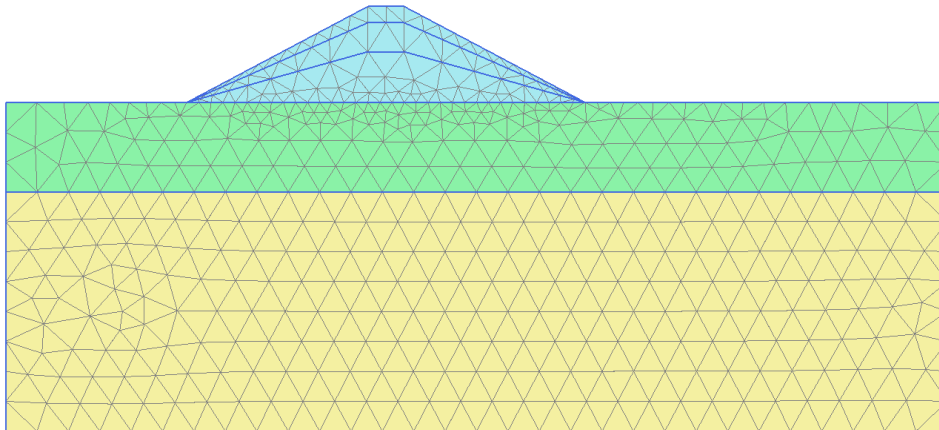


Figure E2: The finite element mesh in Plaxis

Flow Conditions

The dyke at the Leendert de Boerspolder has a water retaining function, which should be simulated in the finite element analysis as well. During the initial construction of the dyke structure and the maintenance steps, the water level will be kept at the initial groundwater level. Afterwards, the water level will be split in three sections: one section for the water level that the dyke should resist, one section for the water level in the soil body of the dyke and one section in the polder at the groundwater level that is currently found in the Leendert de Boerspolder. The increase in water level is obtained by a rapid increase of the water level in five days. The final result of the water levels is shown in Figure E3.

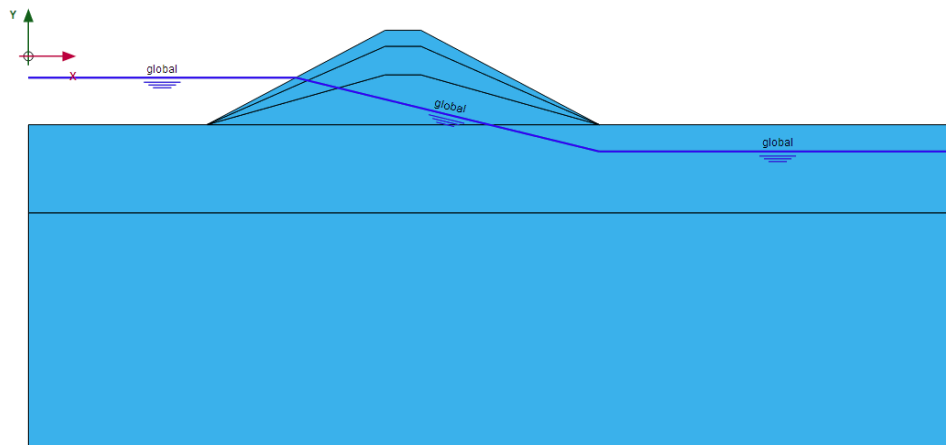


Figure E3: The set water levels after an increase in water level in Plaxis

Construction Stages

The finite element analysis will be done in several steps, called construction stages. An example of a construction stage is the increase of the water level or the consolidation to minimum excess pore pressures. The steps that are set up for the analysis of this research are as follows.

1. The initial phase of the analysis is where the initial conditions are generated. For this research the initial phase is before the construction of the dyke, with just the soil layers and the groundwater being present in this stage. No deformation has occurred yet. The initial stresses are generated by the K0 procedure. Pore water pressures are calculated from the phreatic surface.

2. The next phase is the phase in which the first dyke structure is constructed. This is the structure up to a height of $-0.52\text{m}+\text{NAP}$ in Figure E.1. The calculation type selected for this phase is consolidation with loading type staged construction. The pore water pressures from the previous phase are used and the time interval is set to two days.
3. After the construction a consolidation stage to minimum excess pore pressures is created to allow the excess pore water pressures to dissipate.
4. Due to the first dyke structure an amount of settlement occurred. The second dyke structure up to a height of $0.28\text{m}+\text{NAP}$ is constructed to increase the height of the dyke to $-0.50\text{m}+\text{NAP}$ as is found in the Leendert de Boerspolder. The settings are identical to the first construction phase, but the time interval is set to one day.
5. Once again a consolidation stage to minimum excess pore pressures is created to allow the excess pore water pressures to dissipate.
6. After two construction stages, the crest of the dyke settled once more to a height below the actual crest height found in the polder. The third dyke structure up to a height of $0.73\text{m}+\text{NAP}$ is constructed in this stage. The same settings for the construction are used as before, with a time interval of one day.
7. A consolidation stage to minimum excess pore pressures is added to allow the excess pore water pressures to dissipate.
8. After the previous stage it was found that the crest of the dyke was at approximately $-0.50\text{m}+\text{NAP}$, so no additional structures would have to be constructed to heighten the dyke. The final stage increases the water level to the water level found at the Leendert de Boerspolder of $-0.60\text{m}+\text{NAP}$. The calculation type is set to fully coupled flow-deformation and the time interval is set to five days. Another setting that has to be changed is that a flow function has to be added to the global water level of this stage, which increases the head by 2.07m in five days.